GLOBALLY CONVERGENT NUMERICAL METHODS FOR SEVERAL INVERSE PROBLEMS BASED ON CARLEMAN ESTIMATES

by

Thi Thu Thuy Le

A dissertation submitted to the faculty of
The University of North Carolina at Charlotte
in partial fulfillment of the requirements
for the degree of Doctor of Philosophy in
Applied Mathematics

Charlotte

2023

Approved by:

Dr. Loc Nguyen

Dr. Michael Klibanov

Dr. Taufiquar Khan

Dr. Vasily Astratov

ABSTRACT

THI THU THUY LE. Globally convergent numerical methods for several inverse problems based on Carleman estimates. (Under the direction of DR. LOC NGUYEN and DR. MICHAEL KLIBANOV)

This dissertation focuses on developing efficient numerical methods and theoretical analysis for solving various inverse problems that arise in the fields of mathematics, physics, engineering, and beyond. The goal of inverse problems is to explore inaccessible regions using external measurements, which is essential for non-destructive testing, biomedical imaging, geophysical exploration, and radar applications, among others. However, solving inverse problems is always challenging. This is because they are severely ill-posed and highly nonlinear.

We propose in this dissertation a unified framework to solve severely ill-posed and highly nonlinear inverse problems. The framework is split into two stages:

1. In the first stage, we derive a system of partial differential equations by introducing a new variable and truncating the Fourier series of the solution to the governing equation. The obtained system has only one unknown.

2. In the second stage, we solve the system derived in the first stage using the quasi-reversibility method, the Carleman contraction mapping method, and the convexification method. The obtained solutions of this stage directly yield the desired solutions to the inverse problems.

An important contribution of the dissertation is that we will rigorously and numerically prove the efficiency of this framework, including its global convergence to the true solution. The analytic proofs are based on some Carleman estimates, and the numerical proofs are provided by successfully testing our methods with highly noisy simulated data and experimental data provided by US Army Research Laboratory engineers.

ACKNOWLEDGEMENTS

I express my sincere gratitude to my advisor, Dr. Loc Nguyen, and my co-advisor, Dr. Michael Klibanov, for their invaluable guidance, advice, and feedback throughout my research journey. Their expertise, encouragement, and unwavering support have been crucial in shaping my research project and inspiring me to produce my best work.

I also extend my appreciation to the members of my dissertation committee, Dr. Taufiquar Khan and Dr. Vasily Astratov, for their constructive criticism, helpful suggestions, and encouragement, which have significantly enhanced the quality of my work.

I am also grateful to the faculty and friends at the Department of Mathematics at UNC Charlotte, particularly Dr. Taufiquar Khan and Dr. Shaozhong Deng, for providing a supportive and stimulating academic environment. Additionally, I am thankful for the Graduate School Summer Fellowship 2022 from UNC Charlotte's Graduate School. I acknowledge the support of the US Army Research Office grant W911NF-19-1-0044, National Science Foundation grant DMS-220815, and the Faculty Research Grant program at UNC Charlotte Fund No. 111272. These supports have made the challenges of graduate study much more manageable.

Moreover, I appreciate the time and experiences shared by my friends, Anh Vo, Khoa Vo, Thi Kim Ngan Huynh, Giang Dao, and Phuong Nguyen, which have been instrumental in shaping my research journey and my Ph.D. life.

Finally, I express my deepest gratitude to my family, especially my parents, my husband, my little son, and my brother, for their unwavering support, constant encouragement, and unconditional love. Without their support, this dissertation would not have been possible.

TABLE OF CONTENTS

LIST OF TABLES

LIST OF FIGURES

CHAPTER 1: INTRODUCTION

The field of inverse problems is a diverse and interdisciplinary area of research that has applications in mathematics, physics, engineering, and many other fields. The goal of this field is to explore inaccessible regions through external measurements, which is crucial for non-destructive testing, biomedical imaging, geophysical exploration, and radar, among other applications. This dissertation contributes to this field by developing effective numerical methods and theoretical analysis for various inverse problems.

Specifically, the dissertation has developed methods for solving scattering inverse problems in both the frequency and time domains, inverse source problems for nonlinear parabolic equations, and a linearized kinematic inverse problem with incomplete data. All of these problems are highly ill-posed and often nonlinear, making their solutions challenging. Throughout this dissertation, a unified framework is developed to solve inverse problems. This framework has two stages.

1. In stage 1, we truncate the Fourier series of the solution to the governing equation [1, 2, 3] or introduce a new change of variable [4]. By this step, we obtain a system of partial equations.

2. In stage 2, we compute the solution to this system. As soon as this system is solved, we directly obtain the desired solutions to the inverse problems under consideration.

While stage 1 is straightforward, stage 2 is challenging, especially when the governing equation is nonlinear. There are three numerical methods that are proposed and developed for stage 2 in this dissertation, named the quasi-reversibility method, the

Carleman contraction mapping method, and the convexification method. All of them are based on a sophisticated mathematical tool of Carleman estimates. This tool was first introduced in the field of inverse problems in 1981 in the work of Bukhgeim and Klibanov [5]. Since then, many works of many authors [6, 7, 8, 9, 10, 11, 12, 13, 2] have explored the idea of [5]. See a survey about the Carleman estimates and their applications in [14]. Based on Carleman estimates, these numerical methods are proven to provide reliable solutions even when the data is highly noisy. Importantly, they are "globally" convergent, meaning that they do not require advanced knowledge of the true solution before solving inverse problems. This global property distinguishes this work from many other publications in the field, which often rely on local methods such as least squares optimization. Due to the nonlinear nature of the inverse problems, the least squares functionals are non-convex. They might have multiple local minima and ravines. Therefore, good initial guesses sufficiently close to the true solution are important for optimization-based methods to deliver reliable numerical solutions. However, we only consider the case when such good initial guesses are not available. This is the main reason for us to develop the convexification and Carleman contraction mapping method. These two methods are globally convergent in the following sense:

1. they deliver good numerical solutions to the inverse problem without knowing any information of the true solutions,

2. the claim in #1 above is rigorously proved and numerically verified.

The developed numerical algorithms were successfully tested with highly noisy simulated and experimental data provided by engineers at the US Army Research Laboratory.

The dissertation is organized as follows.

Chapter 2 presents a novel numerical approach for solving the linearized version

of the travel time tomography problem which is given with incomplete data. Our method involves the truncation of Fourier series using a special basis introduced in [15], leading to a boundary value problem for a system of first-order PDEs. We solve this problem using the quasi-reversibility method, which helps to obtain the Fourier coefficients of the solution to the linearized eikonal equation that is spatially dependent. Our method is shown effective even with highly noisy data. We present numerical results to demonstrate its effectiveness. The work in this chapter is adapted from [1].

Chapter 3 proposes a new convergent numerical method for reconstructing the initial condition of a quasilinear parabolic equation from the Dirichlet and Neumann data measured at the boundary of a bounded domain. Unlike previous methods, we do not require any prior knowledge of the true solution, despite the high nonlinearity of the problem. The key in our method is the derivation of a boundary value problem for a system of coupled quasilinear elliptic equations, whose solution is the vector function of the spatially dependent Fourier coefficients of the solution to the governing parabolic equation. We apply an iterative approach to solve this problem and rigorously establish the global convergence of the system using a Carleman estimate. The effectiveness of our method is illustrated through numerical examples. The work in this chapter is adapted from [2]. This work is original and serves as the foundation of one of our numerical methods, named the Carleman contraction mapping method. There also exists a numerical method to solve this inverse problem without truncating the Fourier series of the solution to the governing equation, see [16, Chapter 5, §5.8.2]. However, this method has been developed only theoretically so far and has not been tried numerically yet.

Chapter 4, adapted from [4], develops the Carleman contraction mapping method to solve a Coefficient Inverse Problem for a 1D hyperbolic equation. The numerical method is based on the contraction mapping principle with the involvement of a Car-

leman Weight Function. Using a Carleman estimate, the global convergence of the corresponding numerical method is established. Numerical studies for both computationally simulated and experimentally collected data are presented. The experimental part is concerned with the problem of computing dielectric constants of explosive-like targets in the standoff mode using severely underdetermined data collected by engineers at the US Army Research Laboratory.

Chapter 5, adapted from [3], focuses on analyzing the global convergence of the gradient descent method for minimizing strictly convex functionals on an open and bounded set of a Hilbert space. Unlike the case of the entire Hilbert space, such results are currently unknown for this type of set. We then utilize our findings to establish a comprehensive framework for numerically solving boundary value problems for quasilinear partial differential equations using noisy Cauchy data. This procedure involves using Carleman weight functions to convexify a cost functional from the given boundary value problem, thereby ensuring the convergence of the aforementioned gradient descent method. We prove the global convergence of this method as noise approaches zero, and the convergence rate is Lipschitz. Finally, we apply this method to solve a highly nonlinear and severely ill-posed coefficient inverse problem known as the backscattering inverse problem, which has numerous real-world applications. We present various numerical examples to support our approach.

The final chapter, chapter 6, is for the concluding remarks.

CHAPTER 2: NUMERICAL SOLUTION OF A LINEARIZED TRAVEL TIME TOMOGRAPHY PROBLEM WITH INCOMPLETE DATA

2.1 Introduction

In this chapter, we develop a new numerical method for the linearized Travel Time Tomography Problem (TTTP) for the $d-$D case. Our data are both non-redundant and incomplete. Using results of [1], we establish the convergence of our method. In addition, we provide results of numerical experiments in the 2D case. In particular, we demonstrate that our method provides good accuracy of images of complicated objects with 5% noise in the data. Furthermore, a satisfactory accuracy of images is demonstrated even for very high levels of noise between 80% and 170%.

In fact, both the idea of our method and sources/detectors configuration are close to those of our recent works [2, 1]. However, our case is substantially more difficult one since the waves in our case propagate along geodesic lines, rather than a radiation propagating along straight lines in [2, 1]. Still, although we formulate here results related to the convergence of our method, we do not prove them. The reason is that, as it turns out, proofs are very similar to those in [1]. In other words, surprisingly, the analytical apparatus of the convergence theory developed in [1] works well for the problem considered in this chapter.

In the isotropic case of acoustic/seismic wave propagation, the TTTP is the problem of the recovery of the spatially distributed speed of propagation of acoustic/seismic waves from the first times of arrival of those waves. In the electromagnetic case, this is the problem of the recovery of the spatially distributed dielectric constant from those times. Another name for the TTTP is an inverse kinematic problem (IKP). Waves are originated from some sources located either at the boundary of the closed

bounded domain of interest or outside of this domain. Times of the first arrival from those sources are measured on the part of the boundary of that domain. The TTTP has well-known applications in Geophysics, see, e.g. the book of Romanov [3, Chapter 3].

The pioneering chapters about the solution of the 1D TTTP were published by Herglotz [4] (1905) and then by Wiechert and Zoeppritz [5] (1907). Their method is described in the book of Romanov [3, Section 3 of Chapter 3]. It was recently discovered that, in addition to Geophysics, the IKP has applications in the phaseless inverse scattering problem [6, 7, 8].

The next natural question after the classical 1D case of [4, 5] was about 2 and 3 dimensional cases. The first uniqueness and Lipschitz stability result for the 2D case was obtained by Mukhometov [9], also see [10, 11]. Next, these results were obtained by Mukhometov and Romanov for the 3D case in [12, 3]. We also refer to the work of Stefanov, Uhlmann and Vasy [13] for a more recent publication for the 3D case. As to the numerical methods for the inverse kinematic problem, we refer to [14] for the 2D case and to [15] for the 3D case.

In all past publications about the IKP, the data are redundant in the 3D case and complete in both 2D and 3D cases. In two recent works, the first author [16, 17] two globally convergent numerical methods for the 3D TTTP with non-redundant incomplete data were developed.

Along with the full IKP, a significant applied interest is also in a linearized IKP, see [3, Chapter 3]. Below $d \geq 2$ is the dimension of the space $\mathbb{R}^d$. Points of this space are denoted as $\mathbf{x} \in \mathbb{R}^d$. Let $\overline{c} \equiv const. > 0$ be the speed of sound in a certain reference medium in $\mathbb{R}^d$, which we do not specify, and $c(\mathbf{x}) > 0$ be the variable speed of sound. Then the refractive index is [3, Chapter 3]

$$\mathbf{n}(\mathbf{x}) = \overline{c}/c(\mathbf{x}) \tag{2.1}$$

To linearize, one should assume that $\mathbf{n}(\mathbf{x}) = \mathbf{n}_0(\mathbf{x}) + \mathbf{n}_1(\mathbf{x})$, where $\mathbf{n}_0(\mathbf{x})$ is the known background function and $\mathbf{n}_1(\mathbf{x})$ with $|\mathbf{n}_1(\mathbf{x})| \ll \mathbf{n}_0(\mathbf{x})$ is its unknown perturbation, which is the subject of the solution of the linearized TTTP. Thus, one assumes that the refractive index is basically known, whereas its small perturbation $\mathbf{n}_1$ is unknown. This problem is also called the *geodesic X-ray transform problem*. The Lipschitz stability and uniqueness theorem for this problem in the isotropic case was first obtained in [18], see Theorem 3.2 in Section 4 of Chapter 3 of [3]. In the nonisotropic case this problem was studied in [19]. In [20] numerical studies of this problem in the isotropic case were performed.

In our derivation, we end up with an over-determined boundary value problem for a system of coupled linear PDEs of the first order. It is well known that the quasi-reversibility method is an effective tool for numerical solutions of over determined boundary value problems for PDEs. Lattès and Lions [21] were the first ones who propose the quasi-reversibility method. This technique was developed further in, e.g. [22, 23, 24, 25, 2, 26, 1]. In particular, it was shown in [25] that while it is rather easy to prove, using Riesz theorem, the existence, and uniqueness of the minimizer of a certain functional related to this method, the proof of convergence of those minimizers to the correct solution requires a stronger tool of Carleman estimates.

Another important feature of this chapter is a special orthonormal basis in the space $L^2(-\overline{\alpha}, \overline{\alpha})$, where $\overline{\alpha} > 0$ is a certain number. The functions of this basis depend only on the position of the point source. This basis was first introduced in [27] and was further used in [28, 16, 29, 17, 30, 2, 31, 1]. Just like in these previous publications, we use here an *approximate mathematical model*. More precisely, we assume that a certain function associated with the solution of the governing linearized Eikonal equation can be represented via a truncated Fourier series with respect to this basis. This assumption forms the first element of that model. The second element is that we assume that the first derivatives with respect to all variables are written via finite

differences, and the step size of these finite differences with respect to all variables, except for one, is bounded from below by a positive number $h_0 > 0$.

We do not prove convergence for the case when $h_0 \to 0^+$ and the number N of terms in that truncated series tends to infinity. Thus, we come up with a finite-dimensional approximate mathematical model. We point out that similar approximate mathematical models are used quite often in studies of numerical methods for inverse problems, and numerical results are usually encouraging, see, e.g., [32, 33, 34, 29, 1, 35]. Just as ourselves, proofs of convergence results in such cases when e.g. $N \to \infty, h_0 \to 0^+$ are usually not conducted since they are very challenging tasks due to the ill-posed nature of inverse problems.

The chapter is organized as follows. In Section 2.2, we formulate the inverse problem. Next, in Section 2.3, we introduce the truncation technique and our numerical method. Then, in Section 2.4, we recall the quasi-reversibility method and its convergence in the case of partial finite differences. In Section 2.5 we present the implementation and numerical results. Finally, Section 2.6 is for concluding remarks.

2.2 The linearization

Consider numbers R, a, b such that $R > 1$ and $0 < a < b$. Set

$$\Omega = (-R, R)^{d-1} \times (a, b) \subset \mathbb{R}^d. \tag{2.2}$$

Recall that by (2.1) $\mathbf{n}(\mathbf{x}) = \overline{c}/c(\mathbf{x})$, where $c(\mathbf{x})$ is the speed of sound propagation and $n(\mathbf{x})$ is the refractive index. Let the function $\mathbf{n}_0(\mathbf{x})$ be the known refractive index of the background. We assume that

$$\mathbf{n}_0, \mathbf{n} \in C^2\left(\mathbb{R}^d\right);\ \mathbf{n}_0^2(\mathbf{x}), \mathbf{n}^2(\mathbf{x}) \geq 1 \text{ in } \Omega, \tag{2.3}$$

$$\mathbf{n}_0^2(\mathbf{x}) = \mathbf{n}^2(\mathbf{x}) = 1 \text{ for } \mathbf{x} \in \mathbb{R}^d \setminus \Omega. \tag{2.4}$$

For any two points $\mathbf{x}_1$ and $\mathbf{x}_2$ in $\mathbb{R}^d$, define the geodesic line generated by $\mathbf{n}_0$ connecting $\mathbf{x}_1$ and $\mathbf{x}_2$ as:

$$\Gamma_0(\mathbf{x}_1,\mathbf{x}_2)=\operatorname{argmin}\Big\{\int_\gamma \mathbf{n}_0(\xi)d\sigma(\xi) \text{ where } \gamma:[0,1]\to\mathbb{R}^d \text{ is a smooth map with } \gamma(0)=\mathbf{x}_1,\gamma(1)=\mathbf{x}_2\Big\}. \quad (2.5)$$

Here $d\sigma(\xi)$ is the elementary arc length. Note that by (2.5) the geodesic line $\Gamma_0(\mathbf{x}_1,\mathbf{x}_2)$ connects points $\mathbf{x}_1$ and $\mathbf{x}_2$. Let

$$\mathbf{a}_0(\mathbf{x})=\mathbf{n}_0^2(\mathbf{x}) \quad \text{for all } \mathbf{x}\in\mathbb{R}^d. \quad (2.6)$$

The corresponding travel time between $\mathbf{x}_1$ and $\mathbf{x}_2$ is the integral

$$\int_{\Gamma_0(\mathbf{x}_1,\mathbf{x}_2)} \mathbf{n}_0(\xi)d\sigma(\xi)=\int_{\Gamma_0(\mathbf{x}_1,\mathbf{x}_2)} \sqrt{\mathbf{a}_0(\xi)}d\sigma(\xi).$$

Introduce the line of sources L_{s} located on the x_1-axis as

$$L_{\mathrm{s}}=[-\overline{\alpha},\overline{\alpha}]\times\{(0,0,\dots,0)\}, \quad (2.7)$$

where $\overline{\alpha}$ is a fixed positive number. It follows from (2.2) and (2.7) that

$$\overline{\Omega}\cap L_{\mathrm{s}}=\varnothing. \quad (2.8)$$

For $\mathbf{x}_\alpha\in L_{\mathrm{s}}$, the travel time along $\Gamma_0(\mathbf{x},\mathbf{x}_\alpha)$ of the wave from $\mathbf{x}_\alpha$ to $\mathbf{x}$ is

$$u_0(\mathbf{x},\mathbf{x}_\alpha)=\int_{\Gamma_0(\mathbf{x},\mathbf{x}_\alpha)} \sqrt{\mathbf{a}_0(\xi)}d\sigma(\xi), \quad \mathbf{x}\in\mathbb{R}^d. \quad (2.9)$$

Assumption 2.2.1 (regularity of geodesic lines) *We assume everywhere in this chapter that the geodesic lines are regular in the following sense: for each point* $\mathbf{x}$ *of*

the closed domain $\overline{\Omega}$ *and for each point* $\mathbf{x}_\alpha$ *of the line of sources* L_{s} *there exists a single geodesic line* $\Gamma_0(\mathbf{x}, \mathbf{x}_\alpha)$ *connecting them.*

The inverse problem we consider arises from the highly nonlinear and severely ill-posed inverse kinematic problem. We now present the formal linearization arguments in exactly the same way as they are presented in the book of Romanov [3, Section 4 of Chapter 3]. Just as in this book, we avoid a setting via functional spaces for brevity.

Assume that the function $\mathbf{a}(\mathbf{x}) = \mathbf{n}^2(\mathbf{x})$ contains a perturbation term of the background function $\mathbf{a}_0(\mathbf{x}) = \mathbf{n}_0^2(\mathbf{x})$. In other words,

$$\mathbf{a}(\mathbf{x}) = \mathbf{a}_0(\mathbf{x}) + 2\epsilon\sqrt{\mathbf{a}_0(\mathbf{x})}p(\mathbf{x}), \quad \mathbf{x} \in \mathbb{R}^d, \tag{2.10}$$

where $\epsilon > 0$ is a sufficiently small number. Here, the function $p \in C\left(\mathbb{R}^d\right)$ and $p\left(\mathbf{x}\right) = 0$ for $\mathbf{x} \notin \overline{\Omega}$. Hence, by (2.8) $p(\mathbf{x}) = 0$ for points $\mathbf{x}$ in a small neighborhood of the line of sources L_{s}. Denote

$$u_{\mathbf{n}}(\mathbf{x}, \mathbf{x}_\alpha) = \int_{\Gamma_{\mathbf{n}}(\mathbf{x}, \mathbf{x}_\alpha)} \mathbf{n}(\xi) d\sigma(\xi)$$

the travel time from the point $\mathbf{x}_\alpha \in L_{\mathrm{s}}$ to the point $\mathbf{x} \in \Omega$, where $\Gamma_{\mathbf{n}}(\mathbf{x}, \mathbf{x}_\alpha)$ is the geodesic line generated by the function $\mathbf{n}(\mathbf{x})$. It is well-known that $u_{\mathbf{n}}(\mathbf{x}, \mathbf{x}_\alpha)$ satisfies the Eikonal equation [3, Chapter 3]

$$|\nabla_{\mathbf{x}} u_{\mathbf{n}}(\mathbf{x}, \mathbf{x}_\alpha)|^2 = \mathbf{a}(\mathbf{x}), \quad \mathbf{x} \in \Omega, \mathbf{x}_\alpha \in L_{\mathrm{s}}. \tag{2.11}$$

Let $u_0(\mathbf{x}, \mathbf{x}_\alpha)$ be the travel time function in (2.9) corresponding to the background $\mathbf{a}_0$. Then

$$|\nabla_{\mathbf{x}} u_0(\mathbf{x}, \mathbf{x}_\alpha)|^2 = \mathbf{a}_0(\mathbf{x}), \quad \mathbf{x} \in \Omega, \mathbf{x}_\alpha \in L_{\mathrm{s}}. \tag{2.12}$$

Due to (2.10) we represent $\nabla_{\mathbf{x}} u_{\mathbf{n}}(\mathbf{x}, \mathbf{x}_\alpha)$ as

$$\nabla_{\mathbf{x}} u_{\mathbf{n}}(\mathbf{x}, \mathbf{x}_\alpha) = \nabla_{\mathbf{x}} u_0(\mathbf{x}, \mathbf{x}_\alpha) + \epsilon \nabla_{\mathbf{x}} u^{(1)}(\mathbf{x}, \mathbf{x}_\alpha). \tag{2.13}$$

Hence, ignoring the term with ϵ^2, we obtain

$$|\nabla_{\mathbf{x}} u_{\mathbf{n}}(\mathbf{x}, \mathbf{x}_\alpha)|^2 \approx |\nabla_{\mathbf{x}} u_0(\mathbf{x}, \mathbf{x}_\alpha)|^2 + 2\epsilon \nabla_{\mathbf{x}} u_0(\mathbf{x}, \mathbf{x}_\alpha) \nabla_{\mathbf{x}} u^{(1)}(\mathbf{x}, \mathbf{x}_\alpha). \tag{2.14}$$

Denoting

$$u^{(1)} := u \tag{2.15}$$

and comparing (2.14) with (2.10) and (2.12), we obtain

$$\frac{\nabla_{\mathbf{x}} u_0(\mathbf{x}, \mathbf{x}_\alpha)}{\sqrt{\mathbf{a}_0(\mathbf{x})}} \cdot \nabla_{\mathbf{x}} u(\mathbf{x}, \mathbf{x}_\alpha) = p(\mathbf{x}). \tag{2.16}$$

Thus, equation (2.16) is the “linearization" of the nonlinear equation (2.11). By (2.12) $|\nabla_{\mathbf{x}} u_0(\mathbf{x}, \mathbf{x}_\alpha)| / \sqrt{\mathbf{a}_0(\mathbf{x})} \equiv 1$. Hence, this is a unit vector, which is tangent to the curve $\Gamma_0(\mathbf{x}, \mathbf{x}_\alpha)$ at the point $\mathbf{x}$ [3, Chapter 3]. Hence, the left hand side of (2.16) is the derivative of the function $u(\mathbf{x}, \mathbf{x}_\alpha)$ along the curve $\Gamma_0(\mathbf{x}, \mathbf{x}_\alpha)$. Thus, integrating, we obtain [3, Chapter 3]

$$u(\mathbf{x}, \mathbf{x}_\alpha) = \int_{\Gamma_0(\mathbf{x}, \mathbf{x}_\alpha)} p(\xi) d\sigma(\xi). \tag{2.17}$$

Let $\partial\Omega_{\text{sm}}$ be the smooth part of the boundary $\partial\Omega$ of the domain Ω. For each $\alpha \in (-\overline{\alpha}, \overline{\alpha})$, define

$$\partial\Omega_\alpha^- = \{\mathbf{x} \in \partial\Omega_{\text{sm}} : \nabla_{\mathbf{x}} u_0(\mathbf{x}, \mathbf{x}_\alpha) \cdot \nu(\mathbf{x}) < 0\},$$
$$\partial\Omega_\alpha^+ = \{\mathbf{x} \in \partial\Omega_{\text{sm}} : \nabla_{\mathbf{x}} u_0(\mathbf{x}, \mathbf{x}_\alpha) \cdot \nu(\mathbf{x}) > 0\},$$

where $\mathbf{x}_\alpha = (\alpha, 0, \dots, 0) \in L_{\rm s}$ and $\nu(\mathbf{x})$ is the outward looking unit normal vector at the point $\mathbf{x} \in \partial\Omega_{\rm sm}$. If $\mathbf{n}_0 \equiv 1$, then $\Gamma_0(\mathbf{x}_1, \mathbf{x}_2)$ is the line segment connecting these two points. Hence, it follows from (2.2), (2.7), (2.8), (2.13) and (2.15) that

$$u(\mathbf{x}, \mathbf{x}_\alpha) = 0, \mathbf{x} \in \partial\Omega_\alpha^-. \tag{2.18}$$

The aim of this chapter is to solve the following inverse problem:

Problem 2.2.1 (linearized travel time tomography problem) *Let the function* $u = u(\mathbf{x}, \mathbf{x}_\alpha) \in C^1\left(\overline{\Omega} \times [-\overline{\alpha}, \overline{\alpha}]\right)$ *be the solution of boundary value problem (2.16), (2.18). Given the data* $f(\mathbf{x}, \mathbf{x}_\alpha)$,

$$f(\mathbf{x}, \mathbf{x}_\alpha) = \begin{cases} u(\mathbf{x}, \mathbf{x}_\alpha), \ \mathbf{x} \in \partial\Omega_\alpha^+, \mathbf{x}_\alpha \in L_{\rm s}, \\ 0, \ \mathbf{x} \in \partial\Omega_\alpha^-, \mathbf{x}_\alpha \in L_{\rm s}, \end{cases} \tag{2.19}$$

determine the function $p(\mathbf{x})$, $\mathbf{x} \in \Omega$.

Note that the data (2.19) are non-redundant ones. Indeed, the source $\mathbf{x}_\alpha \in L_{\rm s}$ depends on one variable and the point $\mathbf{x} \in \partial\Omega_\alpha^+$ depends on $d-1$ variables. Hence the function $f(\mathbf{x}, \mathbf{x}_\alpha)$ depends on d variables, so as the target unknown function $p(\mathbf{x})$.

From now on, to separate the coordinate number d of the point $\mathbf{x}$, we write $\mathbf{x} = (x_1, \dots, x_{d-1}, z)$. The transport equation in (2.16) is read as

$$\frac{\partial_z u_0(\mathbf{x}, \mathbf{x}_\alpha)}{\sqrt{\mathbf{a}_0(\mathbf{x})}} \partial_z u(\mathbf{x}, \mathbf{x}_\alpha) + \sum_{i=1}^{d-1} \frac{\partial_{x_i} u_0(\mathbf{x}, \mathbf{x}_\alpha)}{\sqrt{\mathbf{a}_0(\mathbf{x})}} \partial_{x_i} u(\mathbf{x}, \mathbf{x}_\alpha) = p(\mathbf{x}), \tag{2.20}$$

which is equivalent to

$$\partial_z u_0(\mathbf{x}, \mathbf{x}_\alpha) \partial_z u(\mathbf{x}, \mathbf{x}_\alpha) + \sum_{i=1}^{d-1} \partial_{x_i} u_0(\mathbf{x}, \mathbf{x}_\alpha) \partial_{x_i} u(\mathbf{x}, \mathbf{x}_\alpha) = \sqrt{\mathbf{a}_0(\mathbf{x})} p(\mathbf{x}) \tag{2.21}$$

for all $\mathbf{x} \in \Omega$, $\mathbf{x}_\alpha \in L_{\mathrm{s}}$.

2.3 A boundary value problem for a system of coupled PDEs of the first order

This section aims to derive a system of partial differential equations, which can be stably solved by the quasi-reversibility method in the semi-finite difference scheme. The solution of this system yields the desired numerical solution to Problem 2.2.1. Recall that Problem 2.2.1 is the linearized travel time tomography problem, and it is labeled this way by its title.

We will employ a special basis of $L^2(-\overline{\alpha}, \overline{\alpha})$ where $2\overline{\alpha}$ is the length of the line of source L_{sc}, see (2.7). For each $n = 1, 2, \cdots$, let $\phi_n(\alpha) = \alpha^{n-1} \exp(\alpha)$. The set $\{\phi_n\}_{n=1}^{\infty}$ is complete in $L^2(-\overline{\alpha}, \overline{\alpha})$. Applying the Gram-Schmidt orthonormalization process to this set, we obtain a basis of $L^2(-\overline{\alpha}, \overline{\alpha})$, named as $\{\Psi_n\}_{n=1}^{\infty}$. We have the proposition

Proposition 2.3.1 (see [27]) *The basis $\{\Psi_n\}_{n=1}^{\infty}$ satisfies the following properties:*

1. *Ψ_n is not identically zero for all $n \geq 1$.*

2. *For all $m, n \geq 1$*

$$s_{mn} = \int_{-\overline{\alpha}}^{\overline{\alpha}} \Psi_n'(\alpha)\Psi_m(\alpha)d\alpha = \begin{cases} 1 & \text{if } m = n, \\ 0 & \text{if } n < m. \end{cases}$$

Thus, the matrix $S_N = (s_{mn})_{m,n=1}^{N}$, is invertible for all integers $N \geq 1$.

We now derive a system of partial differential equations for the Fourier coefficients of the function

$$w(\mathbf{x}, \mathbf{x}_\alpha) = u(\mathbf{x}, \mathbf{x}_\alpha)\partial_z u_0(\mathbf{x}, \mathbf{x}_\alpha) \quad \mathbf{x} \in \Omega, \mathbf{x}_\alpha \in L_{\mathrm{s}} \tag{2.22}$$

with respect to the basis $\{\Psi_n\}_{n=1}^{\infty}$. Differentiate (2.21) with respect to α. We obtain

$$\frac{\partial}{\partial\alpha}\Big[\partial_z u_0(\mathbf{x},\mathbf{x}_\alpha)\partial_z u(\mathbf{x},\mathbf{x}_\alpha)+\sum_{i=1}^{d-1}\partial_{x_i}u_0(\mathbf{x},\mathbf{x}_\alpha)\partial_{x_i}u(\mathbf{x},\mathbf{x}_\alpha)\Big]=0 \tag{2.23}$$

for all $\mathbf{x}\in\Omega$, $\mathbf{x}_\alpha\in L_{\mathrm{s}}$. From now on, we impose the following condition.

Assumption 2.3.1 (Monotonicity condition in the z-direction) *The traveling time function u_0, defined in* (2.9) *with* $\mathbf{n}$ *replaced by* $\mathbf{n}_0$*, is strictly increasing with respect to z. In other words, $\partial_z u_0(\mathbf{x},\mathbf{x}_\alpha)>0$ for all $\mathbf{x}=(x_1,\dots,x_{d-1},z)\in\Omega$ and for all $\mathbf{x}_\alpha\in L_{\mathrm{s}}$.*

Assumption 2.3.1 means that the higher in the z-direction, the longer the traveling time is. A sufficient condition for Assumption 2.3.1 to be true is formulated in (2.24) of Lemma 3.1. A similar monotonicity condition can be found in formulas (3.24) and (3.24′) of section 2 of chapter 3 of the book [3]. Also, a similar condition was imposed in originating works for the 1D problem of Herglotz and Wiechert and Zoeppritz [4, 5]: see section 3 of chapter 3 of [3]. Besides, figures 5 and 10 of [36] justify this condition from the geophysical standpoint. Recall that by (2.6) and (2.3) $\mathbf{a}_0\in C^2\left(\mathbb{R}^d\right)$ and $\mathbf{a}_0(\mathbf{x})\geq 1$ in $\mathbb{R}^d$. Therefore, the following lemma follows immediately from Lemma 4.1 of [17]:

Lemma 2.3.1 *Let conditions (2.3) and (2.6) hold. Also, let*

$$\partial_z\mathbf{a}_0(\mathbf{x})\geq 0 \text{ for all } \mathbf{x}\in\overline{\Omega}. \tag{2.24}$$

Then

$$\partial_z u_0(\mathbf{x},\mathbf{x}_\alpha)\geq\frac{a}{\sqrt{a^2+2}} \text{ for all } \mathbf{x}\in\overline{\Omega},\alpha\in[-\overline{\alpha},\overline{\alpha}].$$

Although Lemma 2.3.1 is proven in [17] only in the 3D case, the proof in the $d-$D case is very similar and is, therefore, avoided. Let $w(\mathbf{x}, \mathbf{x}_\alpha)$ be the function defined in (2.22). Then

$$\begin{aligned} \partial_z u_0(\mathbf{x}, \mathbf{x}_\alpha)\partial_z u(\mathbf{x}, \mathbf{x}_\alpha) &= \partial_z w(\mathbf{x}, \mathbf{x}_\alpha) - u(\mathbf{x}, \alpha)\partial_{zz} u_0(\mathbf{x}, \mathbf{x}_\alpha) \\ &= \partial_z w(\mathbf{x}, \mathbf{x}_\alpha) - w(\mathbf{x}, \alpha)\frac{\partial_{zz} u_0(\mathbf{x}, \mathbf{x}_\alpha)}{\partial_z u_0(\mathbf{x}, \mathbf{x}_\alpha)}. \end{aligned} \tag{2.25}$$

Also, for $i = 1, \ldots, d-1$

$$\begin{aligned} \partial_{x_i} u(\mathbf{x}, \mathbf{x}_\alpha) &= \frac{\partial}{\partial x_i}\left(\frac{w(\mathbf{x}, \mathbf{x}_\alpha)}{\partial_z u_0(\mathbf{x}, \mathbf{x}_\alpha)}\right) \\ &= \frac{\partial_{x_i} w(\mathbf{x}, \mathbf{x}_\alpha)\partial_z u_0(\mathbf{x}, \mathbf{x}_\alpha) - w(\mathbf{x}, \mathbf{x}_\alpha)\partial_{zx_i} u_0(\mathbf{x}, \mathbf{x}_\alpha)}{(\partial_z u_0(\mathbf{x}, \mathbf{x}_\alpha))^2} \end{aligned} \tag{2.26}$$

for all $\mathbf{x} \in \Omega, \mathbf{x}_\alpha \in L_{\text{sc}}$. Combining (2.23), (2.25) and (2.26), we obtain

$$\begin{aligned} &\frac{\partial}{\partial \alpha}\Big[\partial_z w(\mathbf{x}, \mathbf{x}_\alpha) - w(\mathbf{x}, \mathbf{x}_\alpha)\frac{\partial_{zz} u_0(\mathbf{x}, \mathbf{x}_\alpha)}{\partial_z u_0(\mathbf{x}, \mathbf{x}_\alpha)} \\ &\quad + \sum_{i=1}^{d-1} \frac{\partial_{x_i} w(\mathbf{x}, \mathbf{x}_\alpha)\partial_z u_0(\mathbf{x}, \mathbf{x}_\alpha) - w(\mathbf{x}, \mathbf{x}_\alpha)\partial_{zx_i} u_0(\mathbf{x}, \mathbf{x}_\alpha)}{(\partial_z u_0(\mathbf{x}, \mathbf{x}_\alpha))^2}\partial_{x_i} u_0(\mathbf{x}, \mathbf{x}_\alpha)\Big] = 0. \end{aligned} \tag{2.27}$$

This is equivalent to

$$\begin{aligned} &\partial_{\alpha z} w(\mathbf{x}, \mathbf{x}_\alpha) - \frac{\partial_{zz} u_0(\mathbf{x}, \mathbf{x}_\alpha)}{\partial_z u_0(\mathbf{x}, \mathbf{x}_\alpha)}\partial_\alpha w(\mathbf{x}, \mathbf{x}_\alpha) - \frac{\partial}{\partial \alpha}\left(\frac{\partial_{zz} u_0(\mathbf{x}, \mathbf{x}_\alpha)}{\partial_z u_0(\mathbf{x}, \mathbf{x}_\alpha)}\right) w(\mathbf{x}, \mathbf{x}_\alpha) \\ &\quad + \sum_{i=1}^{d-1}\Big[\frac{\partial_{x_i} u_0(\mathbf{x}, \mathbf{x}_\alpha)}{\partial_z u_0(\mathbf{x}, \mathbf{x}_\alpha)}\partial_{\alpha x_i} w(\mathbf{x}, \mathbf{x}_\alpha) + \frac{\partial}{\partial \alpha}\left(\frac{\partial_{x_i} u_0(\mathbf{x}, \mathbf{x}_\alpha)}{\partial_z u_0(\mathbf{x}, \mathbf{x}_\alpha)}\right)\partial_{x_i} w(\mathbf{x}, \mathbf{x}_\alpha) \\ &\qquad - \frac{\partial_{zx_i} u_0(\mathbf{x}, \mathbf{x}_\alpha)\partial_{x_i} u_0(\mathbf{x}, \mathbf{x}_\alpha)}{(\partial_z u_0(\mathbf{x}, \mathbf{x}_\alpha))^2}\partial_\alpha w(\mathbf{x}, \mathbf{x}_\alpha) \\ &\qquad - \frac{\partial}{\partial \alpha}\left(\frac{\partial_{zx_i} u_0(\mathbf{x}, \mathbf{x}_\alpha)\partial_{x_i} u_0(\mathbf{x}, \mathbf{x}_\alpha)}{(\partial_z u_0(\mathbf{x}, \mathbf{x}_\alpha))^2}\right) w(\mathbf{x}, \mathbf{x}_\alpha)\Big] = 0. \end{aligned} \tag{2.28}$$

We recall now the orthonormal basis $\{\Psi_n\}_{n=1}^{\infty}$ constructed at the beginning of this

section. For each $\mathbf{x} \in \Omega$ and for all $\mathbf{x}_\alpha \in L_{\text{sc}}$, we write

$$w(\mathbf{x}, \mathbf{x}_\alpha) = \sum_{n=1}^{\infty} w_n(\mathbf{x})\Psi_n(\alpha) \approx \sum_{n=1}^{N} w_n(\mathbf{x})\Psi_n(\alpha), \tag{2.29}$$

$$w_n(\mathbf{x}) = \int_{-\overline{\alpha}}^{\overline{\alpha}} w(\mathbf{x}, \mathbf{x}_\alpha)\Psi_n(\alpha)d\alpha. \tag{2.30}$$

The "cut-off" number N is chosen numerically. We discuss the choice of N in more details in Section 2.5. Following our approximate mathematical model introduced in Section 1, we assume that the approximation $\approx$ in (2.29) is an equality as well as

$$\partial_\alpha w(\mathbf{x}, \mathbf{x}_\alpha) = \sum_{n=1}^{N} w_n(\mathbf{x})\Psi_n'(\alpha). \tag{2.31}$$

Plugging (2.29) and (2.31) into (2.28) gives

$$\begin{aligned}
&\sum_{n=1}^{N} \partial_z w_n(\mathbf{x})\Psi_n'(\alpha) - \frac{\partial_{zz}u_0(\mathbf{x}, \mathbf{x}_\alpha)}{\partial_z u_0(\mathbf{x}, \mathbf{x}_\alpha)} \sum_{n=1}^{N} w_n(\mathbf{x})\Psi_n'(\alpha) \\
&\quad - \frac{\partial}{\partial\alpha}\left(\frac{\partial_{zz}u_0(\mathbf{x}, \mathbf{x}_\alpha)}{\partial_z u_0(\mathbf{x}, \mathbf{x}_\alpha)}\right) \sum_{n=1}^{N} w_n(\mathbf{x})\Psi_n(\alpha) + \sum_{i=1}^{d-1}\Big[\frac{\partial_{x_i}u_0(\mathbf{x}, \mathbf{x}_\alpha)}{\partial_z u_0(\mathbf{x}, \mathbf{x}_\alpha)} \sum_{n=1}^{N} \partial_{x_i} w_n(\mathbf{x})\Psi_n'(\alpha) \\
&+ \frac{\partial}{\partial\alpha}\left(\frac{\partial_{x_i}u_0(\mathbf{x}, \mathbf{x}_\alpha)}{\partial_z u_0(\mathbf{x}, \mathbf{x}_\alpha)}\right) \sum_{n=1}^{N} \partial_{x_i} w_n(\mathbf{x})\Psi_n(\alpha) - \frac{\partial_{zx_i}u_0(\mathbf{x}, \mathbf{x}_\alpha)\partial_{x_i}u_0(\mathbf{x}, \mathbf{x}_\alpha)}{(\partial_z u_0(\mathbf{x}, \mathbf{x}_\alpha))^2} \sum_{n=1}^{N} w_n(\mathbf{x})\Psi_n'(\alpha) \\
&\qquad - \frac{\partial}{\partial\alpha}\left(\frac{\partial_{zx_i}u_0(\mathbf{x}, \mathbf{x}_\alpha)\partial_{x_i}u_0(\mathbf{x}, \mathbf{x}_\alpha)}{(\partial_z u_0(\mathbf{x}, \mathbf{x}_\alpha))^2}\right) \sum_{n=1}^{N} w_n(\mathbf{x})\Psi_n(\alpha)\Big] = 0.
\end{aligned}$$

For each $m \in \{1, \ldots, N\}$, multiply the latter equation by $\Psi_m(\alpha)$ and then integrate the resulting equation with respect to α. We get

$$\sum_{n=1}^{N} s_{mn}\partial_z w_n(\mathbf{x}) + \sum_{n=1}^{N} a_{mn}(\mathbf{x})w_n(\mathbf{x}) + \sum_{n=1}^{N}\sum_{i=1}^{d-1} b_{mn,i}(\mathbf{x})\partial_{x_i} w_n(\mathbf{x}) = 0 \tag{2.32}$$

for all $\mathbf{x} \in \Omega$ where s_{mn} is defined as in Proposition 2.3.1,

$$a_{mn}(\mathbf{x}) = \int_{-\overline{\alpha}}^{\overline{\alpha}} \Bigg[-\frac{\partial_{zz} u_0(\mathbf{x}, \mathbf{x}_\alpha)}{\partial_z u_0(\mathbf{x}, \mathbf{x}_\alpha)} \Psi_n'(\alpha) - \frac{\partial}{\partial \alpha} \left(\frac{\partial_{zz} u_0(\mathbf{x}, \mathbf{x}_\alpha)}{\partial_z u_0(\mathbf{x}, \mathbf{x}_\alpha)} \right) \Psi_n(\alpha) - \sum_{i=1}^{d-1} \frac{\partial}{\partial \alpha} \left(\frac{\partial_{z x_i} u_0(\mathbf{x}, \mathbf{x}_\alpha) \partial_{x_i} u_0(\mathbf{x}, \mathbf{x}_\alpha)}{(\partial_z u_0(\mathbf{x}, \mathbf{x}_\alpha))^2} \right) \Psi_n'(\alpha) - \sum_{i=1}^{d-1} \frac{\partial}{\partial \alpha} \left(\frac{\partial_{z x_i} u_0(\mathbf{x}, \mathbf{x}_\alpha) \partial_{x_i} u_0(\mathbf{x}, \mathbf{x}_\alpha)}{(\partial_z u_0(\mathbf{x}, \mathbf{x}_\alpha))^2} \right) \Psi_n(\alpha) \Bigg] \Psi_m(\alpha) d\alpha \quad (2.33)$$

and for $i = 1, \ldots, d-1$

$$b_{mn,i}(\mathbf{x}) = \int_{-\overline{\alpha}}^{\overline{\alpha}} \Big[\frac{\partial_{x_i} u_0(\mathbf{x}, \mathbf{x}_\alpha)}{\partial_z u_0(\mathbf{x}, \mathbf{x}_\alpha)} \Psi_n'(\alpha) + \frac{\partial}{\partial \alpha} \left(\frac{\partial_{x_i} u_0(\mathbf{x}, \mathbf{x}_\alpha)}{\partial_z u_0(\mathbf{x}, \mathbf{x}_\alpha)} \right) \Psi_n(\alpha) \Big] \Psi_m(\alpha) d\alpha, \quad (2.34)$$

for all $\mathbf{x} \in \Omega$. For each $\mathbf{x} \in \Omega$, let $W(\mathbf{x}) = (w_1(\mathbf{x}), \ldots, w_N(\mathbf{x}))^T$, $S = (s_{mn})_{m,n=1}^N$, $A(\mathbf{x}) = (a_{mn}(\mathbf{x}))_{m,n=1}^N$ and $B_i(\mathbf{x}) = (b_{mn,i}(\mathbf{x}))_{m,n=1}^N$ for $i = 1, \ldots, d-1$. Since (2.32) holds true for every $m = 1, \ldots, N$, it can be rewritten as

$$S_N \partial_z W(\mathbf{x}) + A(\mathbf{x}) W(\mathbf{x}) + \sum_{i=1}^{d-1} B_i(\mathbf{x}) \partial_{x_i} W(\mathbf{x}) = 0. \quad (2.35)$$

Since S is invertible, see Proposition 2.3.1, then (2.35) implies the following system of transport equations

$$\partial_z W(\mathbf{x}) + S_N^{-1} A(\mathbf{x}) W(\mathbf{x}) + \sum_{i=1}^{d-1} S_N^{-1} B_i(\mathbf{x}) \partial_{x_i} W(\mathbf{x}) = 0, \quad \mathbf{x} \in \Omega. \quad (2.36)$$

The boundary data for W are:

$$W|_{\partial\Omega} = F(\mathbf{x}) = (f_n)_{n=1}^N, \quad f_n(\mathbf{x}) = \int_{-\overline{\alpha}}^{\overline{\alpha}} f(\mathbf{x}, \mathbf{x}_\alpha) \partial_z u_0(\mathbf{x}, \mathbf{x}_\alpha) \Psi_n(\alpha) d\alpha \quad (2.37)$$

where f is the given data, see (2.19).

Remark 2.3.1 (The approximation context) *Due to the truncation in* (2.29),

equation (2.36) *is within the framework of our approximate mathematical model mentioned in Introduction. Since this chapter is concerned with computational rather than theoretical results, then this model is acceptable. Our approximation leads to good numerical results in Section 2.5.*

Remark 2.3.2 *Problem 2.2.1 is reduced to the problem of finding the vector valued function W satisfying the system* (2.36) *and the boundary condition* (2.37)*. Assume this vector function is computed and denote it as $W^{\text{comp}} = (w_1^{\text{comp}}, \dots, w_n^{\text{comp}})$. Then, we can compute the function $w^{\text{comp}}(\mathbf{x}, \mathbf{x}_\alpha)$ and then the function $u^{\text{comp}}(\mathbf{x}, \mathbf{x}_\alpha)$ sequentially via* (2.29) *and* (2.22)*. The computed target function $p^{\text{comp}}(\mathbf{x})$ is given by* (2.20)*.*

We find an approximate solution of the boundary value problem (2.36)–(2.37) by the quasi-reversibility method. This means that we minimize the functional

$$J_\epsilon(W) = \int_\Omega \left| \partial_z W(\mathbf{x}) + \sum_{i=1}^{d-1} S_N^{-1} B_i(\mathbf{x}) \partial_{x_i} W(\mathbf{x}) + S_N^{-1} A(\mathbf{x}) W(\mathbf{x}) \right|^2 d\mathbf{x} + \epsilon \|W\|^2_{H^1(\Omega)^N} \quad (2.38)$$

on the set of vector functions $W \in H^1(\Omega)^N$ satisfying the boundary constraint (2.37). Here the space $H^1(\Omega)^N = \underbrace{H^1(\Omega) \times \cdots \times H^1(\Omega)}_{N}$ with the commonly defined norm. Similarly to [1], we analyze the functional $J_\epsilon(W)$ for the case when derivatives in (2.38) are written in finite differences.

2.4 The quasi-reversibility method in the finite differences

For brevity, we describe and analyze here the quasi-reversibility method in the case when $d = 2$. The arguments for higher dimensions can be done in the same manner.

In 2D, $\Omega = (-R, R) \times (a, b)$. We arrange an $N_x \times N_z$ grid of points on $\overline{\Omega}$

$$\mathcal{G} = \{(x_i, z_j) : x_i = -R + (i-1)h_x, z_j = a + (j-1)h_z, \\ i = 1, \ldots, N_x, j = 1, \ldots, N_z\}, \quad (2.39)$$

where $h_x \in [h_0, \beta_x)$ and $h_z \in (0, \beta_z)$ are grid step sizes in the x and z directions respectively and and $h_0, \beta_x, \beta_z > 0$ are certain numbers. Here, N_x and N_z are two positive integers. Let $\mathbf{h} = (h_x, h_z)$. We define the discrete set $\Omega^{\mathbf{h}}$ as the set of those points of the set (2.39) which are interior points of the rectangle Ω and $\partial\Omega^{\mathbf{h}}$ is the set of those points of the set (2.39) which are located on the boundary of Ω,

$$\Omega^{\mathbf{h}} = \{(x_i, z_j) : x_i = -R + (i-1)h_x, z_j = a + (j-1)h_z : \\ i = 2, \ldots, N_x - 1; j = 2, \ldots, N_z - 1\}$$
$$\partial\Omega^{\mathbf{h}} = \{(\pm R, z_j) : j = 1, ..., N_z\} \cup \{(x_i, z) : i = 1, ..., N_x, z \in \{a, b\}\},$$
$$\overline{\Omega}^{\mathbf{h}} = \Omega^{\mathbf{h}} \cup \partial\Omega^{\mathbf{h}}.$$

For any continuous function v defined on Ω its finite difference version is $v^{\mathbf{h}} = v|_{\mathcal{G}}$. Here, $\mathbf{h}$ denotes the pair (h_x, h_z). The partial derivatives of the function v are given via forward finite differences as

$$\begin{aligned} \partial_x^{h_x} v^{\mathbf{h}}(x_i, z_j) &= \frac{v^{\mathbf{h}}(x_{i+1}, z_j) - v^{\mathbf{h}}(x_i, z_j)}{h_x} \\ \partial_z^{h_z} v^{\mathbf{h}}(x_i, z_j) &= \frac{v(x_i, z_{j+1}) - v(x_i, z_j)}{h_z} \end{aligned} \quad (2.40)$$

for $i = 0, \ldots, N_x - 1$ and $j = 0, \ldots, N_z - 1$. We denote the finite difference analogs of the spaces $L^2(\Omega)$ and $H^1(\Omega)$ as $L^{2,\mathbf{h}}(\Omega)$ and $H^{1,\mathbf{h}}(\Omega)$. Norms in these spaces are

defined as

$$\|v^{\mathbf{h}}\|_{L^{2,\mathbf{h}}(\Omega^{\mathbf{h}})} = \Big[h_x h_z \sum_{i=0}^{N_x}\sum_{j=0}^{N_z}\big[v^{\mathbf{h}}(x_i,z_j)\big]^2\Big]^{1/2},$$

$$\|v^{\mathbf{h}}\|_{H^{1,\mathbf{h}}(\Omega^{\mathbf{h}})} = \Big[\|v^{\mathbf{h}}\|^2_{L^{2,\mathbf{h}}(\Omega^{\mathbf{h}})} + h_x h_z \sum_{i=0}^{N_x-1}\sum_{j=0}^{N_z-1}\big[\partial_x^{h_x} v^{\mathbf{h}}(x_i,z_j)\big]^2 + \big[\partial_z^{h_z} v^{\mathbf{h}}(x_i,z_j)\big]^2\Big]^{1/2}.$$

Let $F^{\mathbf{h}} = F\mid_{\partial\Omega^{\mathbf{h}}}$. The problem (2.36)–(2.37) becomes

$$L^h\left(W^{\mathbf{h}}\right) = \partial_z^{h_z} W^{\mathbf{h}}(x_i,z_j) + S_N^{-1} B_1(\mathbf{x}_i,z_j)\partial_x^{h_x} W^{\mathbf{h}}(x_i,z_j) + S_N^{-1} A(x_i,z_j) W^{\mathbf{h}}(x_i,z_j) = 0 \quad (2.41)$$

for $i = 0,...,N_x-1; j = 0,...,N_z-1$ and

$$W^{\mathbf{h}}\mid_{\partial\Omega^{\mathbf{h}}} = F^{\mathbf{h}}. \quad (2.42)$$

To solve problem (2.41)-(2.42) numerically, we introduce the finite difference version of the functional J_ϵ, defined in (2.38),

$$J_\epsilon^{\mathbf{h}}(W^{\mathbf{h}}) = h_x h_z \sum_{i=0}^{N_x-1}\sum_{j=0}^{N_z-1}\Big|\partial_z^{h_z} W^{\mathbf{h}}(x_i,z_j) + S_N^{-1} B_1(\mathbf{x}_i,z_j)\partial_x^{h_x} W^{\mathbf{h}}(z_i,z_j) + S_N^{-1} A(x_i,z_j) W^{\mathbf{h}}(x_i,z_j)\Big|^2 + \epsilon\|W^{\mathbf{h}}\|^2_{H_N^{1,\mathbf{h}}(\Omega^{\mathbf{h}})},$$

where $H_N^{1,\mathbf{h}}(\Omega^{\mathbf{h}}) = \big[H^{1,\mathbf{h}}(\Omega^{\mathbf{h}})\big]^N$ and similarly for $L_N^{2,\mathbf{h}}(\Omega^{\mathbf{h}})$. We consider the following problem:

Problem 2.4.1 (Minimization Problem) *Minimize the functional* $J_\epsilon^{\mathbf{h}}(W^{\mathbf{h}})$ *on the set of such vector functions* $W^{\mathbf{h}} \in H_N^{1,\mathbf{h}}(\Omega^{\mathbf{h}})$ *that satisfy boundary condition* (2.42)*.*

The convergence theory for this problem is formulated in Theorems 2.4.1 and 2.4.2.

Proofs of these theorems follow closely the arguments of [1, Section 5] and are, therefore, not repeated in this chapter. Theorem 2.4.1 guarantees the existence and uniqueness of the minimizer of $J_\epsilon^{\mathbf{h}}(W^{\mathbf{h}})$, and this result can be proven on the basis of Riesz theorem. The next natural although a more difficult question is about the convergence of regularized solutions (i.e. minimizers) to the exact one when the level of the noise in the data tends to zero, i.e. Theorem 2.4.2. As it is often the case in the quasi-reversibility method (see, e.g. [25]), a close analog of Theorem 2.4.2 is proven in [1, Section 5] via applying a new discrete Carleman estimate: recall that conventional Carleman estimates are in the continuous form. In other words, these two theorems confirm the effectiveness of our proposed numerical method for solving Problem 2.2.1.

Theorem 2.4.1 (existence and uniqueness of the minimizer) *For any* $\mathbf{h} = (h_x, h_z)$ *with* $h_x \in [h_0, \beta_x), h_z \in (0, \beta_z)$, *any* $\epsilon > 0$ *and for any matrix* $F^{\mathbf{h}}$ *of boundary conditions there exists unique minimizer* $W^{\mathbf{h}}_{\min,\epsilon} \in H_N^{1,\mathbf{h}}(\Omega^{\mathbf{h}})$ *of the functional satisfying boundary condition* (2.42).

As it is always the case in the regularization theory, assume now that there exists an "ideal" solution $W_*^{\mathbf{h}} \in H_N^{1,\mathbf{h}}(\Omega^{\mathbf{h}})$ of problem (2.41)-(2.42) satisfying the following boundary condition:

$$W_*^{\mathbf{h}} \mid_{\partial\Omega^{\mathbf{h}}} = F_*^{\mathbf{h}}, \tag{2.43}$$

where $F_*^{\mathbf{h}}$ is the "ideal" noiseless boundary data. Since $W_*^{\mathbf{h}}$ exists, then (2.43) implies that there exists an extension $G_*^{\mathbf{h}} \in H_N^{1,\mathbf{h}}(\Omega^{\mathbf{h}})$ with $G_*^{\mathbf{h}} \mid_{\partial\Omega^{\mathbf{h}}} = F_*^{\mathbf{h}}$ of the matrix $F_*^{\mathbf{h}}$ in $\Omega^{\mathbf{h}}$. As to the data $F^{\mathbf{h}}$ in (2.42), we assume now that there exists an extension $G^{\mathbf{h}} \in H_N^{1,\mathbf{h}}(\Omega^{\mathbf{h}})$ with $G^{\mathbf{h}} \mid_{\partial\Omega^{\mathbf{h}}} = F^{\mathbf{h}}$ of $F^{\mathbf{h}}$ in $\Omega^{\mathbf{h}}$. Let $\delta > 0$ be the level of the noise in $G^{\mathbf{h}}$, see Remark 5.1. We assume that

$$\left\| G^{\mathbf{h}} - G_*^{\mathbf{h}} \right\|_{H_N^{1,\mathbf{h}}(\Omega^{\mathbf{h}})} < B\delta, \tag{2.44}$$

where the constant $B > 0$ is indpendent on δ.

It is convenient to replace the above notation of the minimizer $W^{\mathbf{h}}_{\min,\epsilon}$ with $W^{\mathbf{h}}_{\min,\epsilon,\delta}$, thus, indicating its dependence on δ. In [1, Section 5], to prove a direct analog of Theorem 2.4.2 (formulated below), a new Carleman estimate for the finite difference operator $\partial_z^{h_z} v$ was proven first. The Carleman Weight Function of this estimate depends only on the discrete variable z. The value of this function at the point $z_j = a + (j-1)h_z$ is $e^{2\lambda(j-1)h_z}$, where $\lambda > 0$ is a parameter. This estimate is valid only if $\lambda h_z < 1$ (Lemma 4.7 of [1, Section 5]). The latter explains the condition of Theorem 2.4.2 imposed on the grid step size h_z in the $z-$direction.

We now explain why do we impose the condition that the grid step size h_x in the $x-$direction must be bounded from below as $h_x \geq h_0 = const. > 0$. Indeed, this bound guarantees that with a constant $C > 0$ independent on $\mathbf{h}$, we have $\left\|\partial_x^{h_x} W^{\mathbf{h}}\right\|_{L^{2,\mathbf{h}}(\Omega^{\mathbf{h}})} \leq C \left\|W^{\mathbf{h}}\right\|_{L^{2,\mathbf{h}}(\Omega^{\mathbf{h}})}$, which is exactly inequality (4.8) of [1, Section 4]. Note that proofs of convergence results in [1, Section 5] use the latter inequality quite essentially.

Theorem 2.4.2 (convergence of regularized solutions) *Let conditions* (2.43) *and* (2.44) *be valid. Let* $L^{\mathbf{h}}$ *be the operator in* (2.41). *Let* $W^{\mathbf{h}}_{\min,\epsilon,\delta} \in H^{1,\mathbf{h}}_N(\Omega^{\mathbf{h}})$ *be the minimizer of the functional* $J^{\mathbf{h}}_\epsilon(W^{\mathbf{h}})$ *with boundary condition* (2.42). *Then there exists a sufficiently small number* $\overline{h}_z > 0$ *depending only on* h_0, a, b, R, N, $L^{\mathbf{h}}$ *such that the following estimate is valid for all* $(h_x, h_z) \in [h_0, \beta_x) \times \left(0, \overline{h}_z\right)$ *and all* $\epsilon, \delta > 0$ *with a constant* $C > 0$ *independent on* ϵ, δ

$$\left\|W^{\mathbf{h}}_{\min,\epsilon,\delta} - W^{\mathbf{h}}_*\right\|_{L^{2,\mathbf{h}}_N(\Omega^{\mathbf{h}})} \leq C\left(\delta + \sqrt{\epsilon}\left\|W^{\mathbf{h}}_*\right\|_{H^{1,\mathbf{h}}_N(\Omega^{\mathbf{h}})}\right).$$

We also note that Lipschitz stability estimate for problem (2.41)-(2.42) is valid as a direct analog of Theorem 5.5 of [1, Section 5]. Therefore, uniqueness also takes place for problem (2.41)-(2.42).

2.5 Numerical Implementation

In this section, we solve Problem 2.2.1 in the 2D case. The domain Ω is

$$\Omega = (-1, 1) \times (1, 3). \tag{2.45}$$

The line of sources L_s is set to be $(-\overline{\alpha}, \overline{\alpha})$ with $\overline{\alpha} = 3$.

We solve the forward problem to compute the simulated data as follows. Given the background function $\mathbf{n}_0$, instead of solving the nonlinear Eikonal equation (2.12), we find $u_0(\mathbf{x}, \mathbf{x}_\alpha)$ using (2.9). To do this, we first find the geodesic line $\Gamma_0(\mathbf{x}, \mathbf{x}_\alpha)$ in (2.9) connecting points $\mathbf{x} \in \Omega$ and $\mathbf{x}_\alpha \in L_s$.We do the latter by using the 2D Fast Marching toolbox which is built in Matlab. Fast Marching is very similar to the Dijkstra algorithm to find the shortest paths on graphs. We refer the reader to [37] for more details about Fast Marching. Next, with this geodesic line $\Gamma_0(\mathbf{x}, \mathbf{x}_\alpha)$ in hand, we compute the function $u(\mathbf{x}, \mathbf{x}_\alpha)$ via (2.17). It is clear that this function u solves (2.16). The point $\mathbf{x}_\alpha$ above is chosen as $(\alpha_i, 0)$ where $\alpha_i = 2(i-1)\overline{\alpha}/N_\alpha$. We set in our computations $N_\alpha = 209$.

Remark 2.5.1 *Denote by $f^*(\mathbf{x}, \mathbf{x}_\alpha)$ the noiseless data $u(\mathbf{x}, \mathbf{x}_\alpha)$, $\mathbf{x} \in \partial\Omega$, $\mathbf{x}_\alpha \in L_s$. The corresponding noisy data at the noise level $\delta > 0$ are set as*

$$f^\delta(\mathbf{x}, \mathbf{x}_\alpha) = f^*(\mathbf{x}, \mathbf{x}_\alpha)(1 + \delta \text{rand}(\mathbf{x}, \mathbf{x}_\alpha)),\ \mathbf{x} \in \partial\Omega_\alpha^+, \mathbf{x}_\alpha \in L_s, \tag{2.46}$$

where rand *is the uniformly distributed function of random numbers taking values in the range $[-1, 1]$. Recall that by (2.19) $f^*(\mathbf{x}, \mathbf{x}_\alpha) = 0$ for $\mathbf{x} \in \partial\Omega_\alpha^-$. This noise generates noise in the boundary condition $F^{\mathbf{h}}$ in (2.42). Hence, using (2.43), we obtain $F^{\mathbf{h}} = F_*^{\mathbf{h}} + \sigma^{\mathbf{h}}$, where $\sigma^{\mathbf{h}}$ is generated by the noisy part of (2.46).*

The choice of appropriate values of parameters is always a difficult task. We have selected an appropriate cut-off number N in (2.29) by a trial and error procedure.

More precisely, we took Test 4 in subsection 2.5.2 with the noise level 5% as a reference test and have selected such a value of N, which gave us the best reconstruction result. We have selected $N = 35$ this way. Then we used the same $N = 35$ for all other tests.

2.5.1 Computing W^{comp}

We arrange the grid $\mathcal{G}$ in $\overline{\Omega}$ as in (2.39). For simplicity, we choose $N_{\mathbf{x}} = N_x = N_z$. The step size $h = h_x = h_z = 2R/(N_{\mathbf{x}} - 1)$. We observe numerically that the matrix S_N^{-1}, present in the definition of J_ϵ in (2.38), contains some large numbers. This causes some unwanted errors in computations. Therefore, using (2.35), we slightly modify the functional J_ϵ of (2.38) as:

$$I_\epsilon(W) = \int_\Omega |S_N \partial_z W(\mathbf{x}) + A(\mathbf{x})W(\mathbf{x}) + \sum_{i=1}^{d-1} B_i(\mathbf{x})\partial_{x_i} W(\mathbf{x})|^2 d\mathbf{x} \\ + \epsilon \|W\|^2_{H^1(\Omega)^N} + \epsilon \left(\|W_{xx}\|^2_{L^2(\Omega)^N} + \|W_{zz}\|^2_{L^2(\Omega)^N} \right). \quad (2.47)$$

We have numerically observed that the additional regularization term with the second derivatives in (2.47) is crucial. If this term is absent, then our numerical results do not meet our expectations; see, Figure 2.1g

Remark 2.5.2 *The above Theorems 2.4.1 and 2.4.2 are valid only for the case when the regularization term with the second derivatives is absent in* (2.47)*. We also recall that proofs of those theorems are presented in [1, Section 5]. We are not sure that those theorems can be extended to the case when the second derivatives are present in* (2.47)*. Thus, we have a discrepancy between the theory and computations. It is well known, however, that such discrepancies quite often occur in numerical studies of truly hard problems, such as e.g. the one of this publication.*

The procedure of computing $p(\mathbf{x})$ is summarized in Algorithm 1.

In all tests with all noise levels in the data, we use $\epsilon = 10^{-8}$. This value was chosen by a trial and error procedure. The finite difference version of the functional I_ϵ for

Algorithm 1 The procedure to solve Problem 2.2.1

1: Choose the cut-off number $N = 35$. Find $\{\Psi_n\}_{n=1}^N$.
2: Compute the boundary data of the vector-valued function $W(\mathbf{x})$.
3: Minimize the functional $I_\epsilon(W)$ subjected to the boundary condition (2.37) to obtain $W^{\text{comp}}(\mathbf{x})$, $\mathbf{x} \in \Omega$.
4: Set $w^{\text{comp}}(\mathbf{x}, \mathbf{x}_\alpha) = \sum_{n=1}^N w_n^{\text{comp}} \Psi_n(\alpha)$, $\mathbf{x} \in \Omega$, $\alpha \in [-\overline{\alpha}, \overline{\alpha}]$.
5: Set $u^{\text{comp}} = w^{\text{comp}}/\partial_z u_0$. Compute p^{comp} by the average of the left hand side of (2.21), namely

$$p^{\text{comp}} = \frac{1}{2\overline{\alpha}\sqrt{\mathbf{a}_0(\mathbf{x})}} \int_{-\overline{\alpha}}^{\overline{\alpha}} \Big[\partial_z u_0(\mathbf{x}, \mathbf{x}_\alpha) \partial_z u^{\text{comp}}(\mathbf{x}, \mathbf{x}_\alpha) + \sum_{i=1}^{d-1} \partial_{x_i} u_0(\mathbf{x}, \mathbf{x}_\alpha) \partial_{x_i} u^{\text{comp}}(\mathbf{x}, \mathbf{x}_\alpha) \Big] d\alpha. \quad (2.48)$$

$d = 2$ is

$$\begin{aligned} I_\epsilon^h(W) = h^2 \sum_{m=1}^N \sum_{i,j=1}^{N_{\mathbf{x}}-1} \Big| \sum_{n=1}^N \Big[& \frac{s_{mn}[w_n(x_i, z_{j+1}) - w_n(x_i, z_j)]}{h} \\ & + a_{mn}(x_i, z_j) w(x_i, y_j) + \frac{b_{mn}(x_i, z_j)(w(x_{i+1}, z_j) - w(x_i, z_j))}{h} \Big] \Big|^2 \\ + \epsilon h^2 \sum_{n=1}^N \sum_{i,j=0}^{N_{\mathbf{x}}} |w_n(x_i, z_j)|^2 + \epsilon h^2 \sum_{n=1}^N \sum_{i,j=0}^{N_{\mathbf{x}}-1} & \big[|\partial_x^h w_n(x_i, z_j)|^2 + |\partial_z^h w_n(x_i, z_j)|^2 \big] \\ + \epsilon h^2 \sum_{n=1}^N \sum_{i,j=1}^{N_{\mathbf{x}}-1} & |\partial_{xx} w_n(x_i, z_j)|^2 + \epsilon h^2 \sum_{n=1}^N \sum_{i,j=1}^{N_{\mathbf{x}}-1} |\partial_{zz}^h w_n(x_i, z_j)|^2, \end{aligned}$$

where a_{mn} and $b_{mn} = b_{mn,1}$ in (2.33) and (2.34) respectively. The partial derivatives ∂_x^h and ∂_z^h are as in (2.40). The second derivative in the finite difference method is understood as usual. We next line up the discrete vector-valued function $w_n(x_i, z_j)$, $1 \le i, j \le N_{\mathbf{x}}$, $1 \le n \le N$ as the vector $(\mathfrak{w}_{\mathfrak{i}})_{\mathfrak{i}=1}^{N_{\mathbf{x}}^2 N}$ with

$$\mathfrak{w}_{\mathfrak{i}} = w_n(x_i, z_j) \quad (2.49)$$

where

$$\mathfrak{i} = (i-1)N_x N + (j-1)N + n. \quad (2.50)$$

The functional I_ϵ^h in the "line up" version is

$$I_\epsilon^h(\mathfrak{w}) = h^2\Big[|\mathcal{L}\mathfrak{w}|^2 + \epsilon|D_x\mathfrak{w}|^2 + \epsilon|D_y\mathfrak{u}|^2 + \epsilon|L\mathfrak{w}|^2\Big]. \tag{2.51}$$

In (2.51),

1. $\mathcal{L}$ is the $N_{\mathbf{x}}^2N \times N_{\mathbf{x}}^2N$ matrix with entries given by

   (a) $(\mathcal{L})_{\mathfrak{ij}} = -s_{mn}/h + a_{mn}(x_i, z_j) - b_{mn}(x_i, y_j)/h$ for $\mathfrak{i} = (i-1)N_xN + (j-1)N + m$ and $\mathfrak{j} = (i-1)N_xN + (j-1)N + n$,

   (b) $(\mathcal{L})_{\mathfrak{ij}} = b_{mn}(x_i, z_j)/h$ for $\mathfrak{i} = (i-1)N_xN + (j-1)N + m$ and $\mathfrak{j} = (i+1-1)N_xN + (j-1)N + n$,

   (c) $(\mathcal{L})_{\mathfrak{ij}} = s_{mn}/h$ for $\mathfrak{i} = (i-1)N_xN + (j-1)N + m$ and $\mathfrak{j} = (i-1)N_xN + (j+1-1)N + n$,

   (d) the other entries of $\mathcal{L}$ are 0

   for $1 \le i, j \le N_{\mathbf{x}} - 1$ and $1 \le m, n \le N$;

2. D_x is the $N_{\mathbf{x}}^2N \times N_{\mathbf{x}}^2N$ matrix with entries are given by

   (a) $(D_x)_{\mathfrak{ii}} = -1/h$ for $\mathfrak{i} = (i-1)N_xN + (j-1)N + m$,

   (b) $(D_x)_{\mathfrak{ij}} = 1/h$ for $\mathfrak{i} = (i-1)N_xN + (j-1)N + m$ and $\mathfrak{j} = (i+1-1)N_xN + (j-1)N + m$,

   (c) the other entries of $\mathcal{L}$ are 0

   for $1 \le i, j \le N_{\mathbf{x}} - 1$ and $1 \le m \le N$;

3. D_y is the $N_{\mathbf{x}}^2N \times N_{\mathbf{x}}^2N$ matrix with entries are given by

   (a) $(D_y)_{\mathfrak{ii}} = -1/h$ for $\mathfrak{i} = (i-1)N_xN + (j-1)N + m$,

(b) $(D_y)_{\mathfrak{ij}} = 1/h$ for $\mathfrak{i} = (i-1)N_xN + (j-1)N + m$ and $\mathfrak{j} = (i-1)N_xN + (j+1-1)N + m$,

(c) the other entries of $\mathcal{L}$ are 0

for $1 \le i, j \le N_{\mathbf{x}} - 1$ and $1 \le m \le N$;

4. L is the $N_{\mathbf{x}}^2 N \times N_{\mathbf{x}}^2 N$ matrix with entries are given by

(a) $(L)_{\mathfrak{ii}} = -4/h^2$ for $\mathfrak{i} = (i-1)N_xN + (j-1)N + m$,

(b) $(L)_{\mathfrak{ij}} = -1/h^2$ for $\mathfrak{i} = (i-1)N_xN + (j-1)N + m$ and $\mathfrak{j} = (i \pm 1 - 1)N_xN + (j-1)N + m$,

(c) $(L)_{\mathfrak{ij}} = -1/h^2$ for $\mathfrak{i} = (i-1)N_xN + (j-1)N + m$ and $\mathfrak{j} = (i-1)N_xN + (j \pm 1 - 1)N + m$,

(d) the other entries of $\mathcal{L}$ are 0

for $2 \le i, j \le N_{\mathbf{x}} - 1$ and $1 \le m \le N$.

The minimizer $\mathfrak{w}$ of I_ϵ^h satisfies the equation

$$\mathcal{L}^T\mathcal{L} + \epsilon(\mathrm{Id} + D_x^T D_x + D_y^T D_y + L^T L)\mathfrak{w} = 0. \tag{2.52}$$

On the other hand, due to the constraint (2.37)

$$\mathcal{D}\mathfrak{w} = \mathfrak{f} \tag{2.53}$$

where $\mathcal{D}$ is a $N_{\mathbf{x}}^2 N \times N_{\mathbf{x}}^2 N$ matrix and $\mathfrak{f}$ is a $N_{\mathbf{x}}^2 N$ dimensional vector, both of which are defined below

1. $(\mathcal{D})_{\mathfrak{ii}} = 1$ for $\mathfrak{i} = (i-1)N_xN + (j-1)N + m$;

2. $(\mathfrak{f})_{\mathfrak{i}} = f_m(x_i, y_j)$ for $\mathfrak{i} = (i-1)N_xN + (j-1)N + m$;

3. the other entries of $\mathcal{L}$ and $\mathfrak{f}$ are 0

for $i \in \{1, N_{\mathbf{x}}\}$, $1 \leq j \leq N_{\mathbf{x}}$ or $2 \leq i \leq N_{\mathbf{x}} - 1$, $j \in \{1, N_{\mathbf{x}}\}$ and $1 \leq m \leq N$. Here, $(f_m)_{m=1}^N$ is in (2.37). Since the data might be noisy, we slightly modify the system constituted by (2.52) and (2.53) to a more stable version

$$\left(\begin{bmatrix} \mathcal{L} \\ \mathcal{D} \end{bmatrix}^T \begin{bmatrix} \mathcal{L} \\ \mathcal{D} \end{bmatrix} + \epsilon(\mathrm{Id} + D_x^T D_x + D_y^T D_y + L^T L) \right) \mathfrak{w} = \begin{bmatrix} 0 \\ \mathfrak{f} \end{bmatrix}. \tag{2.54}$$

Solving the system (2.54), we obtain $\mathfrak{w}^{\text{comp}}$. The values of components of vector valued function $W^{\text{comp}}(\mathbf{x})$ at grid points are computed as $w_n(x_i, z_j) = \mathfrak{w}_{\mathfrak{i}}$ for $\mathfrak{i} = (i-1)N_x N + (j-1)N + m$, $1 \leq i, j \leq N_{\mathbf{x}}$, $1 \leq m \leq N$, see (2.49).

We have presented the implementation of Step 3 in Algorithm 1. The other steps are straight forward.

Remark 2.5.3 *In Step 5 of Algorithm 1 when computing p^{comp} using* (2.48)*, which involves ∇u^{comp}, we smooth out u^{comp} by replacing the value of $u^{\text{comp}}(x, y, \alpha)$, $\alpha \in [-\overline{\alpha}, \overline{\alpha}]$ by the average of u^{comp} on the rectangle of 5×5 points around the point (x, y). We also apply the same smoothing technique to the function p^{comp}.*

2.5.2 Numerical Tests

We perform four (4) numerical tests in this chapter. When indicating dependence of any function below on x, z, we assume that $(x, z) \in \Omega$, where the domain Ω is defined in (2.45). In all our tests, the noise level δ is as in (2.46).

Remark 2.5.4 *In all our tests below the function a_0 is far away from the constant background function. Therefore, Problem 2.2.1 is not considered as a small perturbation of the problem of the inverse Radon transform with incomplete data, see [2]. Some functions a_0 in our tests might not be smooth in $\mathbb{R}^2$. Still, $a_0 \in C^1(\overline{\Omega})$ in Tests 2,3. Thus, the second derivatives of the corresponding function u_0 are well-defined*

in these two tests. Even though $a_0 \notin C^1(\overline{\Omega})$ in Test 1, numerically we have not experienced problems with second derivatives of the function u_0.

Test 1. The true source function p is given by

$$p^{\text{true}}(x,z) = \begin{cases} 8 & (x-0.5)^2 + (z-2)^2 < 0.24^2, \\ 5 & (x+0.5)^2 + (z-2)^2 < 0.22^2, \\ 0 & \text{otherwise.} \end{cases}$$

The background function $\mathbf{a}_0$ is

$$\mathbf{a}_0(x,z) = \begin{cases} 1 + 0.3(1-x^2)(z^2-2) & \text{if } z^2 - 2 > 0, \\ 1 & \text{otherwise.} \end{cases}$$

The numerical results of this test are displayed in Figure 2.1.

The support of p^{true} in Test 1 consists of two discs. The value of the function p in the right disc is higher than the value in the left disc. Our method detects both these inclusions very well, see Figures 2.1c–2.1f. There are some unwanted artifacts near $\partial\Omega$ where we measure the noisy data. The higher level of noisy data, the more artifacts are present. When the noise level $\delta = 5\%$, the computed maximal value of p^{comp} in the left inclusion is 4.97 (relative error 0.6%) and the computed maximal value of p^{comp} in the right inclusion is 7.79 (relative error 2.62%). When the noise level $\delta = 170\%$, the computed maximal value of p^{comp} in the left inclusion is 4.327 (relative error 13.46%) and the computed maximal value of p^{comp} in the right inclusion is 7.811 (relative error 2.36%).

To verify the necessity of the presence of the second derivatives in the regularization term of (2.47), we also conduct computations for Test 2.1 in the case when only the first derivatives are present in the regularization term of (2.47). The result for the case of 5% noise in the data is depicted on Figure 2.1g. Comparison with Figure 2.1c

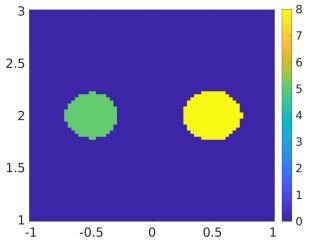

(a) The function p^{pictrue}

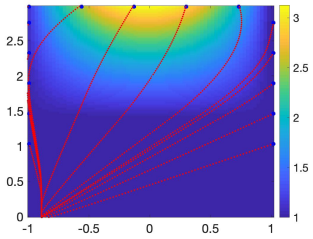

(b) The function $\mathbf{a}_0$ and some geodesic lines, generated by the Fast Marching package in Matlab

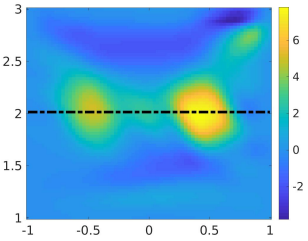

(c) The function p^{comp} computed by Algorithm 1 with 5% noise in the data

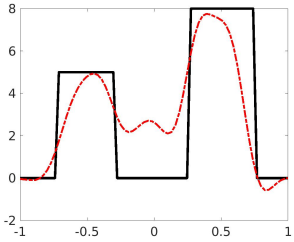

(d) The function p^{true} and p^{comp} with 5% noise in the data on the set $\{z = 2\}$, indicated by a dash-dot line in (c)

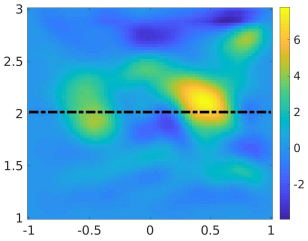

(e) The function p^{comp} computed by Algorithm 1 with 170% noise in the data

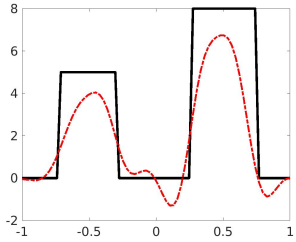

(f) The function p^{true} and p^{comp} with 170% noise in the data on the set $\{z = 2\}$, indicated by a dash-dot line in (e)

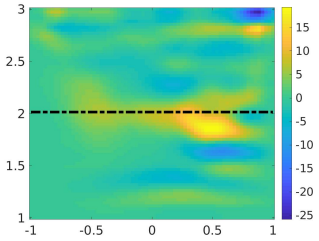

(g) The function p^{comp} in the case when second derivatives are absent in the regularization term of (2.47). 5% noise in the data. The image quality has significantly deteriorated, compared with (c).

Figure 2.1: Test 1. The true and reconstructed source functions using Algorithm 1 from noisy data.

makes it evident that the presence of the second derivatives in the regularization term of (2.47) is important.

Test 2. We test a complicated case when the support of p_{true} looks like a ring. In this test,

$$p^{\text{true}}(x,z) = \begin{cases} 2 & 0.55^2 < r^2 = x^2 + (z-2)^2 < 0.75^2, \\ 0 & \text{otherwise.} \end{cases}$$

The background function $\mathbf{a}_0$ is given by

$$\mathbf{a}_0(x,z) = \begin{cases} 1 + 0.25(x-0.5)^2 \ln(z) & z > 1, \\ 1 & \text{otherwise.} \end{cases}$$

The numerical results of this test are displayed in Figure 2.2.

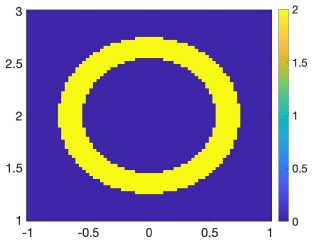

(a) The function p_{true}

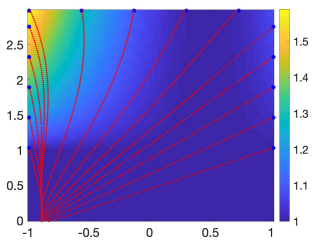

(b) The function $\mathbf{a}_0$ and some geodesic line, generated by the Fast Marching package in Matlab

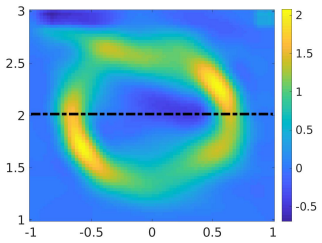

(c) The function p^{comp} computed by Algorithm 1 with 5% noise in the data

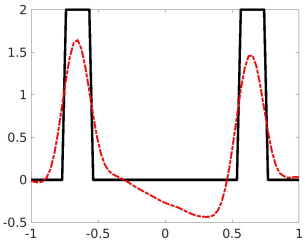

(d) The function p^{true} and p^{comp} with 5% noise in the data on the set $\{z = 2\}$, indicated by a dash-dot line in (c)

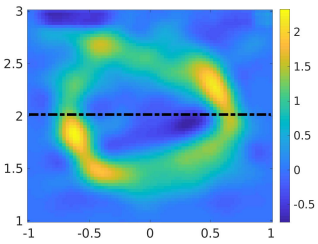

(e) The function p^{comp} computed by Algorithm 1 with 100% noise in the data

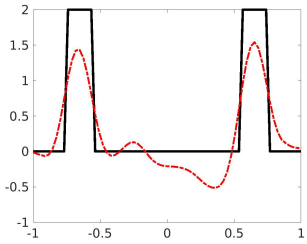

(f) The function p^{true} and p^{comp} with 100% noise in the data on the set $\{z = 2\}$, indicated by a dash-dot line in (e)

Figure 2.2: Test 2. The true and reconstructed source functions using Algorithm 1 from noisy data.

In this test, it is evident that the reconstructed “ring" is acceptable, see Figures

2.2c and 2.2e. The position of the ring is detected quite well, see Figures 2.2d and 2.2f. When the noise level is 5%, the reconstructed maximal value of p^{comp} in the ring is 2.078 (relative error 3.9%). When the noise level is 100%, the reconstructed maximal value of p^{comp} in the ring is 2.329 (relative error 16.45%).

Test 3. We test an interesting and complicated case of the up-side-down letter Y having both positive and negative values. In this test, the function p_{true} is given by

$$p^{\text{true}}(x,z) = \begin{cases} 2.5 & |x-(z-2)| < 0.35, \max\{|x|,|z-2|\} < 0.7, z < 2, x < 0, \\ -2.5 & |x+(z-2)| < 0.2, \max\{|x|,|z-2|\} < 0.7, z < 2, x > 0, \\ 2.5 & |x| < 0.2, \max\{|x|,|z-2|\} < 0.8, z > 2, x < 0, \\ -2.5 & |x| < 0.2, \max\{|x|,|z-2|\} < 0.8, z > 2, x > 0. \end{cases}$$

The background function $\mathbf{a}_0$ is given by

$$\mathbf{a}_0(x,z) = \begin{cases} 1 + 0.5(x+0.5)^2 \ln(z) & z > 1, \\ 1 & \text{otherwise.} \end{cases}$$

The numerical results of this test are displayed in Figure 2.3.

It is clear from Figure 2.3 that both positive and negative parts of the function $p(x,z)$ are successfully identified. When the noise level $\delta = 5\%$, the reconstructed maximal value of the positive part of p^{comp} is 2.186 (relative error 12.56%) and the reconstructed minimal value of p^{comp} of the negative part is -2.482 (relative error 0.72%.) When the noise level is $\delta = 100\%$, the reconstructed maximal value of p^{comp} of the positive part is 2.492 (relative error 0.32%) and the reconstructed minimal value of p^{comp} of the negative part is -3.327 (relative error 33.08%.)

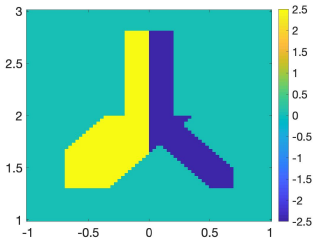

(a) The function p^{true}

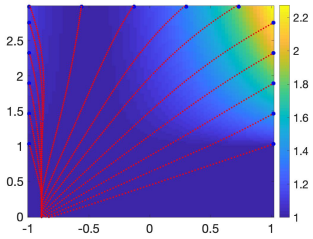

(b) The function $\mathbf{a}_0$ and some geodesic line, generated by the Fast Marching package in Matlab

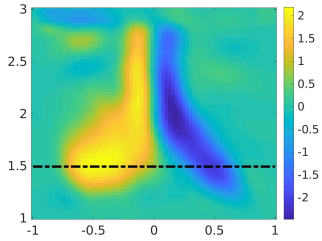

(c) The function p^{comp} computed by Algorithm 1 with 5% noise in the data

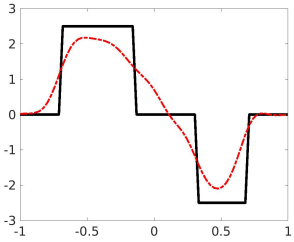

(d) The function p^{true} and p^{comp} with 5% noise in the data on the set $\{z = 1.5\}$, indicated by a dash-dot line in (c)

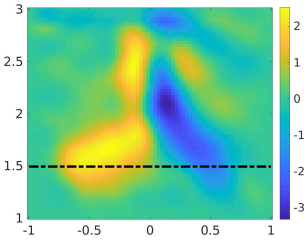

(e) The function p^{comp} computed by Algorithm 1 with 100% noise in the data

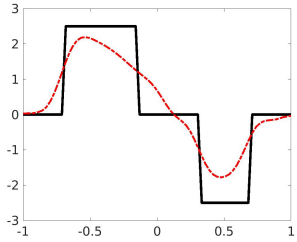

(f) The function p_{true} and p^{comp} with 100% noise in the data on the set $\{z = 1.5\}$, indicated by a dash-dot line in (e)

Figure 2.3: Test 3. The true and reconstructed source functions using Algorithm 1 from noisy data.

Test 4. In this test, we reconstruct the letter λ. The function p^{true} is given by

$$p^{\text{true}}(x,z) = \begin{cases} 2 & |x-(z-2)| < 0.325, \max\{|x|,|z-2|\} < 0.7 \text{ and } x < -0.03, \\ 2 & |x+(z-2)| < 0.2 \text{ and } \max\{|x|,|z-2|\} < 0.7, \\ 0 & \text{otherwise.} \end{cases}$$

In this test, we choose $\mathbf{a}_0$ as

$$\mathbf{a}_0(x,z) = \begin{cases} 1 + x^2 \ln(z) & z > 1, \\ 1 & \text{otherwise.} \end{cases}$$

The numerical results of this test are displayed in Figure 2.4.

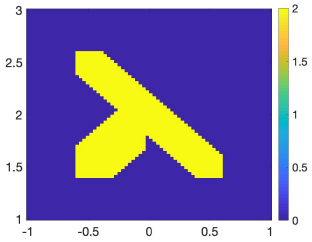

(a) The function p^{true}

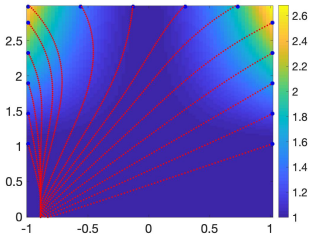

(b) The function $\mathbf{a}_0$ and some geodesic line, generated by the Fast Marching package in Matlab

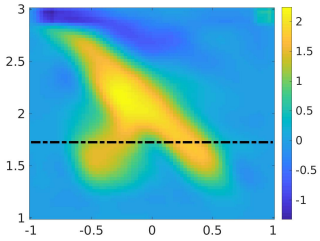

(c) The function p^{comp} by Algorithm 1 with 5% noise in the data

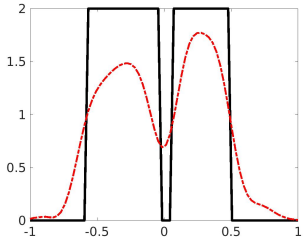

(d) The function p^{true} and p^{comp} with 5% noise in the data on the set $\{z = 1.7\}$, indicated by a dash-dot line in (c)

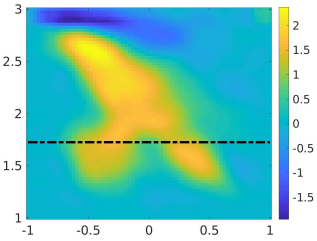

(e) The function p^{comp} computed by Algorithm 1 with 80% noise in the data

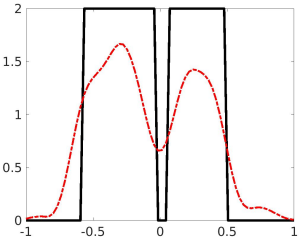

(f) The function p_{true} and p^{comp} with 80% noise in the data on the set $\{z = 1.7\}$, indicated by a dash-dot line in (e)

Figure 2.4: Test 4. The true and reconstructed source functions using Algorithm 1 from noisy data.

The letter λ and the values of the function p^{true} are successfully reconstructed. The computed position of λ is a quite accurate one, see Figures 2.4d and 2.4f. When the noise level $\delta = 5\%$, the computed maximal value of p^{comp} is 2.24 (relative error 12.0%). When the noise level $\delta = 80\%$, the computed maximal value of p^{comp} is 2.375 (relative error 18.75%).

2.6 Concluding Remarks

In this chapter, we have developed a convergent numerical method of the solution of the linearized Travel Time Tomography Problem with non-redundant incomplete data. A good accuracy of numerical results with 5% noise in the data is demonstrated for rather complicated functions to be imaged. It is quite surprising that an acceptable

accuracy of computational results is observed even for very high level of noise in the data varying between 80% and 170%.

REFERENCES

[1] A. V. Smirnov, M. V. Klibanov, and L. H. Nguyen, "On an inverse source problem for the full radiative transfer equation with incomplete data," *SIAM Journal on Scientific Computing*, vol. 41, pp. B929–B952, 2019.

[2] M. V. Klibanov and L. H. Nguyen, "PDE-based numerical method for a limited angle X-ray tomography," *Inverse Problems*, vol. 35, p. 045009, 2019.

[3] V. G. Romanov, *Inverse Problems of Mathematical Physics*. Utrecht: VNU Press, 1986.

[4] G. Herglotz, "Aœber die Elastizitaet der Erde bei Beruecksichtigung ihrer variablen Dichte," *Zeitschr. fur Math. Phys.*, vol. 52, pp. 275–299, 1905.

[5] E. Wiechert and J. Zoeppritz, "Uber Erdbebenwellen," *Nachr. Koenigl. Geselschaft Wiss. Gottingen*, vol. 4, pp. 415–549, 1907.

[6] M. V. Klibanov, L. H. Nguyen, and K. Pan, "Nanostructures imaging via numerical solution of a 3-d inverse scattering problem without the phase information," *Appl. Numer. Math.*, vol. 110, pp. 190–203, 2016.

[7] M. V. Klibanov and V. G. Romanov, "Reconstruction procedures for two inverse scattering problems without the phase information," *SIAM J. Applied Mathematics*, vol. 76, pp. 178–196, 2016.

[8] V. G. Romanov, "Problem of determining the permittivity in the stationary system of Maxwell equations," *Doklady Mathematics*, vol. 93, pp. 1–5, 2017.

[9] R. G. Mukhometov, "The reconstruction problem of a two-dimensional Riemannian metric and integral geometry," *Soviet Math. Dokl.*, vol. 18, pp. 32–35, 1977.

[10] I. N. Bernstein and M. L. Gerver, "On a problem of integral geometry for family of geodesics and the inverse kinematic problem of seismic," *Dokl. Akad. Nauk SSSR*, vol. 243, no. 302–305, 1978.

[11] L. Pestov and G. Uhlmann, "Two dimensional simple Riemannian manifolds are boundary distance rigid," *Annals of Mathematics*, vol. 161, pp. 1093–1110, 2005.

[12] R. G. Mukhometov and V. G. Romanov, "On the problem of determining an isotropic Riemannian metric in the n-dimensional space," *Dokl. Acad. Sci. USSR*, vol. 19, pp. 1330–1333, 1978.

[13] P. Stefanov, G. Uhlmann, and A. Vasy, "Local and global boundary rigidity and the geodesic X-ray transform in the normal gauge," *preprint arXiv: 1702.03638v2, 2017*, 2017.

[14] U. Schrőder and T. Schuster, "An iterative method to reconstruct the refractive index of a medium from time-off-light measurements," *Inverse Problems*, vol. 32, p. 085009, 2016.

[15] H. Zhao and Y. Zhong, "A hybrid adaptive phase space method for reflection travel time tomography," *SIAM J. Imaging Sci.*, vol. 12, pp. 28–53, 2019.

[16] M. V. Klibanov, "On the travel time tomography problem in 3D," *Journal of Inverse and Ill-posed Problems*, vol. 27, pp. 591–607, 2019.

[17] M. V. Klibanov, "Travel time tomography with formally determined incomplete data in 3D," *Inverse Problems and Imaging*, vol. 13, pp. 1367–1393, 2019.

[18] V. G. Romanov, "Integral geometry on isotropic riemannian metric," *Dokl. Akad. Nauk SSSR*, vol. 241, pp. 290–293, 1978.

[19] P. Stefanov, G. Uhlmann, and A. Vasy, "Inverting the local geodesic X-ray transform on tensors," *Journal d'Analyse Mathématique*, vol. 136, pp. 151–208, 2018.

[20] F. Monard, "Numerical implementation of geodesic X-ray transforms and their inversion," *SIAM J. Imaging Sci.*, vol. 7, pp. 1335–1357, 2014.

[21] R. Lattès and J. L. Lions, *The Method of Quasireversibility: Applications to Partial Differential Equations*. New York: Elsevier, 1969.

[22] L. Bourgeois and J. Dardé, "A duality-based method of quasi-reversibility to solve the Cauchy problem in the presence of noisy data," *Inverse Problems*, vol. 26, p. 095016, 2010.

[23] L. Bourgeois, D. Ponomarev, and J. Dardé, "An inverse obstacle problem for the wave equation in a finite time domain," *Inverse Probl. Imaging*, vol. 13, no. 2, pp. 377–400, 2019.

[24] V. Isakov, *Inverse Problems for Partial Differential Equations*. New York: Springer, third ed., 2017.

[25] M. V. Klibanov, "Carleman estimates for the regularization of ill-posed Cauchy problems," *Applied Numerical Mathematics*, vol. 94, pp. 46–74, 2015.

[26] Q. Li and L. H. Nguyen, "Recovering the initial condition of parabolic equations from lateral Cauchy data via the quasi-reversibility method," *Inverse Problems in Science and Engineering*, vol. 28, pp. 580–598, 2020.

[27] M. V. Klibanov, "Convexification of restricted Dirichlet to Neumann map," *J. Inverse and Ill-Posed Problems*, vol. 25, no. 5, pp. 669–685, 2017.

[28] V. A. Khoa, G. W. Bidney, M. V. Klibanov, L. H. Nguyen, L. Nguyen, A. Sullivan, and V. N. Astratov, "Convexification and experimental data for a 3D inverse scattering problem with the moving point source," *Inverse Problems*, vol. 36, p. 085007, 2020.

[29] M. V. Klibanov, A. E. Kolesov, L. Nguyen, and A. Sullivan, "A new version of the convexification method for a 1-D coefficient inverse problem with experimental data," *Inverse Problems*, vol. 34, p. 35005, 2018.

[30] M. V. Klibanov, J. Li, and W. Zhang, "Convexification of electrical impedance tomography with restricted Dirichlet-to-Neumann map data," *Inverse Problems*, vol. 35, p. 035005, 2019.

[31] T. T. Le and L. H. Nguyen, "A convergent numerical method to recover the initial condition of nonlinear parabolic equations from lateral cauchy data," *Journal of Inverse and Ill-posed Problems*, vol. 30, no. 2, pp. 265–286, 2022.

[32] J. Guillement and R. G. Novikov, "Inversion of weighted Radon transforms via finite Fourier series weight approximation," *Inverse Problems in Science and Engineering*, vol. 22, pp. 787–802, 2013.

[33] S. I. Kabanikhin, A. D. Satybaev, and M. A. Shishlenin, *Direct Methods of Solving Inverse Hyperbolic Problems*. Utrecht: VSP, 2005.

[34] S. I. Kabanikhin, K. K. Sabelfeld, N. S. Novikov, and M. A. Shishlenin, "Numerical solution of the multidimensional Gelfand-Levitan equation," *J. Inverse and Ill-Posed Problems*, vol. 23, pp. 439–450, 2015.

[35] B. N. Zakhariev and A. A. Suzko, *Potentials in Quantum Scattering. Direct and Inverse Problems*. Moskow: Energoatomizdat, 1985.

[36] L. Volgyesi and M. Moser, "The inner structure of the Earth," *Periodica Polytechnica Chemical Engineering*, vol. 26, pp. 155–204, 1982.

[37] J. A. Sethian, *Level Set Methods and Fast Marching Methods: Evolving Interfaces in Computational Geometry, Fluid Mechanics, Computer Vision, and Materials Science*. Cambridge Monograph on Applied and Computational Mathematics, Cambridge University Press, 1999.

CHAPTER 3: A CONVERGENT NUMERICAL METHOD TO RECOVER THE INITIAL CONDITION OF NONLINEAR PARABOLIC EQUATIONS FROM LATERAL CAUCHY DATA

3.1 Introduction

Let $d \geq 1$ be the spatial dimension and $T > 0$. Let $q : \mathbb{R} \to \mathbb{R}$ and $c : \mathbb{R}^d \to \mathbb{R}$ be two smooth functions in the class C^1. Assume that $c(\mathbf{x}) \geq c_0$ for some $c_0 > 0$. Consider the problem

$$\begin{cases} c(\mathbf{x})u_t(\mathbf{x},t) &= \Delta u(\mathbf{x},t) + q(u(\mathbf{x},t)) \quad \mathbf{x} \in \mathbb{R}^d, t \in (0,T) \\ u(\mathbf{x},0) &= p(\mathbf{x}) \qquad\qquad\qquad\qquad \mathbf{x} \in \mathbb{R}^d, \end{cases} \tag{3.1}$$

where p is a source function compactly supported in an open and bounded domain Ω of $\mathbb{R}^d$ with smooth boundary $\partial\Omega$. We briefly discuss the unique solvability and some regularity properties of (3.1). Assume that the initial condition of p is in $H^{2+\beta}(\mathbb{R}^d)$ for some $\beta \in [0, 1 + 4/d]$ and has compact support. Assume further that

$$|q(s)| \leq C(1 + |s|) \quad \text{for all } s \in \mathbb{R} \tag{3.2}$$

for some constant $C > 0$. Then (3.1) has a unique solution with $|u(\mathbf{x},t)| \leq M$ and $u \in H^{2+\beta,1+\beta/2}(\mathbb{R}^d \times [0,T])$ for some constant $M > 0$. These unique solvability and regularity properties can be obtained by applying Theorem 6.1 in [1, Chapter 5, §6] and Theorem 2.1 in [1, Chapter 5, §2].

We are interested in the following problem.

Problem 3.1.1 (Inverse Source Problem) *Assume that there is a number $M > 0$*

such that $|u(\mathbf{x},t)| \leq M$ *for all* $\mathbf{x} \in \overline{\Omega}$, $t \in [0,T]$. *Given the lateral Cauchy data*

$$f(\mathbf{x},t) = u(\mathbf{x},t) \quad \textit{and} \quad g(\mathbf{x},t) = \partial_\nu u(\mathbf{x},t) \tag{3.3}$$

for $\mathbf{x} \in \partial\Omega$, $t \in [0,T]$, *determine the function* $u(\mathbf{x},0) = p(\mathbf{x}), \mathbf{x} \in \Omega$.

Problem 3.1.1 arises from the problem of recovering the initial condition $p(\mathbf{x})$ of parabolic equation (3.1) from the lateral Cauchy data. It has many real-world applications, e.g., determination of the spatially distributed temperature inside a solid from the boundary measurement of the heat and heat flux in the time domain [2]; identification the pollution on the surface of the rivers or lakes [3]; effective monitoring the heat conduction processes in steel industries, glass and polymer-forming and nuclear power station [4]. When the nonlinear term $q(u)$ takes the form $u(1-u)$ (or $q(u) = u(1-|u|^\alpha)$) for some $\alpha > 0$, the parabolic equation in (3.1) is called the high dimensional version of the well-known Fisher (or Fisher-Kolmogorov) equation [5]. Although the nonlinearity q does not satisfy condition (3.2), we do not experience any difficulty in numerical computations of the forward problem. It is worth mentioning that the Fisher equation occurs in ecology, physiology, combustion, crystallization, plasma physics, and in general phase transition problems, see [5].

Due to its realistic applications, the problem of determining the initial conditions of parabolic equations has been studied intensively. However, up to the knowledge of the authors, numerical solutions are computed only in the case when the nonlinearity is absent, see e.g., [6]. The uniqueness of Problem 3.1.1 is well-known assuming that the nonlinearity q is in class C^1, see [7]. On the other hand, the logarithmic stability results were rigorously proved in [2, 4].

For completeness, we briefly recall the logarithmic stability of Problem 3.1.1 in this chapter. The natural approach to solve this problem is the optimal control method; that means, minimizing some mismatch functionals. However, since the

known stability is logarithmic [2, 4], the optimal control approach might not give good numerical results; especially, when the initial guess, if provided, is far away from the true solution. A more important reason for us to not use the optimal control method is that the cost functional is nonconvex and, therefore, might have multi-minima. We draw the reader's attention to the convexification methods, see [8, 9, 10, 11, 12, 13, 14, 15], which convexify the cost functional and therefore the difficulty about the lack of the initial guess is avoided. Applying the convexification method to numerically solve Problem 3.1.1 will be studied in the near future project. In this chapter, rather than working on the convexification method, similarly to [16, 17], of which the authors have successfully solved a coefficient inverse problem for a hyperbolic equation and an inverse source problem for a parabolic equation by combining the contraction principle and a new Carleman estimate, we propose a numerical method for Problem 3.1.1. The convergence of our method is proved based on the contraction principle using a new Carleman estimate. The latter is similar to the idea of [16, 18, 17].

As mentioned, since a good initial guess of the true solution of Problem 3.1.1 is not always available, the optimal control method, which is widely used in the scientific community, might not be applicable. To overcome this difficulty, we propose to solve Problem 3.1.1 in the Fourier domain. More precisely, we derive a system of elliptic PDEs whose solution consists of a finite number of the Fourier coefficients of the solution to the parabolic equation (3.1). The solution of this system directly yields the knowledge of the function $u(\mathbf{x}, t)$, from which the solution to our inverse problem follows. We numerically solve this nonlinear system by an iterative process. The initial solution can be computed by solving the system obtained by removing the nonlinear term. Then, we approximate the nonlinear system by replacing the nonlinearity with the one acting on the initial solution obtained in the previous step. Solving this approximation system, we find an updated solution. Continuing this process, we get a fast convergent sequence reaching to the desired function. The convergence of this

iterative procedure is rigorously proved by using a new Carleman estimate and the standard arguments of the contraction principle. The fast convergence will be shown in both analytic and numerical senses.

Two papers closely related to the current one are [17] and [6]. In [17], a source term for a nonlinear parabolic equation is computed, and in [6], the second author and his collaborator computed the initial condition of the linear parabolic equation from the lateral Cauchy data. On the other hand, the coefficient inverse problem for parabolic equations is also very interesting and studied intensively. We draw the reader's attention to [19, 20, 21, 22, 23, 24, 25] for important numerical methods and good numerical results. Besides, the problem of recovering the initial conditions for the hyperbolic equation is very interesting since it arises in many real-world applications. For instance, the problems of thermo- and photo-acoustic tomography play key roles in biomedical imaging. We refer the reader to some important works in this field [26, 27, 28]. Applying the Fourier transform, one can reduce the problem of reconstructing the initial conditions for hyperbolic equations to some inverse source problems for the Helmholtz equation, see [29, 30, 31, 32, 33] for some recent results.

The chapter is organized as follows. In Section 3.2, we derive a nonlinear system of elliptic PDEs, which leads to a numerical method to solve Problem 3.1.1.

This nonlinear system is solved by an iterative scheme. The proof of the convergence of this iteration is based on the contraction principle.

In Section 3.3, we establish and prove a Carleman estimate. This estimate plays an important role in the proof Theorem 3.2.1 that guarantees the existence and uniqueness of the least-squares solution to over-determined elliptic systems. In Section 3.4, we prove the convergence of the iterative sequence. In Section 3.5, we discuss the implementation of our method and show several numerical results. Section 3.6 is for concluding remarks.

3.2 A numerical method to solve Problem 3.1.1

The main aims of this section are to derive a system of nonlinear elliptic equations whose solutions directly yield the solutions to Problem 3.1.1 and then propose a method to solve it.

3.2.1 A system of nonlinear elliptic equations

Let $\{\Psi_n\}_{n\geq 1}$ be an orthonormal basis of $L^2(0,T)$. For each point $\mathbf{x} \in \Omega$, we can approximate $u(\mathbf{x},t)$, $t \in [0,T]$, as

$$u(\mathbf{x},t) = \sum_{n=1}^{\infty} u_n(\mathbf{x})\Psi_n(t) \simeq \sum_{n=1}^{N} u_n(\mathbf{x})\Psi_n(t) \tag{3.4}$$

where

$$u_n(\mathbf{x}) = \int_0^T u(\mathbf{x},t)\Psi_n(t)dt \quad n \geq 1. \tag{3.5}$$

Remark 3.2.1 *Replacing* $\simeq$ *in* (3.4) *by* " $=$ " *forms our approximate mathematical model. We cannot prove the convergence of the model as* $N \to \infty$*. Indeed, such a result is very hard to prove due to both the nonlinearity and the ill-posedness of our inverse problem. Therefore, our goal below is to find spatially dependent Fourier coefficients* u_n *defined in* (3.5)*. The number* N *should be chosen numerically. In fact, in Section 3.5, we verify that with appropriate values of* N*, the error causing from* (3.4) *is small, see also Figure 3.1*

Due to (3.4), the function $u_t(\mathbf{x},t)$ is approximated by

$$u_t(\mathbf{x},t) \simeq \sum_{n=1}^{N} u_n(\mathbf{x})\Psi_n'(t) \quad \mathbf{x} \in \Omega, t \in [0,T]. \tag{3.6}$$

From now on, we replace the approximation "$\simeq$" by equality. This obstacle will be considered numerically in Remark 3.5.1 and Figure 3.1. Plugging (3.4) and (3.6) into

the governing equation in (3.1), we obtain

$$c(\mathbf{x})\sum_{n=1}^{N} u_n(\mathbf{x})\Psi_n'(t) = \sum_{n=1}^{N} \Delta u_n(\mathbf{x})\Psi_n(t) + q\Big(\sum_{n=1}^{N} u_n(\mathbf{x})\Psi_n(t)\Big) \tag{3.7}$$

for all $\mathbf{x} \in \Omega$. For each $m = 1, \ldots, N$, multiply $\Psi_m(t)$ to both sides of (3.7) and then integrate the resulting equation with respect to t on $[0, T]$. For all $\mathbf{x} \in \Omega$, we have

$$\begin{aligned} c(\mathbf{x})\sum_{n=1}^{N} u_n(\mathbf{x}) \int_0^T \Psi_n'(t)\Psi_m(t)dt \\ = \sum_{n=1}^{N} \Delta u_n(\mathbf{x}) \int_0^T \Psi_n(t)\Psi_m(t)dt + \int_0^T q\Big(\sum_{n=1}^{N} u_n(\mathbf{x})\Psi_n(t)\Big)\Psi_m(t)dt. \end{aligned} \tag{3.8}$$

The system (3.8) with $m = 1, \ldots, N$ can be rewritten as

$$c(\mathbf{x})\sum_{n=1}^{N} s_{mn}u_n(\mathbf{x}) = \Delta u_m(\mathbf{x}) + q_m(u_1(\mathbf{x}), u_2(\mathbf{x}), \ldots, u_N(\mathbf{x})) \tag{3.9}$$

where

$$s_{mn} = \int_0^T \Psi_n'(t)\Psi_m(t)dt$$

and

$$q_m(u_1(\mathbf{x}), u_2(\mathbf{x}), \ldots, u_N(\mathbf{x})) = \int_0^T q\Big(\sum_{n=1}^{N} u_n(\mathbf{x})\Psi_n(t)\Big)\Psi_m(t)dt. \tag{3.10}$$

Due to (3.5), each function u_m, $m = 1, \ldots, N$, satisfies the Cauchy boundary conditions

$$\begin{cases} u_m(\mathbf{x}) &= f_m(\mathbf{x}) = \displaystyle\int_0^T f(\mathbf{x}, t)\Psi_m(t)dt \\ \partial_\nu u_m(\mathbf{x}) &= g_m(\mathbf{x}) = \displaystyle\int_0^T g(\mathbf{x}, t)\Psi_m(t)dt \end{cases} \tag{3.11}$$

for all $\mathbf{x} \in \partial\Omega$, $m = 1, \ldots, N$. Here, $f(\mathbf{x}, t)$ and $g(\mathbf{x}, t)$ are the given data.

Remark 3.2.2 *Problem 3.1.1 becomes the problem of finding all functions* $u_m(\mathbf{x})$, $\mathbf{x} \in \Omega$, $m = 1, \ldots, N$, *satisfying (3.9) and the Cauchy boundary conditions (3.11). In fact, if all of those functions are known, we can compute the function* $u(\mathbf{x}, t)$, $\mathbf{x} \in \Omega$, $t \in [0, T]$ *via (3.4). Then, the initial condition* $p(\mathbf{x})$ *is given by the function* $u(\mathbf{x}, 0)$.

Remark 3.2.3 *From now on, we consider the values of* $f_m(\mathbf{x})$ *and* $g_m(\mathbf{x})$ *on* $\partial\Omega$, $m = 1, \ldots, N$, *as the "indirect data", see (3.11). Denote by* $f_m^*(\mathbf{x})$ *and* $g_m^*(\mathbf{x})$ *the noiseless data. In numerical study, we set the noisy data as*

$$f_m^\delta = f_m^*(1 + \delta(-1 + 2\text{rand})) \quad g_m^\delta = g_m^*(1 + \delta(-1 + 2\text{rand}))$$

on $\partial\Omega$, $1 \leq m \leq N$ *where* $\delta > 0$ *is the noise level and* rand *is the function taking uniformly distributed random numbers in the range* $[0, 1]$. *In our numerical study,* $\delta = 20\%$.

3.2.2 An iterative procedure to solve the system (3.9)– (3.11)

We propose a procedure to compute $u_1(\mathbf{x}), \ldots, u_N(\mathbf{x})$. We first approximate (3.9)–(3.11) by solving the following over-determined problem

$$\begin{cases} c(\mathbf{x}) \sum_{n=1}^N s_{mn} u_n^{(0)}(\mathbf{x}) &= \Delta u_m^{(0)}(\mathbf{x}) \quad \mathbf{x} \in \Omega, \\ u_m^{(0)}(\mathbf{x}) &= f_m(\mathbf{x}) \qquad \mathbf{x} \in \partial\Omega, \qquad m = 1, 2, \ldots, N \\ \partial_\nu u_m^0(\mathbf{x}) &= g_m(\mathbf{x}) \qquad \mathbf{x} \in \partial\Omega \end{cases} \tag{3.12}$$

for a vector value function $(u_1^{(0)}, \ldots, u_N^{(0)})$. Then, assume by induction that we know $(u_1^{(k-1)}, \ldots, u_N^{(k-1)})$, $k \geq 1$, we find $(u_1^{(k)}, \ldots, u_N^{(k)})$ by solving

$$\begin{cases} c(\mathbf{x}) \sum_{n=1}^N s_{mn} u_n^{(k)}(\mathbf{x}) = \Delta u_m^{(k)}(\mathbf{x}) \\ \qquad\qquad + q_m[P(u_1^{(k-1)}(\mathbf{x})), \ldots, P(u_N^{(k-1)}(\mathbf{x}))] \quad \mathbf{x} \in \Omega, \\ u_m^{(k)}(\mathbf{x}) = f_m(\mathbf{x}) \qquad\qquad \mathbf{x} \in \partial\Omega, \\ \partial_\nu u_m^{(k)}(\mathbf{x}) = g_m(\mathbf{x}) \qquad\qquad \mathbf{x} \in \partial\Omega \end{cases} \tag{3.13}$$

where q_m is defined in (3.10) for $m = 1, 2, \ldots, N$. Here,

$$P(s) = \begin{cases} M\sqrt{T} & s \in (M\sqrt{T}, \infty), \\ s & s \in [-M\sqrt{T}, M\sqrt{T}], \\ -M\sqrt{T} & s \in (-\infty, -M\sqrt{T}] \end{cases} \quad \text{for all } s \in \mathbb{R}. \tag{3.14}$$

serves as a cut-off function. where $M > \|u^*\|_{L^\infty(\Omega\times[0,T])}$ is a fixed constant.

In practice since both Dirichlet and Neumann conditions are imposed, problem (3.12) and problem (3.13) might have no solution. However, since these two problems are linear, we can use the linear least-squares method to find the "best fit" solutions. In order to guarantee the convergence of the method, we include a Carleman weight function in the linear least-squares functional. Define the set of admissible solution

$$H = \{(u_m)_{m=1}^N \in H^2(\Omega)^N : u_m|_{\partial\Omega} = f_m \text{ and } \partial_\nu u_m|_{\partial\Omega} = g_m, 1 \le m \le N\}.$$

Throughout the chapter, we assume that the set H is nonempty. In the analysis, we will need the following subspace of $H^2(\Omega)^N$

$$H_0 = \left\{(v_1, \ldots, v_N) \in H^2(\Omega) : v_m(\mathbf{x}) = \partial_\nu v_m(\mathbf{x}) = 0\right\}. \tag{3.15}$$

Let $\mathbf{x}_0$ be a point in $\mathbb{R}^d \setminus \Omega$ with $\min\{r(\mathbf{x}) : \mathbf{x} \in \overline{\Omega}\} > 1$ and $b > \max\{r(\mathbf{x}) : \mathbf{x} \in \overline{\Omega}\}$ where

$$r(\mathbf{x}) = |\mathbf{x} - \mathbf{x}_0| \quad \text{for all } \mathbf{x} \in \mathbb{R}^d.$$

We choose $\mathbf{x}_0$ such that $\min\{r(\mathbf{x}) : \mathbf{x} \in \overline{\Omega}\} > 1$. To find $u^{(0)}$, we minimize the functional $J^{(0)} : H \to \mathbb{R}$ with

$$J^{(0)}(u_1, \ldots, u_N) = \sum_{m=1}^N \int_\Omega e^{2\lambda b^{-\beta} r^\beta(\mathbf{x})} \left| \Delta u_m - c(\mathbf{x}) \sum_{n=1}^N s_{mn} u_n \right|^2 d\mathbf{x} \tag{3.16}$$

where λ and β are the numbers as in Corollary 3.3.1. The obtained minimizer $(u_m^{(0)})_{m=1}^N \in H$ is called the regularized solution to (3.12). Next, assume, by induction, that we know $(u_m^{(k-1)})_{m=1}^N$, $k \geq 1$, we set $(u_m^{(k)})_{m=1}^N$ as the minimizer of $J^{(k)} : H \to \mathbb{R}$ defined as

$$J^{(k)}(u_1, \ldots, u_N) = \sum_{m=1}^{N} \int_\Omega e^{2\lambda b^{-\beta} r^\beta(\mathbf{x})} \Big| \Delta u_m - c(\mathbf{x}) \sum_{n=1}^{N} s_{mn} u_n + q_m(P(u_1^{(k-1)}), \ldots, P(u_N^{(k-1)})) \Big|^2 d\mathbf{x}. \quad (3.17)$$

Remark 3.2.4 *The function $e^{2\lambda b^{-\beta} r^\beta(\mathbf{x})}$ in* (3.16) *and* (3.17) *is called the Carleman weight function. Its presence is very helpful to prove the existence and uniqueness of the minimizers for the functionals $J^{(k)}$, $k \geq 0$, see Theorem 3.2.1. On the other hand, this Carleman weight function and the Carleman estimate (see Theorem 3.3.1) play important roles for us to prove the convergence of our method, see Theorem 3.4.1.*

The following result guarantees the existence and uniqueness of the minimizer of (3.12) and the one of (3.13), $k \geq 1$.

Theorem 3.2.1 *Assume that f_m and g_m are in $L^2(\partial\Omega)$, $m = 1, 2, \ldots, N$ and assume that H is nonempty. Then, each functional $J^{(k)}$, $k \geq 0$, has a unique minimizer provided that both λ and β are sufficiently large.*

Proof 3.2.1 *We only prove Theorem 3.2.1 when $k \geq 1$. Since H is nonempty, we can find a vector-valued function $(\varphi_m)_{m=1}^N \in H$. Define*

$$v_m(\mathbf{x}) = u_m(\mathbf{x}) - \varphi_m(\mathbf{x}) \quad \mathbf{x} \in \Omega, m = 1, \ldots, N. \quad (3.18)$$

We minimize

$$I^{(k)}(v_1, \ldots, v_N) = J^{(k)}(u_1 - \varphi_1, \ldots, u_N - \varphi_N)$$

where $(v_m)_{m=1}^N$ varies in H_0, defined in (3.15). If $(v_m)_{m=1}^N$ minimizes $I^{(k)}$, then by the

variational principle,

$$\sum_{m=1}^{N}\Big\langle e^{2\lambda b^{-\beta}r^{\beta}(\mathbf{x})}\Big(\Delta v_m - c(\mathbf{x})\sum_{n=1}^{N}s_{mn}v_n + \Delta\varphi_m - c(\mathbf{x})\sum_{n=1}^{N}s_{mn}\varphi_n$$
$$+q_m(P(u_1^{(k-1)}),\dots,P(u_N^{(k-1)}))\Big), \Delta h_m - c(\mathbf{x})\sum_{n=1}^{N}s_{mn}h_n\Big\rangle_{L^2(\Omega)} = 0 \qquad (3.19)$$

for all $(h_m)_{m=1}^N \in H_0$. *The identity (3.19) is equivalent to*

$$\sum_{m=1}^{N}\Big\langle e^{2\lambda b^{-\beta}r^{\beta}(\mathbf{x})}\Delta v_m - c(\mathbf{x})\sum_{n=1}^{N}s_{mn}v_n, \Delta h_m - c(\mathbf{x})\sum_{n=1}^{N}s_{mn}h_n\Big\rangle_{L^2(\Omega)}$$
$$= -\sum_{m=1}^{N}\Big\langle e^{2\lambda b^{-\beta}r^{\beta}(\mathbf{x})}\Big(\Delta\varphi_m - c(\mathbf{x})\sum_{n=1}^{N}s_{mn}\varphi_n + q_m(P(u_1^{(k-1)}),\dots,P(u_N^{(k-1)}))\Big),$$
$$\Delta h_m - c(\mathbf{x})\sum_{n=1}^{N}s_{mn}h_n\Big\rangle_{L^2(\Omega)}. \qquad (3.20)$$

The left hand side of (3.20) defines a bilinear form $\{\cdot,\cdot\}$ *of a pair* $((v_m)_{m=1}^N,(h_m)_{m=1}^N)$ *in* H_0.

We claim that $\{\cdot,\cdot\}$ *is coercive; that means,*

$$\{(v_m)_{m=1}^N,(v_m)_{m=1}^N\} \geq C\|(v_m)_{m=1}^N\|^2_{H^2(\Omega)^N}$$

for some constant C. *In fact, using the inequality* $(x-y)^2 \geq x^2/2 - y^2$, *we have*

$$\sum_{m=1}^{N}\int_\Omega e^{2\lambda b^{-\beta}r^{\beta}(\mathbf{x})}\Big|\Delta v_m - c(\mathbf{x})\sum_{n=1}^{N}s_{mn}v_n\Big|^2 d\mathbf{x} \geq \sum_{m=1}^{N}\int_\Omega e^{2\lambda b^{-\beta}r^{\beta}(\mathbf{x})}|\Delta v_m|^2 d\mathbf{x}$$
$$-\sum_{m=1}^{N}\int_\Omega e^{2\lambda b^{-\beta}r^{\beta}(\mathbf{x})}\Big|c(\mathbf{x})\sum_{n=1}^{N}s_{mn}v_n\Big|^2 d\mathbf{x}.$$

Applying the Carleman estimate (3.42), which will be proved in Section 3.3, for the

function v_m for each $m \in \{1, \dots, N\}$, we have

$$\sum_{m=1}^{N} \int_{\Omega} e^{2\lambda b^{-\beta} r^{\beta}(\mathbf{x})} \Big| \Delta v_m - c(\mathbf{x}) \sum_{n=1}^{N} s_{mn} v_n \Big|^2 d\mathbf{x}$$
$$\geq \sum_{m=1}^{N} \int_{\Omega} e^{2\lambda b^{-\beta} r^{\beta}(\mathbf{x})} \Big[\frac{C \sum_{i,j=1}^{d} |\partial^2_{x_i x_j} v_m|^2}{\lambda} + C\lambda |\nabla v_m|^2 + C\lambda^3 |v_m|^2 \Big] d\mathbf{x}$$
$$- \sum_{m=1}^{N} \int_{\Omega} e^{2\lambda b^{-\beta} r^{\beta}(\mathbf{x})} \Big| c(\mathbf{x}) \sum_{n=1}^{N} s_{mn} v_n \Big|^2 d\mathbf{x}.$$

Since $c(\mathbf{x})$ and s_{mn} are finite, we can choose λ sufficiently large such that

$$\sum_{m=1}^{N} \int_{\Omega} e^{2\lambda b^{-\beta} r^{\beta}(\mathbf{x})} \Big| \Delta v_m - c(\mathbf{x}) \sum_{n=1}^{N} s_{mn} v_n \Big|^2 d\mathbf{x}$$
$$\geq C \max_{\mathbf{x} \in \overline{\Omega}} \{ e^{2\lambda b^{-\beta} r^{\beta}(\mathbf{x})} \} \lambda^{-1} \sum_{m=1}^{N} \| (v_m)_l \|^2_{H^2(\Omega)}.$$

Applying the Lax-Milgram theorem, we can find a unique vector-valued function $(v_m)_{m=1}^N$ satisfying (3.20). The vector-valued function $(u_m)_{m=1}^N$ can be found via (3.18).

Denote by $\{(u_1^{(k)}, \dots, u_N^{(k)})\}$ the sequence of the minimize of $J^{(k)}$, $k \geq 0$. We claim that this sequence converges to the true solution of (3.9) and (3.11) in $L^2(\Omega)^N$ as $k \to \infty$. The proof of this fact is based on the contraction principle and the Carleman estimate in Section 3.3 plays an important role.

3.3 A new Carleman estimate

In this section, we establish a new Carleman estimate, which has been used to prove Theorem 3.2.1 that guarantees the unique existence of the functional $J^{(k)}$ in (3.17), $k \geq 1$. This estimate and its corollary, Corollary 3.3.1, play a crucial role in the proof of our main result, see Theorem 3.4.1 which guarantees the convergence of our numerical method.

Theorem 3.3.1 (Carleman estimate) *Let $\mathbf{x}_0$ be a point in $\mathbb{R}^d \backslash \overline{\Omega}$ such that $r(\mathbf{x}) =$*

$|\mathbf{x}-\mathbf{x}_0|>1$ for all $\mathbf{x}\in\Omega$. Let $b>\max_{\mathbf{x}\in\overline{\Omega}} r(\mathbf{x})$ be a fixed constant. There exist positive constants β_0 depending only on b, $\mathbf{x}_0$, Ω and d such that for all function $v\in C^2(\overline{\Omega})$ satisfying

$$v(\mathbf{x})=\partial_\nu v(\mathbf{x})=0 \quad \textit{for all } \mathbf{x}\in\partial\Omega,$$

the following estimate holds true

$$\begin{aligned}\int_\Omega e^{2\lambda b^{-\beta}r^\beta(\mathbf{x})}|\Delta v(\mathbf{x})|^2d\mathbf{x} \geq \frac{C}{\lambda\beta^{7/4}b^{-\beta}}\sum_{i,j=1}^{d}\int_\Omega e^{2\lambda b^{-\beta}r^\beta(\mathbf{x})}r^{2\beta}(\mathbf{x})|\partial^2_{x_ix_j}v(\mathbf{x})|^2d\mathbf{x}\\ +C\lambda^3\beta^4b^{-3\beta}\int_\Omega r^{2\beta}(\mathbf{x})e^{2\lambda b^{-\beta}r^\beta}|v(\mathbf{x})|^2d\mathbf{x}\\ +C\lambda\beta^{1/2}b^{-\beta}\int_\Omega e^{2\lambda b^{-\beta}r^\beta(\mathbf{x})}|\nabla v(\mathbf{x})|^2d\mathbf{x} \quad (3.21)\end{aligned}$$

for $\beta\geq\beta_0$ and $\lambda\geq\lambda_0$. Here, $\lambda_0=\lambda_0(b,\Omega,d,\mathbf{x}_0)>1$ is a positive number with $\lambda_0 b^{-\beta}\gg 1$ and $C=C(b,\Omega,d,\mathbf{x}_0)>1$ is a constant. These numbers depend only on the listed parameters.

Remark 3.3.1 *The Carleman estimate in Theorem 3.3.1 is more complicated than the version in [29]. The reason for us to establish this new estimate is that the Carleman weight function in [29] decays fast when $\lambda\gg 1$, causing poor numerical results. Unlike this, the Carleman estimate in Theorem 3.3.1 allows us to choose large λ in implementation, making the theory and the computational codes more consistent.*

Remark 3.3.2 *A new feature in Theorem 3.3.1 is the presence of all second derivatives of the function v on the right-hand side of* (3.21)*. This makes it more convenient for us to prove the existence and uniqueness of the regularized solutions to a system of nonlinear elliptic equations appearing in our analysis in Section 3.2, see Theorem 3.2.1.*

We split the proof of Theorem 3.3.1 into four lemmas, Lemma 3.3.1–Lemma 3.3.4.

Lemma 3.3.1 *Let v be the function as in Theorem 3.3.1. There exists a positive constant β_0 depending only on b, $\mathbf{x}_0$, Ω and d such that*

$$\int_\Omega \frac{e^{2\lambda b^{-\beta} r^\beta(\mathbf{x})}|\Delta v(\mathbf{x})|^2}{4\lambda\beta b^{-\beta} r^{\beta-2}(\mathbf{x})} d\mathbf{x} \geq C\lambda^2\beta^3 b^{-2\beta} \int_\Omega r^{2\beta}(\mathbf{x}) e^{2\lambda b^{-\beta} r^\beta(\mathbf{x})}|v(\mathbf{x})|^2 d\mathbf{x} - C\int_\Omega e^{2\lambda b^{-\beta} r^\beta(\mathbf{x})}|\nabla v(\mathbf{x})|^2 d\mathbf{x} \quad (3.22)$$

for all $\beta \geq \beta_0$ and $\lambda \geq \lambda_0$. Here, λ_0 is a constant such that $\lambda_0 b^{-\beta} \gg 1$.

Proof 3.3.1 *By changing variables, if necessary, we can assume that $\mathbf{x}_0 = 0$. Define the function*

$$w(\mathbf{x}) = e^{\lambda b^{-\beta} r^\beta(\mathbf{x})} v(\mathbf{x}) \quad \text{or} \quad v(\mathbf{x}) = e^{-\lambda b^{-\beta} r^\beta(\mathbf{x})} w(\mathbf{x}) \quad (3.23)$$

for all $\mathbf{x} \in \Omega$. Since v vanishes on $\partial\Omega$, so does w. On the other hand, by the product rule in differentiation, for all $\mathbf{x} \in \Omega$,

$$\nabla v(\mathbf{x}) = e^{-\lambda b^{-\beta} r^\beta(\mathbf{x})} \nabla w(\mathbf{x}) - \beta\lambda b^{-\beta} r^{\beta-2}(\mathbf{x}) e^{-\lambda b^{-\beta} r^\beta(\mathbf{x})} w(\mathbf{x})\mathbf{x} \quad (3.24)$$

It follows that

$$e^{-\lambda b^{-\beta} r^\beta(\mathbf{x})} \nabla w(\mathbf{x}) \cdot \nu = \nabla v(\mathbf{x}) \cdot \nu + \beta\lambda b^{-\beta} r^{\beta-2}(\mathbf{x}) e^{-\lambda b^{-\beta} r^\beta(\mathbf{x})} w(\mathbf{x})\mathbf{x} = 0.$$

for all $\mathbf{x} \in \partial\Omega$. We thus obtain $w(\mathbf{x}) = \partial_\nu w(\mathbf{x}) = 0$ for all $\mathbf{x} \in \partial\Omega$. Hence, from now on, whenever we apply the integration by parts formula on v and w, the integrals on $\partial\Omega$ vanishes. We next compute the Laplacian of v in terms of w. For all $\mathbf{x} \in \Omega$,

$$\begin{aligned}
\Delta v(\mathbf{x}) &= e^{-\lambda b^{-\beta} r^\beta(\mathbf{x})} \Delta w(\mathbf{x}) + 2\nabla e^{-\lambda b^{-\beta} r^\beta(\mathbf{x})} \cdot \nabla w(\mathbf{x}) + w(\mathbf{x}) \Delta(e^{-\lambda b^{-\beta} r^\beta(\mathbf{x})}) \\
&= e^{-\lambda b^{-\beta} r^\beta(\mathbf{x})} \Big[\Delta w(\mathbf{x}) - 2\lambda\beta b^{-\beta} r^{\beta-2}(\mathbf{x}) \nabla w(\mathbf{x}) \cdot \mathbf{x} \\
&\qquad + e^{\lambda b^{-\beta} r^\beta(\mathbf{x})} \Delta(e^{-\lambda b^{-\beta} r^\beta(\mathbf{x})}) w(\mathbf{x}) \Big].
\end{aligned}$$

Using the inequality $(a-b+c)^2 \geq -2ab-2bc$, *we have*

$$|\Delta v(\mathbf{x})|^2 \geq -4\lambda\beta b^{-\beta} r^{\beta-2}(\mathbf{x}) e^{-2\lambda b^{-\beta} r^{\beta}(\mathbf{x})} \Big[\Delta w(\mathbf{x}) \nabla w(\mathbf{x}) \cdot \mathbf{x} + e^{\lambda b^{-\beta} r^{\beta}(\mathbf{x})} \Delta(e^{-\lambda b^{-\beta} r^{\beta}(\mathbf{x})}) w(\mathbf{x}) \nabla w(\mathbf{x}) \cdot \mathbf{x}\Big] \quad (3.25)$$

for all $\mathbf{x} \in \Omega$. *By a straight forward computation, for* $\mathbf{x} \in \Omega$,

$$\Delta(e^{-\lambda b^{-\beta} r^{\beta}(\mathbf{x})}) = -\lambda\beta b^{-\beta} e^{-\lambda b^{-\beta} r^{\beta}(\mathbf{x})} r^{\beta-2}(\mathbf{x}) \big[(\beta - 2 + d) - \lambda b^{-\beta} \beta r^{\beta}(\mathbf{x})\big].$$

Plugging this into (3.25) gives

$$|\Delta v(\mathbf{x})|^2 \geq -4\lambda\beta b^{-\beta} r^{\beta-2}(\mathbf{x}) e^{-2\lambda b^{-\beta} r^{\beta}(\mathbf{x})} \Big[\Delta w(\mathbf{x}) \nabla w(\mathbf{x}) \cdot \mathbf{x} - \lambda\beta b^{-\beta} r^{\beta-2}(\mathbf{x}) \big[(\beta - 2 + d) - \lambda\beta b^{-\beta} r^{\beta}(\mathbf{x})\big] w(\mathbf{x}) \nabla w(\mathbf{x}) \cdot \mathbf{x}\Big]$$

for all $\mathbf{x} \in \Omega$. *Hence,*

$$\int_{\Omega} \frac{e^{2\lambda b^{-\beta} r^{\beta}(\mathbf{x})} |\Delta v(\mathbf{x})|^2}{4\lambda\beta b^{-\beta} r^{\beta-2}(\mathbf{x})} d\mathbf{x} \geq I_1 + I_2 + I_3 \quad (3.26)$$

where

$$I_1 = -\int_{\Omega} \Delta w(\mathbf{x}) \nabla w(\mathbf{x}) \cdot \mathbf{x} d\mathbf{x}, \quad (3.27)$$

$$I_2 = \lambda\beta b^{-\beta} (\beta - 2 + d) \int_{\Omega} r^{\beta-2}(\mathbf{x}) w(\mathbf{x}) \nabla w(\mathbf{x}) \cdot \mathbf{x} d\mathbf{x}, \quad (3.28)$$

$$I_3 = -\lambda^2 b^{-2\beta} \beta^2 \int_{\Omega} r^{2\beta-2}(\mathbf{x}) w(\mathbf{x}) \nabla w(\mathbf{x}) \cdot \mathbf{x} d\mathbf{x}. \quad (3.29)$$

Estimate I_1**.** *Write* $\mathbf{x} = (x_1, \ldots, x_d)$ *and integrating* I_1 *by parts. It follows from*

(3.27) that I_1 is equal to

$$\begin{aligned}
&\int_\Omega \nabla w(\mathbf{x}) \cdot \nabla[\nabla w(\mathbf{x}) \cdot \mathbf{x}] d\mathbf{x} \\
&\qquad = \sum_{i,j=1}^{d} \int_\Omega \partial_{x_i} w(\mathbf{x}) \partial_{x_i} x_j \partial_{x_j} w(\mathbf{x})) d\mathbf{x} \\
&\qquad = \sum_{i,j=1}^{d} \int_\Omega \partial_{x_i} w(\mathbf{x}) [\partial_{x_j} w(\mathbf{x}) \delta_{ij} + x_j \partial_{x_i x_j} w(\mathbf{x})] d\mathbf{x} \\
&\qquad = \sum_{i=1}^{d} \int_\Omega |\partial_{x_i} w(\mathbf{x})|^2 d\mathbf{x} + \sum_{i,j=1}^{d} \int_\Omega x_j \partial_{x_i} w(\mathbf{x}) \partial_{x_j x_i} w(\mathbf{x}) d\mathbf{x}.
\end{aligned}$$

Using the identity $\phi(\mathbf{x})\partial_{x_j}\phi(\mathbf{x}) = \frac{1}{2}\partial_{x_j}(\phi(\mathbf{x})^2)$ with $\Phi(\mathbf{x}) = \partial_{x_i} w(\mathbf{x})$ gives

$$\begin{aligned}
I_1 &= \int_\Omega |\nabla w(\mathbf{x})|^2 d\mathbf{x} + \frac{1}{2} \sum_{i,j=1}^{d} \int_\Omega x_j \partial_{x_j} (\partial_{x_i} w(\mathbf{x}))^2 d\mathbf{x} \\
&= \int_\Omega |\nabla w(\mathbf{x})|^2 d\mathbf{x} - \frac{1}{2} \sum_{i,j=1}^{d} \int_\Omega (\partial_{x_i} w(\mathbf{x}))^2 \partial_{x_j} x_j d\mathbf{x}.
\end{aligned}$$

Hence,

$$I_1 = \left(1 - \frac{d}{2}\right) \int_\Omega |\nabla w(\mathbf{x})|^2 d\mathbf{x}. \tag{3.30}$$

Estimate I_2. *We apply the identity $w\nabla w = \frac{1}{2}\nabla |w|^2$ to get from (3.28)*

$$\begin{aligned}
I_2 &= \frac{\lambda \beta b^{-\beta} (\beta - 2 + d)}{2} \int_\Omega r^{\beta-2}(\mathbf{x}) \nabla |w(\mathbf{x})|^2 \cdot \mathbf{x} d\mathbf{x} \\
&= -\frac{\lambda \beta b^{-\beta} (\beta - 2 + d)}{2} \int_\Omega |w(\mathbf{x})|^2 \mathrm{div}(r^{\beta-2}(\mathbf{x})\mathbf{x}) d\mathbf{x}.
\end{aligned}$$

Here, the integration by parts formula was used. We; therefore, obtain

$$I_2 = -\frac{\lambda \beta b^{-\beta} (\beta - 2 + d)^2}{2} \int_\Omega |w(\mathbf{x})|^2 d\mathbf{x}. \tag{3.31}$$

Estimate I_3. *Using integration by parts formula again, by (3.29),*

$$\begin{aligned} I_3 &= -\frac{\lambda^2\beta^2 b^{-2\beta}}{2}\int_\Omega r^{2\beta-2}(\mathbf{x})\nabla|w(\mathbf{x})|^2\cdot\mathbf{x}d\mathbf{x} \\ &= \frac{\lambda^2\beta^2 b^{-2\beta}}{2}\int_\Omega |w(\mathbf{x})|^2 \mathrm{div}[r^{2\beta-2}(\mathbf{x})\mathbf{x}]d\mathbf{x}. \end{aligned}$$

Hence,

$$\begin{aligned} I_3 &= \frac{\lambda^2\beta^2(2\beta-2+d)b^{-2\beta}}{2}\int_\Omega |w(\mathbf{x})|^2 r^{2\beta-2}(\mathbf{x})d\mathbf{x} \\ &\geq C\lambda^2\beta^3 b^{-2\beta}\int_\Omega r^{2\beta}(\mathbf{x})|w(\mathbf{x})|^2 d\mathbf{x}. \end{aligned} \tag{3.32}$$

Combining (3.26), (3.30), (3.31) and (3.32) and using the fact that $\lambda_0 b^{-\beta} \gg 1$ *(which implies* $\lambda b^{-\beta} \gg 1$*), we get*

$$\begin{aligned} &\int_\Omega \frac{e^{2\lambda b^{-\beta}r^\beta(\mathbf{x})}|\Delta v(\mathbf{x})|^2}{4\lambda\beta b^{-\beta}r^{\beta-2}(\mathbf{x})}d\mathbf{x} \\ &\qquad\geq C\lambda^2\beta^3 b^{-2\beta}\int_\Omega r^{2\beta}(\mathbf{x})|w(\mathbf{x})|^2 d\mathbf{x} - C\int_\Omega |\nabla w(\mathbf{x})|^2 d\mathbf{x}. \end{aligned} \tag{3.33}$$

Recall (3.23) that $w = e^{\lambda b^{-\beta}r^\beta}v$. *We have for all* $\mathbf{x}\in\Omega$,

$$\nabla w(\mathbf{x}) = e^{\lambda b^{-\beta}r^\beta(\mathbf{x})}[\nabla v(\mathbf{x}) + \lambda b^{-\beta}\beta r^{\beta-2}(\mathbf{x})v(\mathbf{x})\mathbf{x}]. \tag{3.34}$$

It follows from (3.23), (3.33), (3.34), the triangle inequality and the fact $\beta^3 \gg \beta^2$ *that*

$$\begin{aligned} \int_\Omega \frac{e^{2\lambda b^{-\beta}r^\beta(\mathbf{x})}|\Delta v(\mathbf{x})|^2}{4\lambda\beta b^{-\beta}r^{\beta-2}(\mathbf{x})}d\mathbf{x} &\geq C\lambda^2\beta^3 b^{-2\beta}\int_\Omega r^{2\beta}(\mathbf{x})e^{2\lambda b^{-\beta}r^\beta(\mathbf{x})}|v(\mathbf{x})|^2 d\mathbf{x} \\ &\quad - C\int_\Omega e^{2\lambda b^{-\beta}r^\beta(\mathbf{x})}|\nabla v(\mathbf{x})|^2 d\mathbf{x}. \end{aligned}$$

Recall that $\rho = \max_{\mathbf{x}\in\overline{\Omega}} r(x)$. *We have obtained the desired inequality (3.22).*

Lemma 3.3.2 *Let v be the function that satisfies all hypotheses of Theorem 3.3.1. There exist positive constants β_0 and λ_0 depending only on b, $\mathbf{x}_0$, Ω and d such that*

$$-\int_\Omega e^{2\lambda b^{-\beta} r^\beta(\mathbf{x})} v(\mathbf{x}) \Delta v(\mathbf{x}) d\mathbf{x} \geq C \int_\Omega e^{2\lambda b^{-\beta} r^\beta(\mathbf{x})} |\nabla v(\mathbf{x})|^2 d\mathbf{x} - C\lambda^2 \beta^2 b^{-2\beta} \int_\Omega e^{2\lambda b^{-\beta} r^{2\beta}(\mathbf{x})} r^{2\beta}(\mathbf{x}) |v(\mathbf{x})|^2 d\mathbf{x} \quad (3.35)$$

for all $\beta \geq \beta_0$ and $\lambda \geq \lambda_0$.

Proof 3.3.2 *By integrating by parts, we have*

$$\begin{aligned} &\int_\Omega e^{2\lambda b^{-\beta} r^\beta(\mathbf{x})} v(\mathbf{x}) \Delta v(\mathbf{x}) d\mathbf{x} \\ &\quad = \int_\Omega \nabla v(\mathbf{x}) \cdot \nabla \big(e^{2\lambda b^{-\beta} r^\beta(\mathbf{x})} v(\mathbf{x}) \big) d\mathbf{x} \\ &\quad = \int_\Omega e^{2\lambda b^{-\beta} r^\beta(\mathbf{x})} |\nabla v(\mathbf{x})|^2 d\mathbf{x} + \int_\Omega v(\mathbf{x}) \nabla v(\mathbf{x}) \cdot \nabla \big(e^{2\lambda b^{-\beta} r^\beta(\mathbf{x})} \big) d\mathbf{x}. \end{aligned} \quad (3.36)$$

The absolute value of the second integral in the right-hand side of (3.36) can be estimated as

$$\begin{aligned} &\Big| \int_\Omega v(\mathbf{x}) \nabla v(\mathbf{x}) \cdot \nabla \big(e^{2\lambda b^{-\beta} r^\beta(\mathbf{x})} \big) d\mathbf{x} \Big| \\ &\quad \leq 2\lambda\beta b^{-\beta} \int_\Omega r^{\beta-1}(\mathbf{x}) e^{2\lambda b^{-\beta} r^\beta(\mathbf{x})} |v(\mathbf{x})| |\nabla v(\mathbf{x})| d\mathbf{x} \\ &\quad \leq C\lambda^2 \beta^2 b^{-2\beta} \int_\Omega e^{2\lambda b^{-\beta} r^\beta(\mathbf{x})} r^{2\beta}(\mathbf{x}) |v(\mathbf{x})|^2 d\mathbf{x} \\ &\qquad\qquad + \frac{1}{2} \int_\Omega e^{2\lambda b^{-\beta} r^\beta(\mathbf{x})} |\nabla v(\mathbf{x})|^2 d\mathbf{x}. \end{aligned} \quad (3.37)$$

This, (3.36) and (3.37) imply

$$-\int_\Omega e^{2\lambda b^{-\beta} r^\beta(\mathbf{x})} v(\mathbf{x}) \Delta v(\mathbf{x}) d\mathbf{x} \geq C \int_\Omega e^{2\lambda b^{-\beta} r^\beta(\mathbf{x})} |\nabla v(\mathbf{x})|^2 d\mathbf{x} - C\lambda^2 \beta^2 b^{-2\beta} \int_\Omega e^{2\lambda b^{-\beta} r^{2\beta}(\mathbf{x})} r^{2\beta}(\mathbf{x}) |v(\mathbf{x})|^2 d\mathbf{x}.$$

The lemma is proved.

Lemma 3.3.3 *Let v be the function satisfying all hypotheses of Theorem 3.3.1. There exist positive constants β_0 depending only on b, $\mathbf{x}_0$, Ω and d such that*

$$\int_\Omega e^{2\lambda b^{-\beta} r^\beta(\mathbf{x})} |\Delta v(\mathbf{x})|^2 d\mathbf{x} \geq C\lambda^3 \beta^4 b^{-3\beta} \int_\Omega r^{2\beta}(\mathbf{x}) e^{2\lambda b^{-\beta} r^\beta} |v(\mathbf{x})|^2 d\mathbf{x} + C\lambda \beta^{1/2} b^{-\beta} \int_\Omega e^{2\lambda b^{-\beta} r^\beta(\mathbf{x})} |\nabla v(\mathbf{x})|^2 d\mathbf{x} \quad (3.38)$$

for all $\beta \geq \beta_0$ and $\lambda \geq \lambda_0$. Here λ_0 is a constant satisfying $\lambda_0 b^{-\beta} > 1$.

Proof 3.3.3 *Multiplying $\beta^{1/4}$ to (3.35) and then applying the inequality $-ab \leq a^2/2 + b^2/2$, we have*

$$\int_\Omega \lambda \beta^{3/2} b^{-\beta} e^{2\lambda b^{-\beta} r^\beta(\mathbf{x})} r^{\beta-2}(\mathbf{x}) |v(\mathbf{x})|^2 d\mathbf{x} + \int_\Omega \frac{e^{2\lambda b^{-\beta} r^\beta(\mathbf{x})}}{4\lambda b^{-\beta} \beta r^{\beta-2}(\mathbf{x})} |\Delta v(\mathbf{x})|^2 d\mathbf{x} \geq C\beta^{1/2} \int_\Omega e^{2\lambda b^{-\beta} r^\beta(\mathbf{x})} |\nabla v(\mathbf{x})|^2 d\mathbf{x} - C\lambda^2 \beta^{5/2} b^{-2\beta} \int_\Omega r^{2\beta}(\mathbf{x}) e^{2\lambda b^{-\beta} r^\beta(\mathbf{x})} |v(\mathbf{x})|^2 d\mathbf{x}.$$

Since $r(\mathbf{x}) > 1$, $\beta^{3/2} r^{\beta-2}(\mathbf{x}) \ll r^{2\beta}(\mathbf{x})$, we have

$$\int_\Omega \frac{e^{2\lambda b^{-\beta} r^\beta(\mathbf{x})}}{4\lambda \beta b^{-\beta} r^{\beta-2}(\mathbf{x})} |\Delta v(\mathbf{x})|^2 d\mathbf{x} \geq C\beta^{1/2} \int_\Omega e^{2\lambda b^{-\beta} r^\beta(\mathbf{x})} |\nabla v(\mathbf{x})|^2 d\mathbf{x} - C\lambda^2 \beta^{5/2} b^{-2\beta} \int_\Omega r^{2\beta}(\mathbf{x}) e^{2\lambda b^{-\beta} r^\beta(\mathbf{x})} |v(\mathbf{x})|^2 d\mathbf{x}. \quad (3.39)$$

Here, we have used the fact that $\lambda b^{-\beta} \gg 1$. Adding (3.39) and (3.22) together, we

obtain

$$\int_\Omega \frac{e^{2\lambda b^{-\beta} r^\beta(\mathbf{x})}}{\lambda\beta b^{-\beta} r^{\beta-2}(\mathbf{x})} |\Delta v(\mathbf{x})|^2 d\mathbf{x} \geq C\lambda^2\beta^3 b^{-2\beta} \int_\Omega r^{2\beta}(\mathbf{x}) e^{2\lambda b^{-\beta} r^\beta} |v(\mathbf{x})|^2 d\mathbf{x} + C\beta^{1/2} \int_\Omega e^{2\lambda b^{-\beta} r^\beta(\mathbf{x})} |\nabla v(\mathbf{x})|^2 d\mathbf{x},$$

which implies (3.38).

Lemma 3.3.4 *Let v be the function satisfying all hypotheses of Theorem 3.3.1. There exist positive constants β_0 and λ_0 depending only on b, $\mathbf{x}_0$, Ω and d such that*

$$\begin{aligned} &\frac{1}{\lambda\beta^{7/4} b^{-\beta}} \int_\Omega e^{2\lambda b^{-\beta} r^\beta(\mathbf{x})} |\Delta v(\mathbf{x})|^2 d\mathbf{x} \\ &\qquad \geq \frac{C}{\lambda\beta^{7/4} b^{-\beta}} \sum_{i,j=1}^d \int_\Omega e^{2\lambda b^{-\beta} r^\beta(\mathbf{x})} r^{2\beta}(\mathbf{x}) |\partial^2_{x_i x_j} v(\mathbf{x})|^2 d\mathbf{x} \\ &\qquad\qquad - C\lambda\beta^{1/4} b^{-\beta} \int_\Omega e^{2\lambda b^{-\beta} r^\beta(\mathbf{x})} |\nabla v(\mathbf{x})|^2 d\mathbf{x} \end{aligned} \tag{3.40}$$

for all $\beta \geq \beta_0$ and $\lambda \geq \lambda_0$.

Proof 3.3.4 *By the density arguments, we can assume that $v \in C^3(\overline{\Omega})$. Write $\mathbf{x} = (x_1, \ldots, x_d)$. We have*

$$\begin{aligned} \int_\Omega e^{2\lambda b^{-\beta} r^\beta(\mathbf{x})} |\Delta v(\mathbf{x})|^2 d\mathbf{x} &= \sum_{i,j=1}^d \int_\Omega e^{2\lambda b^{-\beta} r^\beta(\mathbf{x})} \partial^2_{x_i x_i} v(\mathbf{x}) \partial^2_{x_j x_j} v(\mathbf{x}) d\mathbf{x} \\ &= \sum_{i,j=1}^d \int_\Omega \partial_{x_j} \Big[e^{2\lambda b^{-\beta} r^\beta(\mathbf{x})} \partial^2_{x_i x_i} v(\mathbf{x}) \partial_{x_j} v(\mathbf{x}) \Big] d\mathbf{x} \\ &\quad - \sum_{i,j=1}^d \int_\Omega \partial_{x_j} v(\mathbf{x}) \partial_{x_j} \Big[e^{2\lambda b^{-\beta} r^\beta(\mathbf{x})} \partial^2_{x_i x_i} v(\mathbf{x}) \Big] d\mathbf{x}. \end{aligned}$$

The first integral on the right-hand side above vanishes due to the divergence theorem.

Hence

$$\int_\Omega e^{2\lambda b^{-\beta} r^\beta(\mathbf{x})} |\Delta v(\mathbf{x})|^2 d\mathbf{x} = -\sum_{i,j=1}^{d} \int_\Omega e^{2\lambda b^{-\beta} r^\beta(\mathbf{x})} \partial_{x_j} v(\mathbf{x}) \partial^3_{x_i x_i x_j} v(\mathbf{x}) d\mathbf{x} - \sum_{i,j=1}^{d} \int_\Omega \partial_{x_j} (e^{2\lambda b^{-\beta} r^\beta(\mathbf{x})}) \partial_{x_j} v(\mathbf{x}) \partial^2_{x_i x_i} v(\mathbf{x}) d\mathbf{x}. \quad (3.41)$$

The first term on the right-hand side of (3.41) is rewritten as

$$\begin{aligned} &-\sum_{i,j=1}^{d} \int_\Omega e^{2\lambda b^{-\beta} r^\beta(\mathbf{x})} \partial_{x_j} v(\mathbf{x}) \partial^3_{x_i x_i x_j} v(\mathbf{x}) d\mathbf{x} \\ &\quad = \sum_{i,j=1}^{d} \int_\Omega \partial_{x_i} (e^{2\lambda b^{-\beta} r^\beta(\mathbf{x})} \partial_{x_j} v(\mathbf{x})) \partial^2_{x_i x_j} v(\mathbf{x}) d\mathbf{x} \\ &\quad = \sum_{i,j=1}^{d} \int_\Omega e^{2\lambda b^{-\beta} r^\beta(\mathbf{x})} |\partial^2_{x_i x_j} v(\mathbf{x})|^2 d\mathbf{x} \\ &\qquad + \sum_{i,j=1}^{d} \int_\Omega \partial_{x_j} v(\mathbf{x}) \partial_{x_i} (e^{2\lambda b^{-\beta} r^\beta(\mathbf{x})}) \partial^2_{x_i x_j} v(\mathbf{x}) d\mathbf{x}. \end{aligned}$$

Combining this and (3.41), we have

$$\begin{aligned} \int_\Omega e^{2\lambda b^{-\beta} r^\beta(\mathbf{x})} |\Delta v(\mathbf{x})|^2 d\mathbf{x} &= \sum_{i,j=1}^{d} \int_\Omega e^{2\lambda b^{-\beta} r^\beta(\mathbf{x})} |\partial^2_{x_i x_j} v(\mathbf{x})|^2 d\mathbf{x} \\ &\quad + \sum_{i,j=1}^{d} \int_\Omega \Big[\partial_{x_j} v(\mathbf{x}) \partial_{x_i} (e^{2\lambda b^{-\beta} r^\beta(\mathbf{x})}) \partial^2_{x_i x_j} v(\mathbf{x}) \\ &\qquad - \partial_{x_j} (e^{2\lambda b^{-\beta} r^\beta(\mathbf{x})}) \partial_{x_j} v(\mathbf{x}) \partial^2_{x_i x_i} v(\mathbf{x}) d\mathbf{x} \Big]. \end{aligned}$$

Hence,

$$\begin{aligned} \int_\Omega e^{2\lambda b^{-\beta} r^\beta(\mathbf{x})} |\Delta v(\mathbf{x})|^2 d\mathbf{x} &\geq \sum_{i,j=1}^{d} \int_\Omega e^{2\lambda b^{-\beta} r^\beta(\mathbf{x})} |\partial^2_{x_i x_j} v(\mathbf{x})|^2 d\mathbf{x} \\ &\quad - 2 \sum_{i,j=1}^{d} \int_\Omega |\partial_{x_j} v(\mathbf{x})| |\partial_{x_i} (e^{2\lambda b^{-\beta} r^\beta(\mathbf{x})})| |\partial^2_{x_i x_j} v(\mathbf{x})| d\mathbf{x}. \end{aligned}$$

Note that for all $i = 1, \ldots, d$,

$$\partial_{x_i}(e^{2\lambda b^{-\beta} r^{\beta}(\mathbf{x})}) = 2\lambda b^{-\beta}\beta r^{\beta-2} e^{2\lambda b^{-\beta} r^{\beta}(\mathbf{x})} x_i \quad \textit{for all } \mathbf{x} \in \Omega.$$

Using the inequality $ab \leq a^2/2 + b^2/2$, *we obtain (3.40).*

We now prove Theorem 3.3.1.

Proof 3.3.5 (Proof of Theorem 3.3.1) *Adding (3.38) and (3.40) together, we obtain*

$$\begin{aligned}
(1 + \frac{1}{\lambda^2 \beta^{7/4} b^{-2\beta}}) \int_{\Omega} e^{2\lambda b^{-\beta} r^{\beta}(\mathbf{x})} |\Delta v(\mathbf{x})|^2 d\mathbf{x} \\
\geq \frac{C}{\lambda \beta^{7/4} b^{-\beta}} \sum_{i,j=1}^{d} \int_{\Omega} e^{2\lambda b^{-\beta} r^{\beta}(\mathbf{x})} r^{2\beta}(\mathbf{x}) |\partial^2_{x_i x_j} v(\mathbf{x})|^2 d\mathbf{x} \\
+ C\lambda^3 \beta^4 b^{-3\beta} \int_{\Omega} r^{2\beta}(\mathbf{x}) e^{2\lambda b^{-\beta} r^{\beta}} |v(\mathbf{x})|^2 d\mathbf{x} \\
+ C\lambda \beta^{1/2} b^{-\beta} \int_{\Omega} e^{2\lambda b^{-\beta} r^{\beta}(\mathbf{x})} |\nabla v(\mathbf{x})|^2 d\mathbf{x}.
\end{aligned}$$

Corollary 3.3.1 *Recall* β_0 *and* λ_0 *as in Theorem 3.3.1. Fix* $\beta = \beta_0$ *and let the constant* C *depend on* $\mathbf{x}_0$, Ω, d *and* β. *There exists a constant* λ_0 *depending only on* $\mathbf{x}_0$, Ω, d *and* β *such that for all function* $v \in H^2(\Omega)$ *with*

$$v(\mathbf{x}) = \partial_{\nu} v(\mathbf{x}) = 0 \quad \textit{ on } \partial\Omega,$$

we have

$$\begin{aligned}
\int_{\Omega} e^{2\lambda b^{-\beta} r^{\beta}(\mathbf{x})} |\Delta v(\mathbf{x})|^2 d\mathbf{x} \geq C\lambda^{-1} \sum_{i,j=1}^{d} \int_{\Omega} e^{2\lambda b^{-\beta} r^{\beta}(\mathbf{x})} |\partial^2_{x_i x_j} v(\mathbf{x})|^2 d\mathbf{x} \\
+ C\lambda^3 \int_{\Omega} e^{2\lambda b^{-\beta} r^{\beta}} |v(\mathbf{x})|^2 d\mathbf{x} + C\lambda \int_{\Omega} e^{2\lambda b^{-\beta} r^{\beta}(\mathbf{x})} |\nabla v(\mathbf{x})|^2 d\mathbf{x} \quad (3.42)
\end{aligned}$$

for all $\lambda \geq \lambda_0$.

Remark 3.3.3 *Although there are many versions of the Carleman estimate available, those versions are either too complicated, not suitable for us to prove Theorem 3.2.1 and Theorem 3.4.1, or do not work in computations. The main ideas of the proof follow from [34, 35, 36, 37, 38].*

Remark 3.3.4 *The presence of the second derivatives on the right-hand side of (3.42) is a new feature of our Carleman estimate. The presence of those second derivatives allows us to prove the existence and uniqueness of the minimizers of the cost functionals in Section 3.2.2.*

3.4 The convergence analysis

In this section, we prove a theorem that guarantees that the sequence of vector-valued functions, proposed in Section 3.2.2, converges to the true solution to (3.9)–(3.11). This convergence implies that Algorithm 2 rigorously provides good numerical solutions to Problem 3.1.1.

Theorem 3.4.1 *Assume that problem (3.9)–(3.11) has a unique solution* $(u_m^*)_{m=1}^N$. *Then, there is a constant* λ *depending only on* Ω, T, d *and* N *such that*

$$\sum_{m=1}^{N} \left\| e^{\lambda b^{-\beta} r^{\beta}(\mathbf{x})} (u_m^{(k)} - u_m^*) \right\|_{L^2(\Omega)}^2 \leq \left[\frac{C}{\lambda^3} \right]^{k-1} \sum_{m=1}^{N} \left\| e^{\lambda b^{-\beta} r^{\beta}(\mathbf{x})} (u_m^{(1)} - u_m^*) \right\|_{L^2(\Omega)}^2 \quad (3.43)$$

for $k = 1, 2, \ldots$ *where* C *is a constant depending only on* Ω, T, M, d, N *and* $\|q\|_{C^1(\overline{\Omega})}$. *In particular, if* λ *is large enough such that* $0 < C/\lambda^3 < 1$, $\{u_m^{(k)}\}_{m=1}^N$ *converges to* u_m^* *exponentially. Moreover, with such a* λ, *the sequence* $(p^{(k)})_{k \geq 1}$ *obtained in Step 8 of Algorithm 2 converges to the true function* $p^* = u^*(\mathbf{x}, 0)$ *given by* (3.4) *with* $t = 0$.

Proof 3.4.1 *In the proof,* C *is a generous constant that might change from estimate to estimate.*

Step 1. *Establish a priori bound. Recall H_0 as in (3.15). Since $(u_1^{(k)}, \dots, u_N^{(k)})$ is the minimizer of $J^{(k)}$, by the variational principle, for all $h \in H_0$*

$$\sum_{m=1}^{N} \Big\langle e^{\lambda b^{-\beta} r^{\beta}(\mathbf{x})} \Big[\Delta u^{(k)} - c(\mathbf{x}) \sum_{n=1}^{N} s_{mn} u^{(k)} + q_m(P(u_1^{(k-1)}), \dots, P(u_N^{(k-1)})) \Big], \\ e^{\lambda b^{-\beta} r^{\beta}(\mathbf{x})} \Big[\Delta h_m - c(\mathbf{x}) \sum_{n=1}^{N} s_{mn} h_m \Big] \Big\rangle_{L^2(\Omega)} = 0. \quad (3.44)$$

On the other hand, since $(u_1^*, \dots, u_N^*)$ solves (3.9)–(3.11),

$$\sum_{m=1}^{N} \Big\langle e^{\lambda b^{-\beta} r^{\beta}(\mathbf{x})} \Big[\Delta u^{*} - c(\mathbf{x}) \sum_{n=1}^{N} s_{mn} u^{*} + q_m(u_1^*, \dots, u_N^*) \Big], \\ e^{\lambda b^{-\beta} r^{\beta}(\mathbf{x})} \Big[\Delta h_m - c(\mathbf{x}) \sum_{n=1}^{N} s_{mn} h_m \Big] \Big\rangle_{L^2(\Omega)} = 0. \quad (3.45)$$

It follows from (3.44) and (3.45) that

$$\sum_{m=1}^{N} \Big\langle e^{\lambda b^{-\beta} r^{\beta}(\mathbf{x})} \Big[\Delta(u^{(k)} - u^*) - c(\mathbf{x}) \sum_{n=1}^{N} s_{mn} (u^{(k)} - u^*) \\ + q_m(P(u_1^{(k-1)}), \dots, P(u_N^{(k-1)}))) - q_m(u_1^*, \dots, u_N^*) \Big], \\ e^{\lambda b^{-\beta} r^{\beta}(\mathbf{x})} \Big[\Delta h_m - c(\mathbf{x}) \sum_{n=1}^{N} s_{mn} h_m \Big] \Big\rangle_{L^2(\Omega)} = 0. \quad (3.46)$$

Using the test function $h_m = u_m^{(k)} - u_m^*$, $m = 1, \dots, N$, in (3.46) and using Hölder's inequality, we have

$$\sum_{m=1}^{N} \Big\| e^{\lambda b^{-\beta} r^{\beta}(\mathbf{x})} \Big[\Delta(u^{(k)} - u^*) - c(\mathbf{x}) \sum_{n=1}^{N} s_{mn} (u^{(k)} - u^*) \Big] \Big\|_{L^2(\Omega)}^2 \\ \le \sum_{m=1}^{N} \Big\| e^{\lambda b^{-\beta} r^{\beta}(\mathbf{x})} \Big[q_m(P(u_1^{(k-1)}), \dots, P(u_N^{(k-1)}))) - q_m(u_1^*, \dots, u_N^*) \Big] \Big\|_{L^2(\Omega)} \\ \times \Big\| e^{\lambda b^{-\beta} r^{\beta}(\mathbf{x})} \Big[\Delta(u_m^{(k)} - u_m^*) - c(\mathbf{x}) \sum_{n=1}^{N} s_{mn} (u_m^{(k)} - u_m^*) \Big] \Big\|_{L^2(\Omega)}. \quad (3.47)$$

Using the inequality $\sum_{m=1}^{N} a_m b_m \le (\sum_{m=1}^{N} a_m^2)^{1/2}(\sum_{m=1}^{N} b_m^2)^{1/2}$ *for the right hand side of (3.47) and simplying the resulting, we get*

$$\sum_{m=1}^{N} \Big\| e^{\lambda b^{-\beta} r^{\beta}(\mathbf{x})} \Big[\Delta(u_m^{(k)} - u_m^*) - c(\mathbf{x}) \sum_{n=1}^{N} s_{mn}(u_m^{(k)} - u_m^*) \Big] \Big\|_{L^2(\Omega)}^2$$
$$\le \sum_{m=1}^{N} \Big\| e^{\lambda b^{-\beta} r^{\beta}(\mathbf{x})} \Big[q_m(P(u_1^{(k-1)}), \dots, P(u_N^{(k-1)})))$$
$$- q_m(u_1^*, \dots, u_N^*) \Big] \Big\|_{L^2(\Omega)}^2. \quad (3.48)$$

Step 2. *Estimate the right hand side of (3.48). Since* $\|u^*(\mathbf{x}, t)\|_{L^\infty} \le M$*, we have*

$$|u_m^*(\mathbf{x})| = \Big| \int_0^T u^*(\mathbf{x}, t)\Psi_m(t)dt \Big| \le \|u^*(\mathbf{x}, t)\|_{L^2(0,T)} \|\Psi_m(t)\|_{L^2(0,T)}$$
$$= \Big(\int_0^T |u^*(\mathbf{x}, t)|^2 dx \Big)^{1/2} \le M\sqrt{T}$$

for $m = 1, \dots, N$*. Therefore,*

$$\Big| q_m(P(u_1^{(k-1)}), \dots, P(u_N^{(k-1)})) - q_m(u_1^*, \dots, u_N^*) \Big| \le A_m \sum_{n=1}^{N} \big| u_n^{(k-1)} - u_n^* \big|$$

where

$$A_m = \max \Big\{ |\nabla q_m(s_1, \dots, s_N)| : |s_i| \le M\sqrt{T}, i = 1, \dots, N \Big\} \quad m = 1, \dots, N.$$

Set $A = \sum_{m=1}^{N} A_m$*. The right hand side of (3.48) is bounded from above by*

$$\sum_{m=1}^{N} \Big\| e^{\lambda b^{-\beta} r^{\beta}(\mathbf{x})} \Big[q_m(P(u_1^{(k-1)}), \dots, P(u_N^{(k-1)}))) - q_m(u_1^*, \dots, u_N^*) \Big] \Big\|_{L^2(\Omega)}^2$$
$$\le A \sum_{m=1}^{N} \Big\| e^{\lambda b^{-\beta} r^{\beta}(\mathbf{x})} \big| P(u_m^{(k-1)}) - u_m^* \big| \Big\|_{L^2(\Omega)}^2$$
$$\le A \sum_{m=1}^{N} \Big\| e^{\lambda b^{-\beta} r^{\beta}(\mathbf{x})} \big| u_m^{(k-1)} - u_m^* \big| \Big\|_{L^2(\Omega)}^2. \quad (3.49)$$

Combining (3.48) and (3.49) gives

$$\sum_{m=1}^{N}\left\|e^{\lambda b^{-\beta}r^{\beta}(\mathbf{x})}\Big[\Delta(u_m^{(k)}-u_m^*)-c(\mathbf{x})\sum_{n=1}^{N}s_{mn}(u_m^{(k)}-u_m^*)\Big]\right\|^2_{L^2(\Omega)} \leq A\sum_{m=1}^{N}\left\|e^{\lambda b^{-\beta}r^{\beta}(\mathbf{x})}\big|u_m^{(k-1)}-u_m^*\big|\right\|^2_{L^2(\Omega)}. \quad (3.50)$$

Step 3. *Estimate the left hand side of (3.50). Using the inequality* $(a-b)^2 \geq a^2/2 - 2b^2$, *we have*

$$\begin{aligned}\sum_{m=1}^{N}\left\|e^{\lambda b^{-\beta}r^{\beta}(\mathbf{x})}\Big[\Delta(u_m^{(k)}-u_m^*)-c(\mathbf{x})\sum_{n=1}^{N}s_{mn}(u_n^{(k)}-u_n^*)\Big]\right\|^2_{L^2(\Omega)} &\geq \sum_{m=1}^{N}\frac{1}{2}\left\|e^{\lambda b^{-\beta}r^{\beta}(\mathbf{x})}\Delta(u_m^{(k)}-u_m^*)\right\|^2_{L^2(\Omega)} \\ &\quad - 2\sum_{m=1}^{N}\left\|e^{\lambda b^{-\beta}r^{\beta}(\mathbf{x})}c(\mathbf{x})\sum_{n=1}^{N}s_{mn}(u_n^{(k)}-u_n^*)\right\|^2_{L^2(\Omega)}. \quad (3.51)\end{aligned}$$

Applying Carleman estimate in Corollary 3.3.1, for the function $u_m^{(k)} - u^*$, $m = 1,\ldots,N$, *we estimate*

$$\sum_{m=1}^{N}\frac{1}{2}\left\|e^{\lambda b^{-\beta}r^{\beta}(\mathbf{x})}\Delta(u_m^{(k)}-u_m^*)\right\|^2_{L^2(\Omega)} \geq C\lambda^3\sum_{m=1}^{N}\left\|e^{\lambda b^{-\beta}r^{\beta}(\mathbf{x})}(u_m^{(k)}-u_m^*)\right\|^2_{L^2(\Omega)}. \quad (3.52)$$

Fix $\lambda \geq \lambda_0$ where λ_0 is as in Corollary 3.3.1. It follows from (3.51) and (3.52) that

$$\sum_{m=1}^{N} \frac{1}{2} \left\| e^{\lambda b^{-\beta} r^{\beta}(\mathbf{x})} \Delta(u_m^{(k)} - u_m^*) \right\|_{L^2(\Omega)}^2 - 2 \sum_{m=1}^{N} \left\| e^{\lambda b^{-\beta} r^{\beta}(\mathbf{x})} \sum_{n=1}^{N} s_{mn} (u_n^{(k)} - u_n^*) \right\|_{L^2(\Omega)}^2 \geq C\lambda^3 \sum_{m=1}^{N} \left\| e^{\lambda b^{-\beta} r^{\beta}(\mathbf{x})} (u_m^{(k)} - u_m^*) \right\|_{L^2(\Omega)}^2. \quad (3.53)$$

Combining (3.48), (3.49) and (3.53) gives

$$\sum_{m=1}^{N} \left\| e^{\lambda b^{-\beta} r^{\beta}(\mathbf{x})} (u_m^{(k)} - u_m^*) \right\|_{L^2(\Omega)}^2 \leq \frac{A}{C\lambda^3} \sum_{m=1}^{N} \left\| e^{\lambda b^{-\beta} r^{\beta}(\mathbf{x})} (u_m^{(k-1)} - u_m^*) | \right\|_{L^2(\Omega)}^2.$$

By induction, we have

$$\sum_{m=1}^{N} \left\| e^{\lambda b^{-\beta} r^{\beta}(\mathbf{x})} (u_m^{(k)} - u_m^*) \right\|_{L^2(\Omega)}^2 \leq \left[\frac{A}{C\lambda^3} \right]^{k-1} \sum_{m=1}^{N} \left\| e^{\lambda b^{-\beta} r^{\beta}(\mathbf{x})} (u_m^{(1)} - u_m^*) | \right\|_{L^2(\Omega)}^2.$$

Replacing A/C by the generous constant C, we have proved the estimate (3.43)*. The convergence of $p^{(k)}$ to p^* as $k \to \infty$ is obvious.*

Remark 3.4.1 *The technique of using the Carleman estimate to prove Theorem 3.4.1 is similar to the one in [16] in which a coefficient inverse problem for hyperbolic equations was considered. We also find that this technique is applicable to solve an inverse source problem for nonlinear parabolic equations [17] from the boundary and additional internal measurements.*

Remark 3.4.2 *The convergence of $\{p^{(k)}\}_{k \geq 1}$ to the true solution to the inverse problem in Theorem 3.4.1 is numerically confirmed in Section 3.5. See also Figures 3.2e–3.5e.*

3.5 Numerical implementation

For simplicity, we solve the inverse problem in the case $d = 2$.

3.5.1 The forward problem

We solve the forward problem of Problem 3.1.1 as follows. Let $R_1 > R > 0$ be two positive numbers. Define the domains

$$\Omega_1 = (-R_1, R_1)^2 \quad \text{and} \quad \Omega = (-R, R)^2.$$

We approximate (3.1)defined on $\mathbb{R}^d \times (0, T)$ by the following problem defined on $\Omega_1 \times (0, T)$

$$\begin{cases} c(\mathbf{x})u_t(\mathbf{x}, t) &= \Delta u(\mathbf{x}, t) + q(u(\mathbf{x}, t)) & \mathbf{x} \in \Omega_1, t \in (0, T), \\ u(\mathbf{x}, 0) &= p(\mathbf{x}) & \mathbf{x} \in \Omega_1, \\ u(\mathbf{x}, t) &= 0 & \mathbf{x} \in \partial\Omega_1, t \in [0, T]. \end{cases} \tag{3.54}$$

In our numerical tests, the function c is given by

$$c(x, y) = 1 + 1/30\Big[3(1 - 3x)^2 e^{-9x^2-(3y+1)^2} - 10(3x/5 - 27x^3 - 243y^5)e^{-9x^2-9y^2} - 1/3e^{-(3x+1)^2-9y^2}\Big]$$

for $\mathbf{x} = (x, y) \in \Omega$.

The range of c is $[0.8, 1.25]$, which is not a perturbation of the constant function 1.

We solve (3.54) by the finite difference method using the explicit scheme. The data $f(\mathbf{x}, t) = u(\mathbf{x}, t)$ and $g(\mathbf{x}, t) = \partial_\nu u(\mathbf{x}, t)$ on $\partial\Omega \times [0, T]$ can be extracted easily.

In the next subsection, we discuss our choice of $\{\Psi_n\}_{n\geq 1}$ and the number N in Section 3.2.1 and the truncation in (3.4).

3.5.2 A special orthonormal basis $\{\Psi_n\}_{n\geq 1}$ of $L^2(0,T)$ and the choice of the cut-off number N

We will employ a special basis of $L^2(0,T)$. For each $n = 1, 2, \ldots$, set $\phi_n(t) = (t - T/2)^{n-1} \exp(t - T/2)$. The set $\{\phi_n\}_{n=1}^{\infty}$ is complete in $L^2(0,T)$. Applying the Gram-Schmidt orthonormalization process to this set, we obtain a basis of $L^2(0,T)$, named as $\{\Psi_n\}_{n=1}^{\infty}$.

This basis was originally introduced to solve the electrical impedance tomography problem with partial data in [39]. Since then, this basis was widely used to solve a variety of inverse problems. For instance, in [24], we employ this basis to solve an inverse source problem and a coefficient inverse problem for linear parabolic equations; in [29], this special basis was used to solve an inverse source problem for elliptic equations; in [40], we solve the problem of finding the Radon inverse with incomplete data; in [41], we solve an inverse source problem for the full transport radiative equation. The most related paper to the current one is [6], in which the second author and his collaborator employed this basis to recover the initial condition for linear parabolic equations.

We next discuss the choice of N in (3.4). Fix a positive integer $N_{\mathbf{x}}$. On $\overline{\Omega} = [-R, R]^2$, we arrange an $N_{\mathbf{x}} \times N_{\mathbf{x}}$ uniform grid

$$\mathcal{G} = \Big\{(x_i, y_j) : x_i = -R + (i-1)h, y_j = -R + (j-1)h, 1 \leq i, j \leq N_{\mathbf{x}}\Big\}$$

where $h = 2R/(N_{\mathbf{x}} - 1)$ is the step size. In our computations, we set $R_1 = 6$, $R = 1$, $T = 1.5$ and $N_{\mathbf{x}} = 80$. To solve Problem 3.1.1, we need to compute the discrete values of the function u on the grid $\mathcal{G}$.

The first step in our method is to find an appropriate cut-off number N. We do so as follows. Take the data on $\{(x, y = R) \in \partial\Omega\}$, which is the top part of $\partial\Omega$, $f(x, y = R, t) = u_{\text{true}}(x, y = R, t)$ in Test 1 in Section 3.5.4. Then, we compare the

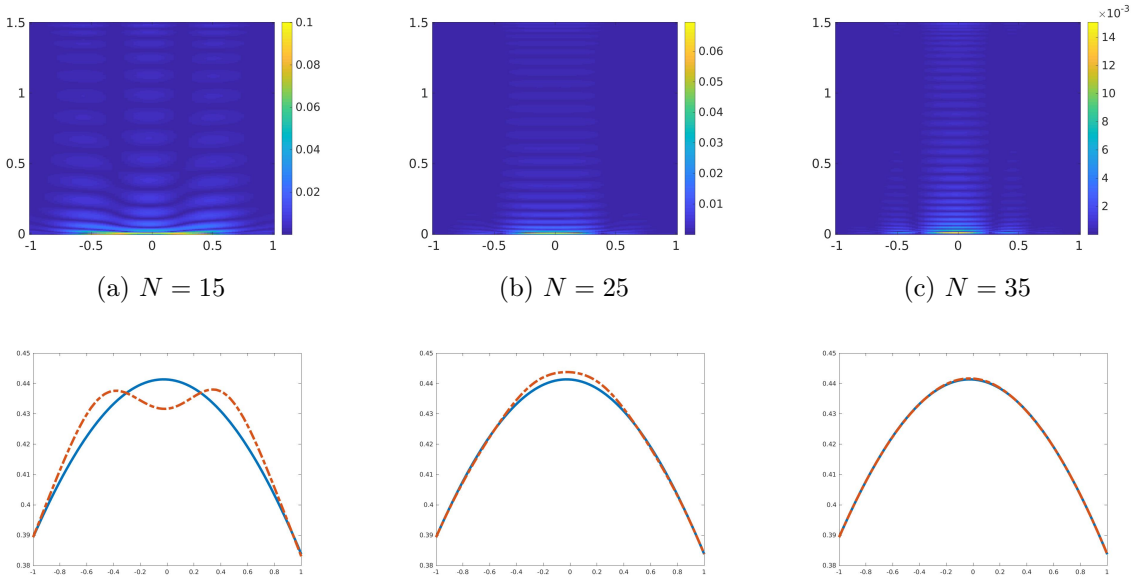

(a) $N = 15$ (b) $N = 25$ (c) $N = 35$

(d) $N = 15$ (e) $N = 25$ (f) $N = 35$

Figure 3.1: The comparison of $f(x, R, t)$ and its partial Fourier sum $\sum_{n=1}^{N} f_m(x, y = R, t)$ on $\{(x, y = R) \in \partial\Omega\}$. The first row displays the graphs of the absolute differences of $f(x, R, t)$ and $\sum_{n=1}^{N} f_n(x, R)\Psi_n(t)$. The horizontal axis indicates x and the vertical axis indicates t. It is evident that the bigger N, the smaller the difference is. The second row shows the true data $f(x, y = R, T)$ (solid line) and its approximation $\sum_{n=1}^{N} f_n(x, y = R)\Psi_n(T)$ (dash–dot line). We observe that when $N = 35$, the two curves coincide.

function $f(x, R, t)$ and the function $\sum_{n=1}^{N} f_n(x, y = R)\Psi_n(t)$ where $f_n(x, y = R)$ is computed by (3.11). Choose N such that the function

$$e_N(\mathbf{x}, t) = \left| f(x, y = R, t) - \sum_{n=1}^{N} f_n(x, y = R)\Psi_n(t) \right|$$

is small enough. We use the same number N for all numerical tests. In this chapter, $N = 35$, see Figure 3.1 for an illustration.

Remark 3.5.1 *In our computations, when the cut-off number N is 15 or 25, the quality of the numerical results is poor. When $N = 35$, we obtain good numerical results. Increasing $N > 35$ does not improve the computed quality.*

Remark 3.5.2 *In this numerical section, we choose the Carleman weight function*

$e^{\lambda b^{-\beta}|\mathbf{x}-\mathbf{x}_0|^\beta}$ when defining $J^{(k)}$, $k \geq 0$, where $\lambda = 40$ and $\beta = 10$. The point $\mathbf{x}_0$ is $(0, 1.5)$ and $b = 5$. This and the condition $\lambda b^{-\beta}$ large conflict. However, in practice, the Carleman weight function with these values of λ and β already helps provide good numerical solutions to Problem 3.1.1. We numerically observe that the weight function blow-up when $\lambda b^{-\beta} \gg 1$, causing some unnecessary numerical difficulties.

We next present the key step in the implementation of the inverse problem.

3.5.3 Computing the vector-valued function $(u_m)_{m=1}^N$

Recall that $(u_m^{(0)}(x, y))_{m=1}^N$ minimizes $J^{(0)}$ on H. Similarly to the argument in the first step of the proof of Theorem 3.4.1, for all $h \in H_0$, see the definition of H_0 in (3.15), by the variational principle, we have

$$\sum_{m=1}^{N} \Big\langle e^{\lambda b^{-\beta} r^\beta(\mathbf{x})} \Big[\Delta u_m^{(0)} - c(\mathbf{x}) \sum_{n=1}^{N} s_{mn} u_m^{(0)}\Big], \\ e^{\lambda b^{-\beta} r^\beta(\mathbf{x})} \Big[\Delta h_m - c(\mathbf{x}) \sum_{n=1}^{N} s_{mn} h_m\Big] \Big\rangle_{L^2(\Omega)} = 0. \quad (3.55)$$

For any $u \in H$, we next associate the values of u_m $\{u_m(x_i, y_j) : 1 \leq m \leq N, 1 \leq i, j \leq N_{\mathbf{x}}\}$ with an $N_{\mathbf{x}}^2 N$ dimensional vector $\mathfrak{u}_{\mathfrak{i}}$ with

$$\mathfrak{u}_{\mathfrak{i}} = u_m(x_i, y_j) \quad (3.56)$$

where

$$\mathfrak{i} = (i-1)N_{\mathbf{x}}N + (j-1)N + m \quad \text{for all } 1 \leq i, j \leq N_{\mathbf{x}}, 1 \leq m \leq N. \quad (3.57)$$

The range of the index $\mathfrak{i}$ is $\{1, \ldots, N_{\mathbf{x}}^2 N\}$. The "line-up" finite difference form of (3.55) is

$$\langle (\mathcal{L} - \mathcal{S})\mathfrak{u}^{(0)}, (\mathcal{L} - \mathcal{S})\mathfrak{h} \rangle = 0 \quad (3.58)$$

where $\mathfrak{W}_\lambda^2$, $\mathfrak{u}^{(0)}$ and $\mathfrak{h}$ are the line-up versions of $(W_\lambda^2)_{m=1}^N$, $(u_m^0)_{m=1}^N$ and $(h_m)_{m=1}^N$ respectively. Here, $\langle\cdot,\cdot\rangle$ is the classical Euclidian inner product. In (3.58)

1. the $N_{\mathbf{x}}^2N \times N_{\mathbf{x}}^2N$ matrix $\mathcal{L}$ is defined as
   (a) $(\mathcal{L})_{\mathfrak{i}\mathfrak{i}} = -\frac{4e^{\lambda b^{-\beta} r^\beta(x_i,y_j)}}{d_{\mathbf{x}}^2}$ for $\mathfrak{i}$ as in (3.57) for $2 \le i,j \le N_{\mathbf{x}}-1$, $1 \le m \le N$;
   (b) $(\mathcal{L})_{\mathfrak{i}\mathfrak{j}} = \frac{e^{\lambda b^{-\beta} r^\beta(x_i,y_j)}}{d_{\mathbf{x}}^2}$ for $\mathfrak{j} = (i \pm 1 - 1)N_{\mathbf{x}}N + (j-1)N + m$ and $\mathfrak{j} = (i-1)N_{\mathbf{x}}N + (j \pm 1 - 1)N + m$; for $2 \le i,j \le N_{\mathbf{x}}-1$, $1 \le m \le N$;
   (c) the other entries are 0.
2. the $N_{\mathbf{x}}^2N \times N_{\mathbf{x}}^2N$ matrix $\mathcal{S}$ is defined as $(\mathcal{S})_{\mathfrak{i}\mathfrak{j}} = e^{\lambda b^{-\beta} r^\beta(x_i,y_j)} c(x_i,y_j) s_{mn}$ for $\mathfrak{i}$ as in (3.57) and $\mathfrak{j} = (i-1)N_{\mathbf{x}}N + (j \pm 1 - 1)N + n$ for $2 \le i,j \le N_{\mathbf{x}}-1$, $1 \le m,n \le N$. The other entries are 0.

On the other hand, since $(u_m^0)_{m=1}^N$ satisfies the boundary constraints (3.11), we have

$$\mathcal{D}\mathfrak{u}^{(0)} = \mathfrak{f} \quad \text{and} \quad \mathcal{N}\mathfrak{u}^{(0)} = \mathfrak{g} \tag{3.59}$$

where

1. The $N_{\mathbf{x}}^2N \times N_{\mathbf{x}}^2N$ matrix $\mathcal{D}$ is defined as $\mathcal{D}_{\mathfrak{i}\mathfrak{i}} = 1$ for $\mathfrak{i}$ as in (3.57), $i \in \{1, N_{\mathbf{x}}\}$, $1 \le j \le N_{\mathbf{x}}$ or $2 \le i \le N_{\mathbf{x}}-1$, $j \in \{1, N_{\mathbf{x}}\}$. The other entries are 0.
2. The $N_{\mathbf{x}}^2N \times N_{\mathbf{x}}^2N$ matrix $\mathcal{N}$ is defined as
   (a) $\mathcal{N}_{\mathfrak{i}\mathfrak{i}} = \frac{1}{d_{\mathbf{x}}}$ for $\mathfrak{i}$ as in (3.57), $i \in \{1, N_{\mathbf{x}}\}$, $1 \le j \le N_{\mathbf{x}}$ or $2 \le i \le N_{\mathbf{x}}-1$, $j \in \{1, N_{\mathbf{x}}\}$, $1 \le m \le N$;
   (b) $\mathcal{N}_{\mathfrak{i}\mathfrak{j}} = -\frac{1}{d_{\mathbf{x}}}$ for $\mathfrak{i}$ as in (3.57) and $\mathfrak{j} = (i+1-1)N_{\mathbf{x}}N + (j-1)N + m$, $i = 1$, $1 \le j \le N_{\mathbf{x}}$, $1 \le m \le N$;
   (c) $\mathcal{N}_{\mathfrak{i}\mathfrak{j}} = -\frac{1}{d_{\mathbf{x}}}$ for $\mathfrak{i}$ as in (3.57) and $\mathfrak{j} = (i-1-1)N_{\mathbf{x}}N + (j-1)N + m$, $i = N_{\mathbf{x}}$, $1 \le j \le N_{\mathbf{x}}$, $1 \le m \le N$;

(d) $\mathcal{N}_{\mathfrak{ij}} = -\frac{1}{d_{\mathbf{x}}}$ for $\mathfrak{i}$ as in (3.57) and $\mathfrak{j} = (i-1)N_{\mathbf{x}}N + (j+1-1)N + m$, $1 \le i \le N_{\mathbf{x}}$, $j = 1$, $1 \le m \le N$;

(e) $\mathcal{N}_{\mathfrak{ij}} = -\frac{1}{d_{\mathbf{x}}}$ for $\mathfrak{i}$ as in (3.57) and $\mathfrak{j} = (i-1)N_{\mathbf{x}}N + (j-1-1)N + m$, $2 \le i \le N_{\mathbf{x}} - 1$, $j = N_{\mathbf{x}}$, $1 \le m \le N$;

(f) The other entries are 0.

3. The $N_{\mathbf{x}}^2 N$ dimensional vector $\mathfrak{f}$ is defined as $\mathfrak{f}_{\mathfrak{i}} = f_m(x_i, y_j)$ for $\mathfrak{i}$ as in (3.57), $i \in \{1, N_{\mathbf{x}}\}$, $1 \le j \le N_{\mathbf{x}}$, $1 \le m \le N$ or $2 \le i \le N_{\mathbf{x}} - 1$, $j \in \{1, N_{\mathbf{x}}\}$.

4. The $N_{\mathbf{x}}^2 N$ dimensional vector $\mathfrak{g}$ is defined as $\mathfrak{g}_{\mathfrak{i}} = g_m(x_i, y_j)$ for $\mathfrak{i}$ as in (3.57), $i \in \{1, N_{\mathbf{x}}\}$, $1 \le j \le N_{\mathbf{x}}$, $1 \le m \le N$ or $2 \le i \le N_{\mathbf{x}} - 1$, $j \in \{1, N_{\mathbf{x}}\}$.

Solving (3.58)–(3.59) by the least square method with the command "lsqlin" built in Matlab, we obtain the vector $\mathfrak{u}^{(0)}$ and hence the initial solution $(u_m^{(0)}(x_i, y_j))_{m=1}^N$ for $1 \le i, j \le N_{\mathbf{x}}$.

Remark 3.5.3 *In computation, defining the matrices above is ineffective due to their large size, $N_{\mathbf{x}}^2 N \times N_{\mathbf{x}}^2 N$ where $N_{\mathbf{x}} = 80$ and $N = 35$. We note that most of those matrices' entries are 0. So, instead of defining dense matrices, we use the invention of sparse matrices. Moreover, using sparse matrices significantly reduces the computational time.*

We next compute the vector valued function $(u_m^{(k)})_{m=1}^N$, $k \ge 1$, assuming by induction that $(u_m^{(k-1)})_{m=1}^N$ is known. Applying a very similar argument when deriving (3.58)–(3.59), the vector $\mathfrak{u}^{(k)}$ the line up version of $(u_m^{(k)}(x_i, y_j))_{m=1}^N$ with $1 \le i, j \le N_{\mathbf{x}}$ satisfies the equations

$$(\mathcal{L} - \mathcal{S})^T (\mathcal{L} - \mathcal{S}) \mathfrak{u}^{(k)} = -(\mathcal{L} - \mathcal{S})^T \mathfrak{q}^{(k-1)}. \tag{3.60}$$

and

$$\mathcal{D}\mathfrak{u}^{(k)} = \mathfrak{f} \quad \text{and} \quad \mathcal{N}\mathfrak{u}^{(k)} = \mathfrak{g} \tag{3.61}$$

where $\mathfrak{q}^{(k-1)}$ is the line up version of $(q_m(u_1^{(k-1)}(x,y),\ldots,u_N^{(k-1)}(x,y)))_{m=1}^N$. To find $\mathfrak{u}^{(k)}$, we solve (3.60)–(3.61) by the least square method with the command "lsqlin" of Matlab. The value of the function $(u_m(x_i,y_j))_{m=1}^N$ follows. We next find $u(x,y,t)$ via (3.4). The desired solution to Problem 3.1.1 $p(x,y)$ is set to be $u(x,y,0)$.

Remark 3.5.4 *In theory, we need to apply the cut-off function P, see (3.14). This is only for our convenience to prove Theorem 3.4.1. However, in computation, we can obtain good numerical results without applying the cut-off technique. This can be explained by setting M sufficiently large.*

We summarize the procedure to find p in Algorithm 2.

Algorithm 2 The procedure to solve Problem 3.1.1

1: Compute $\{\Psi_n\}_{n=1}^N$ as in Section 3.5.2. Choose $N = 35$, see Figure 3.1 and Remark 3.5.1.
2: Compute matrices $\mathcal{L},\mathcal{S},\mathcal{D}$ and $\mathcal{N}$. Find the line up versions $\mathfrak{f}$ and $\mathfrak{g}$ of the data $f_m(x_i,y_j)$ and $g_m(x_i,y_j)$ for $(x_i,y_j)\in\mathcal{G}\cap\partial\Omega$, $1\le m\le N$.
3: Solve (3.58)–(3.59) by the least square method. The solution is denoted by $\mathfrak{u}^{(0)}$. Compute $u_m^{(0)}(x_i,y_j)$, $1\le i,j\le N_{\mathbf{x}}$, $1\le m\le N$ using $u_m^{(0)}(x_i,y_j)=(\mathfrak{u}^{(0)})_{\mathfrak{i}}$ with $\mathfrak{i}$ as in (3.57).
4: Set the initial solution $p^{(0)}=\sum_{n=1}^N u_n^{(0)}(x_i,y_j)\Psi_n(0)$.
5: **for** $k=1$ to 5 **do**
6: Find $\mathfrak{q}^{(k-1)}$, the line up version of $q(P(u_1^{(k-1)}(x_i,y_j)),\ldots,u_N^{(k-1)}(x_i,y_j)))$, $1\le i,j\le N_{\mathbf{x}}$, $1\le m\le N$ in the same manner of (3.56) and (3.57).
7: Solve (3.60)–(3.61) by the least square method. The solution is denoted by $\mathfrak{u}^{(k)}$. Compute $u_m^{(k)}(x_i,y_j)$, $1\le i,j\le N_{\mathbf{x}}$, $1\le m\le N$ using $u_m^{(k)}(x_i,y_j)=(\mathfrak{u}^{(k)})_{\mathfrak{i}}$ with $\mathfrak{i}$ as in (3.57).
8: Set the initial solution $p^{(k)}=\sum_{n=1}^N u_n^{(k)}(x_i,y_j)\Psi_n(0)$.
9: Define the recursive error at step k as $\|p^{(k)}-p^{(k-1)}\|_{L^\infty}(\Omega)$.
10: **end for**

Remark 3.5.5 *We numerically observe that $\|p^{(5)}-p^{(4)}\|_\infty$ is sufficiently small in all tests in Section 3.5.4; i.e., our iterative scheme converges fast. Iterating the loop in Algorithm 2 five (5) times is enough to obtain good numerical results. Therefore, we stop the iterative process when $k=5$.*

3.5.4 Numerical examples

In this section, we show four (4) numerical results.

Test 1. The true source function is given by

$$p_{\text{true}} = \begin{cases} 8 & x^2 + (y - 0.3)^2 < 0.45^2, \\ 0 & \text{otherwise.} \end{cases}$$

The nonlinearity q is given by

$$q(s) = s(1 - s) \quad s \in \mathbb{R}.$$

In this case, the parabolic equation in (3.1) is the Fisher equation. The true and computed source functions p are displayed in Figure 3.2. It appears in the graph of this source function a big inclusion with contrast 8.

Our method to find the initial solution works very well in this case. One can see in Figure 3.2b that by solving the system (3.58)–(3.59), we obtain the initial solution that clearly indicates the position of the inclusion. The value of the reconstructed function inside the inclusion is somewhat acceptable and will improve after several iterations, see Figure 3.2d. The reconstructed function $p_{\text{comp}} = p^{(5)}$ is a good approximation of the true function p_{true}, see Figures 3.2c and 3.2d. It is evident from Figure 3.2e that our method converges fast. The reconstructed maximal value inside the inclusion is 7.202 (relative error 9.98%).

Test 2. We test the case of multiple inclusions, each of which has a different value.

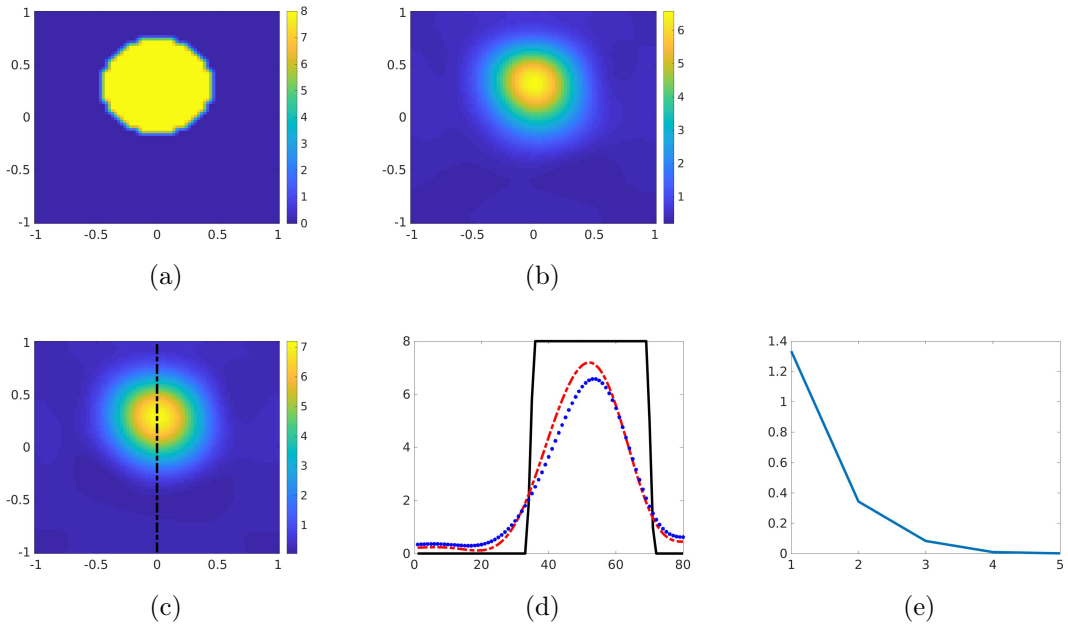

Figure 3.2: Test 1. The reconstruction of the source function. (a) The function p_{true} (b) The initial solution $p^{(0)}$ obtained by Step 3 in Algorithm 2. (c) The function $p^{(5)}$ obtained by Step 8 in Algorithm 2. (d) The true (solid), the initial source function (dot) in (b), and the computed source function (dash-dot) on the vertical line in (c). (e) The curve $\|p^{(k)} - p^{(k-1)}\|_{L^\infty(\Omega)}$, $k = 1, \ldots, 5$. The noise level of the data in this test is 20%.

The true source function p_{true} is given by

$$p_{\text{true}}(x,y) = \begin{cases} 12 & (x-0.5)^2 + (y-0.5)^2 < 0.35^2, \\ 10 & (x+0.5)^2 + (y+0.5)^2 < 0.35^2, \\ 14 & (x-0.5)^2 + (y+0.5)^2 < 0.35^2, \\ 9 & (x+0.5)^2 + (y-0.5)^2 < 0.35^2, \\ 0 & \text{otherwise.} \end{cases}$$

In this test, the nonlinearity q is given by

$$q(s) = -s(1 - \sqrt{|s|}) \quad s \in \mathbb{R}.$$

The true and computed source functions p are displayed in Figure 3.3.

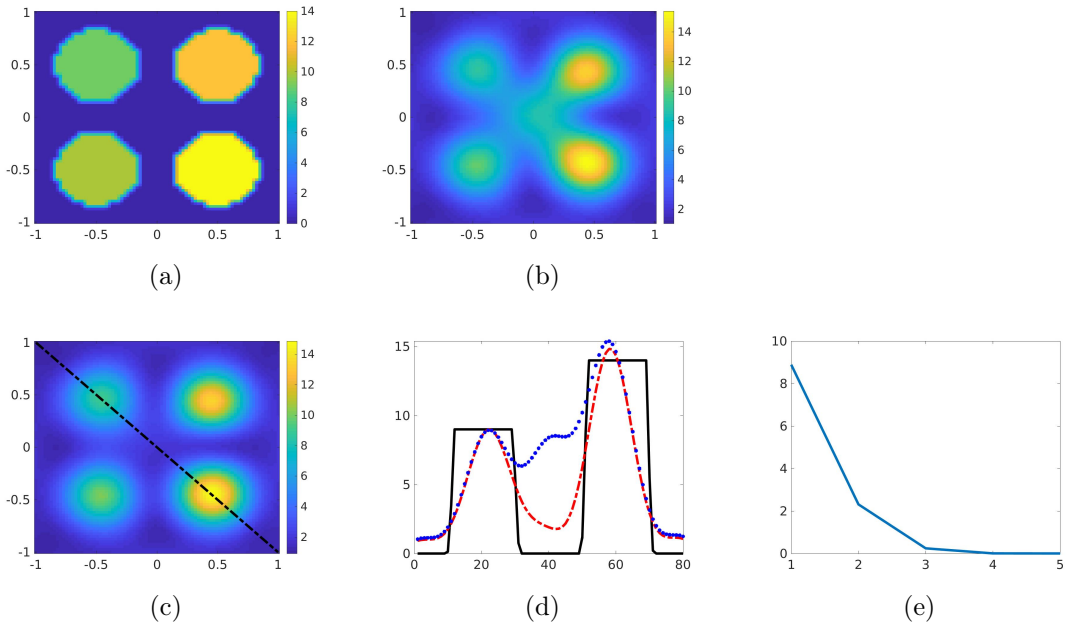

Figure 3.3: Test 2. The reconstruction of the source function. (a) The function p_{true} (b) The initial solution $p^{(0)}$ obtained by Step 3 in Algorithm 2. (c) The function $p^{(5)}$ obtained by Step 8 in Algorithm 2. (d) The true (solid), the initial solution (dot), and computed source function (dash-dot) on the diagonal line in (c). (e) The curve $\|p^{(k)} - p^{(k-1)}\|_{L^\infty(\Omega)}$, $k = 1, \ldots, 5$. The noise level of the data in this test is 20%.

In this test, we successfully recover all four inclusions. On the other hand, the value of p in each inclusion is high, making the true solution far away from the constant background $p_0 = 0$. Hence, $p_0 = 0$ might not serve as the initial guess. Our method to find the initial solution in Step 3 in Algorithm 2 is somewhat effective, see Figure 3.3b. The computed images of the initial solution do not completely separate the inclusions. Both computed values and images of the inclusions improve with iterations. The computed source function $p_{\text{comp}} = p^{(5)}$ is acceptable, see Figure 3.3c. Figure 3.3d shows that the constructed values in the inclusions are good. The procedure converges very fast, see Figure 3.3e.

The true maximal value of the upper left inclusion is 9 and the computed one is 8.992 (relative error 0.0%). The true maximal value of the upper right inclusion is 12 and the computed one is 13.4 (relative error 11.67%). The true maximal value of the

lower left inclusion is 10 and the computed one is 10.13 (relative error 1.3%). The true maximal value of the lower right inclusion is 14 and the computed one is 14.86 (relative error 6.14%).

Test 3. The true source function is given by

$$p_{\text{true}} = \begin{cases} 1 & 0.2^2 < x^2 + y^2 < 0.8^2, \\ 0 & \text{otherwise.} \end{cases}$$

The nonlinearity is given by

$$q(s) = s^2 \quad s \in \mathbb{R}.$$

The support of the function p_{true} is ring-like. This test is interesting due to the presence of the void and the nonlinearity grows fast. The true and computed source functions p are displayed in Figure 3.4.

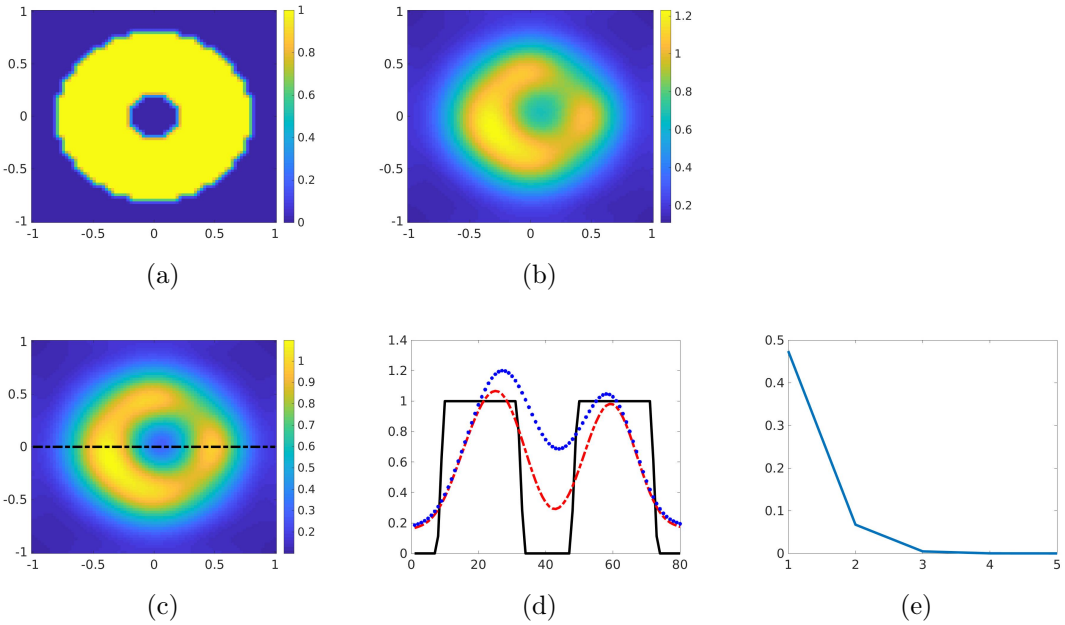

Figure 3.4: Test 3. The reconstruction of the source function. (a) The function p_{true} (b) The initial solution $p^{(0)}$ obtained by Step 3 in Algorithm 2. (c) The function $p^{(5)}$ obtained by Step 8 in Algorithm 2. (d) The true (solid), initial solution (dot) and computed source function (dash-dot) on horizontal line in (c). (e) The curve $\|p^{(k)} - p^{(k-1)}\|_{L^\infty(\Omega)}$, $k = 1, \ldots, 5$. The noise level of the data in this test is 20%.

In this test, our method to find the initial solution in Step 3 in Algorithm 2 is somewhat acceptable. The void in the initial solution $p^{(0)}$ cannot be seen very well, see Figure 3.4b. The contrast and the void are improved with iteration. The final reconstructed source function $p^{(5)}$ is satisfactory, see Figures 3.4c and 3.4d. The computed maximal value inside the ring is 1.094 (relative error = 9.4%).

Test 4. In this test, we identify two high contrast "lines". The true source function is given by

$$p_{\text{true}} = \begin{cases} 10 & \max\{|x|/4, 4|y-0.6| < 0.9\} \text{and } |x| < 0.8, \\ 8 & \max\{|x|/4, 4|y+0.6| < 0.9\} \text{and } |x| < 0.8, \\ 0 & \text{otherwise.} \end{cases}$$

The nonlinearity is given by

$$q(s) = -s^2 \quad s \in \mathbb{R}.$$

The true and computed source functions p are displayed in Figure 3.5.

It is evident that Algorithm 2 provides a good computed source function. The initial solution by Step 3 in Algorithm 2 is quite good although there is a "negative" artifact between the two detected lines, see Figure 3.5b. This artifact is reduced significantly with iteration. We observe that the shape and contrasts of two lines are reconstructed very well, see Figures 3.5c and 3.5d. Our method converges fast, see Figure 3.5e.

The true maximal value of the source function in the upper line is 10 and the computed one is 9.714 (relative error 2.8%). The true maximal value of the source function in the lower line is 8 and the computed one is 8.041 (relative error 0.51%).

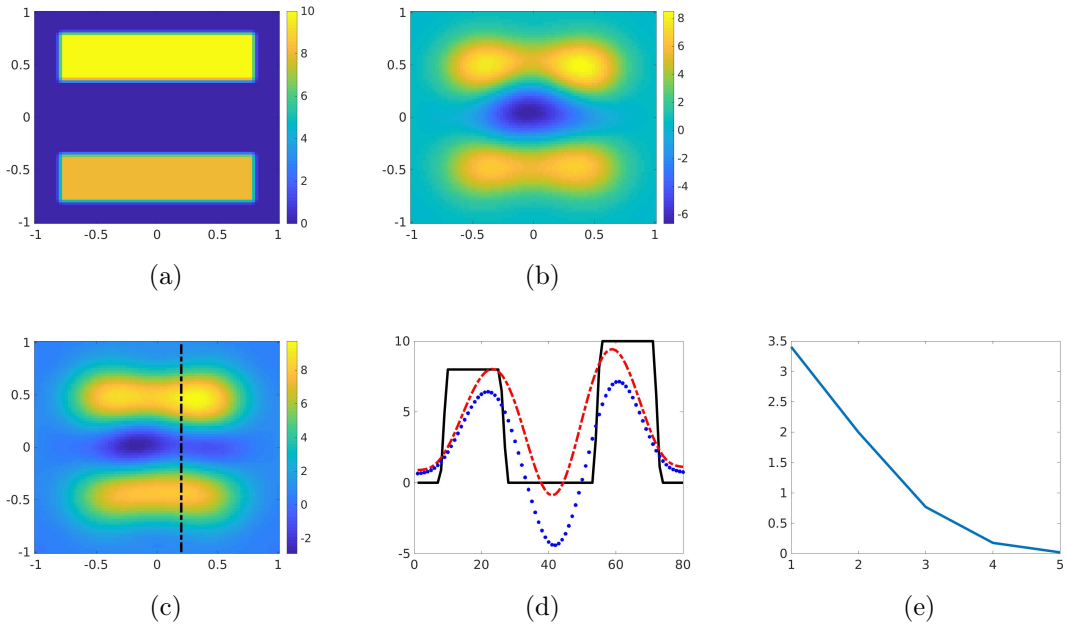

Figure 3.5: Test 3. The reconstruction of the source function. (a) The function p_{true} (b) The initial solution $p^{(0)}$ obtained by Step 3 in Algorithm 2. (c) The function $p^{(5)}$ obtained by Step 8 in Algorithm 2. (d) The true and computed source function on the line (dash-dot) in (c). (e) The curve $\|p^{(k)} - p^{(k-1)}\|_{L^\infty(\Omega)}$, $k = 1, \ldots, 5$. The noise level of the data in this test is 20%.

3.6 Concluding remarks

In this chapter, we analytically and numerically solve the problem of recovering the initial condition of nonlinear parabolic equations. The first step in our method is to derive a system of nonlinear elliptic PDEs whose solutions are the Fourier coefficients of the solution to the governing nonlinear parabolic equation. We propose an iterative scheme to solve the system above. Finding the initial solution for this iterative process is a part of our algorithm. The convergence of this iterative method was proved. We show several numerical results to confirm the theoretical part.

REFERENCES

[1] O. A. Ladyzhenskaya, V. Solonnikov, and N. N. Ural'tseva, *Linear and quasilinear equations of Parabolic Type*, vol. 23. Providence, RI: American Mathematical Society, 1968.

[2] M. V. Klibanov, "Estimates of initial conditions of parabolic equations and inequalities via lateral Cauchy data," *Inverse Problems*, vol. 22, pp. 495–514, 2006.

[3] A. El Badia and T. Ha-Duong, "On an inverse source problem for the heat equation. application to a pollution detection problem," *Journal of Inverse and Ill-posed Problems*, vol. 10, pp. 585–599, 2002.

[4] J. Li, M. Yamamoto, and J. Zou, "Conditional stability and numerical reconstruction of initial temperature," *Communications on Pure and Applied Analysis*, vol. 8, pp. 361–382, 2009.

[5] R. A. Fisher, "The wave of advance of advantageous genes," *Annals of Eugenics*, vol. 7, no. 4, pp. 355–369, 1937.

[6] Q. Li and L. H. Nguyen, "Recovering the initial condition of parabolic equations from lateral Cauchy data via the quasi-reversibility method," *Inverse Problems in Science and Engineering*, vol. 28, pp. 580–598, 2020.

[7] M. M. Lavrent'ev, V. G. Romanov, and S. P. Shishat·skiĭ, *Ill-Posed Problems of Mathematical Physics and Analysis*. Translations of Mathematical Monographs, Providence: RI: AMS, 1986.

[8] M. V. Klibanov and O. V. Ioussoupova, "Uniform strict convexity of a cost functional for three-dimensional inverse scattering problem," *SIAM J. Math. Anal.*, vol. 26, pp. 147–179, 1995.

[9] M. V. Klibanov, "Global convexity in a three-dimensional inverse acoustic problem," *SIAM J. Math. Anal.*, vol. 28, pp. 1371–1388, 1997.

[10] M. V. Klibanov, "Global convexity in diffusion tomography," *Nonlinear World*, vol. 4, pp. 247–265, 1997.

[11] A. B. Bakushinskii, M. V. Klibanov, and N. A. Koshev, "Carleman weight functions for a globally convergent numerical method for ill-posed Cauchy problems for some quasilinear PDEs," *Nonlinear Anal. Real World Appl.*, vol. 34, pp. 201–224, 2017.

[12] M. V. Klibanov, "Carleman weight functions for solving ill-posed Cauchy problems for quasilinear PDEs," *Inverse Problems*, vol. 31, p. 125007, 2015.

[13] M. V. Klibanov and A. E. Kolesov, "Convexification of a 3-D coefficient inverse scattering problem," *Computers and Mathematics with Applications*, vol. 77, pp. 1681–1702, 2019.

[14] M. V. Klibanov, J. Li, and W. Zhang, "Convexification of electrical impedance tomography with restricted Dirichlet-to-Neumann map data," *Inverse Problems*, vol. 35, p. 035005, 2019.

[15] V. A. Khoa, M. V. Klibanov, and L. H. Nguyen, "Convexification for a 3D inverse scattering problem with the moving point source," *SIAM J. Imaging Sci.*, vol. 13, no. 2, pp. 871–904, 2020.

[16] L. Baudouin, M. de Buhan, and S. Ervedoza, "Convergent algorithm based on Carleman estimates for the recovery of a potential in the wave equation," *SIAM J. Nummer. Anal.*, vol. 55, pp. 1578–1613, 2017.

[17] M. Boulakia, M. de Buhan, and E. Schwindt, "Numerical reconstruction based on Carleman estimates of a source term in a reaction-diffusion equation," *ESAIM: COCV*, 2021.

[18] L. Baudouin, M. de Buhan, S. Ervedoza, and A. Osses, "Carleman-based reconstruction algorithm for the waves," *SIAM Journal on Numerical Analysis*, vol. 59, no. 2, pp. 998–1039, 2021.

[19] L. Borcea, V. Druskin, A. V. Mamonov, and M. Zaslavsky, "A model reduction approach to numerical inversion for a parabolic partial differential equation," *Inverse Problems*, vol. 30, p. 125011, 2014.

[20] K. Cao and D. Lesnic, "Determination of space-dependent coefficients from temperature measurements using the conjugate gradient method," *Numer Methods Partial Differential Eq.*, vol. 34, pp. 1370–1400, 2018.

[21] K. Cao and D. Lesnic, "Simultaneous reconstruction of the perfusion coefficient and initial temperature from time-average integral temperature measurements," *Applied Mathematical Modelling*, vol. 68, pp. 523–539, 2019.

[22] Y. L. Keung and J. Zou, "Numerical identifications of parameters in parabolic systems," *Inverse Problems*, vol. 14, pp. 83–100, 1998.

[23] L. H. Nguyen, "A new algorithm to determine the creation or depletion term of parabolic equations from boundary measurements," *Computers and Mathematics with Applications*, vol. 80, pp. 2135–2149, 2020.

[24] P. M. Nguyen and L. H. Nguyen, "A numerical method for an inverse source problem for parabolic equations and its application to a coefficient inverse problem," *Journal of Inverse and Ill-posed Problems*, vol. 38, pp. 232–339, 2020.

[25] L. Yang, J.-N. Yu, and Y.-C. Deng, "An inverse problem of identifying the coefficient of parabolic equation," *Applied Mathematical Modelling*, vol. 32, pp. 1984–1995, 2008.

[26] H. Liu and G. Uhlmann, "Determining both sound speed and internal source in thermo- and photo-acoustic tomography," *Inverse Problems*, vol. 31, p. 105005, 2015.

[27] V. Katsnelson and L. V. Nguyen, "On the convergence of time reversal method for thermoacoustic tomography in elastic media," *Applied Mathematics Letters*, vol. 77, pp. 79–86, 2018.

[28] M. Haltmeier and L. V. Nguyen, "Analysis of iterative methods in photoacoustic tomography with variable sound speed," *SIAM J. Imaging Sci.*, vol. 10, pp. 751–781, 2017.

[29] L. H. Nguyen, Q. Li, and M. V. Klibanov, "A convergent numerical method for a multi-frequency inverse source problem in inhomogenous media," *Inverse Problems and Imaging*, vol. 13, pp. 1067–1094, 2019.

[30] X. Wang, Y. Guo, D. Zhang, and H. Liu, "Fourier method for recovering acoustic sources from multi-frequency far-field data," *Inverse Problems*, vol. 33, p. 035001, 2017.

[31] X. Wang, Y. Guo, J. Li, and H. Liu, "Mathematical design of a novel input/instruction device using a moving acoustic emitter," *Inverse Problems*, vol. 33, p. 105009, 2017.

[32] J. Li, H. Liu, and H. Sun, "On a gesture-computing technique using eletromagnetic waves," *Inverse Probl. Imaging*, vol. 12, pp. 677–696, 2018.

[33] D. Zhang, Y. Guo, J. Li, and H. Liu, "Retrieval of acoustic sources from multi-frequency phaseless data," *Inverse Problems*, vol. 34, p. 094001, 2018.

[34] L. Beilina and M. V. Klibanov, *Approximate Global Convergence and Adaptivity for Coefficient Inverse Problems*. New York: Springer, 2012.

[35] A. L. Bukhgeim and M. V. Klibanov, "Uniqueness in the large of a class of multidimensional inverse problems," *Soviet Math. Doklady*, vol. 17, pp. 244–247, 1981.

[36] M. V. Klibanov, "Carleman estimates for global uniqueness, stability and numerical methods for coefficient inverse problems," *J. Inverse and Ill-Posed Problems*, vol. 21, pp. 477–560, 2013.

[37] M. H. Protter, "Unique continuation for elliptic equations," *Trans. Amer. Math. Soc.*, vol. 95, no. 1, pp. 81–91, 1960.

[38] H. M. Nguyen and L. H. Nguyen, "Cloaking using complementary media for the Helmholtz equation and a three spheres inequality for second order elliptic equations," *Transaction of the American Mathematical Society*, vol. 2, pp. 93–112, 2015.

[39] M. V. Klibanov, "Convexification of restricted Dirichlet to Neumann map," *J. Inverse and Ill-Posed Problems*, vol. 25, no. 5, pp. 669–685, 2017.

[40] M. V. Klibanov and L. H. Nguyen, "PDE-based numerical method for a limited angle X-ray tomography," *Inverse Problems*, vol. 35, p. 045009, 2019.

[41] A. V. Smirnov, M. V. Klibanov, and L. H. Nguyen, "On an inverse source problem for the full radiative transfer equation with incomplete data," *SIAM Journal on Scientific Computing*, vol. 41, pp. B929–B952, 2019.

CHAPTER 4: CARLEMAN CONTRACTION MAPPING FOR A 1D INVERSE SCATTERING PROBLEM WITH EXPERIMENTAL TIME-DEPENDENT DATA

4.1 Introduction

The phenomenon of multiple local minima and ravines of conventional least squares cost functionals for Coefficient Inverse Problems (CIPs) is well known; see, e.g., [38] for a numerical example. Some cost functionals for various CIPs can be found in, e.g., [10, 13, 14]. Due to this phenomenon, the convergence of a numerical method of the minimization of that functional to the true solution of the corresponding CIP can be guaranteed only if its starting point is located in a sufficiently small neighborhood of this solution. To avoid the latter, the so-called convexification method was initially proposed theoretically in [20, 17] and more recently this method was tested on a variety of CIPs. The corresponding results for multidimensional CIPs are summarized in the recently published book [25]. As to the various versions of the convexification method for the 1D CIP of this publication, we refer to publications [22, 23, 24, 40], where the same experimental data as ones discussed in this chapter were treated. In [39] the same CIP, although without experimental data was treated by another version of the convexification method

In the convexification, a weighted Tikhonov-like functional $J_{\lambda,\beta}$ is constructed first, where $\lambda, \beta > 0$ are two parameters. The weight is the Carleman Weight Function (CWF). This is the function, which is used as the weight in the Carleman estimate for the corresponding Partial Differential Operator, see, e.g., [5, 6, 18, 25, 30, 42] for some publications on Carleman estimates. That functional $J_{\lambda,\beta}$ is defined on a bounded convex set $S \subset H$, where H is an appropriate Hilbert space. Next, it is proven that, for an appropriate choice of the parameters λ, β, the functional $J_{\lambda,\beta}$ is

strictly convex on S, has a unique minimizer on S and minimizers generate a sequence, which converges to the true solution of the original CIP as long as the level of noise in the data tends to zero. Let $d(S)$ be the diameter of the set S. An important point here is that a smallness condition is not imposed on $d(S)$. This means that convexification is a globally convergent numerical method in terms of the Definition given below. We call the method outlined in this paragraph the "the first generation of the convexification method".

Definition. *We call a numerical method for a CIP globally convergent if there is a theorem claiming that this method delivers at least one point in a sufficiently small neighborhood of the true solution of that CIP without advanced knowledge of a small neighborhood of this solution.*

The above functional $J_{\lambda,\beta}$ is not a quadratic one. The main new element of this chapter is that we minimize a sequence of quadratic functionals. More precisely, unlike the above, we construct a sequence of linear boundary value problems (BVPs) for certain PDEs with overdetermined boundary conditions and non-local terms. To solve each of these BVPs, we apply a weighted version of the Quasi-Reversibility Method (QRM). The weight is again the CWF. This is the reason why we call this method "Carleman Quasi-Reversibility Method" (CQRM). For each BVP, CQRM minimizes a quadratic weighted functional on a bounded set S', which is an analog of the above-mentioned set S. We analytically establish the key convergence estimate for the sequence of minimizers of these functionals. Our convergence estimate implies the global convergence of that sequence to the true solution of our CIP. We call the technique of this chapter "the second generation of the convexification method".

Remark 1.1. *The convergence estimate mentioned in the previous paragraph is similar to the estimate of the classical contraction mapping principle; see the first item of Remarks 8.1 in section 8. This explains the title of our chapter.*

Furthermore, due to its connection with the contraction mapping, that convergence

estimate implies a rapid convergence of our technique. As a result, computations for our experimental data are performed in *real time* here; also, see Remark 11.1 in section 11 as well as section 12. On the other hand, real-time computations are not claimed in the previous works of this research group on the first generation of the convexification method applied to the same CIP and with the same experimental data as ones used in this chapter [22, 23, 24, 40]. The real-time computations are obviously important for our described Real World application described below in this section. Thus, the real-time computations for experimental data present an *important advantage* of the technique of this chapter over the first generation of the convexification method.

The QRM was first proposed in [29], also, see, e.g. [7, 8, 19, 25] and references cited therein for some follow up publications. Even though Carleman estimates were used in [7, 8, 19, 25] to establish convergence rates, the CWFs were not involved in numerical schemes.

For the first time, the second generation of the convexification method involving CQRM was published in [2]. We also refer to works [3, 4] of the same research group for their later publications. In these papers, globally convergent numerical methods for CIPs for hyperbolic PDEs in $\mathbb{R}^n$ were developed. It is assumed in [2, 3, 4] that one of the initial conditions is not vanishing everywhere in the closed domain of one's interest. In other words, papers [2, 3, 4] work in the framework of the Bukhgeim-Klibanov method, see [9] for the originating work on this method as well as, e.g., [5, 6, 16, 18, 25, 42] for some follow-up publications. The major difference between works [2, 3, 4] and all above-cited publications of our research group on the convexification, including the current one, is that in our works either one of the initial conditions is the $\delta-$function and another one is zero, or a similar requirement holds for the Helmholtz equation. The only exception is the paper [26], which works within the framework of the method of [9], also, see chapter 9 of [25] for the same result as the one in [26]. In [31] the second generation of the convexification was applied to solve an

inverse problem of the determination of the initial condition of a quasilinear parabolic equation. We refer to papers [12, 27] for some globally convergent numerical methods for CIPs with the Dirichlet-to-Neumann map data. In these works, the number m of free variables in the data exceeds the number n of free variables in the unknown coefficient, $m > n$. In our chapter $m = n = 1$. Also, $m = n$ in all other above-cited works on the convexification.

We consider in this chapter a CIP for a 1D hyperbolic PDE. We show that our CIP has a direct application in the problem of the standoff detection and identification of antipersonnel land mines and improvised explosive devices (IEDs). Thus, in the computational part of this chapter, we present results of the numerical performance of our technique for both computationally simulated and experimentally collected data for targets mimicking antipersonnel land mines and IEDs. The experimental data of this chapter were collected by the forward-looking radar of the US Army Research Laboratory [35]. Since these data were described in some previous publications of our research group [15, 22, 23, 24, 28, 40], then we do not describe them here.

From the applied standpoint, our goal is to compute approximate values of dielectric constants of the above-mentioned targets. We point out that our experimental data are *severely under-determined*. Indeed, any target is a 3D object. On the other hand, we have only one experimentally measured time-resolved curve for each target. Therefore, we can compute only a sort of an average value of the dielectric constant of each target. This is the reason of the mathematical modeling of our experimental data by a 1D hyperbolic PDE rather than by its 3D analog. We believe that our results for experimental data might potentially help to decrease the false alarm rate in the problem of the standoff detection and identification of antipersonnel land mines and IEDs.

There is a classical Gelfand-Levitan method [32] for solutions of 1D CIPs for some hyperbolic PDEs. This method does not rely on optimization and, therefore, avoids

the phenomenon of local minima. It reduces the original CIP to a linear integral equation of the second kind. This is the so-called "Gelfand-Levitan equation" (GL). However, the questions of uniqueness and stability of the solution of GL for the case of noisy data are open; see, e.g., Lemma 2.4 in the book [36, Chapter 2]. This lemma is valid only in the case of noiseless data. However, realistic data are always noisy. In addition, it was demonstrated numerically in [15] that GL cannot work well for exactly the same experimental data as the ones we use in the current chapter. On the other hand, it was demonstrated in [22, 23, 24, 40] that the first generation of the convexification method works well with these data. The same is true for the second generation of the convexification method of this chapter.

Uniqueness and Lipschitz stability theorems of the CIP considered here are well known. Indeed, it was shown in, e.g. [40, 39] that, using a change of variables, one can reduce our CIP to a similar CIP for the equation $v_{tt} = v_{yy} + r(y) v, y \in \mathbb{R}$ with the unknown coefficient $r(y)$. We refer to [36, Theorem 2.6 of Chapter 2] for the Lipschitz stability estimate for the latter CIP. In addition, both uniqueness and Lipschitz stability results for our CIP actually follow from Theorem 8.1 below as well as from the convergence analysis of [24] for the first generation of the convexification method for this CIP.

This chapter is arranged as follows. In section 2 we state both forward and inverse problems. In section 3 we derive a nonlinear boundary value problem (BVP) with nonlocal terms. In section 4 we describe our iterative solution of this BVP. In section 5 we formulate the Carleman estimate for the principal part of the PDE operator of that BVP. In section 6 we prove the strong convexity of a functional of section 5 on an appropriate bounded set in a Hilbert space. In section 7 we formulate two methods for finding the unique minimizer of that functional: the gradient descent method and the gradient projection method and prove the global convergence to the minimizer for each of them. In section 8 we establish the contraction mapping property and

prove the global convergence of the method of section 4. In section 9 we formulate two more global convergence theorems, which follow from the results of sections 7 and 8. Numerical results with simulated and experimental data are presented in Section 10 and 11 respectively. Concluding remarks are given in section 12.

4.2 Statements of Forward and Inverse Problems

Below all functions are real-valued ones. Let $b > 1$ be a known number, $x \in \mathbb{R}$ be the spatial variable and the function $c(x) \in C^3(\mathbb{R})$, represents the spatially distributed dielectric constant. We assume that

$$c(x) \in [1, b], x \in \mathbb{R}, \tag{4.1}$$

$$c(x) = 1 \text{ if } x \in (-\infty, \varepsilon] \cup [1, \infty), \tag{4.2}$$

where $\varepsilon \in (0, 1)$ is a small number. Let T be a positive number. We consider the following Cauchy problem for a 1D hyperbolic PDE with a variable coefficient in the principal part of the operator:

$$c(x)u_{tt} = u_{xx},\ x \in \mathbb{R}, t \in (0, T)\,, \tag{4.3}$$

$$u\,(x, 0) = 0, u_t\,(x, 0) = \delta\,(x)\,. \tag{4.4}$$

The problem of finding the function $u(x, t)$ from conditions (4.3), (4.4) is our forward problem.

Let $\tau\,(x)$ be the travel time needed for the wave to travel from the point source at $\{0\}$ to the point x,

$$\tau\,(x) = \int_0^x \sqrt{c(s)}ds \tag{4.5}$$

By (4.5) the following 1D analog of the eikonal equation is valid:

$$\tau'\,(x) = \sqrt{c\,(x)}. \tag{4.6}$$

Let $H(z), z \in \mathbb{R}$ be the Heaviside function,

$$H(z) = \begin{cases} 1, & z > 0, \\ 0, & z < 0. \end{cases}$$

Lemma 2.1 [24, Lemma 2.1]. *For $x \geq 0$, the function $u(x,t)$ has the form:*

$$u(x,t) = H(t - \tau(x)) \left[\frac{1}{2c^{1/4}(x)} + \widehat{u}(x,t) \right], \tag{4.7}$$

where the function $\widehat{u} \in C^2(t \geq \tau(x))$ and $\widehat{u}(x, \tau(x)) = 0$. In particular,

$$\lim_{t \to \tau^+(x)} u(x,t) = \frac{1}{2c^{1/4}(x)}. \tag{4.8}$$

We also refer to books of Romanov [36, formulas (2.50), (2.51)], [37, Lemma 1.2.1] for results, which are similar with the one of Lemma 2.1. Far more challenging similar results in the 3D case can also be found in these books, see [36, Theorem 4.1], [37, Lemma 2.2.1].

Lemma 2.2 (absorbing boundary conditions [24, 40]). *Let $b > \varepsilon$ be the number in (4.1). Let $x_1 \geq b$ and $x_2 \leq \varepsilon$ be two arbitrary numbers. Then the solution $u(x,t)$ of forward problem (4.3), (4.4) satisfies the absorbing boundary conditions at $x = x_1$ and $x = x_2$, i.e.*

$$u_x(x_1,t) + u_t(x_1,t) = 0, \ t \in (0,T), \tag{4.9}$$

$$u_x(x_2,t) - u_t(x_2,t) = 0, \ t \in (0,T). \tag{4.10}$$

We are interested in the following inverse problem:

Coefficient Inverse Problem (CIP). *Suppose that the following two functions $g_0(t)$, $g_1(t)$ are known:*

$$u(\varepsilon,t) = g_0(t), \quad u_x(\varepsilon,t) = g_1(t), \quad t \in (0,T). \tag{4.11}$$

Determine the function $c(x)$ for $x \in (\varepsilon, 1)$, assuming that the number $b > \varepsilon$ in (4.1) is known.

Remark 2.1. *Note that only the function $g_0(t)$ can be measured. As to the function $g_1(t)$, it follows from (4.10) that*

$$g_1(t) = g_0'(t). \tag{4.12}$$

We differentiate noisy functions using the Tikhonov regularization method [41]. Since this method is well known, we do not describe it here.

4.3 A Boundary Value Problem for a Nonlinear PDE With Non-Local Terms

We now introduce a change of variable

$$q(x,t) = u(x, t + \tau(x)). \tag{4.13}$$

We will consider the function $q(x,t)$ only for $t \geq 0$. Using (4.6) and (2.22), we obtain

$$q_{xx} - 2q_{xt}\tau' - q_t\tau'' = 0. \tag{4.14}$$

Furthermore, it follows from (4.8)

$$q(x,0) = \frac{1}{2c^{1/4}(x)} \neq 0. \tag{4.15}$$

By (4.5) and (4.15)

$$\tau''(x) = -\frac{q_x(x,0)}{2q^3(x,0)}. \tag{4.16}$$

Substituting (4.6), (4.15) and (4.16) in (4.14), we obtain

$$L(q) = q_{xx} - q_{xt}\frac{1}{2q^2(x,0)} + q_t\frac{q_x(x,0)}{2q^3(x,0)} = 0. \tag{4.17}$$

Equation, (4.17) is a nonlinear PDE with respect to the function $q(x,t)$ with nonlocal terms $q_x(x,0)$ and $q(x,0)$. We now need to obtain boundary conditions for the function q. By (4.2) and (4.5) $\tau(x) = x$ for $x \in [0,\varepsilon]$. Hence, (4.11), (4.12) and (4.13) lead to

$$q(\varepsilon,t) = g_0(t+\varepsilon), q_x(\varepsilon,t) = 2g_0'(t+\varepsilon),\ t \in (0,T), \tag{4.18}$$

We will solve equation (4.17) in the rectangle

$$\Omega = \{(x,t) : x \in (\varepsilon,b), t \in (0,T)\}. \tag{4.19}$$

By (4.13)

$$q_x(x,t) = u_x(x,t+\tau(x)) + u_t(x,t+\tau(x))\tau'(x) \tag{4.20}$$

By (4.1), (4.2) and (4.5) $\tau'(b) = 1$. Hence, using (4.9) and (4.20), we obtain

$$q_x(b,t) = 0. \tag{4.21}$$

It follows from (4.1) and (4.15) that

$$\frac{1}{2b^{1/4}} \leq q(x,0) \leq \frac{1}{2}, \quad x \in [\varepsilon,b]. \tag{4.22}$$

In addition, we need $q \in C^2(\overline{\Omega})$ and we also need to bound the norm $\|q\|_{C^2(\overline{\Omega})}$ from the above. Let $R > 0$ be an arbitrary number. We define the set $B(R,g_0)$ as

$$B(R,g_0) = \begin{cases} q \in H^4(\Omega) : \|q\|_{H^4(\Omega)} < R, \\ q(\varepsilon,t+\varepsilon) = g_0(t+\varepsilon), q_x(\varepsilon,t) = 2g_0'(t+\varepsilon), \\ q_x(b,t) = 0, \\ \frac{1}{2b^{1/4}} \leq q(x,0) \leq 1/2, x \in [\varepsilon,b]. \end{cases} \tag{4.23}$$

We assume below that

$$B(R, g_0) \neq \varnothing. \tag{4.24}$$

By embedding theorem $\overline{B(R, g_0)} \subset C^2(\overline{\Omega})$ and

$$\|q\|_{C^2(\overline{\Omega})} \leq KR, \ \forall q \in \overline{B(R, g_0)}. \tag{4.25}$$

where the constant $K = K(\Omega) > 0$ depends only on the domain Ω. Using (4.22), we define the function $q^0(x, 0)$ as:

$$\begin{array}{rcl} q^0(x,0) & = & \begin{cases} q(x,0) \ \text{ if } q(x,0) \in \left[1/\left(2b^{1/4}\right), 1/2\right], \\ 1/\left(2b^{1/4}\right), \ \text{ if } q(x,0) < 1/\left(2b^{1/4}\right), \qquad \forall q \in \overline{B(R, g_0)}, \\ 1/2 \text{ if } q(x,0) > 1/2. \end{cases} \\ \forall x & \in & [\varepsilon, b]. \end{array} \tag{4.26}$$

Then the function $q^0(x, 0)$ is piecewise continuously differentiable in $[\varepsilon, b]$ and by (4.25) and (4.26)

$$\left\|q^0(x,0)\right\|_{C[\varepsilon,b]}, \max_{[\varepsilon,b]} \left|q^0_x(x,0)\right| \leq KR, \ \forall q \in B(R, g_0), \tag{4.27}$$

$$\frac{1}{2b^{1/4}} \leq q^0(x,0) \leq \frac{1}{2}, \quad x \in [\varepsilon, b]. \tag{4.28}$$

Thus, (4.17), (4.18), (4.21), (4.26) and (4.28) result in the following BVP for a nonlinear PDE with non-local terms:

$$q_{xx}(x,t) - q_{xt}(x,t)\frac{1}{2\left(q^0(x,0)\right)^2} + q_t(x,t)\frac{q_x(x,0)}{2\left(q^0(x,0)\right)^3} = 0 \text{ in } \Omega, \tag{4.29}$$

$$q(\varepsilon, t) = g_0(t+\varepsilon), \ q_x(\varepsilon, t) = 2g_0'(t+\varepsilon), \ q_x(b, t) = 0. \tag{4.30}$$

Thus, we focus below on the numerical solution of the following problem:

Problem 3.1. *Find a function $q \in B(R, g_0)$ satisfying conditions (4.29), (4.30), where the function $q^0(x,0)$ is defined in (4.26).*

Suppose that we have solved Problem 3.1. Then, using (4.15) and (4.26), we set

$$c(x) = \frac{1}{\left(2q^0(x,0)\right)^4}. \tag{4.31}$$

4.4 Numerical Method for Problem 3.1

4.4.1 The function $q_0(x,t)$

We now find the first approximation $q_0(x,t)$ for the function $q(x,t)$. Using (4.2), we choose $c(x) \equiv 1$ as the first guess for the function $c(x)$. Hence, by (4.15),

$$q_0(x,0) \equiv \frac{1}{2}. \tag{4.32}$$

We now need to find the function $q_0(x,t)$. To do this, drop the nonlinear third term in the left hand side of equation (4.29) and, using (4.32) and (4.26), set $1/\left(2q^0(x,0)\right)^2 := 2$. Then (4.29), (4.30) become:

$$q_{0xx}(x,t) - 2q_{0xt}(x,t) = 0 \text{ in } \Omega, \tag{4.33}$$

$$q_0(\varepsilon,t) = g_0(t+\varepsilon),\ q_{0x}(\varepsilon,t) = 2g_0'(t+\varepsilon), q_{0x}(b,t) = 0. \tag{4.34}$$

BVP (4.33), (4.34) has overdetermined boundary conditions (4.34). Typically, QRM works well for BVPs for PDEs with overdetermined boundary conditions [19, 25]. Therefore, we solve BVP (4.33), (4.34) via CQRM. This means that we consider the following minimization problem:

Minimization Problem Number 0**.** *Assuming (4.24), minimize the functional*

$J^{(0)}_{\lambda,\beta} : \overline{B(R,g_0)} \to \mathbb{R}$ *on the set* ,

$$J^{(0)}_{\lambda,\beta}(q_0) = \int_\Omega \left(q_{0xx} - 2q_{0xt}\right)^2 e^{2\lambda\varphi} dxdt + \beta \|q_0\|^2_{H^4(\Omega)}, \tag{4.35}$$

where $e^{2\lambda\varphi}$ *is the Carleman Weight Function for the operator* $\partial_x - 2\partial_t$ [39, 40]

$$e^{2\lambda\varphi} = e^{-2\lambda(x+\alpha t)}, \tag{4.36}$$

where $\alpha \in (0, 1/2)$ *is the parameter, and* $\beta \in (0,1)$ *is the regularization parameter. Both parameters will be chosen later.*

Theorem 6.1 guarantees that for appropriate values of parameters λ, β, there exists unique minimizer $q_{0,\min}$ $\overline{B(R,g_0)}$ of the functional $J^{(0)}_{\lambda,\beta}(q_0)$.

4.4.2 The function $q_n(x,t)$ for $n \geq 1$

Assume that functionals $J^{(m)}_{\lambda,\beta}(q_m) : \overline{B(R,g_0)} \to \mathbb{R}$ are defined for $m = 0, ..., n-1$, and their minimizers functions $\{q_{m,\min}\}_{m=0}^{n-1} \subset \overline{B(R,g_0)}$ are constructed already, all for the same values of parameters λ, α, β. Replace in (4.29) $q(x,t)$ with $q_n(x,t), q^0(x,0)$ with $q^0_{n-1,\min}(x,0), q_x(x,t)$ with $\partial_x q_{(n-1),\min}(x,t)$ and $q_t(x,t)$ with $\partial_t q_{(n-1),\min}(x,t)$. Then problem (4.29), (4.30) becomes a linear one with respect to the function $q_n(x,t)$,

$$q_{nxx}(x,t) - \frac{q_{nxt}(x,t)}{2\left(q^0_{n-1,\min}(x,0)\right)^2} + \frac{\partial_t q_{(n-1),\min}(x,t)\,\partial_x q_{(n-1)\min}(x,0)}{2\left(q^0_{n-1,\min}(x,0)\right)^3} = 0 \text{ in } \Omega, \tag{4.37}$$

$$q_n(\varepsilon,t) = g_0(t+\varepsilon),\ q_{nx}(\varepsilon,t) = 2g_0'(t+\varepsilon), q_{nx}(b,t) = 0. \tag{4.38}$$

To solve problem (4.37), (4.38), we consider the following minimization problem:

Minimization Problem Number n**.** *Assuming (4.24), minimize the functional* $J^{(n)}_{\lambda,\beta} : H^4(\Omega) \to \mathbb{R}$ *on the set* $B(R,g_0)$,

$$J^{(n)}_{\lambda,\beta}(q_n) = \int_\Omega \Big(q_{nxx}(x,t) - \frac{q_{nxt}(x,t)}{2\big(q^0_{n-1,\min}(x,0)\big)^2} + \frac{\partial_t q_{(n-1),\min}(x,t)\,\partial_x q_{(n-1),\min}(x,0)}{2\big(q^0_{n-1,\min}(x,0)\big)^3}\Big)^2 e^{2\lambda\varphi} dxdt$$

$$+\beta \left\| q_n \right\|^2_{H^4(\Omega)}. \tag{4.39}$$

Suppose that there exists unique minimizer $q_{n,\min} \in \overline{B(R, g_0)}$ of the functional $J^{(n)}_{\lambda,\beta}(q_n)$. Then, following (4.31), (4.26) and (4.31), we set

$$c_n(x) = \frac{1}{\left(2q^0_{n,\min}(x,0)\right)^4}. \tag{4.40}$$

The rest of the analytical part of this chapter is devoted to the convergence analysis of the iterative numerical method presented in this section.

4.5 The Carleman Estimate

In this section, we formulate the Carleman estimate, which is the main tool of our construction. This estimate follows from Theorem 3.1 of [24] as well as from (4.27) and (4.28). Let $q(x,t) \in \overline{B(R, g_0)}$ be an arbitrary function and let the function $q^0(x,0)$ be constructed from the function $q(x,t)$ as in (4.26). Consider the operator $L_0 : H^2(\Omega) \to L_2(\Omega)$,

$$L_0 u = u_{xx}(x,t) - u_{xt}(x,t)\frac{1}{2\left(q^0(x,0)\right)^2}, \quad \text{for all } (x,t) \in \Omega.$$

Theorem 5.1 (Carleman estimate [24]). *There exists a number $\alpha_0 = \alpha_0(R,\Omega) > 0$ depending only on R, Ω such that for any $\alpha \in (0, \alpha_0)$ there exists a sufficiently large number $\lambda_0 = \lambda_0(R, \Omega, \alpha) > 1$ depending only on R,Ω, α such that for all $\lambda \geq \lambda_0$ and for all functions $v \in H^2(\Omega)$ the following Carleman estimate holds:*

$$\int_\Omega (L_0 v)^2 e^{2\lambda\varphi} dxdt$$

$$\geq C\int_\Omega \left(\lambda\left(v_x^2 + v_t^2\right) + \lambda^3 v^2\right) e^{2\lambda\varphi} dxdt + C\int_\varepsilon^b \left(\lambda v_x^2(x,0) + \lambda^3 v^2(x,0)\right) e^{-2\lambda x} dx$$

$$-C\int_0^T \left(\lambda\left(v_x^2(\varepsilon,t) + v_t^2(\varepsilon,t)\right) + \lambda^3 v^2(\varepsilon,t)\right) e^{-2\lambda(\varepsilon+\alpha t)} dt \tag{4.41}$$

$$-C\int_{\varepsilon}^{b}\left(\lambda v_x^2(x,T)+\lambda^3 v^2(x,T)\right)e^{-2\lambda(x+\alpha T)}dx.$$

Remark 5.1. *Here and everywhere below $C=C\left(R,\Omega,\alpha\right)>0$ denotes different constants depending only on listed parameters.*

4.6 Strict Convexity of Functional (4.39) on the Set $B(R,g_0)$, Existence and Uniqueness of Its Minimizer

Functional (4.39) is quadratic. We prove in this section that it is strictly convex on the set $\overline{B(R,g_0)}$. In addition, we prove existence and uniqueness of its minimizer on this set. Although similar results were proven in many of the above-cited publications on the convexification, see, e.g. [24] for the closest one, there are some peculiarities here, which are important for our convergence analysis, see Remarks 6.1, and 6.2 below.

Introduce the subspace $H_0^4\left(\Omega\right)\subset H^4\left(\Omega\right)$ as:

$$H_0^4\left(\Omega\right)=\left\{v\in H^4\left(\Omega\right):v\left(\varepsilon,t\right)=v_x\left(\varepsilon,t\right)=v_x\left(b,t\right)=0\right\}. \tag{4.42}$$

Denote $[,]$ the scalar product in the space $H^4\left(\Omega\right)$. Also, denote

$$A_n\left(q\right)\left(x,t\right)=q_{xx}(x,t)-q_{xt}(x,t)\frac{1}{2\left(q_{n-1,\min}^0(x,0)\right)^2}, \tag{4.43}$$

$$B_n\left(x,t\right)=\partial_t q_{(n-1),\min}\left(x,t\right)\frac{\partial_x q_{(n-1),\min}(x,0)}{2\left(q_{n-1,\min}^0(x,0)\right)^3}. \tag{4.44}$$

Theorem 6.1. *Let $J_{\lambda,\beta}^{(n)}$ be the functional defined in (4.39).* Then:

1. For any set of parameters λ,β and for any $q\in\overline{B(R,g_0)}$ this functional has the Frechet derivative $\left(J_{\lambda,\beta}^{(n)}(q)\right)'\in H_0^4\left(\Omega\right)$. The formula for $\left(J_{\lambda,\beta}^{(n)}(q)\right)'$ is:

$$\left(J_{\lambda,\beta}^{(n)}(q)\right)'(h)$$

$$= 2\int_{\Omega} \left(A_n\left(q\right)\left(x,t\right) + B_n\left(x,t\right)\right) A_n\left(h\right)\left(x,t\right) e^{2\lambda\varphi} dxdt + 2\beta\left[q,h\right],\ \forall h \in H_0^4\left(\Omega\right). \tag{4.45}$$

2. *This derivative is Lipschitz continuous in* $\overline{B(R,g_0)}$*, i.e. there exists a constant* $D > 0$ *such that*

$$\left\| \left(J^{(n)}_{\lambda,\beta}(q_2)\right)' - \left(J^{(n)}_{\lambda,\beta}(q_1)\right)' \right\|_{H^4(\Omega)} \leq D\left\|q_2 - q_1\right\|_{H^4(\Omega)}, \quad \text{for all } q_1, q_2 \in \overline{B(R,g_0)}. \tag{4.46}$$

3. Let $\alpha_0 = \alpha_0\left(R,\Omega\right) > 0, \alpha \in \left(0,\alpha_0\right)$ *and* $\lambda_0 = \lambda_0\left(R,\Omega,\alpha\right) \geq 1$ *be the numbers of Theorem 5.1. Then there exists a sufficiently large constant*

$$\lambda_1 = \lambda_1\left(R,\Omega,\alpha\right) \geq \lambda_0 > 1 \tag{4.47}$$

depending only on listed parameters such that for all $\lambda \geq \lambda_1$ *and for all* $\beta \in \left[2e^{-\lambda\alpha T}, 1\right)$ *the functional* $J^{(n)}_{\lambda,\beta}(q)$ *is strictly convex on the set* $\overline{B\left(R,g\right)}$*. More precisely, let* $q \in \overline{B(R,g)}$ *be an arbitrary function and also let the function* $q + h \in \overline{B(R,g)}$*. Then the following inequality holds:*

$$J^{(n)}_{\lambda,\beta}(q+h) - J^{(n)}_{\lambda,\beta}(q) - \left(J^{(n)}_{\lambda,\beta}(q)\right)'(h) \geq C\int_{\Omega}\left[\lambda\left(h_x^2 + h_t^2\right) + \lambda^3 h^2\right] e^{2\lambda\varphi} dxdt$$

$$+C\int_{\varepsilon}^{b}\left(\lambda h_x^2(x,0) + \lambda^3 h^2(x,0)\right) e^{-2\lambda x} dx + \frac{\beta}{2}\left\|h\right\|^2_{H^4(\Omega)},\ \forall \lambda \geq \lambda_1. \tag{4.48}$$

4. For any $\lambda \geq \lambda_1$ *there exists unique minimizer*

$$q_{n,\min} \in \overline{B(R,g_0)} \tag{4.49}$$

of the functional $J^{(n)}_{\lambda,\beta}(q)$ *on the set* $\overline{B(R,g_0)}$*. Furthermore, the following inequality holds:*

$$\left[\left(J^{(n)}_{\lambda,\beta}(q)\right)', q - q_{n,\min}\right] \geq 0,\ \forall q \in \overline{B(R,g_0)}. \tag{4.50}$$

Remark 6.1. *Even though the expression on the right-hand side of (4.45) is linear with respect to the function q, we cannot use Riesz theorem here to prove the existence and uniqueness of the minimizer $q_{n,\min}$, at which $\left(J^{(n)}_{\lambda,\beta}(q_{n,\min})\right)' = 0$. Rather, all what we can prove is (4.50). This is because we need to ensure that the function $q_{n,\min} \in \overline{B(R,g_0)}$.*

Proof of Theorem 6.1. Since both function $q, q+h \in \overline{B(R,g)}$ satisfy the same boundary conditions, then

$$h \in H_0^4(\Omega). \tag{4.51}$$

By (4.39) and (4.51)

$$J^{(n)}_{\lambda,\beta}(q+h) - J^{(n)}_{\lambda,\beta}(q) = 2\int_\Omega \left(A_n(q)(x,t) + B_n(x,t)\right) A_n(h)(x,t)\, e^{2\lambda\varphi} dxdt + 2\beta[q,h]$$

$$+ \int_\Omega \left[A_n(h)(x,t)\right]^2 e^{2\lambda\varphi} dxdt + \beta \|h\|^2_{H^4(\Omega)},\ \forall h \in H_0^4(\Omega). \tag{4.52}$$

The expression in the first line of (4.52) coincides with the expression in the right-hand side of (4.45). In fact, this is a bounded linear functional mapping $H_0^4(\Omega)$ in $\mathbb{R}$. Therefore, by Riesz theorem, there exists a unique function $\widetilde{J}_n(q) \in H_0^4(\Omega)$ such that

$$\left[\widetilde{J}_n(q), h\right] =$$

$$= 2\int_\Omega \left(A_n(q)(x,t) + B_n(x,t)\right) A_n(h)(x,t)\, e^{2\lambda\varphi} dxdt + 2\beta[q,h],\ \forall h \in H_0^4(\Omega). \tag{4.53}$$

In addition, it is clear from (4.52) and (4.53) that

$$\lim_{\|h\|_{H^4(\Omega)} \to 0} \left\{ \frac{1}{\|h\|_{H^4(\Omega)}} \left[J^{(n)}_{\lambda,\beta}(q+h) - J^{(n)}_{\lambda,\beta}(q) - \left[\widetilde{J}_n(q), h\right] \right] \right\} = 0.$$

Therefore,

$$\widetilde{J}_n(q) = \left(J^{(n)}_{\lambda,\beta}(q)\right)' \in H_0^4(\Omega) \tag{4.54}$$

is the Frechet derivative of the functional $J^{(n)}_{\lambda,\beta}(q) : \overline{B(R,g_0)} \to \mathbb{R}$ at the point $q \in \overline{B(R,g_0)}$, and the right hand side of (4.45) indeed represents $\left(J^{(n)}_{\lambda,\beta}(q)\right)'(h)$. Estimate (4.46) obviously follows from (4.45).

We now prove a strict convexity estimate (4.48). To do this, we apply Carleman estimate (4.41) to the third line of (4.52). We obtain

$$\begin{aligned} &J^{(n)}_{\lambda,\beta}(q+h) - J^{(n)}_{\lambda,\beta}(q) - \left(J^{(n)}_{\lambda,\beta}(q)\right)'(h) \\ &\quad \geq C\int_\Omega \left(\lambda\left(h_x^2+h_t^2\right)+\lambda^3 h^2\right)e^{2\lambda\varphi}dxdt + C\int_\varepsilon^b \left(\lambda h_x^2(x,0)+\lambda^3 h^2(x,0)\right)e^{-2\lambda x}dx \\ &- C\int_\varepsilon^b \left(\lambda h_x^2(x,T)+\lambda^3 h^2(x,T)\right)e^{-2\lambda(x+\alpha T)}dx + \beta\left\|h\right\|^2_{H^4(\Omega)},\ \forall h \in H_0^4(\Omega). \quad (4.55) \end{aligned}$$

By trace theorem there exists a constant $C_1 = C_1(\Omega) > 0$ depending only on the domain Ω such that

$$\left\|v\right\|^2_{H^4(\Omega)} \geq C_1\left\|v(x,T)\right\|^2_{H^1(\Omega)},\ \forall v \in H^4(\Omega).$$

Since the regularization parameter $\beta \in \left[2e^{-\lambda\alpha T},1\right)$, then we can choose λ_1 so large that

$$\frac{\beta}{2}C_1 \geq C_1 e^{-\lambda\alpha T} > Ce^{-2\lambda(x+\alpha T)},\ \forall \lambda \geq \lambda_1, \forall x \in [\varepsilon,b].$$

Hence, for these values of λ, the expression in the last line of (4.55) can be estimated from the below as:

$$-C\int_\varepsilon^b \left(\lambda h_x^2(x,T)+\lambda^3 h^2(x,T)\right)e^{-2\lambda(x+\alpha T)}dx + \beta\left\|h\right\|^2_{H^4(\Omega)} \geq \frac{\beta}{2}\left\|h\right\|^2_{H^4(\Omega)},\ \forall h \in H_0^4(\Omega). \quad (4.56)$$

Hence, (4.55) and (4.56) imply

$$J^{(n)}_{\lambda,\beta}(q+h) - J^{(n)}_{\lambda,\beta}(q) - \left(J^{(n)}_{\lambda,\beta}(q)\right)'(h) \geq C\int_{\Omega}\left(\lambda\left(h_x^2+h_t^2\right)+\lambda^3h^2\right)e^{2\lambda\varphi}dxdt$$
$$+ C\int_{\varepsilon}^{b}\left(\lambda h_x^2(x,0)+\lambda^3h^2(x,0)\right)e^{-2\lambda x}dx + \frac{\beta}{2}\left\|h\right\|^2_{H^4(\Omega)}, \forall\lambda\geq\lambda_1.$$

This proves (4.48). The existence and uniqueness of the minimizer $q_{\min,n}\in\overline{B(R,g_0)}$ and inequality (4.50) follow from (4.48) as well as from a combination of Lemma 2.1 and Theorem 2.1 of [1], also see [33, Chapter 10, section 3]. □

Remark 6.2. *Since the functional $J^{(n)}_{\lambda,\beta}(q)$ is quadratic, then its strict convexity on the whole space $H^4(\Omega)$ follows immediately from the presence of the regularization term $\beta\left\|q_n\right\|^2_{H^4(\Omega)}$ in it. However, in addition to the claim of its strict convexity, we actually need it in our convergence analysis below those terms on the right-hand side of the strict convexity estimate (4.48), which are different from the term $\beta\left\|h\right\|^2_{H^4(\Omega)}/2$. These terms are provided by Carleman estimate (4.48). The condition $\beta\in\left[2e^{-\lambda\alpha T},1\right)$ of Theorem 6.1 is imposed to dominate the negative term in the last line of (4.55): see (4.56).*

4.7 How to Find the Minimizer

Since we search for the minimizer $q_{n,\min}$ of functional (4.39) on the bounded set $\overline{B(R,g_0)}$ rather than on the whole space $H^4(\Omega)$, then we cannot just use Riesz theorem to find this minimizer, also see [1] and [33, Chapter 10, section 3] for the case of finding a minimizer of a strictly convex functional on a bounded set. Two ways of finding the minimizer $q_{n,\min}\in\overline{B(R,g_0)}$ are described in this section.

4.7.1 Gradient descent method

Keeping in mind (4.24), choose an arbitrary function $q_{0,n} \in B(R, g_0)$. We arrange the gradient descent method for the minimization of functional (4.39) as follows:

$$q_{k,n} = q_{(k-1),n} - \eta \left(J^{(n)}_{\lambda,\beta}(q_{(k-1),n}) \right)', \ k = 1, 2, ..., \tag{4.57}$$

where $\eta \in (0,1)$ is a small number, which is chosen later. It is important to note that since functions $J^{(n)}_{\lambda,\beta}(q_{(k-1),n}) \in H^4_0(\Omega)$, then boundary conditions (4.38) are kept the same for all functions $q_{k,n}(x,t)$. Also, using (4.26) and (4.40), we set

$$c_{k,n}(x) = \frac{1}{\left(2q^0_{k,n}(x,0)\right)^4}, \ x \in [\varepsilon, b], \tag{4.58}$$

$$c_{n,\min}(x) = \frac{1}{\left(2q^0_{n,\min}(x,0)\right)^4}, \ x \in [\varepsilon, b]. \tag{4.59}$$

Theorem 7.1 claims the global convergence of the gradient descent method (4.57) to the pair $(q_{n,\min}, c_{n,\min})$ in the case when $q_{\min,n} \in B(R/3, g_0)$, see Remark 7.2.

Theorem 7.1. *Let the number $\lambda_1 = \lambda_1(R, \Omega, \alpha) \geq \lambda_0 > 1$ be the one defined in (4.47). Let $\lambda \geq \lambda_1$. For this value of λ, let $q_{n,\min} \in \overline{B(R, g_0)}$ be the unique minimizer of the functional $J^{(n)}_{\lambda,\beta}(q_n)$ on the set $\overline{B(R, g_0)}$ with the regularization parameter $\beta \in \left[2e^{-\lambda\alpha T}, 1\right)$ (Theorem 6.1). Assume that the function $q_{n,\min} \in B(R/3, g_0)$. For each n, choose the starting point of the gradient descent method (4.57) as $q_{0,n} \in B(R/3, g_0)$. Then, there exists a number $\eta_0 \in (0,1)$ such that for any $\eta \in (0, \eta_0)$ all functions $q_{k,n} \in B(R, g_0)$. Furthermore, there exists a number $\theta = \theta(\eta) \in (0,1)$ such that the following convergence estimates are valid:*

$$\|q_{k,n} - q_{n,\min}\|_{H^4(\Omega)} \leq \theta^k \|q_{0,n} - q_{n,\min}\|_{H^4(\Omega)}, k = 1, ..., \tag{4.60}$$

$$\|c_{k,n} - c_{n,\min}\|_{H^3(\varepsilon,b)} \leq C\theta^k \|q_{0,n} - q_{n,\min}\|_{H^4(\Omega)}, \ k = 1, ... \tag{4.61}$$

Proof. Estimate (4.60) follows immediately from [21, Theorem 4.6] combined with "corrections" of functions $q_{k,n}(x,0), q_{n,\min}(x,0)$ via (4.26). Estimate (4.61) follows immediately from trace theorem, (4.26) and (4.58)-(4.60). $\square$

4.7.2 Gradient projection method

Suppose now that there is no information on whether or not the function $q_{n,\min} \in B(R/3, g_0)$. In this case we construct the gradient projection method. We introduce the function $F(x,t)$ below since it is easy to construct the projection operator on a ball with the center at $\{0\}$.

Consider the function $\chi(x)$ such that

$$\chi(x) \in C^4[\varepsilon, b], \chi(x) = \begin{cases} 1, x \in [\varepsilon, b/4], \\ 0, x \in [b/2, b], \\ \text{between 0 and 1 for } x \in (b/4, b/2). \end{cases}$$

The existence of such functions $\chi(x)$ is well known from the Real Analysis course. Suppose that the function $g_0(t) \in H^5(0, T+\varepsilon)$. Define the function $F \in H^4(\Omega)$ as

$$F(x,t) = \chi(x)\left(g_0(t+\varepsilon) + 2x g_0'(t+\varepsilon)\right).$$

Then

$$F(\varepsilon,t) = g_0(t+\varepsilon),\ F_x(\varepsilon,t) = 2g_0'(t+\varepsilon),\ F_x(b,t) = 0. \tag{4.62}$$

Denote

$$p_n(x,t) = q_n(x,t) - F(x,t). \tag{4.63}$$

Then (4.37), (4.38) become:

$$p_{nxx}(x,t) - p_{nxt}(x,t)\frac{1}{2\left(q^0_{n-1,\min}(x,0)\right)^2} \tag{4.64}$$

$$+F_{xx}(x,t)-F_{xt}(x,t)\frac{1}{2\left(q^0_{n-1,\min}(x,0)\right)^2}+\partial_t q_{(n-1),\min}(x,t)\,\frac{\partial_x q_{(n-1),\min}(x,0)}{2\left(q^0_{n-1,\min}(x,0)\right)^3}=0 \text{ in } \Omega,$$

$$p_n(\varepsilon,t)=0,\ p_{nx}(\varepsilon,t)=0, p_{nx}(b,t)=0. \tag{4.65}$$

Assume that

$$\|F\|_{H^4(\Omega)}<R. \tag{4.66}$$

By (4.62), (4.63), (4.65), (4.66) and triangle inequality

$$p_n\in B_0(2R)=\left\{p\in H^4_0(\Omega):\|p\|_{H^4_0(\Omega)}<2R\right\}. \tag{4.67}$$

To find the function $p_n\in B_0(2R)$ satisfying conditions (4.64), (4.65), we minimize the following functional $I^{(n)}_{\lambda,\beta}(p_n):\overline{B_0(2R)}\to\mathbb{R}$

$$I^{(n)}_{\lambda,\beta}(p_n)=J^{(n)}_{\lambda,\beta}(p_n+F),\ p_n\in B_0(2R). \tag{4.68}$$

Remark 7.1. *An obvious analog of Theorem 6.1 is valid of course for the functional $I^{(n)}_{\lambda,\beta}(p_n)$ defined in (4.68). But in this case, we should have instead of (4.47) $\lambda\geq\widetilde{\lambda}_1=\lambda_1(2R,\Omega,\alpha)\geq\lambda_0>1$. In particular, there exists unique minimizer $p_{n,\min}\in\overline{B_0(2R)}$ of this functional on the closed ball $\overline{B_0(2R)}$. We omit the formulation of this theorem since it is an obvious reformulation of Theorem 6.1.*

Let $P_{\overline{B_0(2R)}}:H^4_0(\Omega)\to\overline{B_0(2R)}$ be the projection operator of the space $H^4_0(\Omega)$ on the closed ball $\overline{B_0(2R)}\subset H^4_0(\Omega)$. Then this operator can be easily constructed:

$$P_{\overline{B_0(2R)}}(p)=\begin{cases} p \text{ if } p\in\overline{B_0(2R)},\\ \frac{2R}{\|p\|_{H^4(\Omega)}}p \text{ if } p\notin\overline{B_0(2R)}.\end{cases}$$

We now construct the gradient projection method of the minimization of the functional $I^{(n)}_{\lambda,\beta}(p_n)$ on the set $\overline{B_0(2R)}$. Let $p_{0,n}\in B_0(2R)$ be an arbitrary function. Then

the sequence of the gradient projection method is:

$$p_{k,n} = P_{\overline{B_0(2R)}}\left(p_{(k-1),n} - \eta\left(I^{(n)}_{\lambda,\beta}(p_{(k-1),n})\right)'\right),\ k = 1, 2, ..., \tag{4.69}$$

where $\eta \in (0,1)$ is a small number, which is chosen later. Using (4.58), (4.59) and (4.63), we set

$$\widetilde{c}_{k,n}(x) = \frac{1}{\left(2\widetilde{q}^{0}_{k,n}(x,0)\right)^4},\ x \in [\varepsilon, b], \tag{4.70}$$

$$\widetilde{c}_{n,\min}(x) = \frac{1}{\left(2\widetilde{q}^{0}_{n,\min}(x,0)\right)^4},\ x \in [\varepsilon, b]. \tag{4.71}$$

Here the function $\widetilde{q}^{0}_{n,k}(x,0)$ is obtained as follows: First, we consider the function $(p_{n,k} + F)(x,0)$. Next, we apply procedure (4.26) to this function. Similarly for $\widetilde{q}^{0}_{n,\min}(x,0)$.

Denote $p_{n,\min} \in \overline{B_0(2R)}$ the unique minimizer of functional (4.68) on the set $\overline{B_0(2R)}$ (Remark 7.1). Following (4.63), denote

$$\widetilde{q}_{n,\min} = p_{n,\min} + F,\ \widetilde{q}_{k,n} = p_{k,n} + F. \tag{4.72}$$

We omit the proof of Theorem 7.2 since it is very similar to the proof of Theorem 7.1. The only difference is that instead of Theorem 4.6 of [21] one should use Theorem 4.1 of [24].

Theorem 7.2. *Let (4.62), (4.66) hold. Let the number* $\lambda_1 = \lambda_1(R, \Omega, \alpha) \geq \lambda_0 > 1$ *be the one defined in (4.47) and let*

$$\lambda \geq \widetilde{\lambda}_1 = \lambda_1(2R, \Omega, \alpha) \geq \lambda_1(R, \Omega, \alpha).$$

For this value of λ *and for* $\beta \in \left[2e^{-\lambda\alpha T}, 1\right)$ *let* $p_{n,\min} \in \overline{B_0(2R)}$ *be the unique minimizer of functional (4.68) on the set* $\overline{B_0(2R)}$ *(Remark 7.1). Let notations (4.70) hold. For each* n*, choose the starting point of the gradient projection method (4.57)*

as $p_{0,n} \in B_0(2R)$. *Then there exists a number* $\eta_0 \in (0,1)$ *such that for any* $\eta \in (0,\eta_0)$ *there exists a number* $\theta = \theta(\eta) \in (0,1)$ *such that the following convergence estimates are valid for the iterative process (4.69):*

$$\|\widetilde{q}_{k,n} - \widetilde{q}_{n,\min}\|_{H^4(\Omega)} \leq \theta^k \|\widetilde{q}_{0,n} - \widetilde{q}_{n,\min}\|_{H^4(\Omega)},$$

$$\|\widetilde{c}_{k,n} - \widetilde{c}_{n,\min}\|_{H^4(\Omega)} \leq C\theta^k \|\widetilde{q}_{0,n} - \widetilde{q}_{n,\min}\|_{H^4(\Omega)},$$

where functions $\widetilde{c}_{k,n}, \widetilde{c}_{n,\min}, \widetilde{q}_{k,n}, \widetilde{q}_{n,\min}$ *are defined in (4.70)-(4.72).*

Remark 7.2. *Both Theorems 7.1 and 7.2 claim the global convergence of corresponding versions of the gradient method to pairs* $(q_{n,\min}, c_{n,\min})$ *and* $(\widetilde{q}_{n,\min}, \widetilde{c}_{n,\min})$. *This is because the starting function in both cases is an arbitrary one either in* $B(R/3, g_0)$ *or in* $B_0(2R)$ *and a smallness condition is not imposed on the number* R. *Also, see the second item of Remarks 8.1 and our definition of the global convergence in Introduction.*

4.8 Contraction Mapping and Global Convergence

In this section, we prove the global convergence of the numerical method of section 4 for solving Problem 3.1. To do this, we first introduce the exact solution of our CIP. Recall that the concept of the existence of the exact solution is one of the main concepts of the theory of ill-posed problems [5, 41]. In particular, an estimate in our global convergence theorem is very similar to the one in contraction mapping.

Suppose that there exists a function $c^*(x)$ satisfying conditions (4.1), (4.2). Let $u^*(x,t)$ be the solution of problem (4.3), (4.4) with $c := c^*$. We assume that the corresponding data $g_0^*(t), \partial_t g_0^*(t)$ for the CIP are noiseless, see (4.11), (4.12). Let $q^*(x,t)$ be the function $q^*(x,t)$ which is constructed from the function $u^*(x,t)$ as in (4.13). Following (4.23), we assume that

$$q^* \in B(R, g_0^*), \tag{4.73}$$

$$B(R,g_0^*)=\left\{\begin{array}{c} q\in H^4(\Omega):\|q\|_{H^4(\Omega)}<R, \\ q(\varepsilon,t+\varepsilon)=g_0^*(t+\varepsilon), q_x(\varepsilon,t)=2\left(g_0^*\right)'(t+\varepsilon), \\ q_x(b,t)=0, \\ \frac{1}{2b^{1/4}}\leq q(x,0)\leq 1/2, x\in[\varepsilon,b] \end{array}\right\}. \tag{4.74}$$

By (4.29)-(4.30)

$$q_{xx}^*(x,t)-q_{xt}^*(x,t)\frac{1}{2\left(q^*(x,0)\right)^2}+q_t^*(x,t)\frac{q_x^*(x,0)}{2\left(q^*(x,0)\right)^3}=0 \text{ in } \Omega, \tag{4.75}$$

$$q^*(\varepsilon,t)=g_0^*(t+\varepsilon),\ q_x^*(\varepsilon,t)=2\partial_t g_0^*(t+\varepsilon), q_x^*(b,t)=0. \tag{4.76}$$

By (4.15)

$$c^*(x)=\frac{1}{\left(2q^*(x,0)\right)^4}. \tag{4.77}$$

It is important in the formulation of Theorem 6.1 that both functions q and $q+h$ should have the same boundary conditions as prescribed in $B(R,g_0)$. However, boundary conditions for functions q_n and q^* are different. Hence, similarly to subsection 7.2, we consider a function $F^*\in H^4(\Omega)$ such that (see (4.62))

$$F^*(\varepsilon,t)=g_0^*(t+\varepsilon),\ F_x^*(\varepsilon,t)=2\partial_t g_0^*(t+\varepsilon),\ F_x^*(b,t)=0. \tag{4.78}$$

We assume similarly to (4.66) that

$$\|F^*\|_{H^4(\Omega)}<R. \tag{4.79}$$

Also, similarly to (4.63), we introduce the function $p^*(x,t)$ as:

$$p^*(x,t)=q^*(x,t)-F^*(x,t). \tag{4.80}$$

Let λ_1 be the number defined in (4.47), let $\lambda\geq\lambda_1$ and the function $q_{n,\min}\in\overline{B(R,g_0)}$

(see (4.49)) be the unique minimizer of the functional $J^{(n)}_{\lambda,\beta}(q_n)$ on the set $\overline{B(R,g_0)}$, the existence of which is established in Theorem 6.1. Following (4.63), denote

$$p_{n,\min}(x,t) = q_{n,\min}(x,t) - F(x,t). \tag{4.81}$$

By (4.49), (4.67), (4.73), (4.74) and (4.79)-(4.81)

$$p_{n,\min}, p^* \in \overline{B_0(2R)}. \tag{4.82}$$

Also, it follows from embedding theorem, (4.25), (4.49), (4.66), (4.79) and (4.82) that

$$\|q^*\|_{C^2(\overline{\Omega})}, \|p^*\|_{C^2(\overline{\Omega})}, \|q_{n,\min}\|_{C^2(\overline{\Omega})}, \|p_{n,\min}\|_{C^2(\overline{\Omega})} \leq C. \tag{4.83}$$

We assume that the data g_0, g_0' for our CIP are given with noise of the level δ, where the number $\delta > 0$ is sufficiently small. More precisely, we assume that

$$\|F - F^*\|_{H^4(\Omega)} < \delta. \tag{4.84}$$

Observe that (4.26), (4.73) and (4.74) imply that

$$\left|q^0_{n-1,\min}(x,0) - q^*(x,0)\right| \leq \left|q_{n-1,\min}(x,0) - q^*(x,0)\right|, \ x \in [\varepsilon, b]. \tag{4.85}$$

By (4.75), (4.76), (4.78) and (4.80)

$$p^*_{xx}(x,t) - p^*_{xt}(x,t)\frac{1}{2\left(q^*(x,0)\right)^2} + q^*_t(x,t)\frac{q^*_x(x,0)}{2\left(q^*(x,0)\right)^3} + F^*_{xx} - F^*_{xt}(x,t)\frac{1}{2\left(q^*(x,0)\right)^2} = 0 \tag{4.86}$$

in $\Omega \times [0,T]$ and

$$p^*(\varepsilon,t) = p^*_x(\varepsilon,t) = p^*_x(b,t) = 0. \tag{4.87}$$

Theorem 8.1 (contraction mapping and the global convergence of the method of

section 3). *Let functions* $F,F^* \in H^4(\Omega)$ *satisfy conditions (4.62), (4.66), (4.78), (4.79) and (4.84). Let a sufficiently large number* $\lambda_1 = \lambda_1(R,\Omega,\alpha) \geq \lambda_0 > 1$ *be the one defined in (4.47). Let*

$$\lambda \geq \widetilde{\lambda}_1 = \lambda_1(2R,\Omega,\alpha) \geq \lambda_1(R,\Omega,\alpha). \tag{4.88}$$

For this value of λ, *let* $q_{n,\min} \in \overline{B(R,g_0)}$ *be the unique minimizer of the functional* $J^{(n)}_{\lambda,\beta}(q_n)$ *on the set* $\overline{B(R,g_0)}$ *with the regularization parameter* $\beta \in \left[2e^{-\lambda\alpha T},1\right)$ *(Theorem 6.1). Let*

$$\overline{q}_n = q_{n,\min} - q^*,\ \overline{c}_n = c_{n,\min} - c^*, \tag{4.89}$$

where $c_{n,\min}$ *is defined in (4.59). Then the following convergence estimate holds*

$$\begin{aligned}
&\int_\Omega \left(\overline{q}^2_{nx} + \overline{q}^2_{nt} + \overline{q}^2_n\right)(x,t)\, e^{2\lambda\varphi} dxdt + \int_\varepsilon^b \left(\overline{q}^2_{nx} + \overline{q}^2_n\right)(x,0)\, e^{-2\lambda x} dx \\
&\leq \frac{C}{\lambda}\int_\Omega \left(\overline{q}^2_{(n-1)x} + \overline{q}^2_{(n-1)t} + \overline{q}^2_{n-1}\right)(x,t)\, e^{2\lambda\varphi} dxdt \qquad (4.90)\\
&+\frac{C}{\lambda}\int_\varepsilon^b \left(\overline{q}^2_{(n-1)x}(x,0) + \overline{q}^2_{n-1}\right)(x,0)\, e^{-2\lambda x} dx + C\left(\delta^2+\beta\right),
\end{aligned}$$

which leads to:

$$\begin{aligned}
&\int_\Omega \left(\overline{q}^2_{nx} + \overline{q}^2_{nt} + \overline{q}^2_n\right)(x,t)\, e^{2\lambda\varphi} dxdt \qquad (4.91)\\
&\leq \frac{C^n}{\lambda^n}\int_\Omega \left(\overline{q}^2_{0x} + \overline{q}^2_{0t} + \overline{q}^2_0\right)(x,t)\, e^{2\lambda\varphi} dxdt + C\left(\delta^2+\beta\right).
\end{aligned}$$

In addition,

$$\|\overline{c}_n\|^2_{H^1(\varepsilon,b)} \leq \frac{C^n}{\lambda^n}\int_\Omega \left(\overline{q}^2_{0x} + \overline{q}^2_{0t} + \overline{q}^2_0\right)(x,t)\, e^{2\lambda\varphi} dxdt + C\left(\delta^2+\beta\right). \tag{4.92}$$

Remarks 8.1:

1. *Due to the presence of the term* C/λ *with a sufficiently large* λ, *estimate (4.90)*

is similar to the one in the classical contraction mapping principle, although we do not claim here the existence of the fixed point.

2. When computing the unique minimizer $q_{0,\min}$ *of functional (4.35) on the set* $\overline{B(R,g_0)}$*, we do not impose a smallness condition on the number* R*. Therefore, Theorem 8.1 claims the global convergence of the method of section 4: see our definition of the global convergence in Introduction. The same is true for Theorems 9.1 and 9.2 in section 9.*

Proof Theorem 8.1. Denote $h_n = p^* - p_{n,\min}$. By (4.81) $h_n = -\overline{q}_n + (F - F^*)$. Hence, (4.84) and embedding theorem imply:

$$h_n^2 \geq \frac{1}{2}\overline{q}_n^2 - C\delta^2, h_{nx}^2 \geq \frac{1}{2}\overline{q}_{nx}^2 - C\delta^2, h_{nt}^2 \geq \frac{1}{2}\overline{q}_{nt}^2 - C\delta^2 \text{ in } \overline{\Omega}, \tag{4.93}$$

$$h_n^2 + h_{nx}^2 + h_{nt}^2 \leq C\left(\overline{q}_n^2 + \overline{q}_{nx}^2 + \overline{q}_{nt}^2 + \delta^2\right) \text{ in } \overline{\Omega}. \tag{4.94}$$

Consider the functional $I_{\lambda,\beta}^{(n)}(p^*) = J_{\lambda,\beta}^{(n)}(p^* + F)$. Since both functions $p_{n,\min}$ and p^* have the same zero boundary conditions (4.65) and since by (4.82) both of them belong to the set $\overline{B_0(2R)}$, then the analog of Theorem 6.1, which is mentioned in Remark 7.1, implies (see (4.48))

$$\begin{aligned} &I_{\lambda,\beta}^{(n)}(p^*) - I_{\lambda,\beta}^{(n)}(p_{n,\min}) - \left(I_{\lambda,\beta}^{(n)}(p_{n,\min})\right)'(h_n) \\ &\geq C\int_\Omega \left[\lambda\left(h_{nx}^2 + h_{nt}^2\right) + \lambda^3 h_n^2\right] e^{2\lambda\varphi} dxdt \\ &+C\int_\varepsilon^b \left(\lambda h_{nx}^2(x,0) + \lambda^3 h_n^2(x,0)\right) e^{-2\lambda x} dx + \frac{\beta}{2}\left\|h_n\right\|_{H^4(\Omega)}^2, \ \forall \lambda \geq \widetilde{\lambda}_1. \end{aligned} \tag{4.95}$$

By (4.50)

$$-\left(I_{\lambda,\beta}^{(n)}(p_{n,\min})\right)'(h_n) \leq 0.$$

Hence, the left hand side of (4.95) can be estimated as:

$$I^{(n)}_{\lambda,\beta}(p^*) - I^{(n)}_{\lambda,\beta}(p_{n,\min}) - \left(I^{(n)}_{\lambda,\beta}(p_{n,\min})\right)'(h) \leq I^{(n)}_{\lambda,\beta}(p^*). \tag{4.96}$$

We now estimate the right-hand side of (4.96) from the above. It follows from (4.39), (4.68) and (4.75) that

$$I^{(n)}_{\lambda,\beta}(p^*) = \int_\Omega G_n^2 e^{2\lambda\varphi} dxdt + \beta \left\| p^* + F \right\|^2_{H^4(\Omega)}, \tag{4.97}$$

where

$$\begin{aligned} G_n = {} & p^*_{xx}(x,t) - p^*_{xt}(x,t)\frac{1}{2\left(q^0_{(n-1),\min}(x,0)\right)^2} + \partial_t q_{(n-1),\min}(x,t)\,\frac{\partial_x q_{(n-1),\min}(x,0)}{2\left(q^0_{(n-1),\min}(x,0)\right)^3} \\ & + F_{xx} - F_{xt}(x,t)\frac{1}{2\left(q^0_{(n-1),\min}(x,0)\right)^2} \\ = {} & q^*_{xx}(x,t) - q^*_{xt}(x,t)\frac{1}{2\left(q^*(x,0)\right)^2} + q^*_t(x,t)\frac{q^*_x(x,0)}{2\left(q^*(x,0)\right)^3} \\ & + (F-F^*)_{xx} - (F-F^*)_{xt}\,\frac{1}{2\left(q^0_{(n-1),\min}(x,0)\right)^2} \\ & - q^*_{xt}\left(\frac{1}{2\left(q^0_{(n-1),\min}(x,0)\right)^2} - \frac{1}{2\left(q^*(x,0)\right)^2}\right) \\ & + \left(\partial_t q_{(n-1),\min}(x,t)\,\frac{\partial_x q_{(n-1),\min}(x,0)}{2\left(q^0_{(n-1),\min}(x,0)\right)^3} - q^*_t(x,t)\frac{q^*_x(x,0)}{2\left(q^*(x,0)\right)^3}\right). \end{aligned} \tag{4.98}$$

By (4.75), the third line of (4.98) equals zero. Hence, (4.98) becomes

$$G_n = (F-F^*)_{xx} + (F-F^*)_{xt}\,\frac{1}{2\left(q^0_{(n-1),\min}(x,0)\right)^2}$$

$$-q^*_{xt}\left(\frac{1}{2\left(q^0_{(n-1),\min}(x,0)\right)^2}-\frac{1}{2\left(q^*(x,0)\right)^2}\right)$$

$$+\left(\partial_t q_{(n-1),\min}(x,t)\,\frac{\partial_x q_{(n-1),\min}(x,0)}{2\left(q^0_{(n-1),\min}(x,0)\right)^3}-q^*_t(x,t)\frac{q^*_x(x,0)}{2\left(q^*(x,0)\right)^3}\right).$$

Hence, by (4.26), (4.84) and embedding theorem

$$|G_n|\le C\delta+C\left|\frac{1}{2\left(q^0_{(n-1),\min}(x,0)\right)^2}-\frac{1}{2\left(q^*(x,0)\right)^2}\right|$$

$$+\left|\partial_t q_{(n-1),\min}(x,t)\,\frac{\partial_x q_{(n-1),\min}(x,0)}{2\left(q^0_{(n-1),\min}(x,0)\right)^3}-q^*_t(x,t)\frac{q^*_x(x,0)}{2\left(q^*(x,0)\right)^3}\right|. \tag{4.99}$$

Using (4.84) and (4.85), we obtain

$$\left|\frac{1}{2\left(q^0_{(n-1),\min}(x,0)\right)^2}-\frac{1}{2\left(q^*(x,0)\right)^2}\right|$$

$$=\frac{\left|\left(q^0_{(n-1),\min}(x,0)-q^*(x,0)\right)-\left(F-F^*\right)(x,0)\right|\left|q^0_{(n-1),\min}(x,0)+q^*(x,0)\right|}{2\left(q^0_{(n-1),\min}(x,0)\right)^2\left(q^*(x,0)\right)^2}.$$

$$\le C\delta+C\left|h_{n-1}(x,0)\right|.$$

Combining this with (4.99), we obtain

$$|G_n|\le C\delta+C\left|h_{n-1}(x,0)\right|$$

$$+\left|\partial_t q_{(n-1),\min}(x,t)\,\frac{\partial_x q_{(n-1),\min}(x,0)}{2\left(q^0_{(n-1),\min}(x,0)\right)^3}-q^*_t(x,t)\frac{q^*_x(x,0)}{2\left(q^*(x,0)\right)^3}\right|. \tag{4.100}$$

Next,

$$\frac{1}{2\left(q^0_{(n-1),\min}(x,0)\right)^3} = \frac{1}{2\left(q^*(x,0)\right)^3}$$

$$+\left(\frac{1}{2\left(q^0_{(n-1),\min}(x,0)\right)^3} - \frac{1}{2\left(q^*(x,0)\right)^3}\right)$$

$$= \frac{1}{2\left(q^*(x,0)\right)^3} + S_{n-1}(x,0)\left[\left(q^0_{(n-1),\min}(x,0) - q^*(x,0)\right) - (F-F^*)(x,0)\right],$$

where the function $S_{n-1}(x,0)$ can be estimated as

$$|S_{n-1}(x,0)| \leq C. \tag{4.101}$$

Hence,

$$\partial_t q_{(n-1),\min}(x,t)\,\frac{\partial_x q_{(n-1),\min}(x,0)}{2\left(q^0_{(n-1),\min}(x,0)\right)^3} =$$

$$\frac{\partial_t q_{(n-1),\min}(x,t)\,\partial_x q_{(n-1),\min}(x,0)}{2\left(q^*(x,0)\right)^3} +$$

$$+\left[\partial_t q_{(n-1),\min}(x,t)\,\partial_x q_{(n-1),\min}(x,0)\right]\times$$

$$\times S_{n-1}(x,0)\left[\left(q^0_{(n-1),\min}(x,0) - q^*(x,0)\right) - (F-F^*)(x,0)\right].$$

Hence, using (4.23), (4.26), (4.73), (4.85) and (4.101), we obtain

$$\left|\partial_t q_{(n-1),\min}(x,t)\,\frac{\partial_x q_{(n-1),\min}(x,0)}{2\left(q^0_{(n-1),\min}(x,0)\right)^3} - q^*_t(x,t)\frac{q^*_x(x,0)}{2\left(q^*(x,0)\right)^3}\right|$$

$$\leq \frac{1}{2\left(q^*(x,0)\right)^3}\left|\partial_t q_{(n-1),\min}(x,t)\,\partial_x q_{(n-1),\min}(x,0) - q^*_t(x,t)q^*_x(x,0)\right| \tag{4.102}$$

$$+C\left(\delta + |h_{n-1}(x,0)|\right)$$

$$\leq C\left(\delta + |h_{n-1}(x,0)| + |\partial_x h_{n-1,x}(x,0)| + |h_{n-1,t}(x,t)|\right).$$

Combining (4.100) with (4.102), we obtain

$$|G_n(x,t)| \leq C\left(\delta + |h_{n-1}(x,0)| + |h_{n-1,x}(x,0)| + |h_{n-1,t}(x,t)|\right).$$

Hence, by (4.97)

$$I^{(n)}_{\lambda,\beta}(p^*) \leq C\int_\Omega \left(\delta^2 + h^2_{n-1}(x,0) + h^2_{n-1,x}(x,0) + h^2_{n-1,t}(x,t)\right) e^{2\lambda\varphi}dxdt + C\beta.$$

Substituting this in (4.96) and then using (4.95), we obtain

$$\int_\Omega \left(h^2_{nx} + h^2_{nt} + h^2_n\right) e^{2\lambda\varphi}dxdt + \int_\varepsilon^b \left(h^2_{nx}(x,0) + h^2_n(x,0)\right) e^{-2\lambda x}dx$$

$$\leq \frac{C}{\lambda}\int_\Omega \left(\delta^2 + h^2_{n-1}(x,0) + h^2_{n-1,x}(x,0) + h^2_{n-1,t}(x,t)\right) e^{2\lambda\varphi}dxdt + C\beta. \tag{4.103}$$

Obviously

$$\int_\Omega \left(h^2_{n-1}(x,0) + h^2_{n-1,x}(x,0)\right) e^{2\lambda\varphi}dxdt \leq \frac{1}{2\lambda\alpha}\int_\varepsilon^b \left(h^2_{(n-1)x}(x,0) + h^2_{n-1}(x,0)\right) e^{-2\lambda x}dx, \tag{4.104}$$

$$\int_\Omega \delta^2 e^{2\lambda\varphi}dxdt \leq C\frac{\delta^2}{\lambda^2}. \tag{4.105}$$

Denote

$$y_n = \int_\Omega \left(h^2_{nx} + h^2_{nt} + h^2_n\right) e^{2\lambda\varphi}dxdt + \int_\varepsilon^b \left(h^2_{nx}(x,0) + h^2_n(x,0)\right) e^{-2\lambda x}dx. \tag{4.106}$$

Then (4.103)-(4.105) imply

$$y_n \leq \frac{C}{\lambda}y_{n-1} + C\left(\frac{\delta^2}{\lambda^2} + \beta\right). \tag{4.107}$$

Iterating (4.107) with respect to n, we obtain

$$\int_\Omega \left(h_{nx}^2 + h_{nt}^2 + h_n^2\right) e^{2\lambda\varphi} dxdt + \int_\varepsilon^b \left(h_{nx}^2(x,0) + h_n^2(x,0)\right) e^{-2\lambda x} dx$$

$$\leq \frac{C}{\lambda^n}\left[\int_\Omega \left(h_{0x}^2 + h_{0t}^2 + h_0^2\right) e^{2\lambda\varphi} dxdt + \int_\varepsilon^b \left(h_{0x}^2(x,0) + h_0^2(x,0)\right) e^{-2\lambda x} dx\right] \quad (4.108)$$

$$+C\left(\frac{\delta^2}{\lambda^2} + \beta\right).$$

Apply (4.93) to the left-hand side of the estimate (4.108). Also, apply (4.94) at $n = 0$ to the right-hand side of (4.108). We obtain (4.91). Estimate (4.92) follows from an obvious combination of (4.91) with (4.59), (4.77), (4.85) and (4.89). Finally, estimate (4.90) follows immediately from (4.93), (4.94) and (4.103). $\square$

4.9 Global Convergence of the Gradient and Gradient Projection Methods to the Exact Solution

First, we consider the gradient method of the minimization of functionals $J_{\lambda,\beta}^{(n)}(q_{(k-1),n})$ on the set $\overline{B(R,g_0)}$, see (4.57). The proof of Theorem 9.1 follows immediately from the triangle inequality combined with Theorems 7.1 and 8.1.

Theorem 9.1. *Let α_0 and λ_0 be the numbers of Theorem 5.1. Let the sufficiently large number $\lambda_1 = \lambda_1(R,\Omega,\alpha) \geq \lambda_0 > 1$ be the one defined in (4.47). Let the number $\widetilde{\lambda}_1$ be the same as in (4.88),*

$$\widetilde{\lambda}_1 = \lambda_1(2R,\Omega,\alpha) \geq \lambda_1(R,\Omega,\alpha).$$

Let $\lambda \geq \lambda_1$ and let the regularization parameter $\beta \in \left[2e^{-\lambda\alpha T}, 1\right)$. Assume that the functions $q_{\min,n} \in B(R/3, g_0)$ for all n. For each n, choose the starting point of the gradient method (4.57) as $q_{0,n} \in B(R/3, g_0)$. Then there exists a number $\eta_0 \in (0,1)$ such that for any $\eta \in (0,\eta_0)$ functions $q_{k,n} \in B(R,g_0), \forall k,n = 1,...$ Furthermore, there exists a number $\theta = \theta(\eta) \in (0,1)$ such that the following convergence estimate

is valid:

$$\|c_{k,n} - c^*\|_{H^1(\varepsilon,b)} \leq C\theta^k \|q_{0,n} - q_{n,\min}\|_{H^4(\Omega)}$$

$$+\frac{C^{n/2}}{\lambda^{n/2}} \left(\int_\Omega \left(\overline{q}_{0x}^2 + \overline{q}_{0t}^2 + \overline{q}_0^2 \right)(x,t)\, e^{2\lambda\varphi} dxdt \right)^{1/2} + C\left(\delta + \sqrt{\beta}\right),$$

where the function $\overline{q}_0$ *is defined in (4.89).*

Consider now the gradient projection method of the minimization of the functionals $I^{(n)}_{\lambda,\beta}(p_n) = J^{(n)}_{\lambda,\beta}(p_n + F)$ in (4.68) on the set $\overline{B_0(2R)}$, see (4.69). We use notations (4.70). Theorem 9.2 follows immediately from the triangle inequality combined with Theorems 7.2 and 8.1.

Theorem 9.2. *Let the number* $\lambda_1 = \lambda_1(R,\Omega,\alpha) \geq \lambda_0 > 1$ *be the one defined in (4.47). Let the number* $\widetilde{\lambda}_1$ *be the same as in (4.88),*

$$\widetilde{\lambda}_1 = \lambda_1(2R,\Omega,\alpha) \geq \lambda_1(R,\Omega,\alpha).$$

Let $\lambda \geq \lambda_1$ *and let the regularization parameter* $\beta \in \left[2e^{-\lambda\alpha T}, 1\right)$. *Consider the gradient projection method (4.69). For each* n, *choose the starting point* $p_{0,n}$ *of this method as an arbitrary point of the ball* $B_0(2R)$. *Then there exists a number* $\eta_0 \in (0,1)$ *such that for any* $\eta \in (0,\eta_0)$ *there exists a number* $\theta = \theta(\eta) \in (0,1)$ *such that the following convergence estimate is valid:*

$$\|\widetilde{c}_{k,n} - c^*\|_{H^1(\varepsilon,b)} \leq C\theta^k \|\widetilde{q}_{0,n} - \widetilde{q}_{n,\min}\|_{H^4(\Omega)}$$

$$+\frac{C^{n/2}}{\lambda^{n/2}} \left(\int_\Omega \left(\overline{q}_{0x}^2 + \overline{q}_{0t}^2 + \overline{q}_0^2 \right)(x,t)\, e^{2\lambda\varphi} dxdt \right)^{1/2} + C\left(\delta + \sqrt{\beta}\right),$$

where functions $\widetilde{c}_{k,n}, \widetilde{q}_{0,n}, \widetilde{q}_{n,\min}$ *and* $\overline{q}_0$ *are defined in (4.70), (4.72) and (4.89) respectively.*

4.10 Numerical Studies

4.10.1 Numerical implementation

To generate the simulated data, we use Lemma 2.2. This means that we solve problem (4.3), (4.4) for the case when the whole real line is replaced by a large interval $(-a, a)$ with the absorbing boundary conditions (4.9)–(4.10). More precisely, just as in Section 6.1 of [24], we use the implicit scheme to numerically solve

$$\begin{cases} c(x)u_{tt}(x,t) = u_{xx}(x,t) & (x,t) \in (-a,a) \times (0,T), \\ u(-a,t) - u_x(-a,t) = 0 & t \in (0,T), \\ u(a,t) + u_x(a,t) = 0 & t \in (0,T), \\ u(x,0) = 0 & x \in \mathbb{R}, \\ u_t(x,0) = \widetilde{\delta}(x) & x \in \mathbb{R}, \end{cases} \tag{4.109}$$

where $a = 5$, $T = 6$ and

$$\widetilde{\delta}(x) = \frac{30}{\sqrt{2\pi}} e^{-\frac{(30x)^2}{2}}$$

is a smooth approximation of the function $\delta(x)$. We solve the problem (4.109) by the implicit finite difference method. In the finite difference scheme, we arrange a uniform partition for the interval $[-a, a]$ as $\{y_0 = -a, y_1, \ldots, y_N = a\} \subset [-a, a]$ with $y_i = a + 2ia/N_x$, $i = 0, \ldots, N_x$, where N_x is a large number. In the time domain, we split the interval $[0, T]$ into $N_t + 1$ uniform sub-intervals $[t_j, t_{j+1}]$, $j = 0, \ldots, N_t$, with $t_j = jT/N_t$, where N_t is a large number. In our computational setting, $N_x = 3001$ and $N_t = 301$. These numbers are the same as in [24].

We observe a computational error for the function u near $(x = 0, t = 0)$. This is due to the fact that the function $\widetilde{\delta}(x)$ is not exactly equal to the Dirac function. We correct the error as follows. It follows from (4.2), (4.7) and (4.8) that $u(x,t) = 1/2$ in a neighborhood of the point $(x,t) = (0,0)$. We, therefore, replace the data $u(\epsilon, t)$ by $1/2$ when $|t|$ is small. In our computation, we set $u(x,t) = 1/2$ for $(x,t) \in$

$[0, 0.0067] \times [0, 0.26]$. This data correction step is exactly the same as in Section 6.1 of [24] and is illustrated by Figure 2 in that publication. Then, we can extract the noiseless data g_0^* easily. We next add the noise into the data via the formula

$$g_0 = g_0^*(1 + \delta \cdot \text{rand}) \tag{4.110}$$

where δ is the noise level, and "rand" is the function that generates uniformly distributed random numbers in the range $[-1, 1]$. In all numerical tests with simulated data below, the noise level $\delta = 0.05$,, i.e., 5%. Due to (4.12), the function $g_1 = g_0'$. Due to the presence of noise, see (4.110), we cannot compute $g_1 = g_0'$ by the finite difference method. Hence, the function g_0' is computed by the Tikhonov regularization method. The version of the Tikhonov regularization method for this problem is well-known. Hence, we do not describe this step here.

Having the data for the function q in hand, we proceed as in Algorithm 1. In step

---

Algorithm 3 A numerical method to solve Problem 3.1

1: Choose a set of parameters λ, α and β.

2: Compute the function q_0 by minimizing the functional $J_{\lambda,\beta}^{(0)}$ defined in (4.35). Due to (4.15), the initial reconstruction is given by

$$c_{\text{init}}(x) = \frac{1}{(2q_0(x,0))^4} \quad \text{for all } x \in [\epsilon, b].$$

3: Assume that the function q_{n-1} is known. We compute the function q_n by minimizing the function $J_{\lambda,\beta}^{(n)}$ defined in (4.39).

4: Set $q_{\text{comp}} = q_n$ when $n = n^*$ is large enough.

5: Due to (4.15), the function c_{comp} is set to be

$$c_{\text{comp}}(x) = \frac{1}{(2q_{\text{comp}}(x,0))^4} \quad \text{for all } x \in [\epsilon, b].$$

---

1 of Algorithm 3, we choose $\lambda = 2$, $\alpha = 0.3$ and $\beta = 10^{-11}$. These parameters were chosen by a trial-error process that is similar to the one in [39]. Just as in [39], we choose a reference numerical test in which we know the true solution. In fact, test

1 of section 10.2 was our reference test. We have tried several values of λ, α, and β until the numerical solution to that reference test became acceptable. Then, we have used the same values of these parameters for all other tests, including all five (5) available cases of experimental data.

We next implement Steps 2 and 3 of Algorithm 1. We write differential operators in the functionals $J^{(0)}_{\lambda,\beta}$ and $J^{(n)}_{\lambda,\beta}$ in the finite differences with the step size in space $\Delta x = 0.0033$ and the step size in time $\Delta t = 0.02$ and minimize resulting functionals with respect to values of corresponding functions at grid points. Since the integrand in the definitions of the functional $J^{(n)}_{\lambda,\beta}, n = 0, 1, ...$ is the square of linear functions, then its minimizer is its critical point. In finite differences, we can write a linear system whose solution is the desired critical point. We solve this system by the command "lsqlin" of Matlab. The details in implementation by the finite difference method including the discretization, the derivation of the linear system for the critical point, and the use of "lsqlin" are very similar to the scheme in [34]. Recall that in our theory, in the definition of the functional $J^{(n)}_{\lambda,\beta}$ acting on q_n, see (4.39), we replaced q_{n-1} with its analog $q_{n-1,\min}$ which belongs to the bounded set $\overline{B(R, g_0)}$, and also replaced $q_{n-1,\min}(x, 0)$ with $q^0_{n-1,\min}(x, 0)$. These replacements are only for the theoretical purpose to avoid the case when q_{n-1} blows up. However, in the numerical studies, these steps can be relaxed. This means that in Step 3, we have minimized the finite difference analog of the functional

$$q_n \mapsto \int_\Omega \Big(q_{nxx}(x,t) - \frac{q_{nxt}(x,t)}{2\big(q_{n-1}(x,0)\big)^2} + \frac{\partial_t q_{n-1}(x,t)\, \partial_x q_{n-1}(x,0)}{2\big(q_{n-1}(x,0)\big)^3} \Big)^2 e^{2\lambda\varphi} dxdt + \beta \left\| q_n \right\|^2_{H^2(\Omega)}, \tag{4.111}$$

subject to the boundary conditions in lines 2 and 3 of (4.23). Another numerical simplification is that rather than using the H^4-norm in the regularization term, we use the H^2- norm in (4.111). Although the theoretical analysis supporting the above simplifications is missing, we did not experience any difficulties in computing

the numerical solutions to Problem 3.1. All of our numerical results are satisfactory.

4.10.2 Numerical results for computationally simulated data

To test Algorithm 3, we present four (4) numerical examples.

Test 1 (the reference test). We first test the case of one inclusion with a high inclusion/background contrast. The true dielectric constant function $c(x)$ has the following form

$$c_{\text{true}}(x) = \begin{cases} 1 + 14e^{\frac{(x-1)^2}{(x-1)^2 - 0.2^2}} & \text{if } |x-1| < 0.2, \\ 1 & \text{otherwise.} \end{cases} \tag{4.112}$$

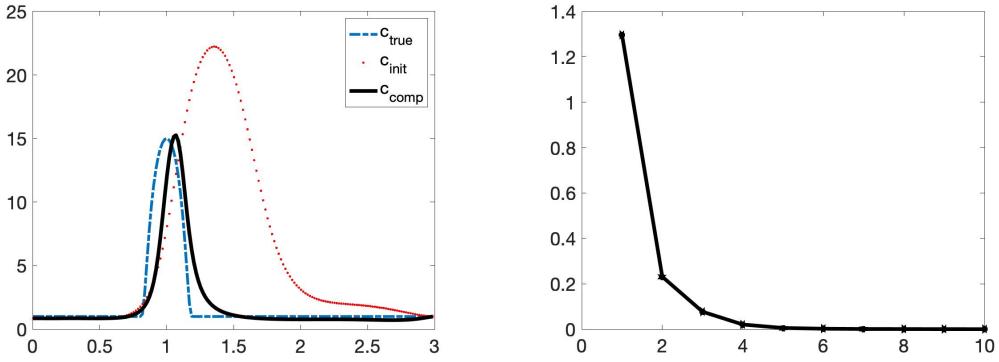

(a) (b)

Figure 4.1: *Test 1. True and reconstructed functions $c(x)$, where c_{true} is given in (4.112). (a) Functions c_{init} and c_{comp} are obtained by Step 2 and Step 5 of Algorithm 3 respectively. (b) The consecutive relative error is $\|c_n - c_{n-1}\|_{L^\infty(\epsilon,M)} / \|c_n\|_{L^\infty(\epsilon,M)}$, $n = 1, \ldots, 10$. The data is with $\delta = 5\%$ noise.*

Thus, the inclusion/background contrast is 15:1. It is evident from Figure 4.1 that we can successfully detect an object. The diameter of this object is 0.4 and the distance between this object and the source is 1. The true inclusion/background contrast is 15/1. The maximal value of the computed dielectric constant is 15.28. The relative error in this maximal value is 1.89% while the noise level in the data is 5%. Although the contrast is high, our method provides a good numerical solution

without requiring any knowledge of the true solution. Our method converges fast. Although the initial reconstruction c_{init} computed in Step 2 of Algorithm 3 is not very good, see Figure 5.1, one can see in Figure 4.1b, that the convergence occurs after only five (5) iterations. This fact verifies numerically the "contraction property" of Theorem 8.1 including the key estimate (4.92).

Test 2. The true function c in this test has two "inclusions",

$$c_{\text{true}}(x) = \begin{cases} 1 + 5e^{\frac{(x-0.6)^2}{(x-0.6)^2 - 0.2^2}} & \text{if } |x - 0.6| < 0.2, \\ 1 + 8e^{\frac{(x-1.4)^2}{(x-1.4)^2 - 0.3^2}} & \text{if } |x - 1.4| < 0.3, \\ 1 & \text{otherwise.} \end{cases} \tag{4.113}$$

The numerical results of this test are displayed in Figure 4.2.

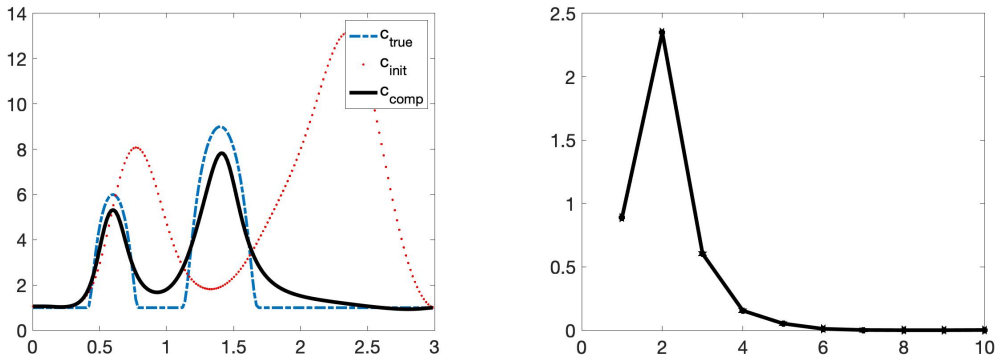

(a) (b)

Figure 4.2: *Test 2. True and reconstructed functions $c(x)$, where c_{true} is given in (4.113). (a) Functions c_{init} and c_{comp} are obtained by Step 2 and Step 5 of Algorithm 3 respectively. (b) The consecutive relative error is $\|c_n - c_{n-1}\|_{L^\infty(\epsilon,M)} / \|c_n\|_{L^\infty(\epsilon,M)}$, $n = 1, \ldots, 10$. The data is with $\delta = 5\%$ noise.*

Test 2 is more complicated than Test 1. However, we still obtain good numerical results. It is evident from Figure 4.2a that we can precisely detect the two inclusions without any initial guess. The true maximal values of the dielectric constant of the inclusions on the left and the right are 6 and 9 respectively. The reconstructed maximal values in those inclusions are acceptable. They are 5.31 (relative error 11.5%)

and 7.8 (relative error 13.3%). As in Test 1, the initial reconstruction c_{init} computed in Step 2 of Algorithm 3 is far from $c_{\text{true}}(x)$. Still, our iterative procedure converges after 7 iterations, see Figure 4.2b.

Test 3 We test the case when the function $c_{\text{true}}(x)$ is discontinuous. It is a piecewise constant function given by

$$c_{\text{true}}(x) = \begin{cases} 10 & \text{if } |x-1| < 0.15, \\ 1 & \text{otherwise.} \end{cases} \tag{4.114}$$

The numerical solution for this test is presented in Figure 4.3.

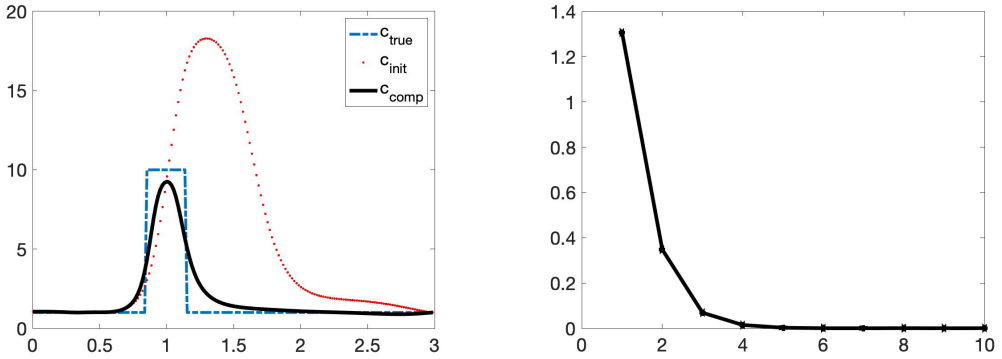

(a) (b)

Figure 4.3: *Test 3. True and reconstructed functions $c(x)$, where c_{true} is given in* (4.114). *(a) Functions c_{init} and c_{comp} are obtained by Step 2 and Step 5 of Algorithm 3 respectively. (b) The consecutive relative error is $\|c_n - c_{n-1}\|_{L^\infty(\epsilon,M)} / \|c_n\|_{L^\infty(\epsilon,M)}$, $n = 1, \ldots, 10$. The data is with $\delta = 5\%$ noise.*

Although the function c_{true} is not smooth and actually not even continuous, Algorithm 3 works and provides a reliable numerical solution. The computed maximal value of the dielectric constant of the object is 9.25 (relative error 7.5%), which is acceptable. The location of the object is detected precisely; see Figure 4.3a. As in the previous two tests, Algorithm 3 converges fast. After the fifth iteration, the reconstructed function c_n becomes unchanged. Again, this fact numerically confirms both Theorem 8.1 and the robustness of our method.

Test 4 In this test, the function $c_{\text{true}}(x)$ has the following form:

$$c_{\text{true}}(x) = \begin{cases} 3.5 + 0.3 \cdot \sin(\pi(x - 1.35)) & \text{if } |x - 0.9| < 0.5, \\ 8 & \text{if } |x - 2| < 0.37, \\ 1 & \text{otherwise.} \end{cases} \tag{4.115}$$

This test is interesting since the graph of the function (4.115) consists of a curve and an inclusion. The numerical solution for this case is presented in Figure 4.4.

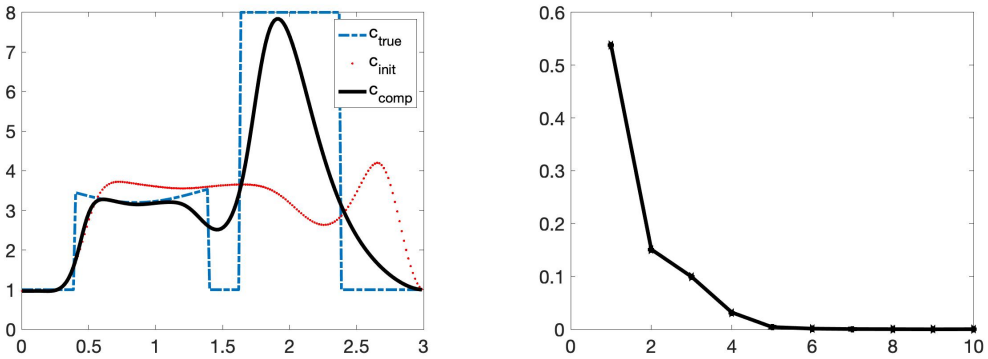

(a) (b)

Figure 4.4: *Test 4. The true and reconstructed functions* $c(x)$*, where* c_{true} *is given in* (4.115)*. (a) The functions* c_{init} *and* c_{comp} *are obtained by Step 2 and Step 5 of Algorithm 3 respectively. (b) The consecutive relative error* $\|c_n - c_{n-1}\|_{L^\infty(\epsilon,M)} / \|c_n\|_{L^\infty(\epsilon,M)}$*,* $n = 1, \ldots, 10$*. The data is with* $\delta = 5\%$ *noise.*

One can observe from Figure 4.4a that our method to compute the initial reconstruction in Step 2 of Algorithm 3 is not very effective. However, after only 6 iterations, good numerical results are obtained. The curve in the first inclusion locally coincides with the true one and the maximal value of the computed dielectric constant within inclusion is quite accurate: it is 7.83 (relative error 2.12%). Our method converges at iteration number 6.

Remark 4.10.1 *It follows from all the above tests that Algorithm 3 is robust in solving a highly nonlinear and severely ill-posed Problem 3.1. It provides satisfactory numerical results with fast convergence. For each test, the computational time to*

compute the numerical solution is about 29 seconds on a MacBook Pro 2019 with a 2.6 GHz processor and 6 Intel i7 cores. This is almost a real-time computation.

4.11 Numerical Results for Experimental Data

We now test Algorithm 3 on experimental data mentioned in Introduction. These data were collected by the US Army Research Laboratory to detect and identify targets mimicking shallow anti-personnel land mines and IEDs. Five tested targets were: a bush, a wood stake, a metal box, a metal cylinder, and a plastic cylinder. The bush and the wood stake were placed in the air, while the other three objects were buried at a few centimeters depth in the ground. Since the locations of targets can be accurately detected by the Ground Position System (GPS), we are only interested in computing the values of their dielectric constants. We are doing so using Algorithm 3.

Just as in our earlier works [15, 22, 23, 24, 28, 40], where these experimental data were used, we compute here the function $c_{\text{rel}}(x)$ defined as:

$$c_{\text{rel}}(x) = \begin{cases} \frac{c_{\text{target}}}{c_{\text{bckgr}}}(x) \text{ if } \max \frac{c_{\text{target}}}{c_{\text{bckgr}}}(x) > 1 & \text{and } x \in D, \\ 1 & \text{otherwise,} \end{cases} \tag{4.116}$$

$$c_{\text{rel}}(x) = \begin{cases} \min \frac{c_{\text{target}}}{c_{\text{bckgr}}}(x) \text{ if } \max \frac{c_{\text{target}}}{c_{\text{bckgr}}}(x) \leq 1 & \text{and } x \in D, \\ 1 & \text{otherwise,} \end{cases} \tag{4.117}$$

where D is a sub-interval of the interval $[\epsilon, M]$, which is occupied by the target. Next, we define the computed value of c_{target} as [24]:

$$c_{\text{comp}} = c_{\text{bckgr}} \times \begin{cases} \max c_{\text{rel}}(x) \text{ if } \max c_{\text{rel}}(x) > 1, \\ \min c_{\text{rel}}(x) \text{ if } \max c_{\text{rel}}(x) < 1. \end{cases} \tag{4.118}$$

As in the above cited publications, we have to preprocess the raw data of [35]

before importing them into our solver. The data preprocessing procedure is exactly the same as the one in [24, Section 7.1]. First, we observe that the $L_\infty-$norm of the experimental data far exceeds the $L_\infty-$norm of the computationally simulated data. Therefore, we need to scale the experimental data by dividing it by a calibration factor $\mu > 0$, i.e. we replace the raw experimental data $f_{\text{raw}}(t)$ with $f_{\text{scale}}(t) = f_{\text{raw}}(t)/\mu$. Then we work only with $f_{\text{scale}}(t)$. To find the calibration factor, we use a trial-and-error process. First, we select a reference target. We then try many values of μ such that the reconstruction of the reference target is satisfactory, i.e. the computed dielectric constant is in its published range, see below in this section about the published range. Then this calibration factor is used is all other tests. When the object is in the air, our reference target is bush. In this case, the calibration factor $\mu_{\text{air}} = 534,592$. When the object is buried under the ground, our reference target is the metal box and the calibration factor was $\mu_{\text{ground}} = 265,223$.

Next, we preprocess the data $f_{\text{scale}}(t)$ as follows. First, we first use a lower envelop (built in Matlab) to bound the data. We then truncate the data that is not in a small interval centered at the global minimizer of the data, see [24, Section 7.1] for the choice of this small interval. But in the case of the plastic cylinder we use the upper envelop. The choice of the upper or lower envelopes is as follows. We look at the function $f_{\text{scale}}(t)$ and find the three extrema with largest absolute values. If the middle extremal value among these three is a minimum, then we bound the data by a lower envelop. Otherwise, we use an upper envelop. See [24, Section 7.1] for more details and the reason of this choice. In particular, Figures 4a, 4b, 4d, 5a, 5b, 5d, 5e, 5g, 5h of [24] provide illustrations. Likewise, our Figures 5 displays computed functions $c_{\text{target}}(x)$ for our five targets. The computed dielectric constants c_{comp} defined in (4.118) by Algorithm 3 are listed in Table 4.1.

The true values of dielectric constants of our targets were not measured in the experiments. Therefore, we compare our computed values with the published ones.

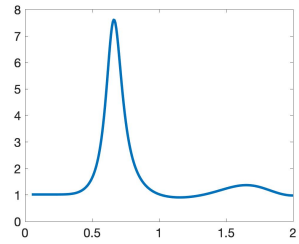

(a) c_{target} for bush

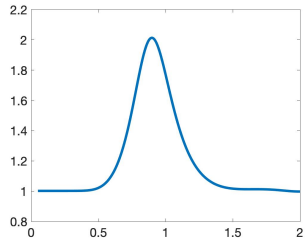

(b) c_{target} for wood stake

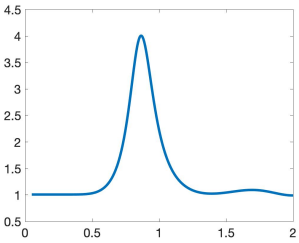

(c) c_{target} for metal box

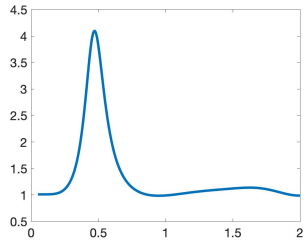

(d) c_{target} for metal cylinder

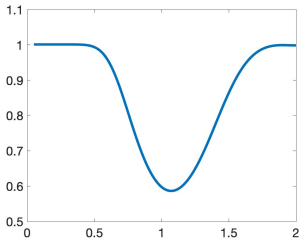

(e) c_{target} for plastic cylinder

Figure 4.5: *Computed functions* $c_{\text{target}}(x, y)$ *for our five targets, also see (4.116)-(4.118) and Table 4.1.*

Table 4.1: Computed dielectric constants of five targets

Target	c_{bckgr}	computed c_{rel}	c_{bckgr}	computed c_{target}	True c_{target}
Bush	1	7.62	1	10.99	$[3, 20]$
Wood stake	1	2.01	1	2.26	$[2, 6]$
Metal box	4	4.00	$[3, 5]$	$[12.00, 20.00]$	$[10, 30]$
Metal cylinder	4	4.01	$[3, 5]$	$[12.3, 20.5]$	$[10, 30]$
Plastic cylinder	4	0.59	$[3, 5]$	$[1.6, 2.95]$	$[1.1, 3.2]$

The published values of the dielectric constants of our targets are listed in the last column of Table 4.1. They can be found on the website of Honeywell (Table of dielectric constants, https://goo.gl/kAxtzB). Also, see [11] for the experimentally measured range of the dielectric constants of vegetation samples, which we assume have the same range as the dielectric constant of bush. In the table of dielectric constants of Honeywell as well as in [11], any dielectric constant is not a number. Rather, each dielectric constant of these references is given within a certain interval. As to the metallic targets, it was established in [28] that they have the so-called "apparent" dielectric constant whose values are in the interval $[10, 30]$.

Conclusion. It is clear from Table 4.1 that our computed dielectric constants are consistent with the intervals of published ones. Therefore, our results for experimental data are satisfactory.

Remark 4.11.1 (Speed of computations) *Our experimental data are sparse. The size of the data in time is* $N_t = 80$*, which is a lot smaller than that in the dense simulated data (*$N_t = 300$*). Therefore, the speed of computations is much faster than for the case of simulated data of section 10. All results of this section were computed in* ***real time*** *on the same computer (MacBook Pro 2019 with 2.6 GHz processor and 6 Intel i7 cores).*

4.12 Concluding Remarks

We have developed a new globally convergent numerical method for a 1-D Coefficient Inverse Problem with backscattering data for the wave-like PDE (4.3). This is the second generation of the above cited convexification method of our research group. The main novelty here is that, rather than minimizing a globally strictly convex weighted cost functional arising in the convexification, we solve on each iterative step a linear boundary value problem. This is done using the so-called Carleman Quasi-Reversibility Method. Just like in the convexification, the key element of the convergence analysis of this chapter is the presence of the Carleman Weight Function in each quadratic functional, which we minimize. The convergence estimate is similar to the well known estimate of the classical contraction mapping principle. The latter explains the title of this chapter. We have proven a global convergence theorem of our method. Our numerical results for computationally simulated data demonstrate high reconstruction accuracies in the presence of 5% random noise in the data.

Furthermore, our numerical results for experimentally collected data have satisfactory accuracy via providing values of computed dielectric constants of explosive-like targets within their published ranges.

A practically important observation here is that our computations for experimental data were performed in *real time*. This observation did not take place for various versions of the first generation of the convexification method of our previous publications [22, 23, 24, 40], which were working with the same experimental data. The latter indicates an important advantage of the second generation of the convexification method of this chapter.

REFERENCES

[1] A. B. Bakushinskii, M. V. Klibanov, and N. A. Koshev. Carleman weight functions for a globally convergent numerical method for ill-posed Cauchy problems for some quasilinear PDEs. *Nonlinear Anal. Real World Appl.*, 34:201–224, 2017.

[2] L. Baudouin, M. de Buhan, and S. Ervedoza. Carleman estimates for waves and applications. *Communications in Partial Differential Equations*, 38:823–59, 2013.

[3] L. Baudouin, M. de Buhan, and S. Ervedoza. Convergent algorithm based on Carleman estimates for the recovery of a potential in the wave equation. *SIAM J. Nummer. Anal.*, 55:1578–1613, 2017.

[4] L. Baudouin, M. de Buhan, S. Ervedoza, and A. Osses. Carleman-based reconstruction algorithm for the waves. *SIAM Journal on Numerical Analysis*, 59(2):998–1039, 2021.

[5] L. Beilina and M. V. Klibanov. *Approximate Global Convergence and Adaptivity for Coefficient Inverse Problems*. Springer, New York, 2012.

[6] M. Bellassoued and M. Yamamoto. *Carleman Estimates and Applications to Inverse Problems for Hyperbolic Systems*. Springer, Japan, 2017.

[7] L. Bourgeois. Convergence rates for the quasi-reversibility method to solve the Cauchy problem for Laplace's equation. *Inverse Problems*, 22:413–430, 2006.

[8] L. Bourgeois and J. Dardé. A duality-based method of quasi-reversibility to solve the Cauchy problem in the presence of noisy data. *Inverse Problems*, 26:095016, 2010.

[9] A. L. Bukhgeim and M. V. Klibanov. Uniqueness in the large of a class of multidimensional inverse problems. *Soviet Math. Doklady*, 17:244–247, 1981.

[10] G. Chavent. *Nonlinear Least Squares for Inverse Problems: Theoretical Foundations and Step-by-Step Guide for Applications, Scientific Computation*. Springer, New York, 2009.

[11] H. T. Chuah, K. Y. Lee, and T. W. Lau. Dielectric constants of rubber and oil palm leaf samples at X-band. *IEEE Trans. Geosci. Remote Sens*, 33(221–223), 1995.

[12] M. de Hoop, P. Kepley, and L. Oksanen. Recovery of a smooth metric via wave field and coordinate transformation reconstruction. *SIAM J. Appl. Math.*, 78:1931–1953, 2018.

[13] A. V. Goncharsky and S. Y. Romanov. Iterative methods for solving coefficient inverse problems of wave tomography in models with attenuation. *Inverse Problems*, 33:025003, 2017.

[14] V. Goncharsky and S. Y. Romanov. A method of solving the coefficient inverse problems of wave tomography. *Comput. Math. Appl.*, 77:967–980, 2019.

[15] A.L. Karchevsky, M.V. Klibanov, L. Nguyen, N. Pantong, and A. Sullivan. The Krein method and the globally convergent method for experimental data. *Applied Numerical Mathematics*, 74:111–127, 2013.

[16] M. V. Klibanov. Inverse problems and Carleman estimates. *Inverse Problems*, 8:575–596, 1992.

[17] M. V. Klibanov. Global convexity in a three-dimensional inverse acoustic problem. *SIAM J. Math. Anal.*, 28:1371–1388, 1997.

[18] M. V. Klibanov. Carleman estimates for global uniqueness, stability and numerical methods for coefficient inverse problems. *J. Inverse and Ill-Posed Problems*, 21:477–560, 2013.

[19] M. V. Klibanov. Carleman estimates for the regularization of ill-posed Cauchy problems. *Applied Numerical Mathematics*, 94:46–74, 2015.

[20] M. V. Klibanov and O. V. Ioussoupova. Uniform strict convexity of a cost functional for three-dimensional inverse scattering problem. *SIAM J. Math. Anal.*, 26:147–179, 1995.

[21] M. V. Klibanov, V. A. Khoa, A. V. Smirnov, L. H. Nguyen, G. W. Bidney, L. Nguyen, A. Sullivan, and V. N. Astratov. Convexification inversion method for nonlinear SAR imaging with experimentally collected data. *to appear on J. Applied and Industrial Mathematics, see also Arxiv:2103.10431*, 2021.

[22] M. V. Klibanov, A. E. Kolesov, L. Nguyen, and A. Sullivan. Globally strictly convex cost functional for a 1-D inverse medium scattering problem with experimental data. *SIAM J. Appl. Math.*, 77:1733–1755, 2017.

[23] M. V. Klibanov, A. E. Kolesov, L. Nguyen, and A. Sullivan. A new version of the convexification method for a 1-D coefficient inverse problem with experimental data. *Inverse Problems*, 34:35005, 2018.

[24] M. V. Klibanov, T. T. Le, L. H. Nguyen, A. Sullivan, and L. Nguyen. Convexification-based globally convergent numerical method for a 1D coefficient inverse problem with experimental data. *preprint, Arxiv:2104.11392*, 2021.

[25] M. V. Klibanov and J. Li. *Inverse Problems and Carleman Estimates: Global Uniqueness, Global Convergence and Experimental Data.* to appear on De Gruyter, 2021.

[26] M. V. Klibanov, J. Li, and W. Zhang. Convexification for an inverse parabolic problem. *Inverse Problems*, 36:085008, 2020.

[27] J. Korpela, M. Lassas, and L. Oksanen. Regularization strategy for an inverse problem for a $1 + 1$ dimensional wave equation. *Inverse Problems*, 32:065001, 2016.

[28] A. Kuzhuget, L. Beilina, M.V. Klibanov, A. Sullivan, Lam Nguyen, and M. A. Fiddy. Blind backscattering experimental data collected in the field and an approximately globally convergent inverse algorithm. *Inverse Problems*, 28:095007, 2012.

[29] R. Lattès and J. L. Lions. *The Method of Quasireversibility: Applications to Partial Differential Equations.* Elsevier, New York, 1969.

[30] M. M. Lavrent'ev, V. G. Romanov, and S. P. Shishat·skiĭ. *Ill-Posed Problems of Mathematical Physics and Analysis.* Translations of Mathematical Monographs. AMS, Providence: RI, 1986.

[31] T. T. Le and L. H. Nguyen. A convergent numerical method to recover the initial condition of nonlinear parabolic equations from lateral cauchy data. *Journal of Inverse and Ill-posed Problems*, 30(2):265–286, 2022.

[32] B. M. Levitan. *Inverse Sturm–Liouville Problems.* VSP, Utrecht, 1987.

[33] M. Minoux. *Mathematical Programming: Theory and Algorithms.* John Wiley & Sons, New York, 1986.

[34] L. H. Nguyen. A new algorithm to determine the creation or depletion term of parabolic equations from boundary measurements. *Computers and Mathematics with Applications*, 80:2135–2149, 2020.

[35] N. Nguyen, D. Wong, M. Ressler, F. Koenig, Stanton B., G. Smith, J. Sichina, and K. Kappra. Obstacle avolidance and concealed target detection using the Army Research Lab ultra-wideband synchronous impulse Reconstruction (UWB SIRE) forward imaging radar. *Proc. SPIE*, 6553:65530H (1)–65530H (8), 2007.

[36] V. G. Romanov. *Inverse Problems of Mathematical Physics.* VNU Press, Utrecht, 1986.

[37] V. G. Romanov. *Investigation Methods for Inverse Problems.* VSP, 2002.

[38] J. A. Scales, M. L. Smith, and T. L. Fischer. Global optimization methods for multimodal inverse problems. *J. Computational Physics*, 103:258–268, 1992.

[39] A. V. Smirnov, M. V. Klibanov, and L. H. Nguyen. Convexification for a 1D hyperbolic coefficient inverse problem with single measurement data. *Inverse Probl. Imaging*, 14(5):913–938, 2020.

[40] A. V. Smirnov, M. V. Klibanov, A. Sullivan, and L. Nguyen. Convexifcation for an inverse problem for a 1d wave equation with experimental data. *Inverse Problems*, 36:095008, 2020.

[41] A. N. Tikhonov, A. Goncharsky, V. V. Stepanov, and A. G. Yagola. *Numerical Methods for the Solution of Ill-Posed Problems*. Kluwer Academic Publishers Group, Dordrecht, 1995.

[42] M. Yamamoto. Carleman estimates for parabolic equations. Topical Review. *Inverse Problems*, 25:123013, 2009.

CHAPTER 5: THE GRADIENT DESCENT METHOD FOR THE CONVEXIFICATION TO SOLVE BOUNDARY VALUE PROBLEMS OF QUASI-LINEAR PDES AND A COEFFICIENT INVERSE PROBLEM

5.1 Introduction

Numerical solutions of ill-posed Cauchy problems for quasi-linear partial differential equations (PDEs) is an important topic that arises in many real-world applications. For example, in the case of parabolic PDEs such problems are common in heat conduction [1, 2]. A natural approach to solve such a problem is to minimize the functional defined by the least-squares method. However, due to the presence of nonlinearity, this functional is non-convex. It might have multiple local minima and ravines. Therefore, a good initial guess, which is located sufficiently close to the true solution, plays an important role in the minimization process. Since such a good initial guess is not always available, we, in this chapter, use the convexification method, in which it is not necessary to have a small distance between the starting point of iterations and the true solution. The main content of the convexification method is to construct a weighted cost functional, which is strictly convex on an a priori chosen bounded set. It is important that smallness condition is not imposed on the diameter of this set. The unique minimizer of that functional on that set is close to the true solution of the given ill-posed Cauchy problem. The key element of that functional is the Carleman Weight Function (CWF), which is involved as weight in the Carleman estimate for the corresponding PDE operator.

An important question arises immediately on how to efficiently find the global minimizer of such a convex functional on that bounded set. It is well known that if a functional is strictly convex on the whole Hilbert space, then the gradient descent

method converges to its unique minimizer if starting from an arbitrary point of that space. However, it is not clear what to do in our case when the strict convexity takes place only on a bounded set. To address this question, it was proposed in [3] to use the gradient projection method. However, this method is a complicated one and is hard to implement numerically. On the other hand, it was heuristically observed in all numerical studies of the convexification conducted so far that a simpler gradient descent method works well; see e.g., [3, 8, 9, 10, 18]. This motivates us to analytically study the question of the global convergence of the gradient descent method.

More precisely, we prove that the gradient descent method delivers a sequence converging to the minimizer of that functional on that bounded set if starting from an arbitrary point of that set. Since smallness conditions are not imposed on the diameter of this set, this is global convergence, see, e.g. [3] where the notion of global convergence is defined. Some numerical results by gradient descent method will be presented.

Another important part of this chapter is to apply this result to solve a highly nonlinear and severely ill-posed coefficient inverse problem with a single measurement of back scattering data in the frequency domain.

As mentioned above, the main idea of the convexification method is to construct a strictly convex functional. To do this, one uses the Carleman weight function to convexify the mismatch functional derived from the given boundary value problem. Several versions of the convexification method have been developed since it was first introduced in [16]. We cite here [14, 12, 3, 19, 10, 20] for some important works in this area and their applications to solve a variety kinds of inverse problems. A comprehensive study of the convexification method is presented in the recent published book [18]. The crucial mathematical results that guarantee the above mentioned properties of the convexification, are the Carleman estimates. The original idea of applying Carleman estimates to coefficient inverse problems was first published in

[5] back in 1981 to prove uniqueness theorems for a wide class of coefficient inverse problems. Some follow up publications can be found in, e.g. [22, 11, 7, 27, 24, 30]. Surveys on the method in [5] can be found in [13, 33], see also [4, Chapter 1] and [18]. It was discovered later in [16], that the idea of [5] can be successfully modified to develop globally convergent numerical methods for coefficient inverse problems using the convexification.

For the convenience of the reader, we will recall in this chapter the convexification method , to solve ill-posed Cauchy problems for quasi-linear PDEs with both Dirichlet and Neumann boundary data [14]. Then, we will prove that if the noise in the boundary data tends to zero, then the convexification method combined with the gradient descent method delivers a close approximation to the solution of that Cauchy problem if starting from an arbitrary point of a selected bounded set. The rate of convergence is Lipschitz. We next apply the above results to solve a highly nonlinear and severely ill-posed coefficient inverse problem, described below. At a point far away from the region of interest, we send out an incident electric wave. The incident wave propagates in the 3D space and scatters when hitting the targets. We measure the back scattering wave on a surface. The aim of the inverse problem is to reconstruct the spatially distributed dielectric constants from this measurement. This coefficient inverse problem is the so-called inverse back scattering problem. It has many real-world applications, including the detection and identification of explosives, nondestructive testing and material characterization, see [9, 8, 29, 32]. We also refer the reader to [6] for the applications of this coefficient inverse problem in sonar imaging, geographical exploration, medical imaging, near-field optical microscopy, nano-optics.

The widely-used method to solve nonlinear coefficient inverse problem is the least squares optimization. This approach requires a good initial guess of the true solution. Unlike this, we assume that the target to be detected is completely unknown. This

means that a good initial guess of its dielectric constant is unavailable. Our numerical procedure is as follows. We first eliminate the unknown dielectric constant from the governing Helmholtz equation. The obtained equation is not a standard PDE. Then, we approximate the solution of the latter PDE via a truncated Fourier series with respect to a special orthonormal basis. Then we obtain an ill-posed Cauchy problem for a coupled system of elliptic of PDEs wih respect to corresponding spatially dependent Fourier coefficients. That special orthonormal basis was originally introduced in [15]. Solving this system by the convexification method and the gradient descent method, we obtain the solution to the above non standard PDE above. Then the solution to the originating coefficient inverse problem follows. We refer the reader to [8, 10, 31] and the references therein for some related versions of this method.

The chapter is organized as follows. In Section 5.2, we prove the convergence of the gradient descent method to the minimizer of a strictly convex functional. In Section 5.3, we present the above mentioned ill-posed Cauchy problem for a quasilinear elliptic PDE with both Dirichlet and Neumann boundary conditions. Also, in this section we present the corresponding functional with the Carleman Weight Function in it. In section 5.4, we recall the convexification method. In this section, we also prove the Lipschitz-like convergence of the minimizers due to the convexification method to the true solution as the noise tends to zero. In section 5.5, we introduce our coefficient inverse problem. In section 5.6, we derive an approximate model to solve this coefficient inverse problem. We present some numerical examples in section 5.7. Section 5.8 is for concluding remarks.

5.2 The gradient descent method to minimize a convex functional

Let X be a Hilbert space and let $J : X \to \mathbb{R}$ be a functional. Assume that J is Fréchet differentiable. Its derivative at the point $v \in X$ is denoted by $DJ(v) : X \to \mathbb{R}$. By the Riesz representation theorem, for each $v \in X$, we can identify $DJ(v)$ with an

element of X, named as $J'(v)$, in the following sense

$$DJ(v)(h) = \langle J'(v), h\rangle_X \quad \text{for all } h \in X.$$

Let $M > 0$ be an arbitrary number. Consider the ball $B(M)$,

$$B(M) = \{v \in X : \|v\|_X < M\}.$$

We assume that the Fréchet derivative J' is Lipschitz continuous in $\overline{B(M)}$, i.e.

$$\|J'(v_2) - J'(v_1)\|_X \leq L\|v_2 - v_1\|_X, \ \forall v_1, v_2 \in \overline{B(M)}, \tag{5.1}$$

where L is a certain number. Assume that J is strictly convex on $\overline{B(M)}$. This means that there exists a constant $\Lambda > 0$ such that

$$\langle J'(v_1) - J'(v_2), v_1 - v_2\rangle_X \geq \Lambda\|v_1 - v_2\|_X^2 \quad \text{for all } v_1, v_2 \in \overline{B(M)}. \tag{5.2}$$

Theorem 5.2.1 follows from a combination of Lemma 2.1 and Theorem 2.1 of [3].

Theorem 5.2.1 *Assume that the functional $J : X \to \mathbb{R}$ is Fréchet differentiable on X and its Fréchet derivative is Lipschitz continuous on $\overline{B(M)}$ as in* (5.1)*. Also, assume that $J(v)$ is strictly convex in $\overline{B(M)}$; i.e., inequality* (5.2) *is true. Then there exists unique minimizer $v_{\min} \in \overline{B(M)}$ of the functional $J(v)$ on the set $\overline{B(M)}$,*

$$\min_{\overline{B(M)}} J(v) = J(v_{\min}).$$

Furthermore, the following inequality holds

$$\langle J'(v_{\min}), v_{\min} - y\rangle_X \leq 0, \quad \textit{for all } y \in \overline{B(M)}.$$

The fact that the minimizer guaranteed by Theorem 5.2.1 can be located on the boundary of the ball $\overline{B(M)}$ prevents us from the proof of the global convergence of the gradient descent method. Hence, we assume in the next theorem that the minimizer is an interior point of $B(M)$.

Theorem 5.2.2 *Assume that the functional $J : X \to \mathbb{R}$ satisfies conditions of Theorem 5.2.1. Let $v_{\min}$ be its minimizer on the set $\overline{B\,(M)}$, the uniqueness and existence of which is guaranteed by Theorem 5.2.1. Suppose that $v_{\min}$ belongs to the interior of $B\,(M)$. Fix $v^{(0)} \in B$. Assume that the ball centered at $v_{\min}$ with the radius $\|v^{(0)} - v_{\min}\|_X$ is contained in $B\,(M)$; i.e.,*

$$B_0 = B(v_{\min}, \|v^{(0)} - v_{\min}\|_X) \subset B\,(M)\,. \tag{5.3}$$

Denote $\eta_0 = \min\,(2\Lambda/L^2, 1)$ and fix $\eta \in (0, \eta_0)$. For each $m \geq 0$, define

$$v^{(m+1)} = v^{(m)} - \eta J'\big(v^{(m)}\big), \quad m \geq 1 \tag{5.4}$$

Then, there exists a number $q \in (0, 1)$ such that

$$v^{(m)} \in B(M) \quad \textit{and } \big\|v^m - v_{\min}\big\|_X \leq q^{m-1}\big\|v^{(0)} - v_{\min}\big\|_X, \quad m \geq 1. \tag{5.5}$$

As a result, the sequence $v^{(m)}$ converges to $v_{\min}$ as m tends to ∞.

The sequence $\{v^{(m)}\}_{m\geq 1}$ defined in (5.4) is generated by the well-known gradient descent method. Although the gradient descent method is widely used in the scientific community, its convergence for a nonconvex functional can be proven only if the starting point of iterations is sufficiently close to the minimizer. Unlike this, Theorem 5.2.2 provides an affirmative answer about the convergence when the starting point is

not necessary located in a sufficiently small neighborhood of the minimizer. Theorem 5.2.2 justifies recent numerical results of our research group where we have used the gradient descent method to minimize globally strictly convex cost functionals arising in convexification even though our past theory said that a more complicated gradient projection method should be used, see e.g., [3, 8, 9, 10, 18, 20].

Proof 5.2.1 (Proof of Theorem 5.2.2) *Let L and Λ be the constants in* (5.1) *and* (5.2) *respectively and let $q = 1 + \eta^2 L^2 - 2\eta\Lambda$. Since $\eta \in (0, \eta_0)$, $q \in (0, 1)$. We prove* (5.5) *by induction. Assume, by induction, that* (5.5) *is true for some $m \geq 1$. Due to assumption* (5.3)*, $v_{\min} \in B(M)$. Thus, $J'(v_{\min}) = 0$. Hence, $v_{\min} = v_{\min} - J'(v_{\min})$. By* (5.4)*, we have*

$$\begin{aligned} \|v^{(m+1)} - v_{\min}\|_X^2 &= \|v^{(m)} - v_{\min} - \eta(J'\left(v^{(m)}\right) - J'(v_{\min}))\|_X^2 \\ &= \|v^{(m)} - v_{\min}\|_X^2 + \eta^2 \|J'\left(v^{(m)}\right) - J'(v_{\min})\|_X^2 \\ &\quad - 2\eta\langle J'^{(m)}) - J'(v_{\min}), v^{(m)} - v_{\min}\rangle_X. \end{aligned}$$

Using this, together with (5.1)*,* (5.2) *and the induction assumption for* (5.5)*, we obtain*

$$\|v^{(m+1)} - v_{\min}\|_X^2 \leq q\|v^{(m)} - v_{\min}\|_X^2 \leq q^m \|v^{(0)} - v_{\min}\|_X^2. \tag{5.6}$$

The last inequality in (5.6) *is deduced from the induction hypothesis. It follows from* (5.6) *that $v^{(m+1)} \in B_0 \subset B$. The assertion* (5.5) *is proved.*

Remark 5.2.1 *1. The hypothesis that the starting point of iterations $v^{(0)}$ is such that the ball centered at $v_{\min}$ with the radius $\|v_{\min} - v_0\|_X$ is contained in $B(M)$ does not weaken Theorem 5.2.2. In fact, if this hypothesis is not satisfied, we can replace $B(M)$ by a larger ball $B(M')$ where $M' > M$. Note that in the convexification method, $B(M)$ is the ball with an arbitrary chosen radius.*

2. The assumption that $v_{\min}$ is inside $B(M)$ is the main reason that helps us to

replace the gradient projection method in [9, 10, 8, 3] with the gradient descent method in Theorem 5.2.2. Without this assumption, elements of the sequence produced by the gradient descent method might be outside of $B(M)$, thus making this sequence diverge.

3. *We refer the reader to [17, Theorem 6], in which the authors proved a less general case of Theorem 5.2.2.*

5.3 A boundary value problem for quasi-linear PDEs

Let $n \geq 2$ be the spatial dimension. Let Ω be an open and bounded domain in $\mathbb{R}^n$ and Γ be a part of $\partial\Omega$. Let $G : \Omega \times \mathbb{R} \times \mathbb{R}^n \to \mathbb{R}$ be a real value function in the class $C^2(\overline{\Omega} \times \mathbb{R} \times \mathbb{R}^n, \mathbb{R})$. Consider the following boundary value problem with both Dirichlet and Neumann boundary conditions

$$\begin{cases} \Delta v(\mathbf{x}) &= G(\mathbf{x}, v(\mathbf{x}), \nabla v(\mathbf{x})) & \mathbf{x} \in \Omega, \\ \partial_\nu v(\mathbf{x}) &= g_0(\mathbf{x}) & \mathbf{x} \in \Gamma, \\ v(\mathbf{x}) &= g_1(\mathbf{x}) & \mathbf{x} \in \partial\Omega \end{cases} \tag{5.7}$$

where g_0 and g_1 are two functions in the class $H^p(\Omega)$ where p is a positive integer with $p > \lceil n/2 \rceil + 2$. In fact, we can say that (5.7) is the Cauchy problem for a quasilinear elliptic equation with the additional Dirichlet boundary data at $\partial\Omega \setminus \Gamma$. Here, $\lceil n/2 \rceil$ is the smallest integer that is greater than $n/2$. This regularity condition guarantees the embedding $H^p(\Omega) \hookrightarrow C^2(\overline{\Omega})$. This embedding will be used for the regularization purpose. In practice, the functions g_0 and g_1 represent the flux and the value information of v on $\partial\Omega$ and Γ respectively. We first recall the convexification method to compute an approximation of the solution, if it exists, to (5.7). Suppose

that

$$H = \{\phi \in H^p(\Omega) : \partial_\nu \phi(\mathbf{x}) = g_0(\mathbf{x}) \quad \text{for all } \mathbf{x} \in \Gamma \text{ and } \phi(\mathbf{x}) = g_1(\mathbf{x}) \text{ for all } \mathbf{x} \in \partial\Omega\} \quad (5.8)$$

is non-empty. Let v_0 be a function in H. Define

$$u(\mathbf{x}) = v(\mathbf{x}) - v_0(\mathbf{x}) \quad \text{for all } \mathbf{x} \in \Omega. \quad (5.9)$$

Then, solving (5.7) is equivalent to solving

$$\begin{cases} \Delta u(\mathbf{x}) &= F(\mathbf{x}, u(\mathbf{x}), \nabla u(\mathbf{x})) & \mathbf{x} \in \Omega, \\ \partial_\nu u(\mathbf{x}) &= 0 & \mathbf{x} \in \Gamma, \\ u(\mathbf{x}) &= 0 & \mathbf{x} \in \partial\Omega \end{cases} \quad (5.10)$$

where

$$F(\mathbf{x}, s, \xi) = \Delta v_0(\mathbf{x}) + G(\mathbf{x}, s + v_0(\mathbf{x}), \xi + \nabla v_0(\mathbf{x})) \quad (5.11)$$

for all $\mathbf{x} \in \Omega, s \in \mathbb{R}, \xi \in \mathbb{R}^n$. Let

$$H_0 = \big\{\phi \in H^p(\Omega) : \partial_\nu \phi(\mathbf{x}) = 0 \quad \text{for all } \mathbf{x} \in \Gamma \text{ and } \phi(\mathbf{x}) = 0 \text{ for all } \mathbf{x} \in \partial\Omega\big\}. \quad (5.12)$$

It is obvious that H_0 is a closed subspace of $H^p(\Omega)$. We consider H_0 a Hilbert space endowed with the usual norm of $H^p(\Omega)$. A widely-used approach to solve (5.10) is to minimize the following least squares functional

$$\int_\Omega \big|\Delta u(\mathbf{x}) - F\big(\mathbf{x}, u(\mathbf{x}), \nabla u(\mathbf{x})\big)\big|^2 d\mathbf{x} + \text{a regularization term.} \quad (5.13)$$

for $u \in H_0$. Due to the nonlinearity of F, and hence L, the functional in (5.13) is nonconvex. It might have multiple local minima and ravines, making the direct optimization approach unpractical. Motivated by this fact, we "convexify" this functional using the idea in [15]. Let $\Psi : \Omega \to \mathbb{R}$ be a C^∞ function with $\nabla\Psi \neq 0$ for all $\mathbf{x} \in \overline{\Omega}$. Introduce the Carleman weight function

$$\mu_\lambda(\mathbf{x}) = \exp(2\lambda\Psi(\mathbf{x})) \quad \text{for all } \mathbf{x} \in \Omega \tag{5.14}$$

where $\lambda > 1$. A Carleman estimate is an inequality of the form below.

Assumption 5.3.1 (Carleman estimate) *There exists $\lambda_0 > 1$ depending only on Ω and n such that for all $\phi \in H^2(\Omega)$ with $\phi|_{\partial\Omega} = 0$ and $\partial_\nu\phi|_\Gamma = 0$, we have*

$$\int_\Omega \mu_\lambda(\mathbf{x})|\Delta\phi|^2 d\mathbf{x} \geq \frac{C}{\lambda}\sum_{i,j=1}^{n}\int_\Omega \mu_\lambda(\mathbf{x})|\partial_{x_i x_j}\phi(\mathbf{x})|^2 d\mathbf{x} + C\lambda\int_\Omega \mu_\lambda(\mathbf{x})[|\nabla\phi|^2 + \lambda^2|\phi|^2]d\mathbf{x} \tag{5.15}$$

for all $\lambda \geq \lambda_0$ for some positive constant C depending only on Ω.

Assumption 5.3.1 holds true for some functions Ψ and μ_λ. For example, Klibanov and his collaborators have established a Carleman estimate in [19, Theorem 4.1], in which $\Omega = (-R, R)^3 \subset \mathbb{R}^3$ for some $R > 0$ and $\Psi(x, y, z) = (z - r)^2$ where r is any number that is greater than R. On the other hand, following the arguments in [19, Theorem 4.1], one can prove a Carleman estimate with $\Psi(x, y, z) = (z + r)^2$, see [10, Theorem 3.1]. This estimate plays an important role in developing a numerical method to solve the backscattering inverse problem with moving point source in [10]. On the other hand, the reader can find another Carleman estimate in [24, Theorem 3.1] when the second derivatives of the test function ϕ are absent in the right-hand side of (5.15). We also cite to [4, 18] for some important versions of the Carleman estimate for other kinds of partial differential operators. Especially, we draw the

reader's attention to [5] for the original idea of using the Carleman estimate to prove the uniqueness of a variety kinds of inverse problems.

Without loss of the generality, we assume that the true solution to (5.10) has a finite $H^p(\Omega)$-norm, which is bounded from above by a known number M. We seek this solution in the set

$$B(M) = \big\{\phi \in H_0 : \|\phi\|_{H^p(\Omega)} < M\big\}. \tag{5.16}$$

More precisely, in order to find a numerical solution to (5.10), we solve the problem below.

Problem 5.3.1 *Fix a regularization parameter $\epsilon > 0$. Minimize the following functional*

$$J_{\epsilon,\lambda}(u) = \int_\Omega \mu_\lambda(\mathbf{x})\big|\Delta u(\mathbf{x}) - F\big(\mathbf{x}, u(\mathbf{x}), \nabla u(\mathbf{x})\big)\big|^2 d\mathbf{x} + \epsilon\|u\|^2_{H^p(\Omega)} \tag{5.17}$$

for all $u \in B(M)$.

In the next section, we will recall the convexification principle to solve Problem 5.3.1. The main content of the convexification principle is that if the Carleman estimate (5.15) holds true then for any arbitrarily large number M, there exists $\lambda_1 > \lambda_0$ such that for all $\lambda > \lambda_1$ and $\epsilon > 0$, $J_{\epsilon,\lambda}$ is strictly convex in $\overline{B(M)}$ where $B(M)$ is the ball in H_0 with center 0 and radius M, see (5.16).

5.4 The convexification method and the convergence of the minimizer to the true solution as the noise tends to zero

In this section, we recall a theorem (Theorem 5.4.1) that guarantees the convexity of the objective functional $J_{\epsilon,\lambda}$ in $\overline{B(M)}$. We write $F = F(\mathbf{x}, s, \xi)$ and the partial derivatives of $F(\mathbf{x}, s, \xi)$ with respect to its variables are written as $\nabla_{\mathbf{x}} F(\mathbf{x}, s, \xi)$, $\partial_s F(\mathbf{x}, s, \xi)$ and $\nabla_\xi F(\mathbf{x}, s, \xi)$. The following theorem, Theorem 5.4.1, guarantees that

$J_{\epsilon,\lambda}$ has Lipschitz continuous Fréchet derivative and, more importantly, that $J_{\epsilon,\lambda}$ is strictly convex if the Carleman weight function μ_λ is such that Assumption 5.3.1 holds true.

Theorem 5.4.1 (Convexification) *1. Let M be an arbitrary positive number and define the ball $B(M)$ as in* (5.16)*. Then, for all $\epsilon > 0$ and $\lambda > 1$, $J_{\epsilon,\lambda} : \overline{B(M)} \subset H_0 \to \mathbb{R}$ is Fréchet differentiable. The derivative of $J_{\epsilon,\lambda}$ is given by*

$$DJ_{\epsilon,\lambda}(u)h = 2\int_\Omega \mu_\lambda(\mathbf{x})\big(\Delta u(\mathbf{x}) - F(\mathbf{x}, u(\mathbf{x}), \nabla u(\mathbf{x}))\big) \big(\Delta h(\mathbf{x}) - DF(u)h(\mathbf{x})\big)d\mathbf{x} + 2\epsilon\langle u, h\rangle_{H^p(\Omega)} \quad (5.18)$$

for all $u \in B(M)$ and $h \in H_0$ where

$$DF(u)h(\mathbf{x}) = \partial_s F(\mathbf{x}, u(\mathbf{x}), \nabla u(\mathbf{x}))h(\mathbf{x}) + \nabla_\xi F(\mathbf{x}, u(\mathbf{x}), \nabla u(\mathbf{x})) \cdot \nabla h(\mathbf{x})$$

for all $\mathbf{x} \in \Omega$. Moreover, the Fréchet derivative $DJ_{\epsilon,\lambda}$ is Lipschitz continuous in $\overline{B(M)}$. That means, there exists a constant $L = L(\Omega, M, F)$, depending only on the listed parameters, such that

$$\|DJ_{\epsilon,\lambda}(u_2) - DJ_{\epsilon,\lambda}(u_1)\|_{\mathcal{L}(H_0)} \leq L\|u_2 - u_1\|_{H^p(\Omega)} \quad (5.19)$$

for all $u_1, u_2 \in \overline{B(M)}$, where $\mathcal{L}(H_0)$ is the set of all bounded linear maps sending functions in H_0 into $\mathbb{R}$.

2. Assume further that the Carleman estimate (5.15) *holds true. Then, there exist $\lambda_1 = \lambda(M, \Omega, F) > \lambda_0$ and $C = C(M, \Omega, F) > 0$, both of which depend only on the*

listed parameters, such that for all $\epsilon > 0$, $\lambda > \lambda_1$, u_1 *and* u_2 *in* $\overline{B(M)}$, *we have*

$$J_{\epsilon,\lambda}(u_2) - J_{\epsilon,\lambda}(u_1) - DJ_{\epsilon,\lambda}(u_1)(u_2 - u_1) \geq C\|u_2 - u_1\|^2_{H^2(\Omega)} + \epsilon\|u_2 - u_1\|^2_{H^p(\Omega)}. \quad (5.20)$$

As a result,

$$\Big(DJ_{\epsilon,\lambda}(u_2) - DJ_{\epsilon,\lambda}(u_1)\Big)(u_2 - u_1) \geq 2C\|u_2 - u_1\|^2_{H^2(\Omega)} + 2\epsilon\|u_2 - u_1\|^2_{H^p(\Omega)} \quad (5.21)$$

for all u_1 *and* u_2 *in* $\overline{B(M)}$.

3. $J_{\epsilon,\lambda}$ *has a unique minimizer in* $\overline{B(M)}$.

We do not present the proof of Theorem 5.4.1 here. The reason is below. One can prove the first part of this theorem with straightforward computations. The proof is similar to that of [3, Theorem 3.1]. The second part of this theorem is a generalization of [3, Theorem 3.2] in the sense that the "convexification" inequalities (5.20) and (5.21) are tighter than the ones in [3, Theorem 3.2]. In fact, in those inequalities, we replace the H^1 norm in [3, Theorem 3.2] by the H^2 norm in the right hand side of (5.20) and (5.21). This is because the right-hand side of the Carleman estimate, see (5.15), contains the second derivatives. The existence of the unique minimizer of $J_{\epsilon,\lambda}$ in part 3 of Theorem 5.4.1 can be proved using the same technique in [10, Theorem 5.3], see also Lemma 2.1 and Theorem 2.1 of [3] and Theorem 5.2.1. On the other hand, we refer the reader to [3, Section 2] for some important facts in convex analysis that are related to the convexification in Theorem 5.4.1.

By using the gradient descent method, we can compute the minimizer of $J_{\epsilon,\lambda}$ in $B(M)$, see Theorem 5.2.2. We are now in the position of solving problem (5.7) with noisy boundary data g_0 and g_1 given. The corresponding noiseless data are denoted by g_0^* and g_1^* respectively. Let $\delta > 0$ be the noise level and assume that there exists

an "error function" $\mathcal{E}$ such that

$$\begin{cases} \|\mathcal{E}\|_{H^p(\Omega)} < \delta, \\ g_0 = g_0^* + \partial_\nu \mathcal{E} \quad \text{on } \partial\Omega, \\ g_1 = g_1^* + \mathcal{E} \qquad \text{in } \Gamma. \end{cases} \tag{5.22}$$

Recall in Section 5.3, we assume that there is a function v_0 satisfying $\partial_\nu g = g_0$ on $\partial\Omega$ and $v_0 = g_1$ on Γ. Let

$$v_{\epsilon,\delta}(\mathbf{x}) = u_{\min}(\mathbf{x}) + v_0(\mathbf{x}) \quad \text{for all } \mathbf{x} \in \Omega \tag{5.23}$$

where $u_{\min}$ is the minimizer of $J_{\epsilon,\lambda}$ obtained in Theorem 5.4.1. The function $v_{\epsilon,\delta}$ is named as the regularized solution to (5.7). Let v^* be the solution to (5.7) with g_0 and g_1 replaced by the corresponding noiseless data g_0^* and g_1^* respectively. The following theorem confirms that the minimizer of $J_{\epsilon,\lambda}$ can be used to approximate the solution to (5.7) via (5.23). It is a generalization of Theorem 4.5 in [10] and Theorem 5.4 in [10]. In fact, in those theorems, the function F has some specific form and does not depend on the first and the second variables $\mathbf{x}$ and $u(\mathbf{x})$.

Theorem 5.4.2 *Assume that problem* (5.7) *with* g_0 *and* g_1 *replaced by* g_0^* *and* g_1^* *respectively has a solution* v^*. *Recall* v_0 *the function we used to change the variable in* (5.9). *Without loss of the generality, assume that*

$$\max\left\{\|v^*\|_{H^p(\Omega)}, \|v_0\|_{H^p(\Omega)}\right\} < \frac{M}{2} - \delta. \tag{5.24}$$

Let $v_{\epsilon,\delta} = u_{\min} + v_0$ *where* $u_{\min}$ *is the minimizer of the strictly convex functional* $J_{\epsilon,\lambda}$. *Then*

$$\|v_{\epsilon,\delta} - v^*\|_{H^2(\Omega)} \leq C(\sqrt{\epsilon}\|v^* - v_0\|_{H^p(\Omega)} + \delta) \tag{5.25}$$

for some constant C *depending on* Ω, M *and* F.

Proof. For $\mathbf{x} \in \Omega$, define

$$u^*(\mathbf{x}) = v^*(\mathbf{x}) - v_0(\mathbf{x}). \tag{5.26}$$

It is obvious that

$$\begin{cases} \partial_\nu u^*(\mathbf{x}) = g_0^*(\mathbf{x}) - g_0(\mathbf{x}) = -\partial_\nu \mathcal{E}(\mathbf{x}) & \text{for all } \mathbf{x} \in \partial\Omega, \\ u^*(\mathbf{x}) = g_1^*(\mathbf{x}) - g_1(\mathbf{x}) = -\mathcal{E}(\mathbf{x}) & \text{for all } \mathbf{x} \in \Gamma \end{cases}$$

Thus, $u^* + \mathcal{E} \in H_0$. Using the triangle inequality, (5.22) and (5.24), we have $u^* + \mathcal{E} \in B(M)$. Using (5.20) with u_1 and u_2 replaced by $u_{\min}$ and $u^* + \mathcal{E}$ respectively, we have

$$\begin{aligned} &J_{\epsilon,\lambda}(u^* + \mathcal{E}) - J_{\epsilon,\lambda}(u_{\min}) - DJ_{\epsilon,\lambda}(u_{\min})(u^* + \mathcal{E} - u_{\min}) \\ &\qquad \geq C\|u^* + \mathcal{E} - u_{\min}\|^2_{H^2(\Omega)} + \epsilon\|u^* + \mathcal{E} - u_{\min}\|^2_{H^p(\Omega)}. \end{aligned} \tag{5.27}$$

Since $u_{\min}$ is the minimizer of $J_{\epsilon,\lambda}$ in $B(M)$, $DJ_{\epsilon,\lambda}(u_{\min}) = 0$. This, together with (5.27) and the fact that $-J_{\epsilon,\lambda}(u_{\min}) \leq 0$, implies

$$J_{\epsilon,\lambda}(u^* + \mathcal{E}) \geq C\|u^* + \mathcal{E} - u_{\min}\|^2_{H^2(\Omega)} + \epsilon\|u^* + \mathcal{E} - u_{\min}\|^2_{H^p(\Omega)}. \tag{5.28}$$

Using the inequality $(a+b)^2 \leq 2a^2 + 2b^2$, we next estimate

$$\begin{aligned} &J_{\epsilon,\lambda}(u^* + \mathcal{E}) \\ &\quad = \int_\Omega \mu_\lambda(\mathbf{x})|\Delta(u^* + \mathcal{E}) - F(\mathbf{x}, u^* + \mathcal{E}, \nabla u^* + \nabla\mathcal{E})|^2 d\mathbf{x} + \epsilon\|u^* + \mathcal{E}\|^2_{H^p(\Omega)} \\ &\quad \leq 2\int_\Omega \mu_\lambda(\mathbf{x})|\Delta u^* - F(\mathbf{x}, u^*, \nabla u^*)|^2 d\mathbf{x} \\ &\qquad + 2\int_\Omega \mu_\lambda(\mathbf{x})|\Delta\mathcal{E} + F(\mathbf{x}, u^*, \nabla u^*) - F(\mathbf{x}, u^* + \mathcal{E}, \nabla u^* + \nabla\mathcal{E})|^2 d\mathbf{x} \\ &\qquad\qquad + \epsilon\|u^* + \mathcal{E}\|^2_{H^p(\Omega)}. \end{aligned} \tag{5.29}$$

Since v^* is the true solution to (5.7), by (5.10), (5.11) and (5.26), we have

$$\Delta u^* - F(\mathbf{x}, u^*, \nabla u^*) = 0 \quad \text{for all } \mathbf{x} \in \Omega.$$

Using (5.22) and (5.29) and the fact that F is in C^1 and hence, Lipschitz, we have

$$J_{\epsilon,\lambda}(u^* + \mathcal{E}) \leq C\delta^2 + \epsilon \|u^* + \mathcal{E}\|^2_{H^p(\Omega)}. \tag{5.30}$$

Combining (5.28) and (5.30) and using the inequality $(a+b)^2 \leq 2(a^2+b^2)$, we have

$$\|u^* - u_{\min}\|^2_{H^2(\Omega)} \leq C(\delta^2 + \epsilon \|u^*\|^2_{H^p(\Omega)}).$$

Estimate (5.25) is proved. □

The procedure to compute v^* is described in Algorithm 4.

Algorithm 4 A numerical method to solve (5.7)

1: Choose M large enough and choose a threshold error $\varepsilon > 0$.
2: Set $m = 0$ and take a function u_0 in $B(M)$.
3: Compute u_{m+1} using the gradient descent method, see (5.4) for some $0 < \eta \ll 1$.
4: If $\|u_{m+1} - u_m\|_{H^2(\Omega)} < \varepsilon$, go to Step 5. Otherwise, set $m = m + 1$ and go back to Step 3.
5: Set $v^{\text{comp}} = u_{m+1} + g$.

Remark 5.4.1 *The choices of M and ε in Step 1 are based on some trial and error processes.*

Remark 5.4.2 *Theorems 5.4.1 and 5.4.2 hold true even when the functions v, u, G, F, g_0 and g_1 take complex values. By splitting* (5.7) *and* (5.10) *into real part and imaginary part, we obtain a system of quasi-linear PDEs on the field of real numbers. Then, we can apply the whole analysis for the case of a single equation to the case of a system of PDEs.*

5.5 A coefficient inverse problem in the frequency domain with back scattering data in $\mathbb{R}^3$

In this section, we introduce a method to solve the backscattering inverse problem with multi-frequency data. This inverse problem has uncountable real-world applications. Solving a system like (5.7) plays an important role in our method. Let Ω be the cube $(-R, R)^3 \subset \mathbb{R}^3$ where R is a positive number. Let $c \in C^1(\mathbb{R}^3)$ represent the dielectric constant of $\mathbb{R}^3$. Assume that

$$\begin{cases} c(\mathbf{x}) = 1 & \text{if } \mathbf{x} \in \mathbb{R}^3 \setminus \Omega, \\ c(\mathbf{x}) \geq 1 & \text{if } \mathbf{x} \in \Omega. \end{cases} \tag{5.31}$$

Assumption (5.31) can be understood as the dielectric constant of the air (or vacuum) is scaled to be 1. Let $[\underline{k}, \overline{k}]$ be an interval of wave number and let $\mathbf{x}_0 = (0, 0, -d)$, with $d > R$, be a point located outside Ω. Let $u = u(\mathbf{x}, k)$, $(\mathbf{x}, k) \in \mathbb{R}^3 \times [\underline{k}, \overline{k}]$, represent the frequency-dependent wave. The function $u(\mathbf{x}, k)$ is governed by the following problem

$$\begin{cases} \Delta u(\mathbf{x}, k) + k^2 c(\mathbf{x}) u(\mathbf{x}, k) &= -\delta(\mathbf{x} - \mathbf{x}_0) & \mathbf{x} \in \mathbb{R}^3, \\ \partial_{|\mathbf{x}|} u(\mathbf{x}, k) - \mathrm{i}k u(\mathbf{x}, k) &= o(|\mathbf{x}|^{-1}) & |\mathbf{x}| \to \infty \end{cases} \tag{5.32}$$

where δ is the Dirac function. The partial differential differential equation in (5.32) is called the Helmholtz equation and the asymptotic behavior of u as $|\mathbf{x}| \to \infty$ is called the Sommerfeld radiation condition. The Sommerfeld radiation condition guarantees the existence and uniqueness of problem (5.32), see [6, Chapter 8]. We are interested in the following problem.

Problem 5.5.1 (Coefficient inverse problem from backscattering data) *Let*

$$\Gamma = \{\mathbf{x} = (x, y, -R) : -R \leq x, y \leq R\} \subset \partial\Omega \tag{5.33}$$

be the measurement site. Given the measurements of

$$f(\mathbf{x},k)=u(\mathbf{x},k)\quad \textit{and}\quad g(\mathbf{x},k)=-\partial_z u(\mathbf{x},k) \tag{5.34}$$

for $(\mathbf{x},k)\in\Gamma\times[\underline{k},\overline{k}]$, *determine the function* $c(\mathbf{x})$, $\mathbf{x}\in\Omega$.

Remark 5.5.1 *We refer the reader to our recent works [9, 10, 8] in which we study a similar inverse problem in which the data are generated by a source moving along a straight line, and only a single frequency was used. Unlike this, the data for the inverse problem under consideration, Problem 5.5.1, are generated by a single source and by multi-frequencies.*

Problem 5.5.1 arises from the following well-known experiment, illustrated in Figure 5.1. Let an optical source illuminate objects inside Ω. The wave generated by the optical source is called the incident wave. The incident wave hits the objects and scatters in all directions. We collect the scattering wave on the part of $\partial\Omega$, named as Γ, that receives the wave coming back from the objects. Solving Problem 5.5.1, with these data, we obtain the dielectric constant of the medium. This information is important in identifying the objects. The forward problem corresponding to Problem 5.5.1 is the problem of computing the function $u(\mathbf{x},k)$, $(\mathbf{x},k)\in\Gamma\times[\underline{k},\overline{k}]$. To solve the forward problem, we first model the incident wave by the point source

$$u_0(\mathbf{x},k)=\frac{\exp(\mathrm{i}k|\mathbf{x}-\mathbf{x}_0|)}{4\pi|\mathbf{x}-\mathbf{x}_0|}\quad (\mathbf{x},k)\in\mathbb{R}^3\times[\underline{k},\overline{k}]. \tag{5.35}$$

It is well-known that

$$\Delta u_0(\mathbf{x},k)+k^2u_0(\mathbf{x},k)=-\delta(\mathbf{x}-\mathbf{x}_0)\quad \mathbf{x}\in\mathbb{R}^3, k\in[\underline{k},\overline{k}]. \tag{5.36}$$

Let

$$u_{\mathrm{sc}}(\mathbf{x},k)=u(\mathbf{x},k)-u_0(\mathbf{x},k)\quad \mathbf{x}\in\mathbb{R}^3, k\in[\underline{k},\overline{k}] \tag{5.37}$$

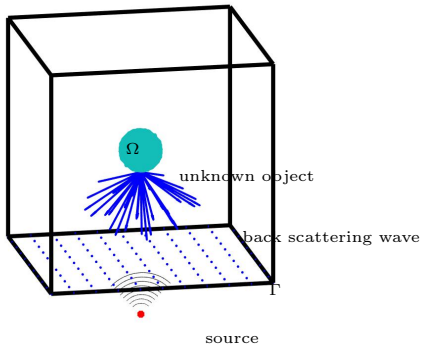

Figure 5.1: A diagram for the experiment that leads to Problem 5.5.1. The unknown object is located inside a box Ω. An emitter (the red dot), located outside Ω, emits the incident wave. The incident wave scatters when hitting an unknown object. The back-scattering waves are represented by blue arrows and collected on an array of detectors located on the part Γ of $\partial\Omega$.

denote the scattering wave. It follows from (5.37) that $u(\mathbf{x}, k)$ is the sum of the scattering wave and the incident wave. We call the function $u(\mathbf{x}, k)$ the total wave. Subtracting the differential equation in (5.32) from (5.36), we obtain

$$\Delta u_{\text{sc}}(\mathbf{x}, k) + k^2 u_{\text{sc}}(\mathbf{x}, k) = -k^2(c(\mathbf{x}) - 1)u(\mathbf{x}, k) \quad \mathbf{x} \in \mathbb{R}^3, k \in [\underline{k}, \overline{k}].$$

Hence, see [6, Chapter 8],

$$u_{\text{sc}}(\mathbf{x}, k) = k^2 \int_{\mathbb{R}^3} \frac{\exp(\mathrm{i}k|\mathbf{x} - \xi|)}{4\pi|\mathbf{x} - \xi|}(c(\xi) - 1)u(\xi, k)d\xi \quad \mathbf{x} \in \mathbb{R}^3, k \in [\underline{k}, \overline{k}]. \tag{5.38}$$

Combining (5.37) and (5.38), we arrive at the Lippmann-Schwinger equation

$$u(\mathbf{x}, k) = u_0(\mathbf{x}, k) + k^2 \int_{\mathbb{R}^3} \frac{\exp(\mathrm{i}k|\mathbf{x} - \xi|)}{4\pi|\mathbf{x} - \xi|}(c(\xi) - 1)u(\xi, k)d\xi \tag{5.39}$$

for all $\mathbf{x} \in \mathbb{R}^3, k \in [\underline{k}, \overline{k}]$. We solve the integral equation (5.39) by the method in [25, 26]. In order to solve the inverse problem, we need to impose the following condition.

Assumption 5.5.1 *The total wave $u(\mathbf{x}, k)$ is nonzero for all $\mathbf{x} \in \Omega$ and $k \in [\underline{k}, \overline{k}]$.*

We provide here an example when Assumption 5.5.1 holds true. In this example, we assume that c is in the class $C^{15}(\mathbb{R}^3)$. Consider the Riemannian metric generated by c

$$d\tau = \sqrt{c(\mathbf{x})}d\mathbf{x}, \quad |d\mathbf{x}| = \sqrt{dx_1^2 + dx_2^2 + dx_3^2}. \tag{5.40}$$

Assume that for each point $\mathbf{x} \in \mathbb{R}^3$, the geodesic line with respect to the Riemannian metric defined (5.40) connecting $\mathbf{x}_0$ and $\mathbf{x}$ is unique, where $\mathbf{x}_0$ is the location of the emitter that emits the point source. Then, it was shown in [21] that

$$u(\mathbf{x}, k) = A(\mathbf{x})e^{\mathrm{i}k\tau(\mathbf{x})} + O\Big(\frac{1}{k}\Big) \quad \text{as } k \to \infty \tag{5.41}$$

for $\mathbf{x} \in \Omega$ where A is a function taking positive value and τ is the travel time of the wave from $\mathbf{x}_0$ to $\mathbf{x}$. Hence, Assumption 5.5.1 holds true when the wave number k is sufficiently large. In the next section, we derive a system of nonlinear partial differential equations. Solution of this system directly yields the solution to Problem 5.5.1.

5.6 A method to solve Problem 5.5.1

Recall that $u = u(\mathbf{x}, k)$, $\mathbf{x} \in \Omega$, $k \in [\underline{k}, \overline{k}]$ is the solution to (5.32). Assume that Assumption 5.5.1 holds true. Define

$$v(\mathbf{x}, k) = \frac{1}{k^2} \log \frac{u(\mathbf{x}, k)}{u_0(\mathbf{x}, k)} \quad \text{for all } \mathbf{x} \in \Omega, k \in [\underline{k}, \overline{k}]. \tag{5.42}$$

Although u/u_0 takes complex values, the function v can be defined. Employing (5.41) and assuming that both $\underline{k}$ and $\overline{k}$ are large, we define the function v as

$$\begin{aligned} v(\mathbf{x},k) &= \frac{1}{k^2}\big[\log u(\mathbf{x},k) - \log u_0(\mathbf{x},k)\big] \\ &= \frac{1}{k^2}\Big[\ln A(\mathbf{x}) - \ln\frac{1}{4\pi|\mathbf{x}-\mathbf{x}_0|} + \mathrm{i}k(\tau(\mathbf{x}) - |\mathbf{x}-\mathbf{x}_0|) + O(1/k)\Big] \end{aligned}$$

for all $\mathbf{x} \in \Omega, k \in [\underline{k}, \overline{k}]$. We now derive a differential equation for the function v. It follows from (5.42) that

$$\nabla v(\mathbf{x},k) = \frac{1}{k^2}\Big(\frac{\nabla u(\mathbf{x},k)}{u(\mathbf{x},k)} - \frac{\nabla u_0(\mathbf{x},k)}{u_0(\mathbf{x},k)}\Big) \quad \text{for all } \mathbf{x} \in \Omega, k \in [\underline{k}, \overline{k}]. \tag{5.43}$$

Taking the divergence of (5.43) gives

$$\Delta v(\mathbf{x},k) = \frac{1}{k^2}\Big(\frac{\Delta u(\mathbf{x},k)}{u(\mathbf{x},k)} - \Big(\frac{\nabla u(\mathbf{x},k)}{u(\mathbf{x},k)}\Big)^2 - \frac{\Delta u_0(\mathbf{x},k)}{u_0(\mathbf{x},k)} + \Big(\frac{\nabla u_0(\mathbf{x},k)}{u_0(\mathbf{x},k)}\Big)^2\Big) \tag{5.44}$$

for all $\mathbf{x} \in \Omega$, $k \in [\underline{k}, \overline{k}]$. Since $u(\mathbf{x},k)$ satisfies the differential equation in (5.32) and $u_0(\mathbf{x},k)$ satisfies the differential equation in (3.1) with $c(\mathbf{x})$ replaced by 1, we have

$$\frac{\Delta u(\mathbf{x},k)}{u(\mathbf{x},k)} = -k^2 c(\mathbf{x}) \quad \text{and} \quad \frac{\Delta u_0(\mathbf{x},k)}{u_0(\mathbf{x},k)} = -k^2 \tag{5.45}$$

for all $\mathbf{x} \in \Omega$, $k \in [\underline{k}, \overline{k}]$. It follows from (5.43), (5.44) and (5.45) that

$$\begin{aligned} \Delta v(\mathbf{x},k) &= \frac{1}{k^2}\Big[-k^2(c(\mathbf{x})-1) - \Big(k^2\nabla v(\mathbf{x},k) + \frac{\nabla u_0(\mathbf{x},k)}{u_0(\mathbf{x},k)}\Big)^2 + \Big(\frac{\nabla u_0(\mathbf{x},k)}{u_0(\mathbf{x},k)}\Big)^2\Big] \\ &= -(c(\mathbf{x})-1) - k^2(\nabla v(\mathbf{x},k))^2 - \frac{2\nabla v(\mathbf{x},k)\cdot\nabla u_0(\mathbf{x},k)}{u_0(\mathbf{x},k)} \end{aligned}$$

for all $\mathbf{x} \in \Omega$, $k \in [\underline{k}, \overline{k}]$. We obtain

$$\Delta v(\mathbf{x},k) + k^2(\nabla v(\mathbf{x},k))^2 + \frac{2\nabla v(\mathbf{x},k)\cdot\nabla u_0(\mathbf{x},k)}{u_0(\mathbf{x},k)} = -c(\mathbf{x}) + 1 \tag{5.46}$$

for all $\mathbf{x} \in \Omega$, $k \in [\underline{k}, \overline{k}]$. Differentiate (5.46) with respect to k. We have

$$\Delta \partial_k v(\mathbf{x}, k) + 2k^2 \nabla v(\mathbf{x}, k) \cdot \nabla \partial_k v(\mathbf{x}, k) + 2k(\nabla v(\mathbf{x}, k))^2 + 2\nabla \partial_k v(\mathbf{x}, k) \cdot \frac{\nabla u_0(\mathbf{x}, k)}{u_0(\mathbf{x}, k)} + 2\nabla v(\mathbf{x}, k) \partial_k \frac{\nabla u_0(\mathbf{x}, k)}{u_0(\mathbf{x}, k)} = 0 \quad (5.47)$$

for all $\mathbf{x} \in \Omega$, $k \in [\underline{k}, \overline{k}]$.

Let $\{\Psi_m\}_{m \geq 1}$ be the orthonormal basis of $L^2(\Omega)$ defined in [15]. This basis is constructed as follows. For each $m \geq 1$, define the function $\phi_m(k) = k^{m-1} e^{k-(\overline{k}+\underline{k})/2}$ for all $k \in [\underline{k}, \overline{k}]$. It is clear that the set $\{\phi_m\}_{m \geq 1}$ is complete in $[\underline{k}, \overline{k}]$. We then apply the Gram-Schmidt orthonormalization process to this set to obtain the basis $\{\Psi_m\}_{m \geq 1}$.

We derive an approximation model for the solution v to (5.47) as follows. For each $\mathbf{x} \in \Omega$ and $k \in [\underline{k}, \overline{k}]$, we write

$$v(\mathbf{x}, k) = \sum_{i=1}^{\infty} v_i(\mathbf{x}) \Psi_i(k) \simeq \sum_{i=1}^{N} v_i(\mathbf{x}) \Psi_i(k) \quad (5.48)$$

for some cut-off number N, determined later in section 5.7, where

$$v_i(\mathbf{x}) = \int_{\underline{k}}^{\overline{k}} v(\mathbf{x}, \kappa) \Psi_i(\kappa) d\kappa \quad i \in \{1, \ldots, N\}. \quad (5.49)$$

In this approximation context,

$$v_k(\mathbf{x}, k) = \sum_{i=1}^{N} v_i(\mathbf{x}) \Psi_i'(k) \quad \text{for all } \mathbf{x} \in \Omega, k \in [\underline{k}, \overline{k}]. \quad (5.50)$$

Plugging (5.48) and (5.50) into (5.47) gives

$$\sum_{i=1}^{N}\Delta v_i(\mathbf{x})\Psi_i'(k)+2\sum_{i,j=1}^{N}\nabla v_i(\mathbf{x})\cdot\nabla v_j(\mathbf{x})\Big(k^2\Psi_i(k)\Psi_j'(k)+k\Psi_i(k)\Psi_j(k)\Big)$$
$$+2\sum_{i=1}^{N}\nabla v_i(\mathbf{x})\cdot\Big(\Psi_i'(k)\frac{\nabla u_0(\mathbf{x},k)}{u_0(\mathbf{x},k)}+\Psi_i(k)\partial_k\frac{\nabla u_0(\mathbf{x},k)}{u_0(\mathbf{x},k)}\Big)=0 \quad (5.51)$$

for all $\mathbf{x}\in\Omega$. For each $l\in\{1,\dots,N\}$, multiplying $\Psi_l(k)$ to both sides of (5.51), we have

$$\sum_{i=1}^{N}s_{li}\Delta v_i(\mathbf{x})+\sum_{i,j=1}^{N}a_{lij}\nabla v_i(\mathbf{x})\cdot\nabla v_j(\mathbf{x})+\sum_{i=1}^{N}B_{li}(\mathbf{x})\cdot\nabla v_i(\mathbf{x})=0 \quad (5.52)$$

where

$$\begin{cases} s_{li}=\displaystyle\int_{\underline{k}}^{\overline{k}}\Psi_i'(k)\Psi_l(k)dk,\\ a_{lij}=2\displaystyle\int_{\underline{k}}^{\overline{k}}\Big(k^2\Psi_i(k)\Psi_j'(k)+k\Psi_i(k)\Psi_j(k)\Big)\Psi_l(k)dk,\\ B_{li}(\mathbf{x})=2\displaystyle\int_{\underline{k}}^{\overline{k}}\Big(\Psi_i'(k)\frac{\nabla u_0(\mathbf{x},k)}{u_0(\mathbf{x},k)}+\Psi_i(k)\partial_k\frac{\nabla u_0(\mathbf{x},k)}{u_0(\mathbf{x},k)}\Big)\Psi_l(k)dk \end{cases} \quad (5.53)$$

for all $i,j,l\in\{1,\dots,N\}$ and $\mathbf{x}\in\Omega$.

We next compute the boundary information for V. For all $\mathbf{x}\in\Gamma$ and $k\in[\underline{k},\overline{k}]$, since $u(\mathbf{x},k)=f(\mathbf{x},k)$ where f is the data for the inverse problem under consideration (see (5.34)), it follows from (5.42) that $v(\mathbf{x},k)=\frac{1}{k^2}\log\frac{f(\mathbf{x},k)}{u_0(\mathbf{x},k)}$. Hence, by (5.49), we have

$$v_i(\mathbf{x})=\int_{\underline{k}}^{\overline{k}}v(\mathbf{x},\kappa)\Psi_i(\kappa)d\kappa=\int_{\underline{k}}^{\overline{k}}\frac{1}{\kappa^2}\log\frac{f(\mathbf{x},\kappa)}{u_0(\mathbf{x},\kappa)}\Psi_i(\kappa)d\kappa \quad i\in\{1,\dots,N\}$$

for all $\mathbf{x}\in\Gamma$. Since we only measure the wave u on Γ, we complement $v_i(\mathbf{x})=0$ for all $i\in\{1,\cdots,N\}$ and $\mathbf{x}\in\partial\Omega\setminus\Gamma$. The boundary value of $V_N=(v_1,v_2,\dots,v_N)^{\mathrm{T}}$ is

given by

$$V_N(\mathbf{x}) = g_1(\mathbf{x}) = \begin{cases} \Big[\int_{\underline{k}}^{\overline{k}} \frac{1}{\kappa^2} \log \frac{f(\mathbf{x},\kappa)}{u_0(\mathbf{x},\kappa)} \Psi_i(\kappa) d\kappa\Big]_{i=1}^{N} & \mathbf{x} \in \Gamma, \\ 0 & \mathbf{x} \in \partial\Omega \setminus \Gamma \end{cases} \tag{5.54}$$

On the other hand, by (5.49), for all $\mathbf{x} \in \Gamma$ and $k \in [\underline{k}, \overline{k}]$,

$$\partial_\nu v(\mathbf{x},k) = \frac{1}{k^2}\Big(\frac{\partial_\nu u(\mathbf{x},k)}{u(\mathbf{x},k)} - \frac{\partial_\nu u_0(\mathbf{x},k)}{u_0(\mathbf{x},k)}\Big) = \frac{1}{k^2}\Big(\frac{g(\mathbf{x},k)}{f(\mathbf{x},k)} - \frac{\partial_\nu u_0(\mathbf{x},k)}{u_0(\mathbf{x},k)}\Big).$$

Therefore, by (5.49),

$$\begin{aligned} \partial_\nu v_i(\mathbf{x}) &= \int_{\underline{k}}^{\overline{k}} \partial_\nu v(\mathbf{x},\kappa)\Psi_i(\kappa) d\kappa \\ &= \int_{\underline{k}}^{\overline{k}} \frac{1}{\kappa^2}\Big(\frac{g(\mathbf{x},\kappa)}{f(\mathbf{x},\kappa)} - \frac{\partial_\nu u_0(\mathbf{x},\kappa)}{u_0(\mathbf{x},\kappa)}\Big)\Psi_i(\kappa) d\kappa \end{aligned} \tag{5.55}$$

for all $i \in \{1,\dots,N\}$ and $\mathbf{x} \in \Gamma$. By setting

$$g_0(\mathbf{x}) = \left[\int_{\underline{k}}^{\overline{k}} \frac{1}{\kappa^2}\Big(\frac{g(\mathbf{x},\kappa)}{f(\mathbf{x},\kappa)} - \frac{\partial_\nu u_0(\mathbf{x},\kappa)}{u_0(\mathbf{x},\kappa)}\Big)\Psi_i(\kappa) d\kappa\right]_{i=1}^{N}, \tag{5.56}$$

we have

$$\partial_\nu V(\mathbf{x}) = g_0(\mathbf{x}) \quad \text{for all } \mathbf{x} \in \Gamma. \tag{5.57}$$

In summary, the vector $V_N = (v_1, v_2, \dots, v_N)^{\mathrm{T}}$ satisfies a Cauchy like boundary value

problem

$$\begin{cases} \sum_{i=1}^{N} s_{li}\Delta v_i(\mathbf{x}) + \sum_{i,j=1}^{N} a_{lij}\nabla v_i(\mathbf{x})\cdot\nabla v_j(\mathbf{x}) & \\ \qquad + \sum_{i=1}^{N} B_{li}(\mathbf{x})\cdot\nabla v_i(\mathbf{x}) = 0, & \mathbf{x}\in\Omega, \\ V_N(\mathbf{x}) = g_1(\mathbf{x}) & \mathbf{x}\in\partial\Omega, \\ \partial_\nu V_N(\mathbf{x}) = g_0(\mathbf{x}) & \mathbf{x}\in\Gamma. \end{cases} \tag{5.58}$$

where s_{ij}, a_{lij}, B_{li}, $1 \le i,j,l \le N$ are given in (5.53), g_1 and g_0, are respectively defined in (5.54) and (5.56).

Remark 5.6.1 *Let $(\tilde{s}_{li})_{l,i=1}^{N}$ denote S^{-1}. Problem* (5.58) *can be rewritten as a particular form of* (5.7) *as*

$$\begin{cases} \sum_{i=1}^{N} \Delta v_i(\mathbf{x}) + \sum_{i,j=1}^{N} \tilde{s}_{li}a_{lij}\nabla v_i(\mathbf{x})\cdot\nabla v_j(\mathbf{x}) & \\ \qquad + \sum_{i=1}^{N} \tilde{s}_{li}B_{li}(\mathbf{x})\cdot\nabla v_i(\mathbf{x}) = 0, & \mathbf{x}\in\Omega, \\ V_N(\mathbf{x}) = g_1(\mathbf{x}) & \mathbf{x}\in\partial\Omega, \\ \partial_\nu V_N(\mathbf{x}) = g_0(\mathbf{x}) & \mathbf{x}\in\Gamma. \end{cases}$$

However, we numerically observe that solving (5.58) *provides better numerical solutions.*

Let $\mu_\lambda(x,y,z) = e^{\lambda(z+r)^2}$ for a number $r > 1$ be a Carleman weight function. We refer the reader to [10, Theorem 3.1] for the proof of Carleman estimate (5.15) with this Carleman weight function in 3D. Thus, we can find the solution to the system of quasi-linear equations (5.58) by the convexification method, see Algorithm 4.

5.7 Numerical tests

In this section, we numerically study Problem 5.3.1 and Problem 5.5.1.

5.7.1 Numerical study for Problem 5.3.1

We present an example in which we apply convexification method to compute the solution to problem of the form (5.7). For simplicity, we consider the case $n = 2$ and the computational domain Ω is chosen to be $(-1, 1)^2$. We choose the set Γ to be $\{(x, y = -1) : |x| \leq 1\} \subset \partial\Omega$, on which we impose the Neumann boundary condition for the solution v. We numerically test the convexification method in the finite difference scheme. That means we compute the values of the solution on the grid

$$\mathcal{G} = \left\{(x_i = -1 + (i-1)d_{\mathbf{x}}, y_j = -1 + (j-1)d_{\mathbf{x}}) : 1 \leq i, j \leq N_{\mathbf{x}}\right\}$$

where $d_{\mathbf{x}} = \frac{2}{N_{\mathbf{x}}-1}$ and $N_{\mathbf{x}}$ is an integer. In our numerical study, $N_{\mathbf{x}} = 41$.

In computation, we use the Carleman weight function $e^{-\lambda(R+1.5)^2} e^{\lambda(y-1.5)^2}$ where $\lambda = 1.1$. This Carleman weight function is the 2D version of the one used in Section 5.7.2. The regularization term is chosen to be $\epsilon = 10^{-6}$. The details in implementation including the discretizing the cost functional $J_{\epsilon,\lambda}$ and the choice of the initial guess are similar to the ones in Section 5.7.2. We do not present in details here. To illustrate the efficiency of Algorithm 4, we compute solution to (5.7) when the nonlineariry G is given by

$$\begin{aligned} G(\mathbf{x}, s, p) = &-\sqrt{|p|^2 + 1} - \sin\left(x + \pi\,(y-0.5)^2\right) + 2\,\pi\,\cos\left(x + \pi\,(y-0.5)^2\right) \\ &- 4\,\pi^2\,(y-0.5)^2 \sin\left(x + \pi\,(y-0.5)^2\right) + \Big[\left(1 + \cos\left(x + \pi\,(y-0.5)^2\right)\right)^2 \\ &+ 4\,\pi^2\,(y-0.5)^2\left(\cos\left(x + \pi\,(y-0.5)^2\right)\right)^2 + 1\Big]^{1/2} \end{aligned} \tag{5.59}$$

for all $\mathbf{x} = (x, y) \in \Omega$, $s \in \mathbb{R}$ and $p \in \mathbb{R}^d$. The exact boundary data are given by

$$\begin{cases} g_1^*(x, y) = x + \sin\left(x + \pi(y-0.5)^2\right) & (x, y) \in \partial\Omega, \\ g_0^*(x, y) = -2\pi(y-0.5)\cos\left(x + \pi(y-0.5)^2\right) & (x, y) \in \Gamma. \end{cases} \tag{5.60}$$

We add noise into the boundary data by the following formulas

$$g_1 = g_1^*(1 + \delta \text{rand}) \quad \text{and} \quad g_0 = g_0^*(1 + \delta \text{rand})$$

where rand is a function taking uniformly distributed random numbers in the range $[-1, 1]$. The noise level δ is set to be 5%, 10% and 20%. The exact solution to (5.7) in this test is $v^*(x, y) = x + \sin\left(x + \pi(y - 0.5)^2\right)$ for all $\mathbf{x} = (x, y) \in \Omega$. The error in computation is given in Table 5.1. The graphs of the exact solution v^*, computed

Table 5.1: The relative error in our computation agaist the noise level δ contained in the boundary data.

δ	relative error $\frac{\|v^* - v^{\text{comp}}\|_{L^\infty(\Omega)}}{\|v^*\|_{L^\infty(\Omega)}}$
5%	4.14%
10%	9.21%
20%	19.40%

solution v^{comp} and their relative differences $\frac{|v^* - v^{\text{comp}}|}{\|v^*\|_{L^\infty(\Omega)}}$, when $\delta = 5\%$, 10% and 20% are displayed in Figure 5.2.

It is evident from Table 5.1 and Figure 5.2 that the convexification method delivers reliable solutions to quasi-linear elliptic equations. The errors in computation are compatible with the noise level and they occur on $\partial\Omega$ where the noise takes place.

5.7.2 Numerical study for Problem 5.5.1

In this section, we present some numerical solutions to Problem 5.5.1. The numerical examples we present in this section illustrate the efficiency of the gradient descent method for the convexification described in section 5.4.

Especially, we will show that the presence of the Carleman weight function in the objective function is crucial. That means, without involving the Carleman estimate, the descent gradient method does not deliver good numerical solutions to the problem of minimizing our nonconvex objective functional.

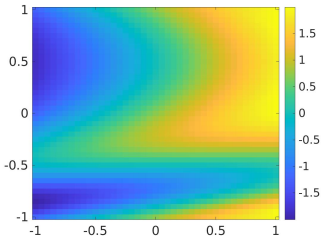

(a) The function v^*

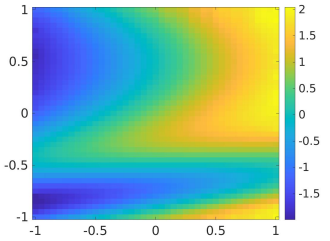

(b) The function v^{comp}. $\delta = 5\%$.

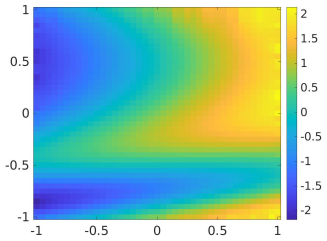

(c) The function v^{comp}. $\delta = 10\%$.

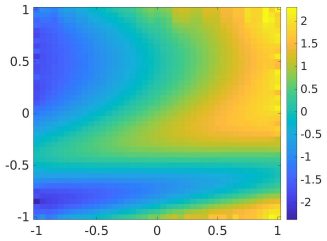

(d) The function v^{comp}. $\delta = 20\%$.

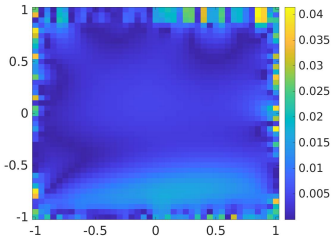

(e) The relative difference $\frac{|v^* - v^{\text{comp}}|}{\|v^*\|_{L^\infty(\Omega)}}$. $\delta = 5\%$

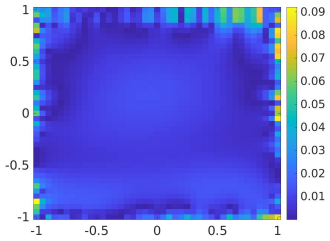

(f) The relative difference $\frac{|v^* - v^{\text{comp}}|}{\|v^*\|_{L^\infty(\Omega)}}$. $\delta = 10\%$

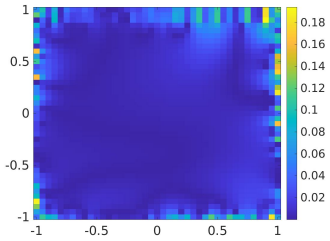

(g) The relative difference $\frac{|v^* - v^{\text{comp}}|}{\|v^*\|_{L^\infty(\Omega)}}$. $\delta = 20\%$

Figure 5.2: Solutions to (5.7) when G and f^* and g^* are given in (5.59) and (5.60) respectively.

5.7.2.1 The forward problem

The experimental setting for Problem 5.5.1 is as follows. Let $R = 1$ and $\Omega = (-R, R)^3$. The source location is placed at $(0, 0, -4)$. The interval of wavenumbers is $[\pi, 2\pi]$, which correspond to the interval of wavelengths $[0.5, 1]$. In order to generate the simulated data, we use the finite difference method in which we decompose Ω as

the uniform partition with grid points

$$\mathcal{G} = \{(x_i = -R + (i-1)h, y_j = -R + (j-1)h, z_l = -R + (l-1)h) : \\ 1 \le i, j, k \le N_{\mathbf{x}}\}$$

where $N_{\mathbf{x}} = 41$ and $h = 2R/(N_{\mathbf{x}} - 1)$. We also split the interval of wavenumbers to the uniform partition

$$\mathcal{K} = \{k_1 = \underline{k}, k_2, \ldots, k_{N_k} = \overline{k}\}$$

where $k_i = \underline{k} + (i-1)(\overline{k} - \underline{k})/(N_k - 1)$ and $N_k = 121$. The forward problem is solved via solving the Lippmann-Schwinger equation (5.39) by the method in [25, 26]. Denote by $u^*(\mathbf{x}, k)$, $\mathbf{x} \in \mathcal{G}$, $k \in \mathcal{K}$ the obtained solution. The noisy data for Problem 5.5.1 is given by

$$f(\mathbf{x}, k) = u(\mathbf{x}, k)(1 + \delta \text{rand}) \quad g(\mathbf{x}, k) = -\partial_z u^*(\mathbf{x}, k)(1 + \delta \text{rand})$$

for all $\mathbf{x} \in \Gamma \cap \mathcal{G}$ and $k \in \mathcal{K}$ where Γ is the measurement site defined in (5.33), $\delta = 10\%$ and rand is the function taking uniformly distributed random numbers in $[-1, 1]$. The truncation number N is 7, which is chosen by a trial-error process.

5.7.2.2 The first approximation of the function V

The first step of our method is to compute a vector-valued function that satisfies

$$\partial_\nu V_0|_\Gamma = g_0 \quad \text{and} \quad V_0|_{\partial\Omega} = g_1. \tag{5.61}$$

This vector-valued function V_0 is used in the change of variable $U = V - V_0$ as in (5.9). Moreover, to guarantee fast convergence, we will find V_0 such that it is close to the solution V. We call this function V_0 the initial solution.

Since our target is to solve the nonlinear system (5.58), it is natural to find $V_0 =$

$(v_1^0, v_2^0, \ldots, v_N^0)$ as the solution to a linear system obtained by removing from (5.58) the nonlinear term, which is

$$\begin{cases} \sum_{i=1}^{N} s_{li}\Delta v_i^0(\mathbf{x}) + \sum_{i=1}^{N} B_{li}(\mathbf{x})\cdot\nabla v_i^0(\mathbf{x}) = 0, & \mathbf{x}\in\Omega, \\ V_0(\mathbf{x}) = g_1(\mathbf{x}) & \mathbf{x}\in\partial\Omega, \\ \partial_\nu V_0(\mathbf{x}) = g_0(\mathbf{x}) & \mathbf{x}\in\Gamma. \end{cases} \tag{5.62}$$

Since (5.62) is a system of linear partial differential equations, we can solve it directly by the quasi-reversibility method involving a Carleman weight function in the finite difference scheme. That means, we minimize the following functional

$$W \mapsto \int_\Omega \mu_\lambda^2 \Big| \sum_{i=1}^{N} s_{li}\Delta w(\mathbf{x}) + \sum_{i=1}^{N} B_{li}(\mathbf{x})\cdot\nabla W(\mathbf{x})\Big|^2 + \epsilon\|W\|^2_{H^2(\Omega)} \tag{5.63}$$

where $W = (w_1, w_2, \ldots, w_N)$ is subject to the boundary conditions $W|_{\partial\Omega} = g_1$ and $\partial_\nu W|_\Gamma = g_0$. In (5.63) and also in this section, the used Carleman weight function is $\mu_\lambda = e^{-\lambda(R+r)^2} e^{\lambda(z-r)^2}$ where $\lambda = 1.1$ and $r = 1.5$ and the regularization parameter $\epsilon = 10^{-6}$. Even though in theory, the value of λ is large. However, we have discovered computationally that a reasonable value $\lambda = 1.1$ works well. So, we use this λ. These observations coincide with those of our previous works on the numerical studies of the convexification [19, 10]. This Carleman weight function is used for all numerical tests in this section.

We refer the reader to [24, 28] for details in the implementation of the quasi-reversibility method to solve a system of linear partial differential equations with Cauchy boundary data.

5.7.2.3 The minimizing sequence

For the simplification in implementation, we skip the step of changing the variable $U = V - V_0$ as in (5.9). Let $U = V - V_0$ where $V_0 = (v_1^0, \ldots, v_N^0)$ is the vector valued

function found in section 5.7.2.2. Then, due to (5.52), we set the cost functional as

$$J(U) = \sum_{l=1}^{N} \int_{\Omega} \mu_{\lambda}^{2} \Big| \sum_{i=1}^{N} s_{li} \Delta v_i - \sum_{i,j=1}^{N} a_{lij} \nabla v_i \cdot \nabla v_j - \sum_{i=1}^{N} B_{li} \nabla v_i \Big)\Big|^2 d\mathbf{x} + \epsilon \|V\|^2_{H^2(\Omega)^N}.$$

The finite difference version of J is

$$\begin{aligned} J(V) = h^3 \sum_{\mathrm{i,j,l=1}}^{N_{\mathbf{x}}} \sum_{l=1}^{N} \mu_{\lambda}^{2}(x_{\mathrm{i}}, y_{\mathrm{j}}, z_{\mathrm{l}}) \Big| \sum_{i=1}^{N} s_{li} \Delta v_i(x_{\mathrm{i}}, y_{\mathrm{j}}, z_{\mathrm{l}}) \\ - \sum_{i,j=1}^{N} a_{lij} \nabla v_i(x_{\mathrm{i}}, y_{\mathrm{j}}, z_{\mathrm{l}}) \cdot \nabla v_j(x_{\mathrm{i}}, y_{\mathrm{j}}, z_{\mathrm{l}}) - \sum_{i=1}^{N} B_{li}(x_{\mathrm{i}}, y_{\mathrm{j}}, z_{\mathrm{l}}) \nabla v_i(x_{\mathrm{i}}, y_{\mathrm{j}}, z_{\mathrm{l}}) \Big|^2 d\mathbf{x} \\ + \epsilon h^3 \sum_{\mathrm{i,j,l=1}}^{N_{\mathbf{x}}} \sum_{l=1}^{N} \Big(|v_l(x_{\mathrm{i}}, y_{\mathrm{j}}, z_{\mathrm{l}})|^2 + |\nabla v_l(x_{\mathrm{i}}, y_{\mathrm{j}}, z_{\mathrm{l}})|^2 + |\Delta v_l(x_{\mathrm{i}}, y_{\mathrm{j}}, z_{\mathrm{l}})|^2 \Big). \quad (5.64) \end{aligned}$$

Remark 5.7.1 *In our computation,* $\epsilon = 10^{-6}$ *for all tests. Also, in* (5.64)*, the regularity term is set to be* $\epsilon\|U\|_{H^2(\Omega)^N}$ *instead of* $H^p(\Omega)^N$*. We observe numerically that using the norm* $\|U\|_{H^2(\Omega)^N}$ *already provides satisfactory numerical solutions. So, it is not necessary for us to choose norm in* $H^p(\Omega)^N$*. This observation significantly reduces the expensive efforts in implementation.*

We now mention that to speed up the minimization procedure, we need to compute the gradient DJ_1 of the discrete functional J_1 in (5.64) above. Having the expression for the gradient via an explicit formula significantly reduces the computational time. We have derived such a formula using the technique of Kronecker deltas, which has been outlined in [23]. For brevity we do not provide this formula here.

5.7.2.4 Numerical examples

We perform three (3) tests.

Test 1. We first consider the case of detecting one target with high dielectric

constant. The dielectric constant of the medium is given by

$$c_{\text{true}} = \begin{cases} 5 & \text{if } 0.6x^2 + y^2 + (z+0.7)^2 \le 0.2^2, \\ 1 & \text{otherwise.} \end{cases}$$

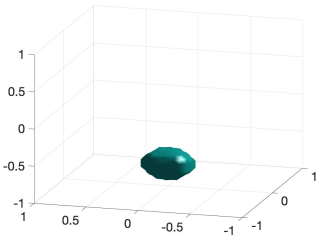

(a) The true 3D image

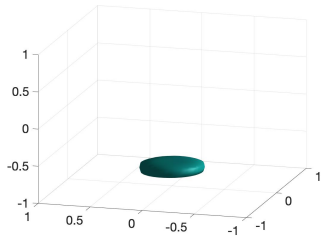

(b) The reconstructed 3D image

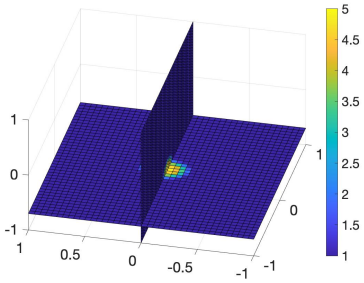

(c) The cross sections $\{z = -0.7\}$ and $\{y = 0\}$ of c_{true}

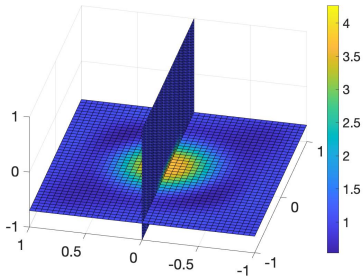

(d) The cross sections $\{z = -0.7\}$ and $\{y = 0\}$ of c_{comp}

Figure 5.3: Test 1. The function c_{true} and its reconstruction c_{comp} from noisy data with noise level of 10%.

The true and computed dielectric constants are displayed in Figure 5.3. It is obvious that the location of the target is detected accurately. The reconstructed shape is somewhat acceptable. The computed maximal value of the dielectric constant is 4.26 (relative error 14.8%)).

Test 2. We test our method when the true dielectric constant is given by

$$c_{\text{true}} = \begin{cases} 3 & \text{if } 0.35^2 \le x^2 + y^2 \le 0.5^2 \text{ and } -0.8 \le z \le -0.65 \\ 1 & \text{otherwise.} \end{cases}$$

The shape of the dielectric constant is a ring.

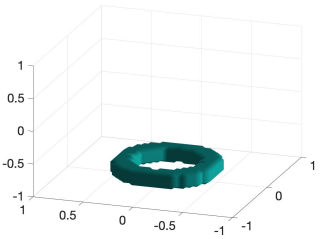

(a) The true 3D image of the ring

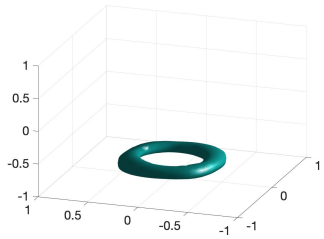

(b) The reconstructed 3D image of the ring

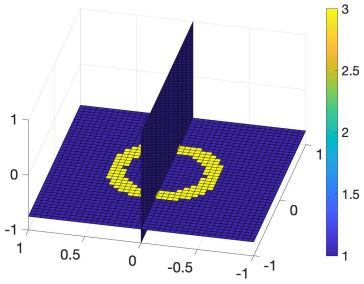

(c) The cross sections $\{z = -0.7\}$ and $\{y = 0\}$ of c_{true}

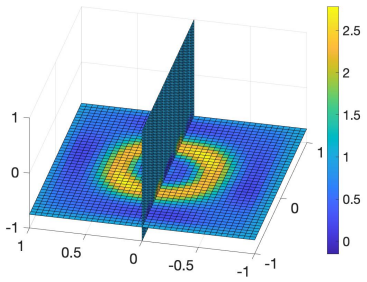

(d) The cross sections $\{z = -0.7\}$ and $\{y = 0\}$ of c_{comp}

Figure 5.4: Test 2. The function c_{true} and its reconstruction c_{comp} from noisy data with noise level of 10%.

The true and computed dielectric constants are displayed in Figure 5.4. It is evident that the dielectric constant is computed successfully. The “ring" shape is clearly detected. The computed maximal value of the dielectric constant is 2.7809 (relative error 7.3%)).

We now consider the direct optimization without using the Carleman weight function. That means we apply the same procedure to compute the dielectric constant except taking $\lambda = 0$. The numerical result in Figure 5.5 show that without the Carleman weight function involving, we reconstruction is poor.

Test 3. We consider dielectric constant with a more complicate geometry. The graph of the dielectric constant is a letter Y located on the plane $z = -.7$ The true and constructed dielectric constants are displayed in Figure 5.6. We observe that our method can detect the shape of the letter Y clearly. Moreover, the reconstructed

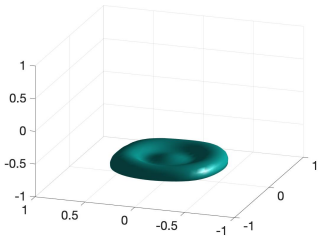

(a) The 3D image computed without using the convexification method

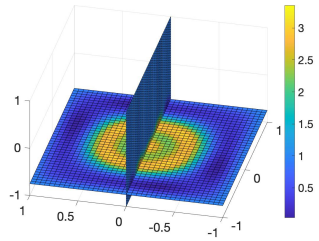

(b) The cross sections $\{z = -0.75\}$ and $\{y = 0\}$ of c_{comp}

Figure 5.5: Test 2. The function c_{true} and its reconstruction c_{comp} from noisy data with noise level of 10% without using Carleman weight function. It is evident that, in this case, the "ring" shape cannot be reconstructed well.

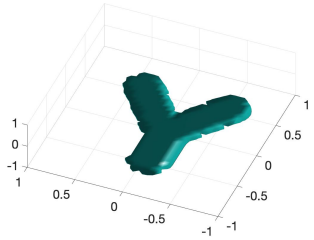

(a) The true 3D image of the letter Y

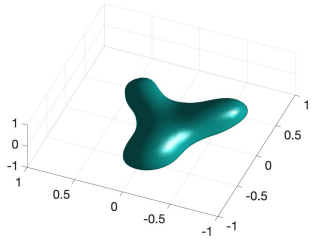

(b) The reconstructed 3D image of the letter Y

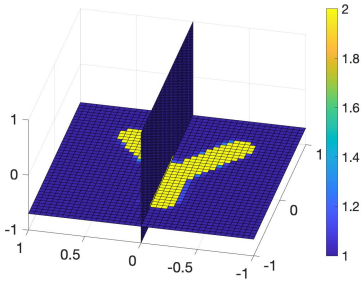

(c) The cross sections $\{z = -0.7\}$ and $\{y = 0\}$ of c_{true}

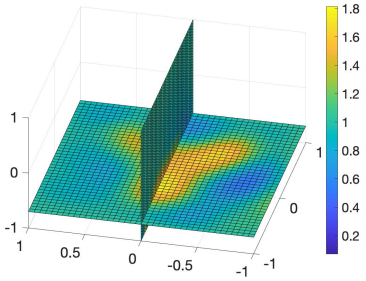

(d) The cross sections $\{z = -0.7\}$ and $\{y = 0\}$ of c_{comp}

Figure 5.6: Test 3. The function c_{true} and its reconstruction c_{comp} from noisy data with noise level of 10%.

value of the dielectric constant is acceptable. The computed maximal value of the function c is 1.8116 (relative error 9.4%).

5.8 Concluding remarks

In the first part of this chapter, we proved the convergence of the gradient descent method to find the minimizer of a functional which is strictly convex on a ball in a Hilbert space rather than on the whole space. This is a new result compared with previously obtained ones by our research team for the case of a more complicated gradient projection method. Then we used the convexification method and gradient descent method to solve a boundary value problem of quasi-linear PDE with both Dirichlet and Neumann data. We proved that this approach provides reasonable numerical solutions as the noise tends to zero. In the second part of the chapter, we applied the theoretical results of the first part to solve an inverse scattering problem. To solve this inverse problem, we derive an approximate mathematical model, which is the Cauchy problem for a coupled system of quasi-linear elliptic partial differential equations. Then, we apply the convexification and the gradient descent method to solve this system. Numerical results for the inverse scattering problem demonstrate a good reconstruction quality.

REFERENCES

[1] O.M. Alifanov. *Inverse heat conduction problems*. Springer, New York, 1994.

[2] O.M. Alifanov, A.E. Artukhin, and S.V. Rumyantcev. *Extreme Methods for Solving Ill-Posed Problems with Applications to Inverse Heat Transfer Problems*. Begell House, New York, 1995.

[3] A. B. Bakushinskii, M. V. Klibanov, and N. A. Koshev. Carleman weight functions for a globally convergent numerical method for ill-posed Cauchy problems for some quasilinear PDEs. *Nonlinear Anal. Real World Appl.*, 34:201–224, 2017.

[4] L. Beilina and M. V. Klibanov. *Approximate Global Convergence and Adaptivity for Coefficient Inverse Problems*. Springer, New York, 2012.

[5] A. L. Bukhgeim and M. V. Klibanov. Uniqueness in the large of a class of multidimensional inverse problems. *Soviet Math. Doklady*, 17:244–247, 1981.

[6] David Colton and Rainer Kress. *Inverse acoustic and electromagnetic scattering theory. Applied Mathematical Sciences*. Springer, New York, 3rd edition, 2013.

[7] V. Isakov. *Inverse Problems for Partial Differential Equations*. Springer, New York, third edition, 2017.

[8] V. A. Khoa, G. W. Bidney, M. V. Klibanov, L. H. Nguyen, L. Nguyen, A. Sullivan, and V. N. Astratov. Convexification and experimental data for a 3D inverse scattering problem with the moving point source. *Inverse Problems*, 36:085007, 2020.

[9] V. A. Khoa, G. W. Bidney, M. V. Klibanov, L. H. Nguyen, L. Nguyen, A. Sullivan, and V. N. Astratov. An inverse problem of a simultaneous reconstruction of the dielectric constant and conductivity from experimental backscattering data. *Inverse Problems in Science and Engineering*, 29(5):712–735, 2021.

[10] V. A. Khoa, M. V. Klibanov, and L. H. Nguyen. Convexification for a 3D inverse scattering problem with the moving point source. *SIAM J. Imaging Sci.*, 13(2):871–904, 2020.

[11] M. V. Klibanov. Inverse problems and Carleman estimates. *Inverse Problems*, 8:575–596, 1992.

[12] M. V. Klibanov. Global convexity in a three-dimensional inverse acoustic problem. *SIAM J. Math. Anal.*, 28:1371–1388, 1997.

[13] M. V. Klibanov. Carleman estimates for global uniqueness, stability and numerical methods for coefficient inverse problems. *J. Inverse and Ill-Posed Problems*, 21:477–560, 2013.

[14] M. V. Klibanov. Carleman weight functions for solving ill-posed Cauchy problems for quasilinear PDEs. *Inverse Problems*, 31:125007, 2015.

[15] M. V. Klibanov. Convexification of restricted Dirichlet to Neumann map. *J. Inverse and Ill-Posed Problems*, 25(5):669–685, 2017.

[16] M. V. Klibanov and O. V. Ioussoupova. Uniform strict convexity of a cost functional for three-dimensional inverse scattering problem. *SIAM J. Math. Anal.*, 26:147–179, 1995.

[17] M. V. Klibanov, V. A. Khoa, A. V. Smirnov, L. H. Nguyen, G. W. Bidney, L. Nguyen, A. Sullivan, and V. N. Astratov. Convexification inversion method for nonlinear SAR imaging with experimentally collected data. *to appear on J. Applied and Industrial Mathematics, see also Arxiv:2103.10431*, 2021.

[18] M. V. Klibanov and J. Li. *Inverse Problems and Carleman Estimates: Global Uniqueness, Global Convergence and Experimental Data.* De Gruyter, 2021.

[19] M. V. Klibanov, J. Li, and W. Zhang. Convexification of electrical impedance tomography with restricted Dirichlet-to-Neumann map data. *Inverse Problems*, 35:035005, 2019.

[20] M. V. Klibanov, Z. Li, and W. Zhang. Convexification for the inversion of a time dependent wave front in a heterogeneous medium. *SIAM J. Appl. Math.*, 79:1722–1747, 2019.

[21] M. V Klibanov and V. G. Romanov. Reconstruction procedures for two inverse scattering problems without the phase information. *SIAM J. Applied Mathematics*, 76:178–196, 2016.

[22] M. V. Klibanov and A. Timonov. *Carleman Estimates for Coefficient Inverse Problems and Numerical Applications.* Inverse and Ill-Posed Problems Series. VSP, Utrecht, 2004.

[23] A. Kuzhuget and M. V. Klibanov. Global convergence for a 1-D inverse problem with application to imaging of land mines. *Applicable Analysis*, 89(1):125–157, 2010.

[24] T. T. Le and L. H. Nguyen. A convergent numerical method to recover the initial condition of nonlinear parabolic equations from lateral cauchy data. *Journal of Inverse and Ill-posed Problems*, 30(2):265–286, 2022.

[25] A. Lechleiter and D.-L. Nguyen. A trigonometric Galerkin method for volume integral equations arising in TM grating scattering. *Adv. Comput. Math.*, 40:1–25, 2014.

[26] D. L. Nguyen. A volume integral equation method for periodic scattering problems for anisotropic Maxwell's equations. *Appl. Numer. Math.*, 98:59–78, 2015.

[27] L. H. Nguyen. An inverse space-dependent source problem for hyperbolic equations and the Lipschitz-like convergence of the quasi-reversibility method. *Inverse Problems*, 35:035007, 2019.

[28] L. H. Nguyen. A new algorithm to determine the creation or depletion term of parabolic equations from boundary measurements. *Computers and Mathematics with Applications*, 80:2135–2149, 2020.

[29] H. Schubert and A. Kuznetsov. *Detection and Disposal of Improvised Explosives*. Springer, Dordrecht, 2006.

[30] R. Triggiani and P.F. Yao. Carleman estimates with no lower order terms for general Riemannian wave equations. Global uniqueness and observability in one shot. *Applied Mathematics and Optimization*, 46:331–375, 2002.

[31] T. Truong, D-L Nguyen, and M. V. Klibanov. Convexification numerical algorithm for a 2D inverse scattering problem with backscatter data. *preprint, arxiv:2002.08427*, 2020.

[32] J. C. Weatherall, J. Barber, and B. T. Smith. Identifying explosives by dielectric properties obtained through wide-band millimeter-wave illumination. In *Passive and Active Millimeter-Wave Imaging XVIII*. Proc. SPIE 9462, 2015.

[33] M. Yamamoto. Carleman estimates for parabolic equations. Topical Review. *Inverse Problems*, 25:123013, 2009.

CHAPTER 6: CONCLUSIONS

In this dissertation, we have made significant contributions to this field by developing effective numerical methods and theoretical analysis for several inverse problems. Our research is motivated by the need to explore inaccessible regions through external measurements, which is crucial for non-destructive testing, biomedical imaging, geophysical exploration, and radar, among other applications.

We have addressed the highly ill-posed and often nonlinear nature of the inverse problems by proposing a unified framework for solving inverse problems. This framework comprises two stages. In stage 1, we truncate the Fourier series of the solution to the governing equation or introduce a new change of variable. By this step, we obtain a system of partial equations. In stage 2, we compute the solution to this system, which directly provides us with the desired solutions to the inverse problems under consideration.

To tackle challenging stage 2, we have proposed and developed three numerical methods based on a sophisticated mathematical tool of Carleman estimates. Based on Carleman estimates, our numerical methods have been proven to provide reliable solutions even when the data is highly noisy. Importantly, they are "globally" convergent, meaning they do not require advanced knowledge of the true solution before solving inverse problems. The numerical algorithms were successfully tested with highly noisy simulated and experimental data provided by engineers at the US Army Research Laboratory. This demonstrates the practicality and efficacy of our proposed methods for real-world applications.

The dissertation has addressed several inverse problems, including scattering inverse problems in both the frequency and time domains, inverse source problems

for nonlinear parabolic equations, and a linearized kinematic inverse problem with incomplete data. Each problem has its unique set of challenges, and our proposed methods have effectively addressed them.

In Chapter 2, we presented a numerical method for solving the linearized travel time tomography problem with incomplete data. The proposed method is based on the truncation of the Fourier series and the quasi-reversibility method. The method is shown to be effective for highly noisy data.

Chapter 3 proposed a numerical method for recovering the initial condition of a quasilinear parabolic equation from lateral Cauchy data. The method is based on the derivation of a boundary value problem for a system of coupled quasilinear elliptic equations and an iterative numerical method named Carleman contraction mapping. The global convergence of the method is rigorously established using a Carleman estimate.

Chapter 4 introduced the Carleman contraction mapping method for solving a coefficient inverse problem for a 1D hyperbolic equation. The method is shown to be effective for both computationally simulated and experimentally collected data provided by engineers at US Army Research Laboratory.

Finally, Chapter 5 studied the global convergence of the gradient descent method for the minimization of strictly convex functionals on a Hilbert space. We apply the numerical method developed in this chapter to solve a challenging inverse backscattering problem with highly noisy simulated data.

In conclusion, the effective algorithms and theoretical analysis in this dissertation provide an essential foundation for future research in the field of inverse problems. We believe that our proposed methods can be applied to numerous real-world applications.

REFERENCES

[1] M. V. Klibanov, T. T. Le, and L. H. Nguyen, "Convergent numerical method for a linearized travel time tomography problem with incomplete data," *SIAM Journal on Scientific Computing*, vol. 42, pp. B1173–B1192, 2020.

[2] T. T. Le and L. H. Nguyen, "A convergent numerical method to recover the initial condition of nonlinear parabolic equations from lateral cauchy data," *Journal of Inverse and Ill-posed Problems*, vol. 30, no. 2, pp. 265–286, 2022.

[3] T. T. Le and L. H. Nguyen, "The gradient descent method for the convexification to solve boundary value problems of quasi-linear PDEs and a coefficient inverse problem," *Journal of Scientific Computing*, vol. 97, no. 74, 2022.

[4] T. T. Le, M. V. Klibanov, L. H. Nguyen, A. Sullivan, and L. Nguyen, "Carleman contraction mapping for a 1D inverse scattering problem with experimental time-dependent data," *Inverse Problems*, vol. 38, no. 4, 2022.

[5] A. L. Bukhgeim and M. V. Klibanov, "Uniqueness in the large of a class of multidimensional inverse problems," *Soviet Math. Doklady*, vol. 17, pp. 244–247, 1981.

[6] O. Y. Imanuvilov and M. Yamamoto, "Global Lipschitz stability in an inverse hyperbolic problem by interior observations," *Inverse Problems*, vol. 17, pp. 717–728, 2001.

[7] O. Y. Imanuvilov, V. Isakov and M. Yamamoto, "An inverse problem for the dynamic Lamé system with two sets of boundary data," *Comm. Pure and Applied Math*, vol. 56, pp. 1–17, 2003.

[8] V. Isakov, *Inverse Problems for Partial Differential Equations*. New York: Springer, third ed., 2017.

[9] M. V. Klibanov, "Inverse problems and Carleman estimates," *Inverse Problems*, vol. 8, pp. 575–596, 1992.

[10] M. V. Klibanov and A. Timonov, *Carleman Estimates for Coefficient Inverse Problems and Numerical Applications*. Inverse and Ill-Posed Problems Series, Utrecht: VSP, 2004.

[11] L. H. Nguyen, "An inverse space-dependent source problem for hyperbolic equations and the Lipschitz-like convergence of the quasi-reversibility method," *Inverse Problems*, vol. 35, p. 035007, 2019.

[12] A. V. Smirnov, M. V. Klibanov, and L. H. Nguyen, "Convexification for a 1D hyperbolic coefficient inverse problem with single measurement data," *Inverse Probl. Imaging*, vol. 14, no. 5, pp. 913–938, 2020.

[13] L. H. Nguyen, Q. Li, and M. V. Klibanov, "A convergent numerical method for a multi-frequency inverse source problem in inhomogenous media," *Inverse Problems and Imaging*, vol. 13, pp. 1067–1094, 2019.

[14] M. V. Klibanov, "Carleman estimates for global uniqueness, stability and numerical methods for coefficient inverse problems," *J. Inverse and Ill-Posed Problems*, vol. 21, pp. 477–560, 2013.

[15] M. V. Klibanov, "Convexification of restricted Dirichlet to Neumann map," *J. Inverse and Ill-Posed Problems*, vol. 25, no. 5, pp. 669–685, 2017.

[16] M. V. Klibanov and J. Li, *Inverse Problems and Carleman Estimates: Global Uniqueness, Global Convergence and Experimental Data*. De Gruyter, 2021.

APPENDIX A: Permission Letters

Thuy Le <tle55@uncc.edu>

[EXTERNAL] RE: Contact Request From SIAM
1 message

Kelly Thomas <Thomas@siam.org> Mon, Feb 27, 2023 at 12:17 PM
To: "tle55@uncc.edu" <tle55@uncc.edu>

Dear Ms. Le:

SIAM is happy to give permission to reuse material from the article mentioned below in your dissertation. Please acknowledge the original publication, using the complete bibliographic information.

Sincerely,

Kelly Thomas
Managing Editor
Society for Industrial and Applied Mathematics
3600 Market Street - 6th Floor
Philadelphia, PA 19104
thomas@siam.org / (267) 350-6387

-----Original Message-----
From: noreply@siam.org <noreply@siam.org>
Sent: Sunday, February 26, 2023 10:55 AM
To: Kelly Thomas <Thomas@siam.org>
Subject: Contact Request From SIAM

Dear Kelly Thomas,

This message was sent to you from the SIAM contact request system on behalf of Thuy T Le.

Below is the information provided by Thuy T Le:

Email address: tle55@uncc.edu
Phone number: 7043459265
This request was made from the following page on the SIAM website:
https://www.siam.org/about-siam/staff

The following message was provided by Thuy T Le:

Dear Ms. Thomas,

I am completing my doctoral dissertation at the University of North Carolina at Charlotte entitled "Globally convergent numerical methods for several inverse problems based on Carleman estimates". I am writing to request permission to use material from the following SIAM publication in my doctoral thesis:
M. V. Klibanov, T. T. Le and L. H. Nguyen, Convergent numerical method for a linearized travel time tomography problem with incomplete data, SIAM Journal on Scientific Computing 42(2020) B1173-B1192, 2020.
I am the author of this article, and SIAM holds the copyright. I plan to reuse this paper's text, figures, and tables in my thesis.

The requested permission extends to any future revisions and editions of my dissertation, including non-exclusive world rights in all languages, and the prospective publication of my dissertation by ProQuest through its UMI® Dissertation Publishing business. ProQuest may produce and sell copies of my dissertation on demand and may make my dissertation available for free internet download at my request. These rights will in no way restrict the republication of the material in any other form by you or by others authorized by you. Your approval will confirm that your company owns the copyright to the above-described material.

Figure A.1: Permission letter - Society for Industrial and Applied Mathematics

Marketplace

This is a License Agreement between Thuy T. Le ("User") and Copyright Clearance Center, Inc. ("CCC") on behalf of the Rightsholder identified in the order details below. The license consists of the order details, the Marketplace Permissions General Terms and Conditions below, and any Rightsholder Terms and Conditions which are included below.

All payments must be made in full to CCC in accordance with the Marketplace Permissions General Terms and Conditions below.

Order Date	13-Feb-2023	**Type of Use**	Republish in a thesis/dissertation
Order License ID	1323158-1		
ISSN	0928-0219	**Publisher**	VSP BV,
		Portion	Chapter/article

LICENSED CONTENT

Publication Title	Journal of inverse and ill-posed problems	**Country**	Germany
		Rightsholder	Walter de Gruyter and Company
Date	01/01/1993		
Language	English	**Publication Type**	Journal

REQUEST DETAILS

Portion Type	Chapter/article	**Rights Requested**	Main product
Page Range(s)	256-286	**Distribution**	Worldwide
Total Number of Pages	31	**Translation**	Original language of publication
Format (select all that apply)	Print, Electronic	**Copies for the Disabled?**	No
Who Will Republish the Content?	Author of requested content	**Minor Editing Privileges?**	No
		Incidental Promotional Use?	No
Duration of Use	Life of current edition		
Lifetime Unit Quantity	Up to 2,000,000	**Currency**	USD

NEW WORK DETAILS

Title	Globally convergent numerical methods for several inverse problems based on Carleman estimates	**Institution Name**	University of North Carolina at Charlotte
		Expected Presentation Date	2023-05-12
Instructor Name	Thuy Le		

ADDITIONAL DETAILS

Order Reference Number	N/A	**The Requesting Person/Organization to Appear on the License**	Thuy T. Le

REQUESTED CONTENT DETAILS

Figure A.2: Republication License - De Gruyter

Marketplace

This is a License Agreement between Thuy T. Le ("User") and Copyright Clearance Center, Inc. ("CCC") on behalf of the Rightsholder identified in the order details below. The license consists of the order details, the Marketplace Permissions General Terms and Conditions below, and any Rightsholder Terms and Conditions which are included below.

All payments must be made in full to CCC in accordance with the Marketplace Permissions General Terms and Conditions below.

Order Date	15-Feb-2023	**Type of Use**	Republish in a thesis/dissertation
Order License ID	1324311-1		
ISSN	0266-5611	**Publisher**	IOP Publishing
		Portion	Chapter/article

LICENSED CONTENT

Publication Title	Inverse Problems	**Country**	United Kingdom of Great Britain and Northern Ireland
Author/Editor	Institute of Physics (Great Britain)	**Rightsholder**	IOP Publishing, Ltd
Date	01/01/1985	**Publication Type**	Journal
Language	English		

REQUEST DETAILS

Portion Type	Chapter/article	**Rights Requested**	Main product
Page Range(s)	045002	**Distribution**	Worldwide
Total Number of Pages	31	**Translation**	Original language of publication
Format (select all that apply)	Print, Electronic	**Copies for the Disabled?**	No
Who Will Republish the Content?	Author of requested content	**Minor Editing Privileges?**	No
Duration of Use	Life of current edition	**Incidental Promotional Use?**	No
Lifetime Unit Quantity	Up to 2,000,000	**Currency**	USD

NEW WORK DETAILS

Title	Globally convergent numerical methods for several inverse problems based on Carleman estimates	**Institution Name**	University of North Carolina at Charlotte
		Expected Presentation Date	2023-05-12
Instructor Name	Thuy Le		

ADDITIONAL DETAILS

Order Reference Number	N/A	**The Requesting Person/Organization to Appear on the License**	Thuy T. Le

REQUESTED CONTENT DETAILS

Figure A.3: Republication License - IOP Publishing

Marketplace

This is a License Agreement between Thuy T. Le ("User") and Copyright Clearance Center, Inc. ("CCC") on behalf of the Rightsholder identified in the order details below. The license consists of the order details, the Marketplace Permissions General Terms and Conditions below, and any Rightsholder Terms and Conditions which are included below.

All payments must be made in full to CCC in accordance with the Marketplace Permissions General Terms and Conditions below.

Order Date	17-Feb-2023	**Type of Use**	Republish in a thesis/dissertation
Order License ID	1325207-1		
ISSN	0885-7474	**Publisher**	SPRINGER NEW YORK LLC
		Portion	Chapter/article

LICENSED CONTENT

Publication Title	Journal of scientific computing	**Rightsholder**	Springer Nature BV
		Publication Type	Journal
Date	01/01/1986	**URL**	http://www.springer.com/mathematics/computational+science+%26+engineering/journal/10915
Language	English		
Country	United States of America		

REQUEST DETAILS

Portion Type	Chapter/article	**Rights Requested**	Main product
Page Range(s)	91:74	**Distribution**	Worldwide
Total Number of Pages	23	**Translation**	Original language of publication
Format (select all that apply)	Print, Electronic	**Copies for the Disabled?**	No
Who Will Republish the Content?	Author of requested content	**Minor Editing Privileges?**	No
		Incidental Promotional Use?	No
Duration of Use	Life of current edition		
Lifetime Unit Quantity	Up to 2,000,000	**Currency**	USD

NEW WORK DETAILS

Title	Globally convergent numerical methods for several inverse problems based on Carleman estimates	**Institution Name**	University of North Carolina at Charlotte
		Expected Presentation Date	2023-05-12
Instructor Name	Thuy T. Le		

ADDITIONAL DETAILS

The Requesting Person/Organization to Appear on the License	Thuy T. Le

Figure A.4: Republication License - Springer New York